ADVANCES IN LATERAL TORSIONAL BUCKLING ANALYSIS OF BEAM-COLUMNS AND PLANE FRAMES

by

Arash Sahraei

Thesis submitted to the
Faculty of Graduate and Postdoctoral Studies
in partial fulfillment of
the requirements for the degree of
DOCTOR OF PHILOSOPHY
in Civil Engineering

Department of Civil Engineering
Faculty of Engineering
University of Ottawa

Abstract

The present study provides a series of contributions to the advancement of methods of lateral torsional buckling analysis of beam-columns and plane frames.

The first contribution develops a family of three finite elements for the lateral torsional buckling analysis of members with doubly symmetric cross-sections. The elements capture warping, shear deformation, and load position effects as well as the destabilizing effects due to strong axis bending, associated shear forces, and axial forces. The formulation starts with a recently developed variational principle based on an advanced kinematic model that incorporates shear deformation effects due to flexure and warping. Unlike previous shear deformable solutions that exhibit slow convergence due to shear locking, the present study develops an innovative interpolation scheme that circumvents shear locking. One of the elements is devised to attain fast convergence. The second element is devised to guarantee convergence to the buckling loads from below while the third element is guaranteed to converge from above, thus providing lower and upper bounds for the buckling loads. The formulation is equipped with a versatile multi-point constraint feature enabling the analyst to model, among other applications, the effect of lateral braces that are offset from the shear center.

The second contribution extends the formulation to members with mono-symmetric sections. A closed-form shear deformable solution is derived for the case of a mono-symmetric simply supported beam subjected to uniform bending moments. A beam finite element is developed and adopted to provide solutions for simply supported beams, cantilevers, and developing moment gradient factors for beams under linear moments. The formulation is shown to successfully capture interaction effects between axial forces and bending moments and the destabilizing effect of loads offset from the shear center.

The third contribution devises a technique to extend present lateral torsional buckling solutions originally intended for beam analysis to the modelling of plane frames. The technique involves developing a generalized four-node joint finite element that accurately quantifies the partial warping restraint provided by common moment connections to adjoining members framing at right angles. The joint element is intended to seamlessly interface either with the classical beam buckling elements or the shear deformable finite elements developed in the present study. A systematic static condensation scheme is devised to adapt the joint element for cases where a joint interfaces with only two or three elements. Careful consideration is taken to incorporate for the finite rotation effect for the joints. The formulation adopts multi-point constraints to characterize the in-plane pre-buckling behavior and out-of-plane buckling behavior of the joints. The methodology is shown to involve considerably fewer degrees of freedom than shell based solutions while leading to accurate predictions of the buckling loads. The technique is then adopted to characterize the elastic lateral torsional buckling of sample plane frame configurations and thus provides a basis to assess the validity of the Salvadori hypothesis commonly adopted in present design standards whereby buckling loads for members are quantified by separating the members from the entire structure. The study suggests that for plane frames with lateral restraints at the joints, the application of the Salvadori hypothesis typically leads to conservative buckling load estimates. In contrast, for cases where some of the joints are laterally free, the Salvadori hypothesis may overestimate the buckling strength.

Acknowledgment

I would like to express my sincere gratitude and deepest appreciation to my knowledgeable supervisor, Professor Magdi Mohareb, for his patient guidance, assistance, advice, support and continuous encouragement throughout this work. I have been extremely lucky to have a supervisor who cared so much about my work, and who responded to my questions and queries so promptly. In fact, without his support, I would have not been able to accomplish this study.

I would also thank my beloved parents, Hossein and Farideh, and my nice sister, Avid, for their endless support and sacrifice for me during the years.

My special thanks go to my lovely wife, Mozhgan, for her precious and continuous moral support, patience and tireless encouragement during my study. Honestly, without her encouragement and unconditional love, I would have not been able to conquer the long-distance challenges and complete my degree.

Finally, my thanks should be extended to my colleagues and friends for their help and friendship during my doctoral study.

Table of Contents

List of Figures

List of Tables

Chapter 1 Introduction

1.1 Background and motivation

Lateral torsional buckling is a mode of failure typically governing the flexural resistance of laterally unsupported long span members bent about their strong axis. Structural steel design standards such as CAN/CSA S16 (2014), ANSI/AISC 360 (2016), AS4100 (1998) and EN 1993-1-1 (2005) recognize lateral torsional buckling as a mode of failure and provide expressions to estimate the elastic lateral torsional buckling resistance for beams with simple configuration and idealized boundary conditions. For example, ANSI/AISC 360 (2016) describes the lateral torsional buckling phenomenon as a buckling mode of a flexural member in which it simultaneously twists about its shear center and moves out of its bending plane. Most standards use the classical lateral torsional buckling expression for simply supported beams with doubly symmetric cross-section subjected to uniform bending moments as a starting point and apply moment gradient factors to accommodate for practical loading scenarios where the moments are non-uniform. Barsoum and Gallagher (1970) developed a beam finite element formulation to compute the elastic lateral torsional buckling moment for general loading and boundary conditions. For non-uniform moments, standard provisions provide moment gradient factor expressions. Such moment gradient factors are obtained by dividing the critical moments as computed based on the conventional finite element by Barsoum and Gallagher (1970) for non-uniform bending moments, by the critical uniform bending moment expression as given by the classical solution. Recently, design standards such as CAN/CSA S16 (2014), ANSI/AISC 360 (2005) and the subsequent editions (2010, 2016) have provided expressions for quantifying the lateral torsional buckling resistance for simply supported members with mono-symmetric cross-sections subjected to general loading. More complex cases involving continuous beams, cantilever suspended construction and cantilevers are beyond the scope of North American design standards.

Beams with wide flange cross-sections are commonly used in structural steel assemblies. Due to their inherently weak torsional stiffness, they are particularly prone to lateral torsional buckling when subjected to transverse loads. The beneficial effects of end and intermediate partial and full restraints provided by roof purlins and framing cross-beams are typically not addressed within existing design standard provisions as they are applicable only to simple cases. In practice, I-beams can also be restrained laterally at locations along the section depth that are offset from the section shear center. Thus, it is of interest to develop an effective lateral torsional buckling analysis tool capable of modelling the effect of intermediate rigid or elastic restraints that are offset from the shear center. Within this context, the present research aims to advance present methods of lateral torsional buckling analysis and provide a better understanding and insight on the effect of restraints on the resistance and behavior of steel beams while accounting for the beneficial effects of lateral and rotational restraints.

Another limitation in the present design standards in treating lateral torsional buckling, is that they omit interaction effects among various members of a frame, i.e., when performing design interaction checks, each member of a frame is assumed to buckle independently. The validity of such an approach needs to be assessed by conducting a lateral torsional buckling analysis on the whole structure. In principle, such a buckling analysis can be performed using shell elements. However, for typical multi-bay multi-story frames, the modelling effort and running time can be prohibitively expensive. Within this context, the present study aims at developing computationally efficient and accurate means of determining the lateral torsional buckling strength of plane frames as a whole while accounting for the interaction between various adjoining members of a frame.

1.2 Objectives and scope

The objective of the present study is to improve methods of lateral torsional buckling analysis of steel assemblies in several respects. These are:

(1) In a relatively recent study, Wu and Mohareb (2011a) developed a variational principle for a shear deformable buckling theory and adopted the principle to develop a finite element formulation for the lateral torsional buckling analysis of doubly symmetric cross-sections (Wu and Mohareb (2011b)). The element is based on linear interpolation functions and has C0 continuity. The element was shown to a) converge from above to the buckling load in a manner similar to other finite element formulations, and b) exhibit particularly slow-convergence characteristics as hundreds of degrees of freedom were needed to model simple problems. The present study starts with the variational principle in Wu and Mohareb (2011a) and develops an innovative interpolation scheme leading to C1 continuity, resulting in a family of three finite elements for the lateral torsional buckling analysis of doubly symmetric members. The elements exhibit superior convergence characteristics and are developed such that one of the elements is guaranteed to

converge to the buckling load from above, the other one is guaranteed to converge from below, and the third element is devised to exhibit the fastest convergence rate.

(2) Extending the solution in (1) for the lateral torsional buckling analysis of beams with mono-symmetric cross-sections by developing a finite element that accounts for mono-symmetry effects and shear deformation effects.

(3) Within items (1) and (2), developing a feature for incorporating any number mp of user-specified linear Multiple Point Constraints (MPCs) of the type

$$[A]_{mp\times np}\{u_p\}_{np}=\{B\}_{mp} \tag{1.1}$$

within the pre-buckling analysis module, where $[A]_{mp\times np}$ is a user-input matrix of coefficients, $\{u\}_{np}$ is the vector of pre-buckling nodal displacements for the structure, and $\{B\}_{mp}$ a user input right hand side vector. Pre-buckling MPCs are useful in several practical engineering applications. For example, consider a continuous beam with four supports in which the middle supports are constrained to move vertically and the other two supports to settle by half of that amount by a specified vertical displacement v_1 as shown in Figure 1-1.

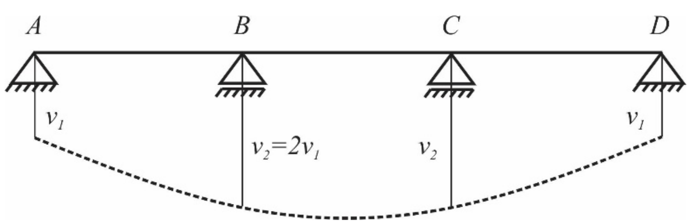

Figure 1-1 Example of pre-buckling MPCs

The pre-buckling constraint equations can be written as

$$\begin{aligned} v_{PA} &= v_1 \\ v_{PB}-2v_{PA} &= 0 \\ v_{PC}-2v_{PA} &= 0 \\ v_{PD}-v_{PA} &= 0 \end{aligned} \tag{1.2}$$

or, in a matrix form, one has

$$\begin{bmatrix} 1 & 0 & 0 & 0 \\ -2 & 1 & 0 & 0 \\ -2 & 0 & 1 & 0 \\ -1 & 0 & 0 & 1 \end{bmatrix} \begin{Bmatrix} v_{PA} \\ v_{PB} \\ v_{PC} \\ v_{PD} \end{Bmatrix} = \begin{Bmatrix} v_1 \\ 0 \\ 0 \\ 0 \end{Bmatrix} \quad (1.3)$$

Equation (1.3) is a special case of Eq. (1.1). It is thus of practical interest to add a feature which seamlessly enforce any set of linear kinematic constraints of the form of Eq. (1.1). The solution also extends the multiple point constraint capability to the buckling analysis by incorporating any number mb of linear Multiple Point Constraints (MPCs) of the form

$$[B]_{mb\times nb}\{u_b\}_{nb} = \{0\}_{mb} \quad (1.4)$$

where $[B]_{mb\times nb}$ is a matrix of user-input coefficients and $\{u\}_{nb}$ is the vector of buckling nodal displacements for the structure. The usefulness of the buckling MPCs is illustrated by considering a doubly symmetric beam laterally braced at the top flange at the third points as shown in Figure 1-2.

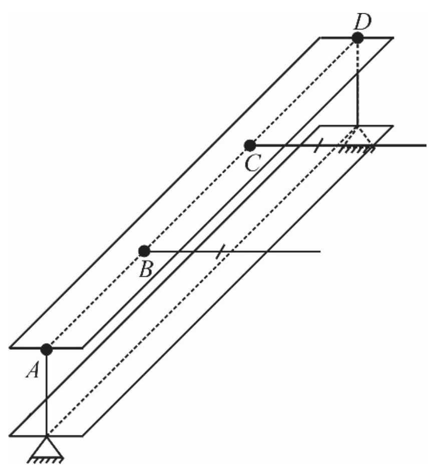

Figure 1-2 Example of buckling MPCs

The corresponding buckling constraint equations can be written as

$$\begin{aligned} \left(\frac{h}{2}\right)\theta_B - u_B &= 0 \\ \left(\frac{h}{2}\right)\theta_C - u_C &= 0 \end{aligned} \quad (1.5)$$

where h is the section depth, θ_B and θ_C are the angles of twist at points B and C, and u_B and u_C are lateral displacements of the shear center at points B and C, respectively. In a matrix form, the constraints can be written as

$$\begin{bmatrix} \frac{h}{2} & -1 & 0 & 0 \\ 0 & 0 & \frac{h}{2} & -1 \end{bmatrix} \begin{Bmatrix} \theta_B \\ u_B \\ \theta_C \\ u_C \end{Bmatrix} = \begin{Bmatrix} 0 \\ 0 \end{Bmatrix} \tag{1.6}$$

which is a special case of Eq. (1.4). Thus, the present study incorporates a feature that seamlessly incorporates pre-buckling and buckling MPCs within the analysis.

(4) Developing a generalized coupled spring element

In practical design problems, it is often desirable to isolate a member from the rest of the structure to investigate its buckling strength or link components of the structure such a column and beam using an intermediate elastic body (such a joint). Since buckling problems are particularly sensitive to boundary conditions, it is important to realistically represent the end constraints at the end of the member(s). Given that the surrounding structure (or adjoining elastic body) has some flexibility, the constraints at member ends are only partial and can be approximately modelled, for example, through spring elements. Under thin-walled beam theories, nodal degrees of freedom relevant to lateral torsional buckling are lateral, torsional, warping or related to weak axis rotation. Further, these constraints are coupled, in the sense that, for example, if an end of the member is moved laterally, the remainder of the structure would generate twisting moments, bimoments, weak axis moments, lateral forces at both ends of the member. Present FEA programs do not incorporate such coupling effects. Thus, one of the objectives of the present study is to incorporate a generalized spring feature which allows the user to define a coupled multi-degree of spring element that links any set of user specified degrees of freedom within the structure.

(5) Extending existing beam lateral torsional buckling solutions for co-linear elements to non-collinear planar frame structures

Present design standard provisions isolate the member from the rest of the structure and conduct separate code checks. In order to assess the validity of this common practice, shell finite element modelling for the whole structure can be conducted. However, the associated computational cost can be prohibitive. Thus, under the present study, lateral torsional buckling solutions for co-linear elements are extended to plane frames subjected to in-plane loads. A challenge encountered in such a treatment is illustrated in Figure 1-3. As the shown frame undergoes lateral buckling, the three members connected to the identified joint element exhibit different warping deformations $\psi_i\left(i=1,2,3\right)$ at their ends. This signifies that the joint element has three different warping deformations $\psi_i\left(i=1,2,3\right)$ at each of its three faces i. In general, a warping deformation ψ_i induces not only a bimoment B_i on the same face, but also bimoments on the other two faces $B_j(i \neq j)$, i.e., the joint warping-bimoment response can be characterized by a 3x3 bimoment-warping stiffness matrix and the nodal bimoments $\left\{B_i\right\}$ are thus related to the warping degrees of freedom $\left\{\psi_i\right\}$ through

$$\left\{B_i\right\}_{3\times1}=\left[K_\omega\right]_{3\times3}\left\{\psi_i\right\}_{3\times1} \tag{1.7}$$

in which $\left[K_\omega\right]_{3\times3}$ is a fully coupled matrix. In order to obtain the matrix $\left[K_\omega\right]_{3\times3}$, a detailed shell type analysis needs to be conducted and a special static condensation procedure needs to be performed to recover matrix $\left[K_\omega\right]_{3\times3}$. This approach was attempted in a pilot study by Wu and Mohareb (2012) on joints connecting only two members. The present study aims at generalizing the joint element formulation for joints connecting 2, 3, and 4 beam elements. Another challenge in generalizing the beam lateral torsional buckling analysis to frames is the fact that as the joint element undergoes buckling rotations, it can be shown that conventional treatment based on the small rotation assumption leads to loss of equilibrium of the joint. This phenomenon has been reported in McGuire et al. (2000) but received little attention in various published lateral torsional buckling solutions. Within this context, the present study provides a robust treatment of finite rotation effects for joints which turns out to be of prime importance for the correct prediction of lateral torsional buckling of frames. The study then integrates the warping stiffness, finite rotation effects, along with conventional beam lateral torsional buckling elements to investigate the lateral torsional buckling of planar frames.

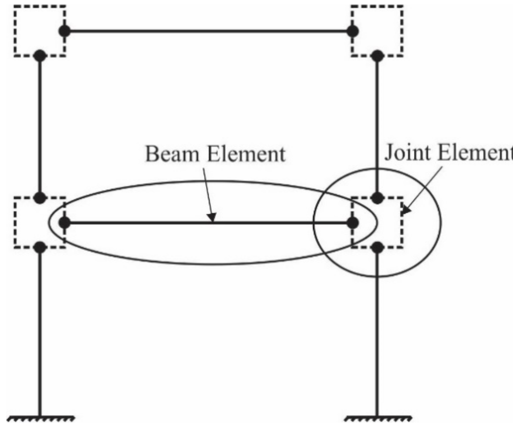

Figure 1-3 Typical Plane Frame model

1.3 Outline of the thesis

The body of the present thesis consists of six chapters. The contents of chapters are as follows:

Chapter 1 provided an introduction and a description of the scope of the thesis,

Chapter 2 provides a review of the literature relevant to lateral torsional buckling and is divided into three parts. The first part reviews relevant standard provisions. The second introduces two ABAQUS elements used throughout the study as benchmark solutions for comparison purposes. Also summarized are available features to model multiple point constraints (MPCs) in ABAQUS. Available spring elements in ABAQUS are discussed and their limitations are outlined. Finally, a comprehensive literature review is provided on various lateral torsional buckling (LTB) studies for beams with doubly symmetric and mono-symmetric cross-sections. Lateral torsional buckling solutions involving elastic restraints are also provided in the review. Comparative tables are also provided to summarize various aspects of past work and situate the contributions of the present study within the existing body of knowledge.

Chapter 3 Develops a formulation for a family of beam elements for the LTB for members with doubly symmetric cross-sections. The validity of the formulation is then assessed against other solutions. The applicability of the new formulation to practical engineering problems is then illustrated through a series of examples.

Chapter 4 extends the formulation for LTB analysis of mono-symmetric thin-walled members. The validity of formulation is then assessed against benchmark solutions and the new solution is applied to a series of practical problems including developing moment gradient values for beams under linear moment gradients.

Chapter 5 develops the features necessary to extend lateral torsional buckling analysis to plane frames. This includes the development of joint elements intended to interface seamlessly with existing finite elements such as those developed in Chapters 3 and 4 and others. A robust treatment of finite rotation effect is also presented. The features developed in Chapters 3-5 are then integrated to analyze a variety of plane frames for lateral torsional buckling analysis. Comparisons with other modelling techniques are also provided for assessment, and the advantages of an integrated analysis are outlined.

Chapter 6 then summarizes the research developed in the thesis, the various observations and conclusions and recommends ideas for further research in the area.

Chapters 3-5 are written in a paper format. Chapters 3 and 4 have been published in Sahraei and Mohareb (2016) and Sahraei et al. (2015) and Chapter 5 has been submitted for review into an international journal. All the formulations developed in the present study, have been implemented under the MATLAB platform.

1.4 REFERENCES

Standards Association of Australia (SAA), (1998). Steel Structures, AS4100-1998, SAA, Australian Institute of Steel Construction. Sydney, Australia.

American Institute of Steel Construction, (AISC), (2005). Specification for Structural Steel Buildings, ANSI/AISC 360-05, AISC. Chicago, IL.

CEN, Eurocode 3: Design of Steel Structures, (2005). Part 1-1: General Rules and Rules for Buildings, ENV 1993-1-1, Comité Européen de Normalisation. Brussels, Belgium.

American Institute of Steel Construction, (AISC), (2010). Specification for Structural Steel Buildings, ANSI/AISC 360-10, AISC. Chicago, IL.

Canadian Standards Association, (CSA), (2014). Limit States Design of Steel Structures, CAN/CSA S16-14. Toronto, Ontario, Canada.

American Institute of Steel Construction, (AISC), (2016). Specification for Structural Steel Buildings, ANSI/AISC 360-16, AISC. Chicago, IL.

Barsoum, R. S. and R. H. Gallagher (1970). "Finite element analysis of torsional and torsional–flexural stability problems." International Journal for Numerical Methods in Engineering 2(3): 335-352.

McGuire, W., R. H. Gallagher and R. D. Ziemian (2000). Matrix Structural Analysis. New York, John Wiley & Sons, Inc.

Sahraei, A. and M. Mohareb (2016). "Upper and lower bound solutions for lateral-torsional buckling of doubly symmetric members." Thin-Walled Structures 102: 180-196.

Sahraei, A., L. Wu and M. Mohareb (2015). "Finite element formulation for lateral torsional buckling analysis of shear deformable mono-symmetric thin-walled members." Thin-Walled Structures 89(0): 212-226.

Wu, L. and M. Mohareb (2011a). "Buckling of shear deformable thin-walled members—I. Variational principle and analytical solutions." Thin-Walled Structures 49(1): 197-207.

Wu, L. and M. Mohareb (2011b). "Buckling formulation for shear deformable thin-walled members—II. Finite element formulation." Thin-Walled Structures 49(1): 208-222.

Wu, L. and M. Mohareb (2012). "Finite-Element Formulation for the Lateral Torsional Buckling of Plane Frames." Journal of Engineering Mechanics 139(4): 512-524.

Chapter 2 Literature Review

2.1 General

The present chapter provides an overview of relevant studies and is divided into three parts. Firstly, the elastic lateral torsional buckling provisions in Canadian, American, Australian and Eurocode standards for doubly symmetric and mono-symmetric cross-sections are reviewed in Section 2.2. Secondly, a brief review of the shell S4R element and the open thin-walled beam element B31OS in ABAQUS is presented in Section 2.3 since both elements will be used to assess the validity of the solutions developed in Chapters 3 through 5. Also presented are available features in ABAQUS to enforce multiple point constraints (MPCs) and a review of spring elements is provided. Lastly, Section 2.4 provides a detailed review of lateral torsional buckling studies for members with doubly symmetric and mono-symmetric cross-sections. Also, reviewed under the same section are the studies that incorporate elastic restraints within lateral torsional buckling solutions given their relevant to the objectives of the present study.

2.2 Standard provisions on lateral torsional buckling

Most steel design standards start with the classical closed-form solution of critical buckling moment M_u for a simply supported beam relative to twist and lateral displacement subject to uniform bending moments to develop expressions for both doubly symmetric and mono-symmetric cross-sections. For doubly symmetric sections, the equation takes the form

$$M_u = \frac{\pi}{L_u}\sqrt{EI_yGJ + \left(\frac{\pi E}{L_u}\right)^2 I_yC_w} \qquad (2.1)$$

in which L_u is the unbraced length of the beam, E is elastic modulus of steel, I_y is the weak axis moment of inertia, G is the shear modulus of elasticity of steel, J is torsional constant and C_w is the warping constant. For mono-symmetric sections, the critical moment equation takes the form

$$M_u = \frac{\pi^2 EI_y}{2L_u}\left[\beta_x + \sqrt{\beta_x^2 + 4\left(\frac{GJL_u^2}{\pi^2 EI_y} + \frac{C_w}{I_y}\right)}\right] \qquad (2.2)$$

where for a wide flange section with unequal legs, the mono-symmetry parameter can be approximated by

$$\beta_x = 0.9\left(d-t\right)\left(\frac{2I_{yc}}{I_y}-1\right)\left(1-\left(\frac{I_y}{I_x}\right)^2\right) \tag{2.3}$$

in which d is the section depth, t is the flange thickness, I_{yc} and I_{yt} are the moment of inertia of the compression and tension flanges about the y-axis, respectively. In the following, the design provisions for doubly symmetric sections will first be reviewed and then the review will extend to mono-symmetric sections.

2.2.1 Doubly symmetric sections

2.2.1.1 CAN/CSA S16-14

One of the objectives of the present study is to provide moment gradient factors for mono-symmetric I-beams. Thus, it is of interest to review the elastic lateral torsional buckling equations presented in various design standards. According to the Canadian Standards (2014), for laterally unsupported beams with doubly symmetric cross-sections bent about their strong axis, the elastic lateral torsional buckling is given by

$$M_{cr} = C_{CAN} M_u \tag{2.4}$$

where C_{CAN} is the moment gradient factor and is used to account for general non-uniform moment distribution. It is obtained through

$$C_{CAN} = \frac{4M_{\max}}{\sqrt{M_{\max}^2 + 4M_A^2 + 7M_B^2 + 4M_C^2}} \le 2.5 \tag{2.5}$$

in which $M_{\max}$ is the maximum bending moment along the beam, M_A, M_B and M_C are bending moments at the quarter, mid-point and three-quarter points of the beam span, respectively.

2.2.1.2 ANSI/AISC 360-16

For doubly symmetric cross-sections, the elastic lateral torsional buckling strength suggested by ANSI/AISC 360 (2016) is

$$M_{cr} = C_{AISC} M_u \tag{2.6}$$

in which M_u is again the classical critical moment and C_{AISC} is the ANSI/AISC 360 (2016) moment gradient factor given by

$$C_{AISC} = \frac{12.5M_{\max}}{2.5M_{\max} + 3M_A + 4M_B + 3M_C} \tag{2.7}$$

2.2.1.3 AS-4100-1998

The Australian standard (1998) provides the equation

$$M_{cr} = C_{AUS}\alpha_s M_p \leq M_p \tag{2.8}$$

to calculate both elastic and inelastic lateral torsional buckling strength of beams with doubly symmetric cross-sections where C_{AUS} is the AS-4100-1998 (1998) moment gradient factor given by

$$C_{AUS} = \frac{1.7M_{\max}}{\sqrt{M_A^2 + M_B^2 + M_C^2}} \leq 2.5 \tag{2.9}$$

and α_s is referred to as the slenderness reduction factor obtained through

$$\alpha_s = 0.6\left\{\sqrt{\left[\left(\frac{M_p}{M_o}\right)^2 + 3\right]} - \left(\frac{M_p}{M_o}\right)\right\} \tag{2.10}$$

in which M_p is the plastic moment resistance and M_o is a modified version of classical critical buckling solution M_u and is given as

$$M_o = \frac{\pi}{L_e}\sqrt{EI_yGJ + \left(\frac{\pi E}{L_e}\right)^2 I_yC_w} \tag{2.11}$$

where $L_e = k_tk_lk_rL_u$ is an effective span accounting for the end twist restraint through constant k_t, for the load height relative to the shear center through coefficient k_l, and for the weak axis restraint via k_r and L_u being the span of the member.

2.2.1.4 EN 1993-1-1:2005

Under the Eurocode (2005), the elastic critical moment for lateral torsional buckling of mono-symmetric and doubly symmetric I-beams bent about the major axis is given by

$$M_{cr} = C_1 \frac{\pi^2 EI_z}{(kL)^2} \left\{ \sqrt{\left[\left(\frac{k}{k_w}\right)^2 \frac{C_w}{I_z} + \frac{(kL)^2 GI_t}{\pi^2 EI_z} + \left(C_2 z_g - C_3 z_j\right)^2 \right]} - \left(C_2 z_g - C_3 z_j\right) \right\} \tag{2.12}$$

where G is the shear modulus, I_t is the Saint Venant torsional constant, C_w is the warping constant, I_z is the moment of inertia about the weak axis, L is the length of the beam between two points that have lateral restraint, C_1 is the factor depending on the bending moment distribution, C_2 is a factor depending on the load height, C_3 is a factor depending on the degree of mono-symmetry of the section, k and k_w are effective length factors refers to end rotation and end warping, respectively and varying between 0.5 for full fixation restraint and 1.0 for restraints simply supported against lateral movement and twist, z_g is the load height distance $z_g = z_a - z_s$ in which z_a is the load application height, z_s is the shear center height and z_g is negative for loads acting towards the shear center from their points of application and $z_j = z_s - 0.5\int_A \left(y^2 + z^2\right)\frac{z}{I_y} dA$ is the mono-symmetric parameter and is equal to zero for doubly symmetric sections.

2.2.2 Mono-symmetric sections

2.2.2.1 CAN/CSA S16-14

For mono-symmetric sections, CAN/CSA S16 (2014) provides the following expression for the critical moment

$$M_{cr} = \frac{\omega_3 \pi^2 EI_y}{2L_u} \left[\beta_x + \sqrt{\beta_x^2 + 4\left(\frac{GJL_u^2}{\pi^2 EI_y} + \frac{C_w}{I_y}\right)} \right] \tag{2.13}$$

where $\omega_3 = C_{CAN}$ for mono-symmetric I-beams under single curvature and $\omega_3 = C_{CAN}\left[0.5 + 2\left(I_{yc}/I_y\right)^2\right]$ for mono-symmetric I-beams under double curvature. In the absence of accurate values for cross-sectional properties β_x and C_w, they can be evaluated through

$$\beta_x = 0.9\left(d-t\right)\left(\frac{2I_{yc}}{I_y} - 1\right)\left(1 - \left(\frac{I_y}{I_x}\right)^2\right) \tag{2.14}$$

$$C_w = \frac{I_{yc} I_{yt} \left(d-t\right)^2}{I_y} \tag{2.15}$$

in which d is the section depth, t is the flange thickness, I_{yc} and I_{yt} are the moment of inertia of the compression and tension flanges about the y-axis respectively; and I_y and I_x are also moment of inertia about y-axis and x-axis correspondingly.

2.2.2.2 ANSI/AISC 360-16

To determine the elastic lateral torsional buckling strength for mono-symmetric I-beams, the American standards ANSI/AISC 360 (2016) provide the equation

$$M_{cr} = \frac{C_{AISC}\pi^2 E I_y}{2L_u}\left\{\frac{\beta_x}{2} + \sqrt{\left(\frac{\beta_x}{2}\right)^2 + \frac{C_w}{I_y}\left[1 + 0.0390\frac{J}{C_w}L_b^2\right]}\right\} \tag{2.16}$$

in which C_{AISC} is the moment gradient factor identical to that provided for doubly symmetric cross-sections but it is applicable for mono-symmetric under single curvature. For mono-symmetric cross-sections subjected to reverse curvature bending, the commentary stipulates that each flange should be separately considered as a compression flange and the lateral torsional buckling resistance should be evaluated by comparing the available flexural resistance against the external moments that induce compression in the flange which is under consideration.

2.2.2.3 AS-4100-1998

Under the Australian Standards (1998), the flexural resistance of I-beams with mono-symmetric cross-sections is obtained from Equation (2.8) with the following definitions for M_o

$$M_o = \sqrt{\left(\frac{\pi^2 EI_y}{L_e^2}\right)}\sqrt{\left[(GJ) + \left(\frac{\pi^2 EC_w}{L_e^2}\right) + \left(\frac{\beta_x^2 \pi^2 EI_y}{4L_e^2}\right)\right]} + \frac{\beta_x}{2}\sqrt{\left(\frac{\pi^2 EI_y}{L_e^2}\right)} \quad (2.17)$$

where the mono-symmetry section constant β_x is obtained through

$$\beta_x = 0.8 d_f \left[\left(\frac{2I_{cy}}{I_y}\right) - 1\right] \quad (2.18)$$

in which d_f is the distance between flange centroids, I_{cy} is the moment of inertia of the compression flange about the y-axis and I_y is the moment of inertia about y-axis.

2.3 Review of relevant modelling features in ABAQUS

Among the large number of elements in the ABAQUS library, the shell element S4R and the open section beam element B31OS will be used for benchmark comparisons against various solutions to be implemented in the present study. The features of the S4R element is reviewed under Section 2.3.1 and those of the B31OS element are reviewed under Section 2.3.2. Also, reviewed are the Multiple Point Constraint (MPC) feature under Section 2.3.3 and the available spring features under Section 2.3.4.

2.3.1 The S4R element

The S4R is a general-purpose doubly curved shell (S) element with four (4) nodes and reduced (R) integration. Externally, the element has three translational and three rotational degrees of freedom per node in which each independent degree of freedom uses bi-linear interpolation function. Reduced integration is adopted to reduce the computational run time and avoid shear locking. The element predicts accurate results for thin shells and captures shear deformations and distortional effects. Since it is a reduced integration element, it may yield deformation modes causing zero strains at integration points. These zero-energy modes propagate throughout the mesh and can cause “hourglassing” resulting in inaccurate results. To prevent this phenomenon, an hourglass stabilization control feature is built into the element by allocating a small fictitious stiffness associated with zero-energy deformation modes. Also, ABAQUS automatically checks the mode shapes for possible hourglassing.

2.3.2 The B31OS element

B31OS element is beam (B) for 3D analysis (3) using a linear or first order and hence the designation (1) interpolation. The element is based on an open section (OS) formulation and involves two nodes. Each node has seven degrees of freedom; three translational and three rotational degrees of freedom and an additional degree of freedom representing the warping deformation. The element can be used for beams with arbitrary sections. The element captures shear deformation effects only due to bending, but omits shear deformation effects due to warping.

2.3.3 Multiple Point Constraints (MPCs) in ABAQUS

The various degrees of freedom in an ABAQUS model can be related through user-specified linear or non-linear relations using various features. Following are the features available in ABAQUS to enforcing common restraints.

*MPC Type TIE couples all the active degrees of freedom between two specified nodes and is ideal for joining two parts of a mesh when they are fully connected.

*MPC Type SLIDER constrains the specified node(s) on a straight line defined by two specified nodes but allows them to move along the line and permits the line to change length.

Keyword *EQUATION can be used to express any linear relationship between any set of nodes. This feature will be used in the present research under Chapter 3 to define MPCs for the B31OS element.

2.3.4 Springs elements in ABAQUS

ABAQUS is able to incorporate linear and nonlinear springs into the model. The spring element type *SPRING1 can be used to model an elastic foundation-like feature in the model. This element type has a single node and serves to elastically connect a specified node to a rigid surface. This type of spring does not rotate within a large displacement analysis. The force-displacement relationship for this type of spring elements takes the form

$$\begin{Bmatrix} F_x \\ F_y \\ F_z \end{Bmatrix} = [K]_{3\times 3}\{u\}_{3\times 1} = \begin{bmatrix} k_x & & \\ & k_y & \\ & & k_z \end{bmatrix}_{3\times 3} \begin{Bmatrix} u_x \\ u_y \\ u_z \end{Bmatrix}_{3\times 1} \tag{2.19}$$

where F_x, F_y, F_z are the forces in the spring along the global directions, u_x, u_y, u_z are the corresponding displacements in the spring, and k_x, k_y, k_z are user-specified spring constants.

Another type of spring element provided in the ABAQUS library is *SPRING2 element type which connects two nodes within the model and is assumed to act along a fixed direction. In this case, depending on the orientation defined by the user, the spring can be modeled as an element transferring normal loads or shear loads. The force-displacement equation is characterized by the relation

$$\begin{Bmatrix} \begin{Bmatrix} F_x \\ F_y \\ F_z \end{Bmatrix}_1 \\ \begin{Bmatrix} F_x \\ F_y \\ F_z \end{Bmatrix}_2 \end{Bmatrix} = \left[\begin{array}{ccc|ccc} k_{x1} & & & -k_{x2} & & \\ & k_{y1} & & & -k_{y2} & \\ & & k_{z1} & & & -k_{z2} \\ \hline -k_{x1} & & & k_{x2} & & \\ & -k_{y1} & & & k_{y2} & \\ & & -k_{z1} & & & k_{z2} \end{array}\right] \begin{Bmatrix} \begin{Bmatrix} u_{x1} \\ u_{y1} \\ u_{z1} \end{Bmatrix}_1 \\ \begin{Bmatrix} u_{x2} \\ u_{y2} \\ u_{z2} \end{Bmatrix}_2 \end{Bmatrix} \tag{2.20}$$

In contrast to *SPRING1, the presence of off-diagonal entries in stiffness matrices of *SPRING2 implies limited spring coupling. As part of the developments to be presented in Chapter 5 of the present study, a generalized coupled spring feature is developed with full coupling between any number n of user specified degrees of freedom. Such a feature will be used, for example, to connect beams to columns through a coupled warping matrix which accounts for the flexibility of the joint. In general, the coupled spring feature enables the user to define a user-specified matrix $\left[K_s\right]$ connecting the degrees of freedom, i.e.,

$$\{F\}_{n\times 1} = \left[K_s\right]_{n\times n} \{u\}_{n\times 1} \tag{2.21}$$

Presently, there is no feature within the ABAQUS element library to handle full coupling between specified degrees of freedom. Thus, developing a coupled spring element under the present study will fill this gap and will help conduct buckling analyses for frame assemblies.

2.4 Studies on elastic lateral torsional buckling

This section will review the most relevant studies to the objectives defined in Chapter 1. The gaps to be covered within the present the present thesis will be identified. A detailed review is provided for elastic lateral torsional buckling beams with doubly symmetric and mono-symmetric cross-sections. Also, covered are studies on incorporating elastic restraints in lateral torsional buckling solutions beams. In the majority of the studies, the following hypotheses are essentially assumed to be valid, unless otherwise mentioned: (1) Rigid in-plane cross-sectional deformation, (2) Elastic behavior of material, (3) Neglecting distortional and local deformations, (4) Discarding shear deformation of the section mid-line, and (5) Large angle of twist but small deformations.

2.4.1 Beams with doubly symmetric cross-sections

Early Studies

Using the Rayleigh-Ritz method, Salvadori (1955) developed the lateral torsional buckling solution of simply supported and continuous I-beams subject to a combination of axial and unequal end moments. Based on the finite difference technique, Poley (1956) solved the governing buckling differential equations for cantilever beams under uniformly distributed load. Using a successive-approximation technique for solving differential equations, Austin et al. (1957) developed the critical lateral torsional buckling solutions for beams with full torsional end restraints and partial rotational end restraints about the weak axis subjected to uniformly distributed loads and mid-span point loads. Load heights relative to the section centroid were also considered in their solution. Powel and Klingner (1970) developed a thin-walled beam finite element to obtain the lateral torsional buckling capacity of simply supported and continuous beams subject to arbitrary loading. Their solution was applicable to variable and mono-symmetric cross-sections. Load position effects and the presence of lateral and torsional restraints were incorporated into the solution.

Kitipornchai and Richter (1978)

The study of Kitipornchai and Richter (1978) investigated the elastic lateral buckling of simply supported beams with doubly symmetric I-sections and rigid discrete intermediate translational and rotational restraints. The finite integral method was used in the solution. Three types of loads were investigated in the solution; concentrated loads, end moments and uniformly distributed loads. The effects of location of discrete braces along the span, level at which the restraint is attached, load height, beam parameter and type of restraint on the buckling resistance of these beams were investigated. They conducted experiments on the beams under concentrated loads. They concluded that the buckling strength was considerably influenced by the beam parameter.

For beams under uniformly distributed loads, the best location for a single restraint was the mid-span but for the beams with a single translational or rotational restraint, the effective location would be a point above the shear center. Tested beams were made of extruded high-strength aluminum. The loaded points were designed such that they could restrain rigidly against lateral displacement and rotation of the cross-section but they were free to move vertically, longitudinally and rotate about their minor axis. Results showed that there existed a good agreement between both experimental and theoretical results.

Wang et al. (1995)

The study of Wang et al. (1995) proposed a numerical solution based on Rayleigh-Ritz method for buckling analysis to determine the optimal locations for rigid restraints and internal supports in order to maximize the elastic lateral torsional capacity of doubly symmetric I-beams. They also conducted a sensitivity analysis for buckling solutions to examine the effect of restraints and internal roller supports under various loading and bracing conditions and quantified the optimal locations of restraints. Selected beams were braced with three types of rigid restraints including lateral, rotational and full restraints attached to the centroidal axis and had various end conditions such as free, simply supported and fixed end under an arbitrary load distribution. The effects of residual stresses and initial imperfection were neglected. Three special cases were considered for more investigations: singly braced cantilevers under uniformly distributed load, cantilevers with two restraints under a point load at tip and uniformly loaded propped cantilevers. Loads were applied at the top flange, shear center and bottom flange of the beams.

For the first case, it was seen that solutions were affected by the load position, restraint type and beam parameter. Rotational restraints were as effective as full (rotational and lateral) restraints and hence lateral restraints were effective only were loads were applied to the bottom flange. It was observed that buckling loads were sensitive to restraint location especially in the neighbor of optimal restraint location. It was also found that the optimal restraint location was independent of load position and beam parameter. Unlike the first case, the optimal restraint location of the second case was dependent to the restraint type, load position and beam parameter. It could be seen in the third case that the buckling capacity was considerably enhanced by applying internal roller support at its optimal location.

Lim et al. (2003)

Using two independent methods; the Bubnov-Galerkin method and the finite element analysis, Lim et al. (2003) evaluated the effects of moment gradient and end warping, lateral, and torsional restraints on lateral torsional buckling capacity of beams. They also proposed equations to evaluate moment gradient correction factors which incorporate end restraint conditions of the beam which are applicable for both doubly symmetric and mono-symmetric cross-sections and compared their results with those of obtained from design standards formulae.

Park et al. (2004)

Park et al. (2004) reviewed existing expressions (2010) and their applicability to cases involving lateral restraints at both ends and along the top flange by comparing predictions based on existing expressions with finite element results. They proposed a new equation for lateral torsional buckling of beams laterally restrained along the top flange and end supports subject to concentrated load at top flange and end moments.

Larue et al. (2007)

Larue et al. (2007) developed an approximate method for determining the flexural-torsional buckling moment of doubly symmetric steel beams with rigid continuous lateral restraint applied to the tension flange. The beams were restrained at their end by fork supports with the same boundary conditions as those for simply supported beams. The effect of moment distribution on the mode of failure was also studied and design procedures were proposed. They developed the software MGv3 to solve differential equations resulting from the second order solution, which is based on trigonometric functions to approximate the rotations to obtain critical moments from an eigenvalue analysis. Results were compared to those obtained from the finite element-based program LTBEAM (2003). To derive buckling moments, it was assumed the beams are elastically braced against the lateral displacement at one of the flanges. Results obtained agreed well with those obtained from finite element approach. In contrast to results of previous studies, it was concluded that restraining the tension flange had only a small influence on the buckling moment capacity of beams and it was found that sometimes it was inadequate to stabilizing the beam with respect to buckling.

Khelil and Larue (2008)

Using the Galerkin method, Khelil and Larue (2008) investigated the same class of problems as in (2007) with similar conclusions.

Trahair (2008)

Using a finite element program, FTBER, an extension of the commercial finite element program, PRFELB (1997, 1998), Trahair (2008) developed a design approach for obtaining lateral buckling resistance of monorail beams, cantilevers and overhangs loaded at the bottom flange and laterally and transversely supported at the top flange.

Erkmen and Mohareb (2008a, b)

A common feature among the above studies is that they focused on doubly symmetric cross-sections. Other shear deformable theories were also developed. This includes the work of Erkmen and Mohareb (2008a) who developed a complementary energy variational principle and formulated a finite element (2008b) for doubly symmetric sections.

Wu and Mohareb (2011a, b)

Wu and Mohareb developed a shear deformable theory (2011a) and finite element formulation (2011b) for the lateral-torsional buckling of members with doubly-symmetric cross-sections. The element developed was based on linear interpolation of the displacement fields and was based on non-orthogonal coordinate systems. Slow convergence was observed due to shear locking. As a result, a very fine mesh was needed to achieve convergence.

Summary

Table 2.1 presents a comparative summary of the lateral torsional buckling of doubly symmetric beams. As can be observed, only two studies have incorporated shear deformation effects. Although three of these investigations were carried out on beams with lateral or rotational intermediate discrete rigid restraints, none of the three studies examined the effect of eccentric rigid lateral restraint along the web height on lateral torsional buckling capacity of doubly symmetric beam. Within this context, the present study aims to partially fill this gap by introducing a family of computationally efficient shear deformable finite elements with desirable convergence characteristics (Chapter 3) that are equipped with multi-point constraint features which enables, among other things, the modelling of lateral braces offset from the shear center.

Table 2.1 A comparative study on lateral torsional buckling of doubly symmetric I-beams

Author(s)	Boundary Condition Types		Loading Types					Assumptions			Rigid Discrete Restraints		Soloutions Developed
	Simply Supported	Cantilever	Concentrated Transverse Load(s)	Uniformly Distributed Load	Uniform Bending Moment	Linear Moment	Axial load	Distortional effects	Shear Deformations	Pre-buckling Deformations	Translational	Rotational	
Barsoum and Gallagher (1970)	✓	✓	✓	✓	✓	✓	✓						FEA
Powel and Klingner (1970)	✓	✓	✓	✓	✓	✓	✓				✓	✓	FEA
Kitipornchai and Richter (1978)	✓		✓	✓	✓	✓					✓	✓	Finite Integral Method
Wang et al. (1995)	✓	✓	✓	✓							✓	✓	Reyleigh-Ritz Method
Erkmen and Mohareb (2008)	✓	✓	✓	✓	✓	✓	✓		✓				FEA
Wu and Mohareb (2011)	✓	✓	✓	✓	✓	✓	✓		✓				FEA
Present Study	✓	✓	✓	✓	✓	✓	✓		✓		✓	✓	**FEA**

2.4.2 Beams with mono-symmetric cross-sections

Anderson and Trahair (1972)

Using finite integral method, Anderson and Trahair (1972) presented tabulated values of critical loads for mono-symmetric I-beam cantilevers and simply supported beams. Uniformly distributed and concentrated point loading were applied at different heights of various cross-sections examined. They ignored major axis curvature and solved the governing deferential equations numerically. Several experimental tests were carried out to verify the numerical results. Four high-strength aluminum I-section cantilevers with bottom and top larger flange were subjected to concentrated point load applied at different heights. Close agreement was reached. The authors examined the combined effect of beam mono-symmetry and position of load relative to the shear center on the lateral torsional buckling resistance. They concluded that, for simply supported beams, these two effects are additive i.e., when top flange is larger, the elastic buckling load is always greater while for cantilevers these effects are contrary due to Wagner effect.

Robert and Burt (1985)

Robert and Burt (1985) investigated the lateral torsional buckling capacity of mono-symmetric I-beams based on the stationarity of the total potential energy. Simply supported beams and cantilevers were investigated based on three types of loading including uniform moments, uniformly distributed and concentrated loads. For simply supported beams, closed-form solutions containing pre-buckling displacements were derived. For cantilever beams, solutions were developed based on trigonometric approximations of the buckling displacements. Results were in agreement with those presented in Anderson and Trahair (1972). They proposed an approximation method in order to incorporate the effect of pre-buckling displacements in numerical solutions.

Kitipornchai et al. (1986)

Based on the finite integral method and the Rayleigh-Ritz energy-based approach, Kitipornchai et al. (1986) investigated the elastic lateral torsional buckling resistance of mono-symmetric simply supported I-beams subject to moment gradients. Solutions were expressed in terms of the beam parameter, the degree of beam mono-symmetry and the end moment ratio. The authored showed that for mono-symmetric beams with nearly equal flanges, the conventional moment gradient factor accurately predicted the buckling capacity while for beams with high mono-symmetry, the conventional moment gradient equation leads to un-conservative results. To compensate for this deficiency, they proposed an approximate expression for buckling moments within ten percent of the solution. Their solution is not applicable for tee sections.

Wang and Kitipornchai (1986)

Wang and Kitipornchai (1986) investigated the lateral torsional capacity of simply supported mono-symmetric I-beams under transverse loads. Loading conditions included point load, symmetrical two-point loads, and uniformly distributed loads. They adopted the Rayleigh-Ritz method for their solution and presented the results in terms of beam mono-symmetry parameter and the beam parameter. Half-sine Fourier series were used to approximate the displacements. They showed that the moment modification factor used for doubly symmetric sections predicts buckling loads for mono-symmetric beams to lead to errors either on the conservative or un-conservative sides. Thus, they proposed new moment gradient factor equations specifically tailored for mono-symmetric sections, which is highly dependent on the beam mono-symmetry parameter, load height ratio and the beam parameter. Finally, for a given beam parameter (defined as the ratio of the warping to Saint Venant stiffness), they derived an expression for determining the mono-symmetry parameter which maximizes the beam lateral buckling strength.

Wang and Kitipornchai (1986)

Wang and Kitipornchai (1986) investigated the elastic lateral torsional capacity of mono-symmetric cantilevers under various load conditions including concentrated transverse load, concentrated end moment and uniformly distributed load. Using the finite integral method and the Rayleigh-Ritz energy-based approach, buckling estimates were derived and expressed in terms of meaningful mono-symmetric parameters. Load height effects were considered within the study. They validated their solutions with those based on Anderson and Trahair (1972) and their experiments. Finally, they proposed an approximate equation for predicting the lateral torsional buckling capacity of mono-symmetric cantilevers under uniform bending moments. Results obtained from this approximation were in close agreement with energy-based solutions.

Attard (1990)

Attard (1990) derived an approximate non-dimensional equation for estimating the elastic lateral-torsional capacity of mono-symmetric cross-sections with general boundary conditions and subject to general loading. The author incorporated the effect of initial pre-buckling bending curvature in his study. Using the second variation of total potential energy, and limiting the derivation to sections with small torsional to flexural rigidity, he tabulated values for buckling coefficients to estimate the elastic lateral torsional buckling capacity of mono-symmetric sections. He concluded that cross-sections where the flexural rigidity of the weak axis is equal or greater than the flexural rigidity of the strong axis, are prone to buckling phenomena provided that the transverse loads are offset the shear center in such a way that it induces a destabilizing effect into the beam.

Mohri et al. (2003)

Mohri et al. (2003) developed an analytical model for estimating the lateral torsional buckling resistance of mono-symmetric simply supported I-beams. Using the Ritz and Galerkin's methods and based of Vlasov's assumptions (1961), the buckling capacity was compared to that of obtained from Eurocode 3 (2005). The authors investigated the transverse loading including uniformly distributed load, symmetrical two-point load configurations, and load height effect. They showed that lateral buckling coefficients adopted for mono-symmetric sections in Eurocode 3 (2005) are in agreement with the ones developed in their study. To verify their analytical solutions, a numerical simulation was performed. Using ABAQUS, several buckling analyses were conducted based on the shell S8R5 element. It was shown that the proposed analytical solutions agreed with results obtained from FEA and the regular code solutions overestimated the lateral torsional buckling resistance of mono-symmetric I-sections.

Andrade et al. (2007)

Andrade et al. (2007) extended application of the equation provided in Eurocode 3 (Section 2.2.1.4) for estimating lateral torsional buckling resistance of mono-symmetric I-beams, to cantilevers subject to transverse uniformly distributed and concentrated tip loads acting at various section heights. A theoretical study based on elastic lateral torsional buckling was carried out by presenting the buckling problem in a non-dimensional form. The effect of warping restraint at fixed-ends was considered throughout the investigation. Pre-buckling deformations were neglected and analyses were conducted under the small strain Vlasov hypotheses (1961). The authors performed a parametric study and presented numerical results based on Rayleigh-Ritz method. Close agreement was obtained with the results from Wang and Kitipornchai (1986) for cases of restrained warping and free warping at both ends. Approximate equations were developed for calculating three coefficients $\left(C_1 - C_3\right)$ involved in estimating lateral torsional buckling capacity of mono-symmetric beams.

Erkmen and Mohareb (2008)

Using the principle of stationary of complementary energy, Erkmen and Mohareb (2008a, 2008b) developed a shear deformable element to determine the LTB capacity of open thin-walled members. The solution is applicable both for mono-symmetric and doubly symmetric cross-sections. In some of the problems investigated, discretization errors provided lower bound predictions for the critical loads.

Zhang and Tong (2008)

Zhang and Tong (2008) proposed a new solution for estimating lateral torsional buckling analysis of mono-symmetric cantilevers based on energy method. I-beams were subject to uniform bending moment and two typical transverse loads including free-end point load and uniformly distributed load. Results were compared with two other energy-based theories including traditional solutions by Wang and Kitipornchai (1986) and those of obtained from Lu's theory reported in Tong and Zhang (2003a, 2003b, 2003c, 2004). Differences with previous formulations were attributed to using linear versus nonlinear distributions of shear and linear versus nonlinear normal strain energy terms involved in the total potential energy equation. They also compared their results with those of obtained from experimental test adopted from Anderson and Trahair (1972), Attard and Bradford (1990) and shell FEA. It was demonstrated that their results agreed well with solutions obtained from Lu's theory reported in Tong and Zhang (2003a, 2003b, 2003c, 2004) for cantilevers under pure bending. Finally, they proposed approximate expressions to capture the load height effect for estimating lateral torsional buckling capacity of cantilevers with doubly symmetric sections subject to free-end point load and uniformly distributed loads.

Erkmen et al. (2009)

Erkmen et al. (2009) investigated the torsional buckling of columns with shear deformable elements developed based on a complementary energy variational principle. The study provided the conditions under which the formulation would be guaranteed to converge from below.

Mohri et al. (2010)

Mohri et al. (2010) developed linear and nonlinear models to investigate into the lateral- torsional buckling capacity of simply supported mono-symmetric I-beams under moment gradient. Pre-buckling deformations were considered throughout the study. Results based on a 3D finite element model, which captured warping and large angles of twist, were compared to those obtained from a numerical simulation using the large torsion element B3Dw presented in the FE package developed by Mohri et al. (2008). The effect of pre-buckling deflections was found to be tangible in the lateral buckling resistance of mono-symmetric beams. For mono-symmetric sections, the study shows that under moment gradient, the effect of pre-buckling deformation is more pronounced when the larger flange is under compression.

Attard and Kim (2010)

Based on a hyper-elastic constitutive model, Attard and Kim (2010) formulated a lateral torsional buckling solution and equilibrium equations of simply supported shear deformable beams with mono-symmetric cross-sections. They adopted large rotations and finite shear rotations. Warping deformation was taken normal to the plane of cross-section in the displaced configuration. The solution was based on second order approximations for the displacements, curvatures, twists and internal forces, which lead to new coupling terms between bending moments, twisting moments and bi-moments. A closed-form solution was developed for the lateral torsional buckling of mono-symmetric simply supported beams under uniform moments. The flexural-torsional buckling of axially loaded columns was also examined. It was shown that the solution is consistent with that of obtained from traditional Haringx's column buckling formula (1942) in which shear deformations were included. Solutions were provided for beams under transverse mid-point loads and uniformly distributed load. The effect of shear deformation was found to be more pronounced in short-span beams and those with flexible shear rigidity.

Camotim et al. (2012)

Using the LTBEAM (2003) and GBTUL (2008) codes developed for LTB and vibration analysis of thin-walled members under generalized beam theory, Camotim et al. (2012) modeled fork-type end supports under uniform moments, mid-span point load, symmetrical two-point load, distributed load and unequal end moments and provided various numerical results. They observed that, for mono-symmetric sections among all loading conditions including end moments and transverse loads applied at shear center, the lowest critical buckling moment did not necessarily correspond to uniform bending moments. They also investigated the moment gradient effect on the LTB resistance.

Mohri et al. (2013)

Mohri et al. (2003) developed a non-linear model to investigate the effect of axial forces on the lateral torsional buckling resistance of mono-symmetric simply supported members. Members were investigated under distributed and concentrated transverse loads along with axial forces. A closed-form solution for the interaction effect was developed by applying Galerkin's method. The solution captures the effect of pre-buckling deformation, load height effect, Wagner's coefficient, and interaction between flexural buckling and lateral torsional buckling. The formulation is based on large angles of twist but small deformations. The model was validated thorough numerical comparisons using the beam element b3Dw which captures warping and large displacements. Analytical solutions were compared with those obtained from linear and non-linear FEA. The closed-form solution was shown to be in close agreement to FEM simulations. They concluded that classical linear solutions underestimated the resistance of beam-columns especially for H-sections. Stability of I-beams was investigated by applying downward and upward transverse loads. They showed that for downward acting loads, the axial-bending interaction curve was more non-linear and complex compared to that based on upward-acting loads.

Erkmen (2014)

Using the Hellinger-Reissner principle, Erkmen (2014) developed a hybrid finite element formulation for shear deformable elements. Load position effects were incorporated in his solutions. The solution was applied to simply supported and cantilever beams with doubly symmetric and mono-symmetric cross-sections subjected to concentrated point load, uniform and linear bending moments. He compared results based on his study with those obtained from complementary energy in Erkmen and Mohareb (2008b) and those based on shell element solutions.

Summary

A comparative summary of the most relevant studies is shown in Table 2.2 As seen, all of the aforementioned studies, excluding the work Erkmen and Mohareb (2008a, 2008b), Attard and Kim (2010) and Erkmen (2014), neglect shear deformation due to bending and warping. Within this context, shear deformable elements with desirable convergence characteristics will be developed in Chapter 4.

Table 2.2 A comparative study on lateral torsional buckling of mono-symmetric I-beams by Sahraei et al. (2015)

Author(s)	Boundary Condition Types		Loading Types					Assumptions			Solutions Developed			Analysis Type
	Simply Supported	Cantilever	Concentrated Transverse Load(s)	Uniformly Distributed Load	Uniform Bending Moment	Linear Moment	Axial load	Distortional effects	Shear Deformations	Pre-buckling Deformations	Closed-form	FEA	Other Numerical Methods	
Anderson and Trahair (1972)	✓	✓	✓	✓									Finite Integral	
Bradford (1985)	✓	✓	✓	✓	✓	✓	✓	✓				✓		
Roberts and Burt (1985)	✓	✓	✓	✓						✓	✓		Stationarity of the Total Potential Energy	
Kitipornchai et al. (1986)	✓				✓	✓							Rayleigh-Ritz	
Wang and Kitipornchai (1986)	✓		✓	✓									Rayleigh-Ritz	
Wang and Kitipornchai (1986)		✓	✓	✓									Rayleigh-Ritz	
Attard (1990)	✓	✓	✓	✓	✓	✓				✓			Stationarity of the Total Potential Energy	
Helwig et al. (1997)	✓		✓	✓										Shell FEA
Mohri et al. (2003)	✓		✓	✓									Ritz and Galerkin	
Andrade et al. (2007)		✓	✓	✓									Rayleigh-Ritz	
Zhang and Tong (2008)		✓	✓	✓	✓								Stationarity of the Total Potential Energy	
Erkmen and Mohareb (2008)	✓	✓	✓	✓	✓	✓	✓		✓			✓	Stationarity of the Complementary Energy	
Mohri et al. (2010)	✓	✓	✓	✓	✓	✓	✓			✓		✓		Beam 3D FEA
Attard and Kim (2010)	✓				✓				✓		✓			Hyperelastic
Camotim et al. (2012)	✓		✓	✓	✓	✓							Stationarity of the Total Potential Energy	LTBEAM Shell FEA GBT
Mohri et al. (2013)	✓		✓	✓			✓			✓	✓		Galerkin	Beam 3D FEA
Erkmen (2014)	✓	✓	✓	✓	✓	✓	✓		✓			✓	Hellinger-Reissner	
Present Study	✓	✓	✓	✓	✓	✓	✓		✓		✓	✓	**Stationarity of the Total Potential Energy**	

2.4.3 Effect of intermediate restraints on lateral torsional buckling capacity of beams

One of the motivations for the implementation of the kinematic constraint feature is to provide means of modelling full restraints within a member span. Also, a key motivation for developing the coupled spring feature is to provide means to model partial restraints either within member spans, or at the ends. Thus, the present section aims at covering relevant studies which aim at investigating the effect of elastic restraints on lateral torsional buckling capacity of beams.

Flint (1951)

Flint (1951) was one of the first investigators to present solutions for the buckling resistance of beams that are restrained either with central elastic lateral or torsional restraints. In the derivation, the author neglected the effect of warping. Using the principle of minimum total potential energy method, expressions were developed which relate the support stiffness to the ratio of critical load for braced beams to that of unbraced beam. The author considered simply supported beams with rectangular cross-sections that are laterally restrained at mid-span and subject to mid-span loading acting through the shear center. Also considered was the case of torsional restraint at mid-span under a uniform bending moment. The author showed that the stability of the beams considerably increases with the presence of end fixity and torsional stiffness at supports, and lateral and torsional restraints within the span.

Schmidt (1965)

Schmidt (1965) examined the effect of interaction between elastic end torsional restraints and elastic central lateral restraint on the buckling load of simply supported beams. In the study, the central restraint was taken at the same level as the central point load and considered various load heights above the shear center. The study used the elastic center line of the beam to derive approximations by using the Timoshenko's theory (1936). Using Bessel functions, expressions where derived for the critical load and presented a conservative estimate for the maximum load capacity of beams with the aforementioned restraints.

Taylor and Ojalvo (1966)

Taylor and Ojalvo (1966) extended Flint's study (1951) on torsional restraints while considering the effect of warping on buckling moments of simply supported I-beams. In their investigations, closely spaced beams were considered to provide continuous torsional restraints. The study also considered pointwise elastic torsional restraints at mid-span. Three types of loadings were investigated; uniform moments, central concentrated load and uniformly distributed loads. Starting with the differential equations of buckling developed by Vlasov (1961) and using the numerical method presented originally by Young (1945) and generalized later on by Hoblit (1951) to solve the resulted boundary value problem, they obtained the buckling loads for the problems investigated. Torsional restraints were shown to be effective in increasing the critical buckling moments. For beams with continuous torsional restrained, this increase was observed to be tangible and unbounded as the stiffness increases.

Hartman (1967)

Hartman (1967) adopted a numeric technique which integrates simultaneous differential equations while satisfying equilibrium and continuity at interior joints. The study evaluated the effect and partial lateral, torsional, and weak axis rotation constraints on the lateral torsional buckling capacity of beams subjected to point loads with interior supports. The study focused on simply supported beams, and continuous two-span and three-span beams.

Nethercot and Rockey (1971)

Nethercot and Rockey (1971) investigated the lateral stability of beams. The study focused on beams with lateral, torsional or both lateral and torsional restraints within the beam span. The authors derived relations between the buckling load and the non-dimensional lateral and torsional stiffness parameters. Using an approximate two dimensional beam finite element, they also provided charts to quantify theoretical limiting values for the elastic restraint stiffness which allow the member to attain the critical moment based on full restraint conditions. Solutions were obtained for simply supported beams subjected to a uniform moment. Lateral and torsional restraints were modeled using elastic translational and rotational springs, respectively acting at the shear center. The study investigated the effect of the location of a single support on the ratio of buckling load of a braced beam to that of an unbraced beam as a function of the non-dimensional support stiffness. The influence of lateral, torsional and combined restraints on the stability of the beams was investigated. It was observed that the largest critical moment capacity is obtained for the case of combined restraints. Combined restraints were also observed to be effective in controlling distortional buckling.

Nethercot (1973)

Nethercot (1973b) investigated the effect of load type on the lateral stability of elastically stabilized beams. He used the beam finite element by Barsoum and Gallagher (1970) to obtain critical moments for simply supported symmetrical I-section beams braced laterally or torsionally. Lateral restraints were assumed at mid-span at either the shear center or top flange of the beam while torsional restraints were assumed to be located at the shear center of the mid-span point. Spring arrangements were used to model lateral restraints. The author also investigated the influence of top flange restraints subject to various load configurations and load heights: equal end moments, central load applied at bottom flange, central load applied at shear center, central load applied at top flange, uniform load applied at bottom flange, uniform load applied at shear center, and uniform load applied at top flange.

The influence of warping, which was characterized by the ratio of torsional rigidity to warping rigidity, on critical moments was investigated in the study. When the top flange is laterally restrained at the level of top flange, a noticeable increase in buckling resistance is attained. This beneficial effect was observed to be more tangible for beams subjected to top flange loading compared to shear center loading. The accuracy of the solutions was validated against previous experimental results on cold-formed sections in his earlier investigations (Nethercot (1971)).

Hancock and Trahair (1978)

Hancock and Trahair (1978) extended the finite element formulation developed by Barsoum and Gallagher (1970) to incorporate the effect of continuous elastic and discrete restraints along the element. They generalized their formulations for LTB analysis of mono-symmetric beam-columns subject to moment gradients as well. They have shown the validity of their results based on the LTB analysis of a simply supported beam under uniform moment and continuous elastic restraints provided by diaphragm sheeting, against the closed-form solutions developed by Trahair (1979) and also LTB analysis of mono-symmetric cantilevers under moment gradient against solutions provided by Anderson and Trahair (1972).

Bose (1982)

One of the assumptions made for critical moment expressions of beams in design standards is that beam ends are fully restrained, both laterally and torsionally, at supports but are free to warp and undergo lateral bending rotation. Bose (1982) assessed the validity of the theoretical solutions presented in British standard (1982) by conducting experimental tests designed for this purpose and investigated into the effect of torsional restraint stiffness at supports on the buckling strength of beams and compared the results with the design values extracted from British code. In his tests, at each support, the compression flange was connected to a torsional spring to provide torsional bracing.

Simply supported beams were tested and subjected to a central point load acting at the top flange. The torsional restraint stiffness at supports was varied. In some cases, full twist restraint conditions were found to be practically unattainable. Beams with limited torsional stiffness at the supports were observed to attain a lower buckling resistance than those based on the idealized case where full torsional restraints are provided. As a general observation, good agreement was observed between results based on beams with partial torsional stiffness and code design values for beams with slenderness ratio higher than 250. In contrast, for beams with slenderness ratios less than 130, failure corresponded to a lower load compared to those estimated by code equations.

Roeder and Assadi (1982)

Roeder and Assadi (1982) derived expressions for the lateral torsional buckling capacity of beams with laterally restrained tension flanges and compared their solutions with experimental results. They surveyed various studies and concluded that while design standard provisions were valid for beams with laterally restrained compression flanges in some applications such as continuous beams, the tension flange happens to be restrained.

Cantilever problems under tip load were also investigated. No closed-form solution was available for this case. Thus, a numerical solution was developed based on the finite difference method. A validation of their theoretical predictions was conducted through experimental results. Two simply supported steel and aluminum beams were built and tested twice. First, they were tested with no lateral restraint and the same boundary conditions as the ones used by Timoshenko. Then, they were retested with the tension flange restrained through a metal sheet membrane and the same boundary conditions used for the first test. Both beams were subjected to pure bending moments. The experimental results substantiated the theoretical results. It was concluded that when the warping stiffness is small compared to Saint Venant stiffness, lateral deformations were observed to be small and the buckling capacity of the beam was found to be higher.

Wakabayashi and Nakamura (1983)

Wakabayashi and Nakamura (1983) investigated the effect of bending moment distribution, lateral bracing provide by purlins and sub-beams, and restraining influence of neighboring members on lateral buckling strength and post-lateral buckling behavior of H-section beams. They conducted a large-scale experimental study and simulated the tests conducted by performing finite element analyses. Beams were subjected to moments with various gradients. Twisting and lateral deformations were prevented at supports. In the finite element models, the purlins were modeled by an elastic-perfectly plastic springs while sub-beams were treated as linear elastic springs. The FEA results were found to agree well with experimental results in many cases. The effect of moment distribution was observed to be considerable on the lateral buckling strength. Thus, they recommended adopting a moment gradient moment gradient factor for design. The maximum load carrying capacity was found to increase due to the restraining action of purlins which provided twisting restraint to the beams. The bracing effect of sub-beams and adjacent members were estimated using the proposed effective length factor method.

Kitipornchai et al. (1984)

Kitipornchai et al. (1984) investigated into the elastic buckling resistance of cantilever I-beams having discrete lateral, rotational or both restraints along the beam. The influence of the beam parameter, load height, type of restraint, location of restraints along the beam and the level at which restraints are attached across the cross-section of the beam on the elastic buckling resistance was examined by using finite integral method. Two types of loads including concentrated point load and uniformly distributed load were used throughout the study and several experiments were conducted to validate the theoretical results. Translational and rotational springs were used in order to model the lateral and rotational stiffness respectively. A computer program based on the finite integral method was used to solve the governing differential equations and obtain elastic buckling loads. The authors assessed several cantilevers with discrete partial or full restraints along the beam and different locations across the height of cross-section subjected to concentrated and distributed loads applied at top flange, shear center and bottom flange with various beam parameters. They illustrated their results based on the ratio of buckling load of beams with restraint arrangement to buckling load of unrestrained cantilevers. For beams with small beam parameters, the location of optimum restraint could be obtained at a point near mid-span under a point tip load and near 0.4 of the length from the clamped support under uniformly distributed load. For higher values of beam parameters, this distance for most cases varied between 0.4 and 0.7 of the length from fixed support. To substantiate their theoretical results, several experiments on extruded high-strength aluminum I-beam cantilevers were conducted. These beams were under concentrated tip loads. Restraints attached along the test beams were lateral restraints at top flange, shear center, bottom flange and full restraints. The modified Southwell plot was used to obtain experimental critical loads. Experimental results were in a reasonable agreement with theoretical results and confirmed them. They were lower than theoretical results in general. It was concluded that for cantilevers with a simple lateral restraint, the best place for the restraint was near the top flange level. Nevertheless, if the full restraint could not be obtained, the next best option was rotational restraint while the lateral bracing at the bottom flange was not as effective as the two aforementioned restraints.

Assadi and Roeder (1985)

Assadi and Roeder (1985) derived a theoretical solution for lateral torsional buckling of cantilevers with continuous elastic or rigid restraints. They used the direct variational method to formulate the governing differential equations and natural boundary conditions. The study examined the effect of three parameters: the lateral restraint height, the load height, and the stiffness of lateral elastic restraints. They also conducted an experimental investigation on cantilevers under point loads which are offset from the shear center. Lateral restraints were provided by attaching angles to the tension flange and clamped support conditions were attained by grouting. A comparison was performed between the analytical and experimental results.

Wang et al. (1987)

Using energy-based solutions, Wang et al. (1987) investigated the effect of various types of discrete intermediate restraints, restraint locations, and beam parameters, on the buckling capacity of wide variety of mono-symmetric beams. Results were in good agreement with those experimentally and theoretically obtained by Kitipornchai et al. (1984). Discrete bracings investigated consisted of four types: full bracings including both rigid lateral and rotational restraints, rigid rotational restraint, rigid lateral restraint attached to the beam at a specific distance above the shear center, and elastic restraint. Lateral restraints included top flange, shear center, and bottom flange bracing. Loading conditions included concentrated end moments, concentrated point load applied at the tip, and distributed loading.

Twisting restraint was shown to be more effective than lateral restraint. As such, twist restraint was found adequate in some cases and full bracing was deemed unnecessary. In mono-symmetric cantilevers under concentrated end moments, a twist restraint can be as effective as a full restraint when placed approximately at 70% of the span length from the fixed support. For beams under a point load at tip, full or rotational restraint at mid-span were observed to be optimal. In cantilevers with a larger top flange and subjected to bottom flange loading, lateral restraint at the bottom near the tip was found to be most effective location for bracing.

Wang and Nethercot (1990)

Wang and Nethercot (1990) developed a finite element program for three-dimensional ultimate-strength analysis to assess bracing requirements for laterally unrestrained beams. Their solution is based on a beam element with seven degrees of freedom per node. Purlins and sub-beams were modeled as torsional and rotational braces attached to nodal points. Plasticity and initial imperfection effects were incorporated into the model. The results were verified against the experimental work done by Wakayabashi and Nakamura (1983) and Wong-Chung and Kitipornchai (1987). Beams under mid-span concentrated load applied to the upper flange were investigated. The interaction between restraint stiffness, restraint strength and load carrying capacity was examined for a number of simply supported I-beams with single, three or five equally spaced discrete torsional restraints. A parametric study indicated 1% of the axial force in the flange at failure could be taken that for single bracing, and 2% of the axial force in the flange for multiple-restraint systems.

Yura (2001)

Based on the elastic finite element program BASP developed by Akay et al. (1977) and Choo (1987). Yura (2001) conducted a comprehensive study on bracing requirements for beams. Examined in the study were factors that affect bracing requirement such as loading configuration, load level, location of restraint and cross-sectional distortion. Relative and discrete lateral restraints and discrete torsional restraints were considered. Loading cases investigated involved uniform moments, equal and opposite end moments and central point load applied at either the top flange or the beam centroid.

For flexural members, the study extended the concepts introduced by Winter (1960) regarding strength and stiffness requirements for column bracing. Equations were developed for stiffness and strength requirements for laterally and torsionally restrained simply supported I-beams. Due to web distortion, stiffer lateral restraints were found to be required when no stiffeners are provided. Centroidal lateral restraints were observed to be less effective than top flange lateral restraint. Lateral restraints provided near the top flange of simply supported beams and overhanging spans were observed to be effective in controlling web distortion. The study also investigated the buckling strength of beams with top flange discrete torsional restraints under uniform moments and pointed out that the results are fundamentally different from those based on lateral bracing. The study demonstrated that the presence of stiffeners does not increase the effectiveness of torsional restraints at the tension or compression flanges. Torsional restraints were found not to be as effective as lateral restraints, to top flange loading, restraint location and number of restraints, but were observed to have more influence on cross-sectional distortion.

Nguyen et al (2010)

Nguyen et al. (2010) developed analytical solutions for the lateral torsional buckling strength for I-girders with equidistant discrete torsional restraints and quantified the torsional stiffness requirements for the restraints. Their study focused on simply supported beams against torsion and flexure and subject to linear bending moments. Moments at both ends were applied in the form of two equal and opposite forces at each flange. For the case of uniform moments, they derived a solution using the Rayleigh-Ritz method. Torsional bracings were modeled as torsional springs. By considering the out of plane displacement and twisting angle as sinusoidal functions series, they compared their solutions to those based on the shell solutions in BASP program (Yura and Kim (1993)). I-girder cross-sections were chosen such that the local buckling is avoided according to AISC specifications (2001). In the BASP solution, transverse stiffeners with equal height and width to those of cross-section were provided at torsional bracing points in order to prevent distortion of the web. The study also investigated other cases involving moment gradients and effects of imperfections through a series of finite element models in ABAQUS. They compared their results against previous solutions by Yura (2001) and Trahair (1993) and concluded that the equivalent continuous bracing concept introduced by Yura (2001) and Trahair (1993) underestimated the torsional stiffness requirements in some cases.

Lee et al. (2011)

Lee et al. (2011) provided an analytical solution for lateral torsional buckling strength and torsional stiffness requirements of I-girders subjected to non-uniform moments, concentrated loads, and distributed loads that are discretely braced using torsional restraints. Results were compared against FEA analyses based on BASP program (1987). Cross-sections were selected so as to meet AISC (2001) criteria to prevent local buckling. Beams were stiffened by transverse stiffeners attached at the restrained sections. An equivalent moment gradient factor was also proposed for fully braced I-girder and results were compared to those based on the study by Yura (2001) and FEA. The equivalent continuous brace stiffness method proposed by Yura (2001) was found to considerably underestimate the torsional stiffness requirement compared to FEA results.

Nguyen et al. (2012)

Nguyen et al. (2012) conducted an FEA which captures geometry and material non-linearity, initial imperfections and residual stresses. Transverse stiffeners were modeled as rotational springs. Bending moments were represented as the product of maximum moment at mid-span and a load dependent Fourier series. Beam sizes were selected to fail by flexural lateral buckling prior to local buckling according to Eurocode (2005) specifications.

They extended their previous study on the effect of discrete torsional braces on the lateral torsional buckling resistance of I-girder beams under uniform moments to other loading conditions. They substantiated their solutions against those of Yura (2001), Valentino and Trahair (1998) and finite element analysis based on ABAQUS. The inelastic buckling strength of I-girders with discrete torsional restraints was also examined through non-linear finite element analyses which incorporate the effects of residual stresses and initial imperfection. They formulated a solution for the flexural buckling resistance of I-girders under mid-span point load and uniformly distributed load by extending their previous solutions in Nguyen et al. (2010). They determined the stiffness requirement that provides buckling moment resistance of fully restrained I-girders. Again, they showed that the flexural torsional buckling strength and stiffness requirement of I-girders in Yura (2001) and Valentino and Trahair (1998) give un-conservative results as the number of torsional restraints increases compared to finite element analysis. The study showed that the inelastic stiffness requirement is smaller than that based on elastic analysis.

McCann et al. (2013)

Using the Rayleigh-Ritz method, McCann et al. (2013) derived expressions for lateral torsional buckling capacity of simply supported beams under uniform moments braced with elastic off-center discrete lateral restraints along the beam. Considering both stiffness and strength effects, they also developed a method to optimize design of bracing members locating at even intervals discretely above the shear center.

Hu (2016)

Hu (2016) conducted an analytical and numerical investigation on the lateral trosional buckling analysis of wooden beams with mid-span lateral braces subjected to symmetrically distributed loads. The study considered the cases of rigid and flexible braces. The analytical solutions were developed based on the principle of stationary potential energy using a Fourier expansion of the buckling displacement fields and bending moments. The validity of solutions agreed well with 3D ABAQUS model results based on the C3D8 element.

Summary

A common feature among the studies under Section 2.4.3 is that they individually incorporated the effect of elastic lateral or rotational restraints on lateral torsional buckling of beams but neglected any coupling that may arise between lateral and torsional bracing. Thus, the proposed study attempts to fill this gap by developing a coupled spring formulation capable of incorporating full spring coupling effects. An example of the application of this feature will be illustrated in Chapter 5 to define the warping matrices to connect the ends of beams and adjoined columns.

2.5 REFERENCES

BS 5400: Steel, concrete and composite bridges, (1982). Part 3: Code of practice for the design of steel bridges. London, British Standards Institution.

Standards Association of Australia (SAA), (1998). Steel Structures, AS4100-1998, SAA, Australian Institute of Steel Construction. Sydney, Australia.

Manual of steel construction, load and resistance factor design, AISC, (2001).

CEN, Eurocode 3: Design of Steel Structures, (2005). Part 1-1: General Rules and Rules for Buildings, ENV 1993-1-1, Comité Européen de Normalisation. Brussels, Belgium.

Canadian Standards Association, (CSA), (2014). Limit States Design of Steel Structures, CAN/CSA S16-14. Toronto, Ontario, Canada.

American Institute of Steel Construction, (AISC), (2016). Specification for Structural Steel Buildings, ANSI/AISC 360-16, AISC. Chicago, IL.

Akay, H. U., C. P. Johnson and K. M. Will (1977). "Lateral and Local Buckling of Beams and Frames." Journal of the Structural Division, ASCE, ST9 103(9): 1821-1832.

Anderson, J. M. and N. S. Trahair (1972). "Stability of Monosymmetric Beams and Cantilevers." Journal of the Structural Division, ASCE 98(ST1): 269-286.

Andrade, A., D. Camotim and P. Providência e Costa (2007). "On the evaluation of elastic critical moments in doubly and singly symmetric I-section cantilevers." Journal of Constructional Steel Research 63(7): 894-908.

Assadi, M. and C. Roeder (1985). "Stability of Continuously Restrained Cantilevers." Journal of Engineering Mechanics 111(12): 1440-1456.

Attard, M. M. (1990). "General non-dimensional equation for lateral buckling." Thin-Walled Structures 9(1–4): 417-435.

Attard, M. M. and M. A. Bradford (1990). Bifurcation experiments on mono-symmetric cantilevers. In: 12th Australasian conference on the mechanics of structures and materials: 207–213.

Attard, M. M. and M.-Y. Kim (2010). "Lateral buckling of beams with shear deformations – A hyperelastic formulation." International Journal of Solids and Structures 47(20): 2825-2840.

Austin, W. J., S. Yegian and T. P. Tung (1957). "Lateral Buckling of Elastically End-Restrained I-Beams." Transactions of the American Society of Civil Engineers 122(1): 374–388.

Barsoum, R. S. and R. H. Gallagher (1970). "Finite element analysis of torsional and torsional–flexural stability problems." International Journal for Numerical Methods in Engineering 2(3): 335-352.

Bebiano, R., N. Silvestre and D. Camotim (2008). GBTUL – Code for Buckling and Vibration Analysis of Thin-Walled Members. Technical University of Lisbon, Instituto Superior Tecnico (IST).

Bose, B. (1982). "THE INFLUENCE OF TORSIONAL RESTRAINT STIFFNESS AT SUPPORTS ON THE BUCKLING STRENGTH OF BEAMS." Institution of Engineers (Australia) Civ. Eng. Trans. 60B(4): 69-75.

Camotim, D., A. Andrade and C. Basaglia (2012). "Some thoughts on a surprising result concerning the lateral-torsional buckling of monosymmetric I-section beams." Thin-Walled Structures 60(0): 216-221.

Choo, K. M. (1987). Building Program BASP for Use on a Micro Computer MS, University of Texas at Austin.

Erkmen, R. E. (2014). "Shear deformable hybrid finite-element formulation for buckling analysis of thin-walled members." Finite Elements in Analysis and Design 82(0): 32-45.

Erkmen, R. E. and M. Mohareb (2008a). "Buckling analysis of thin-walled open members—A complementary energy variational principle." Thin-Walled Structures 46(6): 602-617.

Erkmen, R. E. and M. Mohareb (2008b). "Buckling analysis of thin-walled open members—A finite element formulation." Thin-Walled Structures 46(6): 618-636.

Erkmen, R. E., M. Mohareb and M. Bradford (2009). "Complementary Energy Based Formulation for Torsional Buckling of Columns." Journal of Engineering Mechanics 135(12): 1420-1426.

Flint, A. R. (1951). "The influence of restraint on the stability of beams." The Structural Engineer 29(9): 235-246.

Galea, Y. (2003). Moment critique de deversement elastique de poutre flechies— Presentation du logiciel LTBEAM, Revue Construction Metallique, CTICM.

Hancock, G. J. and N. S. Trahair (1978). "FINITE ELEMENT ANALYSIS OF THE LATERAL BUCKLING OF CONTINUOUSLY RESTRAINED BEAM-COLUMNS." Institution of Engineers (Australia) Civ. Eng. Trans. CE2(2): 120-127.

Haringx, J. A. (1942). On the buckling and lateral rigidity of helical springs, Proceedings of the Koninklijke Nederlandse Akademie van Wetenschappen 45:533.

Hartmann, A. J. (1967). "Elastic Lateral Buckling of Continuous Beams." Journal of the Structural Division 93(4): 11-26.

Hoblit, F. M. (1951). "Buckling Load of a Stepped Column." Journal of the Aeronautical Sciences 18(2): 124-126.

Hu, Y. (2016). Lateral Torsional Buckling of Wooden Beams with Mid-span Lateral Bracing. in partial fulfillment of the requirements for the degree of Master of Applied Science in Civil Engineering, University of Ottawa.

Khelil, A. and B. Larue (2008). "Simple solutions for the flexural-torsional buckling of laterally restrained I-beams." Engineering Structures 30(10): 2923-2934.

Kitipornchai, S., P. Dux and N. Richter (1984). "Buckling and Bracing of Cantilevers." Journal of Structural Engineering 110(9): 2250-2262.

Kitipornchai, S. and N. J. Richter (1978). "Elastic lateral buckling of I-beams with discrete intermediate restraints." Civil Engineering Transactions, Institution of Engineers, Australia CE20(No. 2): 105-111.

Kitipornchai, S., C. Wang and N. Trahair (1986). "Buckling of Monosymmetric I-Beams under Moment Gradient." Journal of Structural Engineering 112(4): 781-799.

Larue, B., A. Khelil and M. Gueury (2007). "Elastic flexural–torsional buckling of steel beams with rigid and continuous lateral restraints." Journal of Constructional Steel Research 63(5): 692-708.

Lee, H. E., C. T. Nguyen, J. H. Moon and H. S. Joo (2011). "Lateral-torsional buckling of discretely-braced i-girder." Procedia Engineering 14(0): 264-271.

Lim, N.-H., N.-H. Park, Y.-J. Kang and I.-H. Sung (2003). "Elastic buckling of I-beams under linear moment gradient." International Journal of Solids and Structures 40(21): 5635-5647.

McCann, F., L. Gardner and M. A. Wadee (2013). "Design of steel beams with discrete lateral restraints." Journal of Constructional Steel Research 80(0): 82-90.

Mohri, F., A. Brouki and J. C. Roth (2003). "Theoretical and numerical stability analyses of unrestrained, mono-symmetric thin-walled beams." Journal of Constructional Steel Research 59(1): 63-90.

Mohri, F., N. Damil and M. P. Ferry (2008). "Large torsion finite element model for thin-walled beams." Computers & Structures 86(7–8): 671-683.

Mohri, F., N. Damil and M. Potier-Ferry (2010). "Linear and non-linear stability analyses of thin-walled beams with monosymmetric I sections." Thin-Walled Structures 48(4–5): 299-315.

Nethercot, D. A. (1971). The lateral stability of beams supported by corrugated sheeting Doctor of Philosophy, Cardiff University.

Nethercot, D. A. (1973b). "buckling of laterally or torsionally restrained beams." Journal of the Engineering Mechanics Division ASCE, 99(No. EM4): 773-791.

Nethercot, D. A. and K. C. Rockey (1971). "Finite element solutions for the buckling of columns and beams." International Journal of Mechanical Sciences 13(11): 945-949.

Nguyen, C. T., H.-S. Joo, J. Moon and H.-E. Lee (2012). "Flexural-torsional buckling strength of I-girders with discrete torsional braces under various loading conditions." Engineering Structures 36(0): 337-350.

Nguyen, C. T., J. Moon, V. N. Le and H.-E. Lee (2010). "Lateral–torsional buckling of I-girders with discrete torsional bracings." Journal of Constructional Steel Research 66(2): 170-177.

Papangelis, J. P., N. S. Trahair and G. J. Hancock (1997). PRFELB, Finite element flexural-torsional buckling analysis of plane frames. University of Sydney, Centre for Advanced Structural Engineering.

Papangelis, J. P., N. S. Trahair and G. J. Hancock (1998). "Elastic flexural–torsional buckling of structures by computer." Computers & Structures 68(1–3): 125-137.

Park, J. S., J. M. Stallings and Y. J. Kang (2004). "Lateral–torsional buckling of prismatic beams with continuous top-flange bracing." Journal of Constructional Steel Research 60(2): 147-160.

Poley, S. (1956). "Lateral Buckling of Cantilevered I-Beams Under Uniform Load." Transactions of the American Society of Civil Engineers 121(1): 786–790.

Powell, G. and R. Klingner (1970). "Elastic Lateral Buckling of Steel Beams." Journal of the Structural Division 96(9): 1919-1932.

Roberts, T. M. and C. A. Burt (1985). "Instability of monosymmetric I-beams and cantilevers." International Journal of Mechanical Sciences 27(5): 313-324.

Roeder, C. and M. Assadi (1982). "Lateral Stability of I-Beams with Partial Support." Journal of the Structural Division 108(ST8): 1768-1780.

Sahraei, A., L. Wu and M. Mohareb (2015). "Finite element formulation for lateral torsional buckling analysis of shear deformable mono-symmetric thin-walled members." Thin-Walled Structures 89(0): 212-226.

Salvadori, M. G. (1955). "Lateral Buckling of I-Beams." Transactions of the American Society of Civil Engineers 120(1): 1165-1177.

Schmidt, L. C. (1965). "RESTRAINTS AGAINST ELASTIC LATERAL BUCKLING." Journal of Engineering Mechanics 91(No. EM6): 1-10.

Taylor, A. C. and M. Ojalvo (1966). "Torsional Restraint of Lateral Buckling." Journal of the Structural Division 92(2): 115-130.

Timoshenko, S. (1936). Theory of Elastic Stability, Mcgraw Hill Co., NY.

Tong, G. and L. Zhang (2003a). "An Analysis of Current Stability Theories for Thin-walled Members." Advances in Structural Engineering 6(4): 283-292.

Tong, G. and L. Zhang (2003b). "A General Theory for the Flexural-Torsional Buckling of Thin-Walled Members I: Energy Method." Advances in Structural Engineering 6(4): 293-298.

Tong, G. and L. Zhang (2003c). "A General Theory for Flexural-Torsional Buckling of Thin-Walled Members II: Fictitious Load Method." Advances in Structural Engineering 6(4): 299-308.

Trahair, N. S. (1979). "Elastic lateral-buckling of continuously beam-columns." The Profession of a Civil Engineer, University Press, Sydney: 61-73.

Trahair, N. S. (1993). Flexural-Torsional Buckling of Structures, CRC Press. USA.

Trahair, N. S. (2008). "Lateral buckling of monorail beams." Engineering Structures 30(11): 3213-3218.

Valentino, J. and N. Trahair (1998). "Torsional Restraint against Elastic Lateral Buckling." Journal of Structural Engineering 124(10): 1217-1225.

Vlasov, V. Z. (1961). Thin-walled elastic beams, 2nd Edition, Israel Program for Scientific Translation. Jerusalem.

Wakabayashi, M. and T. Nakamura (1983). "Buckling of laterally braced beams." Engineering Structures 5(2): 108-118.

Wang, C. and S. Kitipornchai (1986). "Buckling Capacities of Monosymmetric I-Beams." Journal of Structural Engineering 112(11): 2373-2391.

Wang, C. M., K. K. Ang and L. Wang (1995). "Optimization of bracing and internal support locations for beams against lateral buckling." Structural optimization 9(1): 12-17.

Wang, C. M. and S. Kitipornchai (1986). "On stability of monosymmetric cantilevers." Engineering Structures 8(3): 169-180.

Wang, C. M., S. Kitipornchai and V. Thevendran (1987). "Buckling of braced monosymmetric cantilevers." International Journal of Mechanical Sciences 29(5): 321-337.

Wang, Y. C. and D. A. Nethercot (1990). "Bracing requirements for laterally unrestrained beams." Journal of Constructional Steel Research 17(4): 305-315.

Winter, G. (1960). "Lateral Bracing Of Columns And Beams." Transactions of the American Society of Civil Engineers 125(1): 807-826.

Wong-Chung, A. D. and S. Kitipornchai (1987). "Partially braced inelastic beam buckling experiments." Journal of Constructional Steel Research 7(3): 189-211.

Young, D. H. (1945). "Inelastic Buckling of Variable-Section Columns." ASME Trans. 12(3): 165-169.

Yura, J. (2001). "Fundamentals of beam bracing." Engineering Journal, AISC (First Quarter): 11-26.

Yura, J. A. and J. H. Kim (1993). Buckling analysis of stiffened plates (BASP).

Zhang, L. and G. Tong (2004). "Flexural–torsional buckling of thin-walled beam members based on shell buckling theory." Thin-Walled Structures 42(12): 1665-1687.

Zhang, L. and G. S. Tong (2008). "Elastic flexural-torsional buckling of thin-walled cantilevers." Thin-Walled Structures 46(1): 27-37.

Ziemian, R. D. (2010). Guide to stability design criteria for metal structures. New York, John Wiley & Sons.

Chapter 3 Upper and lower bound solutions for lateral-torsional buckling of doubly symmetric members

Abstract

A family of three finite elements is developed for the lateral-torsional buckling analysis of thin-walled members with doubly symmetric cross-sections. The elements are based on a recently derived variational principle which incorporates shear deformation effects in conjunction with a special interpolation scheme ensuring C1 continuity. One of the elements is developed such that it consistently converges from above while another element is intended to consistently converge from below. The third element exhibits fast convergence characteristics compared to other shear deformable elements but cannot be guaranteed to provide either an upper or a lower bound solution. The formulation can incorporate any set of linear multi-point kinematic constraints. The validity of the solution is established through comparisons with other well-established numerical solutions. The elements are then used to solve practical problems involving simply supported beams, cantilevers and continuous beams under a variety of loading conditions including concentrated loads, linear bending moments and uniformly distributed loads. The effect of lateral and torsional restraints and the location of lateral restraint along the section height on lateral-torsional buckling capacity of beams are also examined through examples.

Keywords: Upper and lower bounds, computational efficiency, finite element, lateral-torsional buckling, lateral and torsional restraints, doubly-symmetric sections, thin-walled members.

3.1 Motivation

In a recent study, Wu and Mohareb (2011a, 2011b) developed a shear deformable theory and finite element formulation for lateral-torsional buckling of doubly-symmetric cross-sections. The element developed was based on linear interpolation of the displacement fields, leading to a C0 continuous element, and was shown to a) converge from above, in a manner similar to conventional finite element formulations, and b) to exhibit particularly slow-convergence characteristics as hundreds of degrees of freedom were needed to model simple problems. Starting with the same variational principle, the present study develops an elaborate interpolation scheme leading to C1 continuity and resulting in a family of finite elements for the lateral torsional buckling analysis of members with superior characteristics; (1) it considerably accelerates the convergence characteristics of the solution, and (2) in one of the resulting elements, discretization errors are shown to lead to lower bound estimates of the buckling capacity, a desirable feature from a design viewpoint. In the second element, they were shown to lead to an upper bound estimate, while the third element exhibits the fastest convergence characteristics. The new solution is subsequently used to investigate the effect of lateral and/or torsional restraints and the effect of lateral bracing location along the web height on the lateral torsional buckling capacity of simple and multi-span beams.

3.2 Literature review

Numerous studies have investigated the elastic lateral-torsional buckling (LTB) resistance of doubly-symmetric I-beams. Using the Rayleigh-Ritz method, Salvadori (1955) developed the LTB solution of simply supported and continuous beams subject to a combination of axial and unequal end moments. Based on the finite difference technique, Poley (1956) solved the governing buckling differential equations for cantilever beams under uniformly distributed load. Using a successive-approximation technique for solving differential equations, Austin et al. (1957) developed the critical LTB solutions for beams with full torsional end restraints and partial rotational end restraints about the weak axis subjected to uniformly distributed loads and mid-span point loads. Load locations relative to the section centroid were also considered. Based on a numerical integration technique, Hartmann (1967) evaluated the effect and partial lateral, torsional, and weak axis bending constraints on the LTB capacity of beams subjected to point loads, with interior supports for simply supported and continuous two-span and three-span beams. Krajcinovic (1969) and Barsoum and Gallagher (1970) developed a finite element for buckling analysis based on the Vlasov thin-walled beam theory. Powel and Klingner (1970) developed a thin-walled beam finite element to obtain the LTB capacity of simply supported and continuous beams subject to general loading. Their solution was applicable to doubly symmetric and mono-symmetric cross-sections. The effect of load position relative to shear center and that of lateral and torsional restraints were incorporated into the solution. Using the beam element developed by Gallagher and Padlog (1963), Nethercot and Rockey (1971) investigated the lateral stability of simply supported beams with discrete lateral restraints, discrete torsional restraints, and both lateral and torsional restraints, subject to uniform moments. Also, Based on the element, Nethercot (1973a) examined the effect of load type and lateral, torsional, and warping restraints on LTB of cantilevers and proposed expressions for the effective length of cantilevers governed by LTB. Using the same element, Nethercot (1973b) studied the effect of load type on LTB of simply supported beams braced laterally or torsionally under uniform moments, mid-span point load, and uniformly distributed load. Based on the finite integral method, Kitipornchai and Richter (1978) studied the LTB of simply supported beams with discrete rigid intermediate translational and rotational restraints and subjected to concentrated load, end moments and uniformly distributed load. Kitipornchai et al. (1984) extended their work to investigate the effect of intermediate translational and rotational discrete restraints on LTB capacity of cantilevers under uniformly distributed and concentrated loads. Based on the direct variational approach, Assadi and Roeder (1985) studied the LTB of cantilevers with continuous rigid and elastic lateral restraints. Their study investigated the effects of load height, height of lateral restraint and stiffness. Based on a closed-form solution, Tong and Chen (1988) investigated the LTB capacity of simply supported beams with symmetrical or mono-symmetrical I-sections, either restrained laterally or torsionally at mid-span, subjected to uniform bending moments. Wang and Nethercot (1990) developed a thin-walled beam element for conducting a three-dimensional ultimate-strength analysis to assess bracing requirements for laterally unrestrained beams. They investigated simply supported I-beams with a single, three, or five equally spaced discrete torsional restraints subjected to central transverse concentrated load applied to the upper flange. Attard (1990) developed solutions for estimating LTB capacity of beams with mono-symmetric and doubly symmetric sections and general boundary conditions. Albert et al. (1992) developed a finite element model consisting of four-node plate elements for the web and two-node line elements for the flanges. This model predicts the LTB resistance of beams under various loading and boundary conditions while capturing distortional effects. Using this finite element model, Essa and Kennedy (1994) developed effective length factors for built-in cantilevers under top and bottom flange lateral restraints and load positions relative to the shear center. Using the same element, they also developed a design approach for cantilever-suspended-span constructions (1995). Wang et al. (1995) used the Rayleigh-Ritz method to determine the optimal locations for rigid lateral and torsional intermediate restraints to maximize the elastic LTB capacity of I-beams. Using the elastic buckling finite element program, BASP (Buckling Analysis of Stiffened Plates) developed by

Akay et al. (1977) and Choo (1987), Yura (2001) developed rules for bracing requirements based on the loading configuration, load height relative the shear center, location of restraint and cross-section distortion. Based on the Babnov-Galerkin method and the two-node beam finite element, Lim et al. (2003) evaluated the effects of moment gradient and end warping, lateral, and torsional restraints on LTB capacity of beams. Park et al. (2004) examined the effect of continuous top flange bracing on LTB capacity of simply supported and multi-span beams subject to uniformly distributed and concentrated loads based on the four-node plate element within the finite element program MSC/NASTRAN. Using shell analysis, Ozdemir and Topkaya (2006) examined LTB capacity of overhanging monorails under various loading and boundary conditions. Based on a shell element solution and the finite difference method, Serna et al. (2006) proposed a new moment gradient factor for simply supported beams restrained torsionally at both ends and subject to general loads applied at the shear center. Using the Rayleigh-Ritz method, Andrade et al. (2007) extended the application of the Eurocode 3 (1992) three-factor method for LTB to cantilevers with doubly and mono-symmetric sections subject to uniformly distributed and concentrated transverse tip loads. Their solution incorporated the effect of load height relative to the shear center. Larue et al. (2007) developed a code based on a mathematical software, called MGv3, for determining the LTB moment of I-beams with rigid continuous lateral restraint applied at the tension flange. The same problem was solved by Khelil and Larue (2008) who adopted the Galerkin method. Using a finite element program, FTBER, an extension of the commercial finite element program, PRFELB, Trahair (2008) developed a design approach for obtaining lateral buckling resistance of monorail beams, cantilevers and overhangs loaded at the bottom flange and laterally and transversely supported at the top flange. Based on the Rayleigh-Ritz approach, Nguyen et al. (2010) developed LTB solutions for I-girders subject to linear bending moments with equidistant discrete torsional restraints and quantified the torsional stiffness requirements for the restraints to maximize the LTB capacity.

A common feature about the previous studies is the fact that they neglect shear deformation. Shear deformable buckling solutions were developed relatively recently. Using the stationary complementary energy variational principle, Erkmen and Mohareb (2008a, 2008b) developed a shear deformable element to determine the LTB capacity of open thin-walled members. Erkmen et al. (2009) investigated the conditions under which the elastic torsional buckling of columns is guaranteed to converge from below. Based on a hyper-elastic constitutive model, Attard and Kim

(2010) developed a shear deformable element to determine LTB solutions of simply supported beams subject to uniform bending moment. Another shear deformable element was developed by Wu and Mohareb (2011a, 2011b) based on the principle of stationary potential energy. Erkmen and Attard (2011) and Erkmen (2014) also developed shear deformable elements to predict LTB capacity of thin-walled members. Examples on shear deformable elements in composite beams include the work of Kim and Lee (2013) and Kim and Choi (2013). Within the above context, the present solution provides a shear deformable solution.

In the majority of the above studies, discretization errors are observed to lead to upper bound predictions of the critical loads. Exceptions to that trend are observed in Erkmen and Mohareb (2008a, 2008b), Erkmen et al. (2009), Erkmen (2014), Santos (2011) and Santos (2012) which provide lower bound predictions of the critical loads in some of problems investigated. However, none of the above studies reached an unconditional lower bound buckling load prediction. In this context, one of the finite elements developed under the present study is shown to consistently provide a lower bound buckling prediction.

3.3 Assumptions

The variational principle (Wu and Mohareb (2011b)) is based on the following assumptions:

1. Beam cross-sections are open and doubly-symmetric,
2. Regarding shear/bending action, the cross-section is assumed to remain rigid in its own plane during deformation but does not remain perpendicular to the neutral axis after deformation in line with the Timoshenko theory (Wu and Mohareb (2011a)). The hypothesis is further generalized for torsion/warping action,
3. Strains are assumed small but rotations are assumed to be moderate (Wu and Mohareb (2010, 2011a)). Rotation effects are thus included in the formulation by retaining the non-linear strain components,
4. The member buckles in an inextensional mode (Trahair (1993)) which means that throughout buckling, the centroidal longitudinal strain and curvature in yz-plane remain zero. This signifies that the member is assumed to buckle under constant axial load and bending moments,
5. The material is assumed to be linearly elastic and obeys Hooke’s law, and
6. Pre-buckling deformation and distortional effects are neglected.

3.4 Problem description, convention and notation

A right-handed Cartesian coordinate system is adopted in the present study. The z-axis is oriented along the axial direction while x-axis and y-axis are parallel to major and minor principal axes, respectively. The origin coincides with the cross-section centroid $C(x_c = 0, y_c = 0)$, sectorial origin S_0, Pole A_p and shear center SC to form an orthogonal coordinate system. The member is assumed to be subjected to a uniformly distributed transverse load q_y applied at a distance $y_{qy}(z)$ from the shear center and a uniformly distributed axial load q_z acting at distance $y_{qz}(z)$ from the origin. Under such external loads, the member deforms from configuration 1 to 2 as shown in Figure 3-1 and undergoes displacements $v_p(z)$, $w_p(z)$ and rotation $\theta_{xp}(z)$. As a convention, subscript *p* represents pre-buckling displacement, strain and stress fields. The applied loads are assumed to increase by a factor λ and attain the values λq_y and λq_z at the onset of buckling (Configuration 3). Under the load increase, it is assumed that pre-buckling deformations linearly increase to $\lambda v_p(z)$, $\lambda w_p(z)$ and $\lambda \theta_p(z)$. The section then undergoes LTB (Configuration 4) manifested by lateral displacement u_b, weak-axis rotation θ_{yb}, angle of twist θ_{zb} and warping deformation ψ_b. Again, as a matter of convention, subscript *b* denotes field displacements, strains, or stresses, occurring during the buckling stage (i.e., in going from configuration 3 to 4).

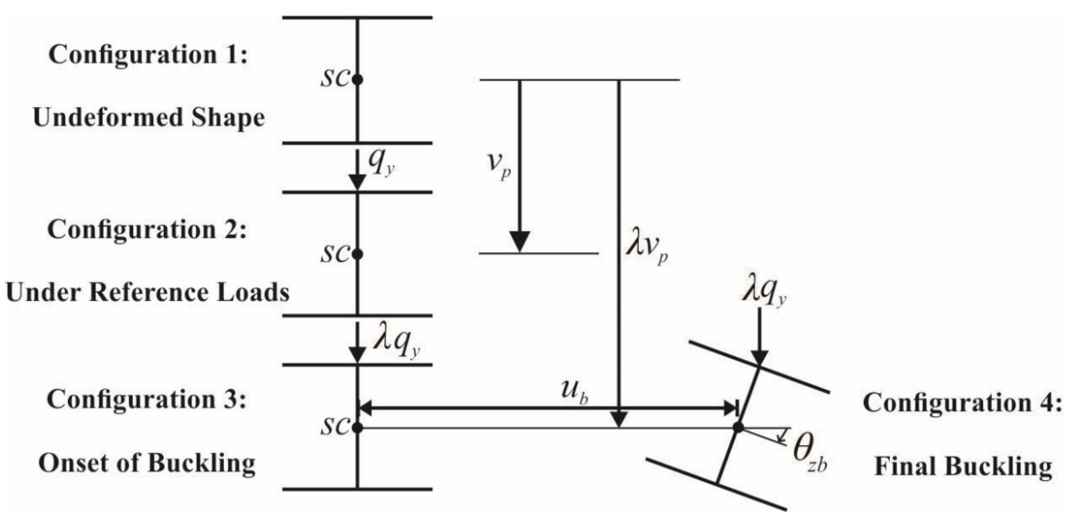

Figure 3-1 Different stages of deformation

3.5 Variational principle

When the member is at the onset of buckling (Configuration 3 in Figure 3-1), the first variation of total potential energy $\delta\pi$ has to vanish to meet the equilibrium condition and also the variation of the second variation of total potential energy $\delta^2\pi$ has to vanish to meet condition of neutral stability, i.e., $\delta\left[(1/2)\delta^2\pi\right]=\delta\left[(1/2)\delta^2(U+V)\right]=0$, in which U is the internal strain energy and V is the load potential energy gained by externally applied loads. For a doubly-symmetric cross-section and using orthogonal coordinates, the condition of neutral stability leads to (Wu and Mohareb (2011a))

$$\delta\left(\frac{1}{2}\delta^2\pi\right)=\delta\left[\frac{1}{2}\delta^2\left(U_b+U_{sv}+U_s+V_N+V_M+V_V+V_{qy}+V_{qz}\right)\right]=0 \tag{3.1}$$

in which U_b, U_{sv} and U_s are, respectively, the internal strain energy due to normal stresses, Saint-Venant shear stresses, and other shearing stresses induced by bending and warping. The terms V_N, V_M, V_V, V_{qy} and V_{qz} represent the destabilizing effects due to normal forces, bending moments, shear forces, transverse load position effect, and longitudinal load position effect, respectively. For orthogonal coordinates, the second variations of the above energy terms take the form (Wu and Mohareb (2011a, 2011b))

$$\delta^2 U_b = \int_0^L \left[EI_{yy}\left(\theta'_{yb}\right)^2 + EI_{\omega\omega}\left(\psi'_b\right)^2 \right] dz$$

$$\delta^2 U_{sv} = \int_0^L GJ\left(\theta'_{zb}\right)^2 dz$$

$$\delta^2 U_s = G\int_0^L \left[\left(D_{xx}u'_b - D_{xx}\theta_{yb}\right)u'_b + \left(-D_{xx}u'_b + D_{xx}\theta_{yb}\right)\theta_{yb} + \left(D_{hh}\theta'_{zb} + D_{hh}\psi_b\right)\theta'_{zb} \right.$$
$$\left. + \left(D_{hh}\theta'_{zb} + D_{hh}\psi_b\right)\psi_b \right] dz$$

$$\delta^2 V_N = -\lambda\int_0^L \left(\frac{N_p(z)}{A}\right)\left[-Au'^2_b - \left(I_{xx} + I_{yy}\right)\theta'^2_{zb}\right] dz$$

$$\delta^2 V_M = -\lambda\int_0^L M_{xp}(z)\left[-2\left(\theta'_{yb}\theta_{zb} + \theta_{yb}\theta'_{zb}\right) + 2u'_b\theta'_{zb}\right] dz$$

$$\delta^2 V_V = -\lambda\int_0^L V_{yp}(z)\left(-2\theta_{yb}\theta_{zb} + 2u'_b\theta_{zb}\right) dz$$

$$\delta^2 V_{qy} = -\lambda\int_0^L -q_y y_{qy}\left(\theta_{zb}\right)^2 dz \qquad \text{(3.2)a-h}$$

$$\delta^2 V_{qz} = -\lambda\int_0^L 2q_z y_{qz}\theta_{yb}\theta_{zb} dz$$

in which E is Young's modulus, A is the cross-sectional area, G is the shear modulus, J is the Saint-Venant torsional constant and the cross-sectional properties $I_{yy} = \int_A x^2 dA$, $I_{\omega\omega} = \int_A \omega^2 dA$, $D_{hh} = \int_A h^2 dA$, $D_{xx} = \int_A \left(dx/ds\right)^2 dA$ have been defined. Also, ω is the Vlasov warping function, s is a tangential coordinate along the section mid-surface and h is the distance perpendicular from the section shear center to the tangent to the section mid-line at the point of interest. In Eqs. (3.2)a-h, the pre-buckling internal forces $N_p(z), M_{xp}(z), V_{yp}(z)$ denote the normal force, bending moments about the strong axis, and associated shear force, respectively.

3.6 Overview of the finite element formulation in Wu and Mohareb (2011b)

The variational expressions in Eqs (3.2)a-h consist of the buckling displacement functions u_b θ_{yb} θ_{zb} ψ_b and their first derivatives with respect to coordinate *z*. Thus, each of the assumed four displacement functions needs to satisfy only C0 continuity. By taking two nodes per element and adopting a linear interpolation scheme between the two nodal values, the displacement fields $\langle u_b(z) \quad \theta_{yb}(z) \quad \theta_{zb}(z) \quad \psi_b(z)\rangle^T$ were related (Wu and Mohareb (2011b)) to the nodal displacements through

$$\langle u_b(z) \quad \theta_{yb}(z) \quad \theta_{zb}(z) \quad \psi_b(z)\rangle_{1\times4} = \langle H_b(z)\rangle_{1\times2} \left[\begin{Bmatrix} u_1 \\ u_2 \end{Bmatrix}_{2\times1} \quad \begin{Bmatrix} \theta_{y1} \\ \theta_{y2} \end{Bmatrix}_{2\times1} \quad \begin{Bmatrix} \theta_{z1} \\ \theta_{z2} \end{Bmatrix}_{2\times1} \quad \begin{Bmatrix} \psi_1 \\ \psi_2 \end{Bmatrix}_{2\times1} \right]$$

(3.3)a-d

in which $\langle H_b(z)\rangle_{1\times2} = \langle(1-z/L) \quad (z/L)\rangle$ is the vector of linear shape functions and $u_1, u_2, \theta_{y1}, ...\psi_2$ are the nodal displacement. In a similar manner, the pre-buckling stress resultants $N_p(z) \quad V_{yp}(z) \quad M_{xp}(z)$ are linearly interpolated between the internal forces $N_1, N_2, V_1, V_2, M_1, M_2$ at the nodes as obtained from the pre-buckling analysis, i.e.,

$$\langle N_p(z) \quad V_{yp}(z) \quad M_{xp}(z)\rangle = \langle H_b(z)\rangle_{1\times2} \left[\begin{Bmatrix} N_1 \\ -N_2 \end{Bmatrix}_{2\times1} \quad \begin{Bmatrix} V_1 \\ -V_2 \end{Bmatrix}_{2\times1} \quad \begin{Bmatrix} M_1 \\ -M_2 \end{Bmatrix}_{2\times1} \right] \qquad (3.4)\text{a-c}$$

The resulting element, to be subsequently referred as the WM element, was successful in converging to the buckling solutions (Wu and Mohareb (2011b)) only when a rather large number of elements were taken. Coarser meshes were observed to grossly overestimate buckling loads due to shear locking. Thus, the present formulation circumvents such problems by developing special shape functions featuring C1 continuity while preserving the minimal number degrees of freedom adopted in the WM element.

3.7 Conditions of neutral stability

Eqs. (3.2)a-h are integrated by parts and common terms are grouped together. Since functions δu_b, $\delta\theta_{yb}$, $\delta\theta_{zb}$ and $\delta\psi_b$ are arbitrary, one can rewrite the conditions of neutral stability in a matrix form as

$$\left[\begin{array}{c|c|c|c} \begin{array}{c}-\left(\lambda N_p+GD_{xx}\right)\mathscr{D}^2\\ -\lambda N_p'\mathscr{D}\end{array} & GD_{xx}\mathscr{D} & \lambda\left(V_{yp}\mathscr{D}+\dfrac{V_{yp}'}{2}+M_{xp}\mathscr{D}^2\right) & 0 \\ \hline GD_{xx}\mathscr{D} & -GD_{xx}+EI_{yy}\mathscr{D}^2 & \lambda q_z y_{qz} & 0 \\ \hline \lambda\left(V_{yp}\mathscr{D}+\dfrac{V_{yp}'}{2}+M_{xp}\mathscr{D}^2\right) & -\lambda q_z y_{qz} & \begin{array}{c}\lambda q_y y_{qy}-G\left(J+D_{hh}\right)\mathscr{D}^2\\ -\lambda\dfrac{\left(I_{xx}+I_{yy}\right)}{A}\left(N_p'\mathscr{D}+N_p\mathscr{D}^2\right)\end{array} & -GD_{hh}\mathscr{D} \\ \hline 0 & 0 & -GD_{hh}\mathscr{D} & -GD_{hh}+EI_{\omega\omega}\mathscr{D}^2 \end{array}\right]$$

$$\times\begin{Bmatrix} u_b \\ \theta_{yb} \\ \theta_{zb} \\ \psi_b \end{Bmatrix}=\begin{Bmatrix} 0 \\ 0 \\ 0 \\ 0 \end{Bmatrix} \tag{3.5}$$

in which $\mathscr{D}=\partial/\partial z$, $\mathscr{D}^2=\partial^2/\partial z^2$.

3.8 Finite element formulation

As discussed earlier, the element developed in Wu and Mohareb (2011b) has a minimum number of degrees of freedom (8 DOFs for the buckling solution) but exhibited slow-convergence, thus needing hundreds of elements to model simple problems. In order to develop computationally more efficient solutions, the present study devises a set of approximation schemes of the pre-buckling internal forces (Section 3.8.1), followed by formulating shape functions with superior convergence characteristics (Section 3.8.2) while keeping the number of degrees of freedom per element to a minimum. These shape functions are then used to develop a family of finite elements with various superior characteristics.

3.8.1 Approximation of pre-buckling internal forces

In general, the pre-buckling internal forces $N_p\left(z\right)$, $V_{yp}\left(z\right)$ and $M_{xp}\left(z\right)$ are non-constant functions. Conventional solutions (e.g., Barsoum and Gallagher (1970), Wu and Mohareb (2011b)) capture the exact distribution of internal forces [Figure 3-2(a)], as predicted from the pre-buckling analysis, when formulating the geometric stiffness matrices arising from Eqs. (3.2)d-h. In the present study, we deviate from this convention by subdividing the member(s) into a series of small elements such that the internal forces $N_p(z) \approx \overline{N}_p$, $V_{yp}(z) \approx \overline{V}_{yp}$ and $M_{xp}(z) \approx \overline{M}_{xp}$ can be considered constant within each element. The advantages of the proposed treatment are:

a) Unlike the case where $N_p(z)$, $V_{yp}(z)$ and $M_{xp}(z)$ are non-constant, under the approximations $N_p(z) \approx \overline{N}_p$, $V_{yp}(z) \approx \overline{V}_{yp}$ and $M_{xp}(z) \approx \overline{M}_{xp}$, a closed-form solution for the conditions of neutral stability [Eq. (3.5)] becomes attainable. This outcome is key in developing the superior shape functions proposed under the present study (Section 3.8.2).

b) It is clear that the proposed approximation would converge to the correct solution when enough elements are taken, and

c) Within each element, the magnitudes of constants $\overline{N}_p$, $\overline{V}_{yp}$ and $\overline{M}_{xp}$ can be taken to target either a fast-converging solution (Case 1), an upper bound solution (Case 2), or a lower bound solution (Case 3) as describe in the following section.

Case 1: Fast-converging solution

Under this case, the internal forces are taken equal to the mean value of the internal forces [Figure 3-2(b)] within the element i.e.,

$$\left[N_p(z), V_{yp}(z), M_{xp}(z)\right] \approx \left(\overline{N}_p, \overline{V}_{yp}, \overline{M}_{xp}\right) = \left[\left(N_1 - N_2\right)/2 \quad, \left(V_1 - V_2\right)/2, \quad \left(M_1 - M_2\right)/2\right] \tag{3.6a-c}$$

A similar approach was adopted in Sahraei et al. (2015) for mono-symmetric sections. It is stressed however, that the solution in (Sahraei et al. 2015) is not applicable to doubly symmetric sections which are the focus of the present study. This is the case since, as will be discussed under Section 3.8.2, the closed-form solution for the neutral stability conditions for the present problem as given in Eq. (3.5) takes a different form from that reported in (Sahraei et al. 2015). Thus, the direct application of the solution in (Sahraei et al. 2015) is found to lead to singularity problems when applied to doubly symmetric sections. Within this context, the present treatment circumvents these difficulties by treating the case of doubly symmetric separately. The finite element resulting from the approximation in Eq. (3.6)a-c will be shown to have excellent convergence characteristics compared to that in Wu and Mohareb (2011b). The element resulting from Case 1 will be referred to as the SM-M element.

Case 2: Upper-bound solution

An upper bound prediction of the buckling load is targeted by adopting internal force approximations which consistently underestimate the destabilizing effect as given by Eqs. (3.2)d-h, leading to a larger buckling load multiplier λ and hence over-predicting the critical loads. The following approximations satisfy this requirement

$$\begin{aligned} N_p(z) &\approx \overline{N}_p = s_n(N_1, N_2)\min(|N_1|,|N_2|) \\ V_{yp}(z) &\approx \overline{V}_{yp} = s_n(V_1, V_2)\min(|V_1|,|V_2|) \\ M_{xp}(z) &\approx \overline{M}_{xp} = s_n(M_1, M_2)\min(|M_1|,|M_2|) \end{aligned} \qquad (3.7)\text{a-c}$$

where $s_n(a_1, a_2)$ is the sign of argument (a_1 or a_2) with the smaller absolute value. Mathematically, it is given by

$$s_n(a_1,a_2) = \begin{cases} +1 & \text{if } \left[(a_1>0)\text{and}(a_2>0)\right] \\ -1 & \text{if } \left[(a_1>0)\text{and}(a_2<0)\text{and}(|a_1|>|a_2|)\right] \\ +1 & \text{if } \left[(a_1>0)\text{and}(a_2<0)\text{and}(|a_1|\le|a_2|)\right] \\ -1 & \text{if } \left[(a_1<0)\text{and}(a_2<0)\right] \\ +1 & \text{if } \left[(a_1<0)\text{and}(a_2>0)\text{and}(|a_1|>|a_2|)\right] \\ -1 & \text{if } \left[(a_1<0)\text{and}(a_2>0)\text{and}(|a_1|\le|a_2|)\right] \\ 0 & \text{if } \left[(a_1=0)\text{or}(a_2=0)\right] \end{cases}$$

It is clear that, as the number of elements are increased, Eqs. (3.7)a-c lead to $N_p(z) \to \overline{N}_p$, $V_{yp}(z) \to \overline{V}_{yp}$, $M_{xp}(z) \to \overline{M}_{xp}$ and in the limit, the approximate destabilizing term approaches that based on the exact distribution of the internal forces within the element, i.e., the solution is guaranteed to converge to the buckling load from above. The element based on approximations (3.7)a-c will be referred to as the SM-N element [Figure 3-2(c)].

Case 3: Lower-bound solution

In a similar manner, a guaranteed lower bound prediction of the buckling load is targeted by adopting internal force approximations which consistently overestimating the magnitudes of the destabilizing terms as given by Eqs. (3.2)d-h, thus leading to a smaller buckling load multiplier λ. Towards this goal, the following approximations are proposed

$$N_p(z) \approx \overline{N}_p = s_x(N_1, N_2)\max(|N_1|, |N_2|)$$
$$V_{yp}(z) \approx \overline{V}_{yp} = s_x(V_1, V_2)\max(|V_1|, |V_2|) \qquad (3.8)\text{a-c}$$
$$M_{xp}(z) \approx \overline{M}_{xp} = s_x(M_1, M_2)\max(|M_1|, |M_2|)$$

where $s_n(a_1, a_2)$ is the sign of argument (a_1 or a_2) with the larger absolute value, i.e.,

$$s_x(a_1, a_2) = \begin{cases} +1 & \text{if } \left[(a_2 \geq -a_1)\text{and}(a_1 > 0)\right] \\ -1 & \text{if } \left[(a_2 < -a_1)\text{and}(a_1 > 0)\right] \\ +1 & \text{if } \left[(a_2 > -a_1)\text{and}(a_1 < 0)\right] \\ -1 & \text{if } \left[(a_2 \leq -a_1)\text{and}(a_1 < 0)\right] \\ \text{sign}(a_1) & \text{if } a_2 = 0 \\ \text{sign}(a_2) & \text{if } a_1 = 0 \\ 0 & \text{if } \left[(a_1 = 0)\text{and}(a_2 = 0)\right] \end{cases}$$

The resulting element will be referred to as the SM-X element [Figure 3-2(d)] and will be shown to consistently converge from below.

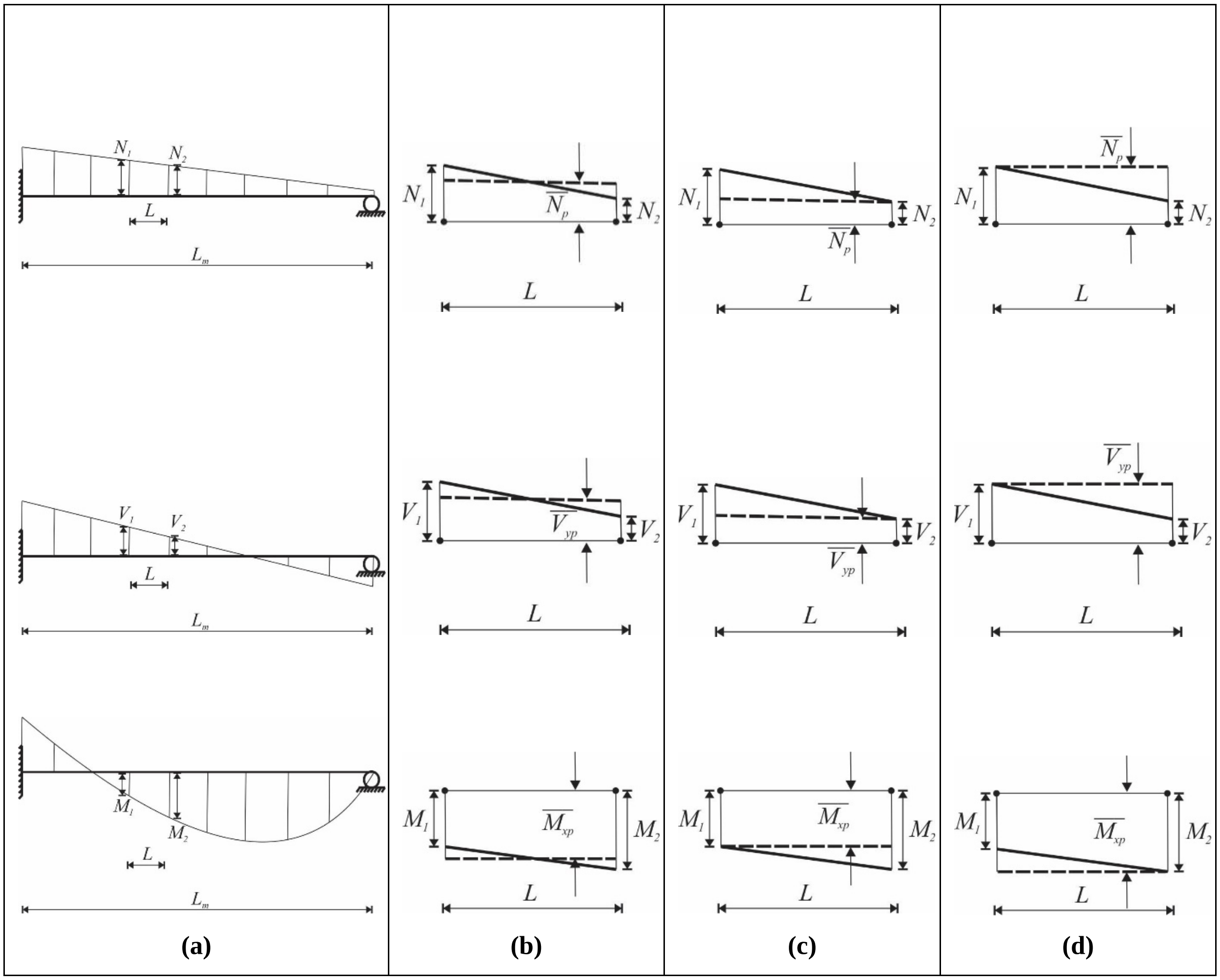

Figure 3-2 (a) Pre-buckling internal forces and approximations for (b) SM-M element, (c) SM-N element and (d) SM-X element (all solid lines denote exact internal force diagrams and dashed lines denote internal force approximations)

Within an element length L, any of the approximations provided in Eqs. (3.6)a-c, (3.7)a-c or (3.8) a-c leads to the following approximate expressions for the destabilizing energy terms in Eqs. (3.2) d-f

$$\delta^2 V_N \approx -\lambda \bar{N}_p \int_0^L \left(\frac{1}{A}\right)\left[-A u_b'^2 - \left(I_{xx} + I_{yy}\right)\theta_{zb}'^2\right] dz$$

$$\delta^2 V_M \approx -\lambda \bar{M}_{xp} \int_0^L \left[-2\left(\theta_{yb}'\theta_{zb} + \theta_{yb}\theta_{zb}'\right) + 2u_b'\theta_{zb}'\right] dz \qquad (3.9)\text{a-c}$$

$$\delta^2 V_V \approx -\lambda \bar{V}_{yp} \int_0^L \left(-2\theta_{yb}\theta_{zb} + 2u_b'\theta_{zb}\right) dz$$

It is clear that under all three approximations in Cases (1-3), as the number of elements is sufficiently large, the piecewise approximations of the destabilizing terms in Eqs. (3.9)a-c would approach that based on actual internal force distributions in Eqs. (3.2)d-f, thus guaranteeing convergence to the critical loads.

3.8.2 Formulating shape functions

As observed in Wu and Mohareb (2011b), by adopting linear interpolation functions to relate the displacement fields $u_b, \theta_{yb}, \theta_{zb}, \psi_b$ to the nodal displacements, it was observed that the resulting element suffers from shear locking. This was manifested by the large number of elements needed to attain convergence. Within this context, the present section aims at developing improved shape functions which avoid shear locking. Towards this goal, the shape functions will be based on closed-form solutions of the equilibrium equations. The presence of the unknowns $\lambda N_p, \lambda V_{yp}, \lambda M_{xp}$ arising in Eq. (3.5), makes such a solution unattainable given that λ is unknown a-priori. Thus, when formulating shape functions, the terms involving $\lambda N_p, \lambda V_{yp}, \lambda M_{xp}$ are assumed negligible. The validity of this hypothesis is numerically assessed and verified in Appendix A.

It is emphasized that this simplification will be used only for the purpose of developing shape functions. Once the shape functions are developed, they will be substituted into the stationary condition of the second variation of the total potential energy functional [Eq. (3.1)] while retaining the contributions $\delta^2 V_N, \delta^2 V_M, \delta^2 V_V$ of destabilizing terms.

By neglecting the destabilizing terms, the differential equations of neutral stability can be expressed as two sets of coupled differential equations [Eq. (3.25)]

$$\begin{bmatrix} -GD_{xx}\mathscr{D}^2 & GD_{xx}\mathscr{D} \\ GD_{xx}\mathscr{D} & -GD_{xx} + EI_{yy}\mathscr{D}^2 \end{bmatrix} \begin{Bmatrix} u_b \\ \theta_{yb} \end{Bmatrix} = \begin{Bmatrix} 0 \\ 0 \end{Bmatrix}$$
$$\begin{bmatrix} -GJ\mathscr{D}^2 - GD_{hh}\mathscr{D}^2 & -GD_{hh}\mathscr{D} \\ -GD_{hh}\mathscr{D} & -GD_{hh} + EI_{\omega\omega}\mathscr{D}^2 \end{bmatrix} \begin{Bmatrix} \theta_{zb} \\ \psi_b \end{Bmatrix} = \begin{Bmatrix} 0 \\ 0 \end{Bmatrix} \qquad (3.10)\text{a-b}$$

The solution is assumed to take the form $\langle u_b, \theta_{yb}, \theta_{zb}, \psi_b \rangle^T = \langle A_i, B_i, C_i, D_i \rangle^T e^{m_i z}$. By substituting into Eqs. (3.10)a-b and expanding the determinant of coefficients for each set, one has

$$\left[\begin{array}{c|c} -GD_{xx}m^2 & GD_{xx}m \\ \hline GD_{xx}m & -GD_{xx}+EI_{yy}m^2 \end{array}\right]\begin{Bmatrix} A \\ B \end{Bmatrix}=\begin{Bmatrix} 0 \\ 0 \end{Bmatrix}, \quad \left[\begin{array}{c|c} -GJm^2-GD_{hh}m^2 & -GD_{hh}m \\ \hline -GD_{hh}m & -GD_{hh}+EI_{\omega\omega}m^2 \end{array}\right]\begin{Bmatrix} C \\ D \end{Bmatrix}=\begin{Bmatrix} 0 \\ 0 \end{Bmatrix}$$

(3.11)a-b

By setting the determinant of the matrix of coefficients of Eq. (3.11)a to zero, one obtains four zero roots, i.e., $m_1 = m_2 = m_3 = m_4 = 0$. Also, by setting the determinant of the matrix of coefficients of Eq. (3.11)b to zero, one obtains

$$m_1 = m_2 = 0, \quad m_3 = -m_4 = \sqrt{\frac{GJD_{hh}}{EI_{\omega\omega}\left(D_{hh}+J\right)}} \tag{3.12}$$

The corresponding solution can be shown to take the form

$$\begin{Bmatrix} u_b(z) \\ \theta_{yb}(z) \end{Bmatrix} = \left[B_1(z)\right]_{2\times4}\{A\}_{4\times1}, \qquad \left[B_1(z)\right]_{2\times4} = \left[\begin{array}{c|c|c|c} 1 & z & z^2 & z^3 \\ \hline 0 & 1 & 2z & \dfrac{6EI_{yy}}{GD_{xx}}+3z^2 \end{array}\right] \tag{3.13a-b}$$

where the vector of integration constants $\langle A\rangle^T = \langle A_1 \quad A_2 \quad A_3 \quad A_4\rangle$ has been defined. Also, one has

$$\begin{Bmatrix} \theta_{zb}(z) \\ \psi_b(z) \end{Bmatrix} = \left[B_2(z)\right]_{2\times4}\{C\}_{4\times1}, \quad \left[B_2(z)\right]_{2\times4} = \left[\begin{array}{c|c|c|c} 1 & z & e^{m_3 z} & e^{m_4 z} \\ \hline 0 & -1 & \dfrac{-\left(J+D_{hh}\right)}{D_{hh}}m_3 e^{m_3 z} & \dfrac{-\left(J+D_{hh}\right)}{D_{hh}}m_4 e^{m_4 z} \end{array}\right]$$

(3.14)a-b

where vector $\langle C\rangle^T = \langle C_1 \quad C_2 \quad C_3 \quad C_4\rangle$ consists of the integration constants. Eqs. (3.13)a and (3.14)a are consolidated to yield

$$\{d(z)\}_{4\times1} = \left[\begin{array}{c|c} \left[B_1(z)\right] & [0] \\ \hline [0] & \left[B_2(z)\right] \end{array}\right]_{4\times8} \{C_{st}\}_{8\times1} \tag{3.15}$$

where $\langle d(z)\rangle^T = \langle u_b(z) \quad \theta_{yb}(z) \quad \theta_{yb}(z) \quad \psi_b(z)\rangle^T$ consist of the displacement functions, and the vector of integration constants $\langle C_{st}\rangle^T = \langle \langle A\rangle^T \mid \langle C\rangle^T \rangle$ has been defined. The nodal displacements

$\langle \delta u_N \rangle^T = \langle \delta u_{b1} \quad \delta\theta_{yb1} \quad \delta\theta_{zb1} \quad \delta\psi_{b1} \quad \delta u_{b2} \quad \delta\theta_{yb2} \quad \delta\theta_{zb2} \quad \delta\psi_{b2} \rangle^T$ can be related to the vector of integration constants $\{C_{st}\}$ by setting $z=0$ and $z=L$ in Eq. (3.15) via

$$\{\delta u_N\}_{8\times1} = [H]_{8\times8}\{C_{st}\}_{8\times1}, \qquad [H]_{8\times8} = \begin{bmatrix} [B(0)]_{4\times8} \\ \hline [B(l)]_{4\times8} \end{bmatrix} \tag{3.16)a-b}$$

From Eq. (3.16)a, by solving for the integration constants and substituting into Eq. (3.15), one obtains

$$\{d(z)\}_{4\times1} = [L(z)]_{4\times8}\{\delta u_N\}_{8\times1} \tag{3.17}$$

in which $[L(z)]_{4\times8} = [B(z)]_{4\times8}[H]_{8\times8}^{-1}$ is a matrix of 32 shape functions. Shape functions $[L(z)]_{4\times8}$ ensure C1 continuity of the displacement fields while exactly satisfy the neutral stability conditions in Eqs. (3.10)a-b.

3.8.3 Element stiffness matrices

From Eq. (3.17), by substituting field displacements into Eqs. (3.2)a-h and then Eq. (3.1) and evoking the stationarity condition, one obtains the stationarity condition

$$([K]-\lambda[K_G])\{\delta u_n\} = \{0\} \tag{3.18}$$

where the element elastic stiffness matrix $[K]$ and geometric matrix $[K_G]$ are defined as

$$\begin{aligned} [K] &= [K]_f + [K]_{sv} + [K]_s \\ [K_G] &= [K_G]_N + [K_G]_M + [K_G]_V + [K_G]_{qy} + [K_G]_{qz} \end{aligned} \tag{3.19)a-b}$$

in which the elastic stiffness matrices contributions $[K]_f$, $[K]_{sv}$, $[K]_s$ are due to flexural stresses, the Saint-Venant shear stresses and the remaining shear stresses, respectively and the geometric matrices contributions $[K_G]_N$, $[K_G]_M$, $[K_G]_V$, $[K_G]_{qy}$, $[K_G]_{qz}$ are due to normal forces, bending moments, shear forces, transverse load position effect and distributed axial load, respectively. These stiffness matrices are obtained from

$$\begin{aligned}&\left\{[K]_f,[K]_{sv},[K]_s,[K_G]_N,[K_G]_M,[K_G]_V,[K_G]_{qy},[K_G]_{qz}\right\}=\\&\left[H^{-1}\right]^T_{8\times8}\left\{[M_1],[M_2],[M_3],[M_4],[M_5],[M_6],[M_7],[M_8]\right\}[H]^{-1}_{8\times8}\end{aligned} \tag{3.20}$$

in which closed-form expressions for matrices $[M_1]$ to $[M_8]$ have been provided in Appendix B.

3.8.4 Stiffness matrix for the structure

The element elastic and geometric matrices $[K]$ and $[K_G]$ are assembled to form the structure elastic and geometric matrices $[S]$ and $[S_G]$, respectively and the boundary conditions are enforced. In order to incorporate kinematic constraints into the formulation (such as the presence of eccentric supports, etc.), the structure is assumed to be subjected to a set of m multiple point constraints of the form of

$$[P]_{m\times n}\{u_s\}_{n\times1}=\{0\}_{m\times1} \tag{3.21}$$

where $[P]_{m\times n}$ is a matrix of user-input coefficients which linearly relate any set of nodal displacements, $\{u_s\}_{n\times1}$ is the vector of nodal displacements for the structure and n is the number of degrees of freedom. It is then required to extremize the second variation of the total potential energy π of the system subject to the set of constraints in Eq. (3.21). This is formally achieved by introducing an auxiliary functional π^* through augmenting the total potential energy π by an additional term resulting from pre-multiplying the constraints in Eq. (3.21) by a vector of Lagrange multipliers $\langle F\rangle^T_{1\times m}$ such that

$$\begin{aligned}\delta\left(\frac{1}{2}\delta^2\pi^*\right)&=\delta\left(\frac{1}{2}\delta^2\pi+\langle F\rangle^T_{1\times m}[P]_{m\times n}\{u_s\}_{n\times1}\right)\\&=\delta\left(\frac{1}{2}\langle u_s\rangle^T_{1\times n}\left([S]_{n\times n}-\lambda[S_G]_{n\times n}\right)\{u_s\}_{n\times1}+\langle F\rangle^T_{1\times m}[P]_{m\times n}\{u_s\}_{n\times1}\right)=0\end{aligned} \tag{3.22}$$

By evoking the stationarity conditions of the second variation of the functional π^*, $\partial\left((1/2)\delta^2\pi^*\right)/\partial\{u_s\}_{n\times1}=\{0\}_{n\times1}$, $\partial\left((1/2)\delta^2\pi^*\right)/\partial\{F\}_{m\times1}=\{0\}_{m\times1}$, one obtains

$$\left\{\begin{bmatrix}[S]_{n\times n} & [P]^T_{n\times m}\\ [P]_{m\times n} & [0]_{m\times m}\end{bmatrix}-\lambda\begin{bmatrix}[S_G]_{n\times n} & [0]_{n\times m}\\ [0]_{m\times n} & [0]_{m\times m}\end{bmatrix}\right\}\begin{Bmatrix}\{u_s\}_{n\times1}\\ \{F\}_{m\times1}\end{Bmatrix}=\begin{Bmatrix}\{0\}_{n\times1}\\ \{0\}_{m\times1}\end{Bmatrix} \tag{3.23}$$

The modified eigenvalue problem defined by Eq. (3.23) is then solved for the load multiplier λ, the associated eigen displacement vector $\{u_s\}_{n\times 1}$ and Lagrange multipliers $\{F\}_{m\times 1}$.

3.9 Examples

This section provides various buckling examples and evaluates the convergence characteristics of the proposed elements against other numerical solutions. Comparisons are also provided to the other solutions. The number of degrees of freedom needed to achieve convergence is established and the convergence behavior for the three element is discussed. The effects of lateral and torsional restraints and their location of lateral restraints relative to the shear center on lateral-torsional capacity are also assessed for simply supported and continuous multiple-span beams. In all examples, steel material is considered with $E = 200,000$ MPa and $G = 77,000$ MPa. The W250x45 section is adopted (Figure 3-3). Cross-sectional properties are $I_{xx} = 71.887\times 10^6\,\text{mm}^4$, $I_{yy} = 7.033\times 10^6\,\text{mm}^4$, $A = 5770.8\text{mm}^2$, $I_{\omega\omega} = 1.124\times 10^{11}\,\text{mm}^6$, $J = 2.538\times 10^5\,\text{mm}^4$, $D_{xx} = 3848\text{mm}^2$ and $D_{hh} = 61.577\times 10^6\,\text{mm}^4$.

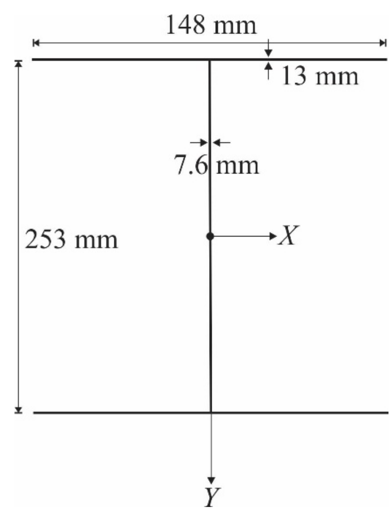

Figure 3-3 Dimensions of the W250x45 cross-section

3.9.1 Example 1: Mesh density analysis and comparison with other solutions for cantilevers

A comparison is provided with solution developed by Wu and Mohareb (2011b) (WM element), the SM-M, SM-N and SM-X elements developed in the present study and the classical Barsoum and Gallagher element (referred to as BG element). The example was solved in Wu and Mohareb (2011b) and is revisited here for comparison. It consists of a cantilever beam under a vertical concentrated load applied at the tip and acting at the shear center. Two spans are investigated: 5m and 1m. A mesh study analysis is provided in Figure 3-4 and Figure 3-5. In Figure 3-4, the horizontal line provides the converged value for the buckling load when a large number of elements are taken, i.e., 8 BG elements (non-shear deformable) and 320 WM elements (shear deformable). Both elements predicted the same critical load 41.3 kN within three significant digits since shear deformation effects are negligible for long spans. For the elements developed in the present study, 120 SM-X elements yielded a critical load prediction of 40.9 kN while 120 SM-N elements yielded a value of 41.5 kN. The best and fastest prediction among the shear deformable elements was obtained using the SM-M element where 8 elements were enough to reach a critical load of 41.1 kN. As seen, results based on all four shear deformable elements (WM, SM-M, SM-N and SM-X) and the classical non-shear deformable BG element are in a close agreement for the beam with larger span. The SM-M element involves the smallest number of degrees of freedom (i.e., 8 elements) and unlike other displacement-based elements such as WM and BG elements, it is observed to converge from below in the present problem. On the other hand, the SM-N element converges from above at a relatively slow rate compared to SM-M, but still at a faster rate than the WM element. It is also observed that the resulting SM-X element converges from below again, albeit the convergence rate is in line with that of the SM-N element, but still faster than the WM element for the present example. For the 1m span cantilever, Figure 3-5 shows that all four shear deformable elements (SM-N, SM-M, SM-X and WM) converge to the same critical load, while the classical shear non-deformable BG element is observed to slightly overestimate the buckling load, which is more pronounced in short span beams.

For comparison, a solution based on the ABAQUS S4R shell element as reported in Wu and Mohareb (2011b) was also provided. The ABAQUS S4R solution yielded buckling load estimates of 39.98 kN and 2396 kN for the long and short span members, respectively. Both predictions are slightly lower than those based on the shear deformable elements. The difference is attributed to the fact that the shell element captures both the distortional and shear deformation effects and thus provides the most flexible representation of all solutions. The largest buckling load observed is that based on the BG element. This is expected since the BG element neglects distortional and shear deformation effects and thus provides the stiffest representation of the member.

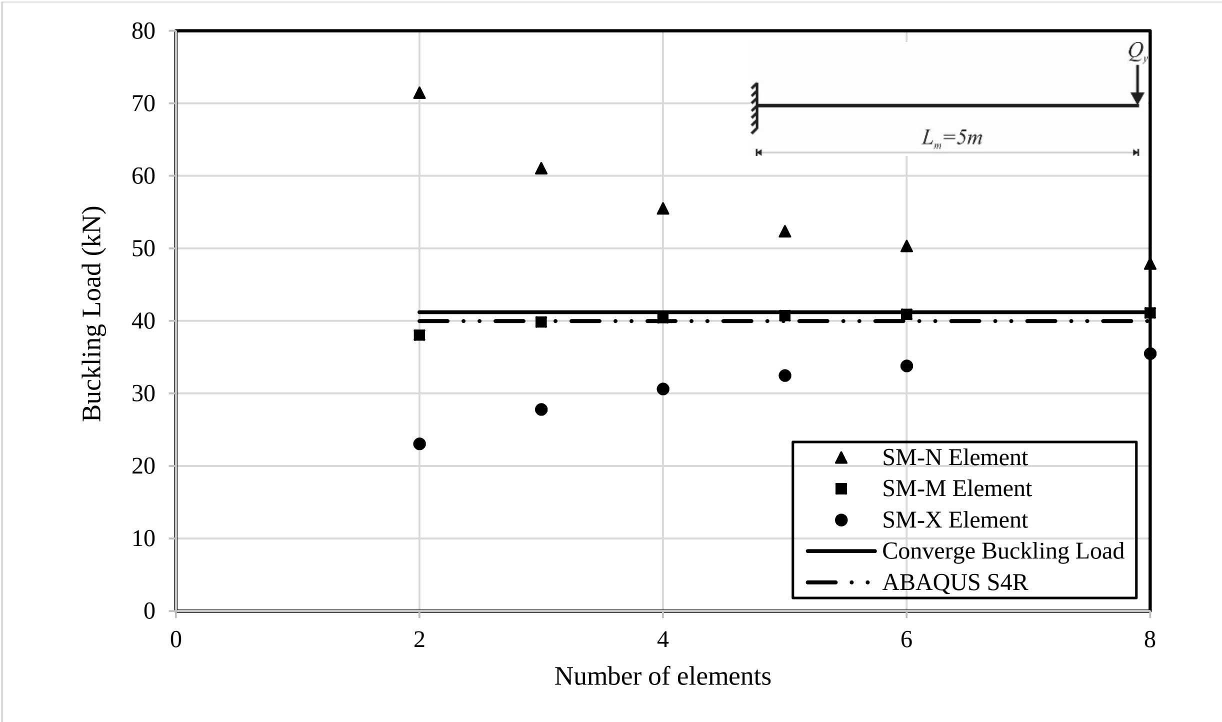

Figure 3-4 Mesh study analysis for the cantilever beam with larger span

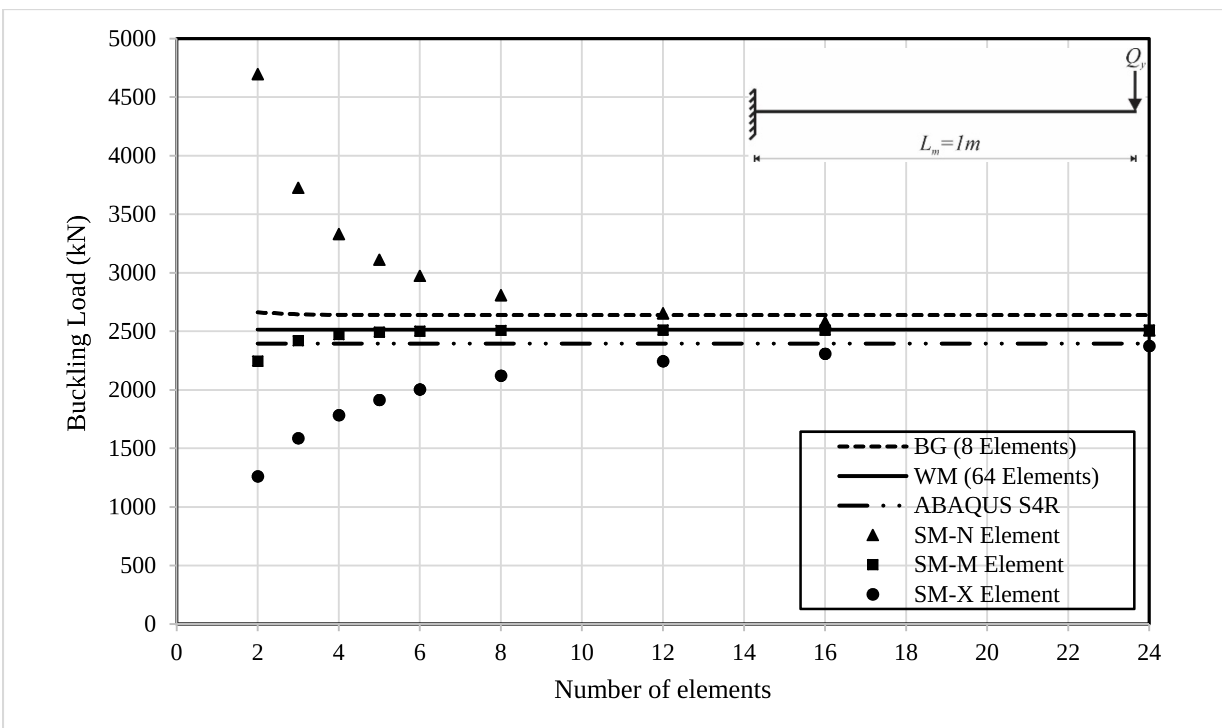

Figure 3-5 Mesh study analysis for the cantilever beam with shorter span

3.9.2 Example 2: Convergence characteristics for other loading conditions

While Example 1 has shown the convergence characteristics of the elements SM-N, SM-M and SM-X for the particular case of a cantilever under tip load, the present example is aimed to investigate the convergence characteristics for other types of loading. Four additional loading cases are considered for a 5m span simply supported beam under the following loads:

a) Mid-span point load,
b) Uniformly distributed load,
c) Uniform bending moments, and
d) Linear reverse moments.

A mesh density study was performed for each of the five cases using each of the three elements. The results are summarized in Table 3.1 for SM-M element, Table 3.2 for SM-N element and Table 3.3 for SM-X elements. In all five cases, the SM-M is observed to be fast converging compared to the other two elements. Mesh refinements from 8 to 120 elements were associated with a difference in the predicted buckling moments of less the 2% in all five cases. The solution is observed to converge from below for the cases of reverse moments and cantilever and from above in other cases, i.e., no specific convergence trend can be guaranteed under the SM-M element.

For element SM-N, Table 3.2 indicates that convergence is from above in all cases. The number of elements needed for convergence is higher than the SM-M, where 48 elements were associated with a 3% difference compared to solutions based on 120 elements.

For element SM-X, Table 3.3 indicates that convergence is from below in all cases, i.e., discretization errors consistently result in an underestimation of the buckling moments. This feature is desirable from a design viewpoint, since it consistently errs on the conservative side. Solutions based on 48 elements are observed to agree within 3% of those based on 120 elements. The present study suggests that both elements SM-N and SM-X are comparatively more computationally efficient than the WM element (Wu and Mohareb (2011b)), where 320 elements have been reported to be needed for convergence. While elements SM-N and SM-X appear to consistently provide upper and lower bounds of the buckling moments, element SM-M is most efficient in terms of computational effort required for convergence. A comparison for the results of SM-X, SM-M and SM-N elements are provided in Table 3.4. When the same number of elements are taken (120 elements in the present study), the buckling moments predicted by SM-M element are observed to always lie between those based on SM-X and SM-N elements. Results based on SM-X thus appear to provide lower bound predictions while those based on SM-N provide upper bound predictions of the buckling moments. Table 3.5 provides a comparison of the merits of each of the three formulations developed in the present and relevant past studies.

Table 3.1 Buckling moments (kNm) and convergence characteristics predicted by SM-M element

Problem	**Number of SM-M elements**				**(1)/(4)**	**(2)/(4)**	**(3)/(4)**	**Converge from**
	(1) n=2	**(2) n=4**	**(3) n=8**	**(4) n=120**				
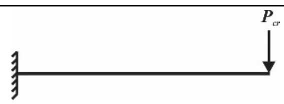	190.2	202.3	205.5	**206.4**	0.92	0.98	1.00	Below
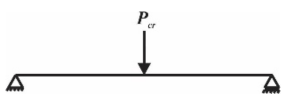	250.3	179.6	170.6	**167.9**	1.49	1.07	1.02	Above
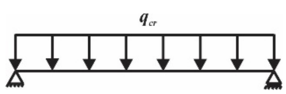	250.3	152.9	142.7	**139.6**	1.79	1.10	1.02	Above
	125.4	123.6	123.5	**123.5**	1.02	1.00	1.00	Above
	251.3	310.4	327.6	**332.7**	0.76	0.93	0.98	Below

Table 3.2 Buckling moments (kNm) and convergence characteristics predicted by SM-N element

Problem	**Number of SM-N elements**				**(1)/(4)**	**(2)/(4)**	**(3)/(4)**
	(1) **n=24**	**(2)** **n=48**	**(3)** **n=72**	**(4)** **n=120**			
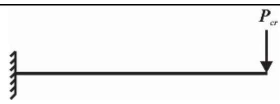	216.7	211.3	209.5	**208.0**	1.04	1.02	1.01
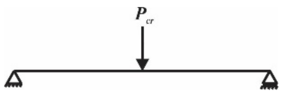	178.0	172.8	171.1	**169.9**	1.05	1.02	1.01
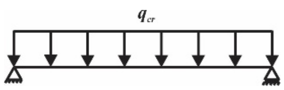	143.5	141.5	140.9	**140.4**	1.02	1.01	1.00
	123.5	123.5	123.5	**123.5**	1.00	1.00	1.00
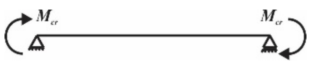	364.8	348.3	343.0	**338.8**	1.08	1.03	1.01

Table 3.3 Buckling moments (kNm) and convergence characteristics predicted by SM-X element

Problem	**Number of SM-X elements**				**(1)/(4)**	**(2)/(4)**	**(3)/(4)**
	(1) **n=24**	**(2)** **n=48**	**(3)** **n=72**	**(4)** **n=120**			
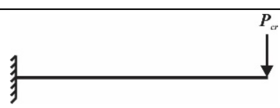	196.5	201.2	202.9	**204.3**	0.96	0.98	0.99
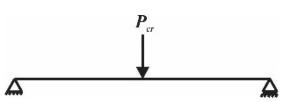	159.6	163.6	165.1	**166.3**	0.96	0.98	0.99
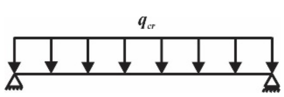	136.8	138.2	138.7	**139.1**	0.98	0.99	1.00
	123.5	123.5	123.5	**123.5**	1.00	1.00	1.00
	304.2	318.1	322.9	**326.8**	0.93	0.97	0.99

Table 3.4 Comparison between buckling moments (kNm) predicted by SM-X, SM-M and SM-N elements (120 elements were taken in all cases)

Problem	**SM-X Lower Bound**	**SM-M**	**SM-N Upper Bound**
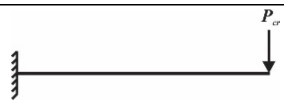	204.3	**206.4**	208.0
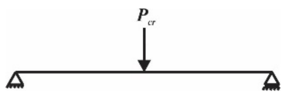	166.3	**167.9**	169.9
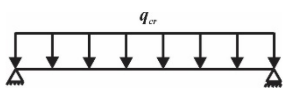	139.1	**139.6**	140.4
	123.5	**123.5**	123.5
	326.8	**332.7**	338.8

Table 3.5 Comparison between the features of the SM-N, SM-M, and SM-X elements

	SM-N	**SM-M**	**SM-X**
Advantage compared to the classical BG element (Barsoum and Gallagher (1970))	Account for shear deformation		
Advantage compared to shear deformable WM element (Wu and Mohareb (2011b))	Avoids shear locking		
Additional advantages compared to other elements in the present study	Is guaranteed to converge from above	Fast-converging element	Is guaranteed to converge from below
Disadvantages compared to other elements in the present study	Slow convergence compared to SM-M and SM-X	Cannot be guaranteed to converge from below or from above	Slower convergence compared to SM-M

3.9.3 Example 3: Effect of lateral and torsional restraints on buckling capacity of beams

A 4m span simply supported beam with a W250x45 cross-section is subject to reverse end moments as shown in Figure 3-6. Five bracing scenarios were considered: Case 1 involved a lateral restraints at shear center $(u_b = 0)$, Case 2 involved a lateral restraint at the bottom flange i.e., $\left[\theta_{zb}(d/2) - u_b = 0\right]$, Case 3 involved a lateral restraint at the top flange, i.e., $\left[\theta_{zb}(d/2) + u_b = 0\right]$, Case 4 involved a torsional restraint, i.e., $(\theta_{zb} = 0)$ and Case 5 considered torsional and lateral restraints at shear center, i.e., $(u_b = 0, \theta_{zb} = 0)$. All constraints were used to form the matrix of coefficients $[P]$ introduce in Eqs. (3.21)-(3.23) and the resulting constrained eigenvalue problem was solved to yield the critical load combinations. Results are illustrated in Table 3.6. For each scenario, five solutions based on SM-X, SM-M, SM-N, BG elements and ABAQUS B31OS element are provided.

According to ABAQUS documentation[1], B31OS is listed among Timoshenko-type beam elements, in which the flexural shear stiffness values are internally computed from user-input section geometries. It is the authors' experience (e.g., Hjaji and Mohareb (2014)) that shear deformation effects within the element are limited to flexural shear and the element omits shear deformation effects due to non-uniform warping.

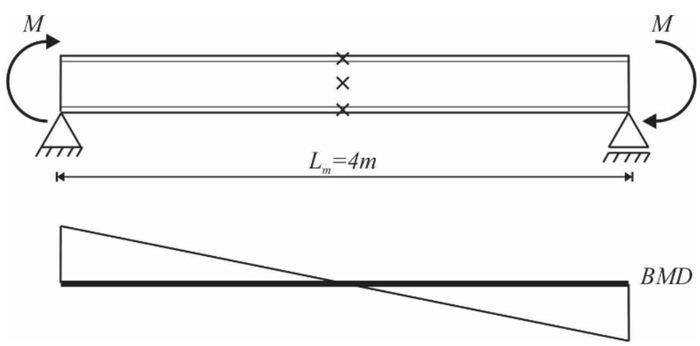

Figure 3-6 Simply supported beam restrained at mid-span subject to reverse end moments

[1] ABAQUS 6.12, Analysis User's Manual, Volume VI: Elements, Section 29.3.3-3

Table 3.6 Critical moments (kNm) for various mid-span constraints

Constraint Type	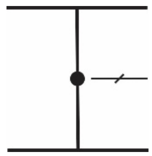	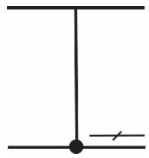	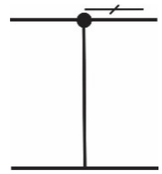	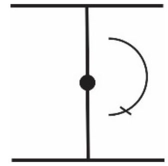	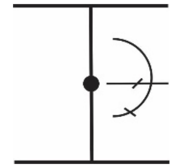
Equation	$u_b = 0$	$\theta_{zb}\left(d/2\right) - u_b = 0$	$\theta_{zb}\left(d/2\right) + u_b = 0$	$\theta_{zb} = 0$	$u_b = 0$ $\theta_{zb} = 0$
Lower bound I (8 SM-X elements)	355.2	362.8	362.8	734.6	873.0
Lower bound II (48 SM-X elements)	429.6	490.9	490.9	865.4	1053
(8 SM-M elements)	**442.9**	**508.5**	**508.5**	**891.3**	**1075**
Upper bound I (48 SM-N elements)	470.6	539.1	539.1	929.3	1115
Upper bound II (8 SM-N elements)	591.8	676.8	676.8	1123	1290
ABAQUS B31OS (40 elements)	451.7	518.2	518.2	906.6	1099
BG (8 elements)	452.7	519.4	519.4	908.8	1106
SM-M/B31OS	**98.0%**	**98.1%**	**98.1%**	**98.3%**	**98.0%**

Results based on the SM-X, SM-M and SM-N elements (which capture shear deformation due to bending and warping) are compared with those predicted by the ABAQUS B31OS element (which captures shear deformation effects due to bending, but neglects shear deformation effects due to warping) and those based on the BG element (neglecting both shear deformation effects due to bending and warping).

Eight elements were needed for convergence under the SM-M and BG solutions while 40 B31OS elements were needed to attain convergence. Results based on the SM-M are shown to agree well with those based on the B31OS solution.

On average, the SM-M solution is observed be about 2.0% less than the B31OS solution and 2.2% less than the BG solution. The difference is attributed to shear deformation which is entirely captured in the SM-M element, only in part in the B31OS, and neglected in the BG element. In all cases, taking 8 SM-N and 8 SM-X elements is observed to respectively provide upper and lower bounds for the 8 SM-M solutions. Also, improved upper and lower bounds were observed by taking 48 SM-N and SM-X elements, thus narrowing the band between both bounds.

Restraining the bottom or top flanges (Cases 2 and 3) laterally is observed to increase the buckling capacity of the beam more than the case where the shear center is laterally restrained (Case 1). As expected, restraining the shear center both laterally and torsionally (Case 5) is found to significantly increase the buckling load by more than twice the capacity compared to the case where no restraints are provided. Restraining the section torsionally (Case 4) is observed to be more effective in increasing the buckling capacity compared to cases where either the shear center or one of the flanges is laterally restrained (Cases 1-3). Figure 3-7 depicts the lateral buckling displacements for the top and bottom flanges for all five cases as calculated by the expressions $u_b \pm \theta_b \left(h/2 \right)$ versus the longitudinal coordinate *z*. In all cases, the buckling mode shapes were normalized with respect to the peak flange displacement. In Cases 1 and 5, the average top and bottom displacements (or mid-height) at mid-span, vanishes given the presence of a lateral restraint at mid-height. Also, for Cases 4 and 5, the top and bottom flange displacements are equal since twist was restrained in both cases. For Case 2, it is clear that the bottom flange is successfully restrained at mid-span. Also, in Case 3, the mid-span top flange was restrained. In Case 1, the peak flange displacements take place near $z = 1.5m$ and $2.5m$. It is also shown that, when one of the flanges is laterally restrained (Cases 2 and 3), the peak lateral displacement occurs at about $z = 2.5m$. The maximum lateral displacements for Cases 4 and 5 are observed at nearby $z = 1m$ and $z = 3m$.

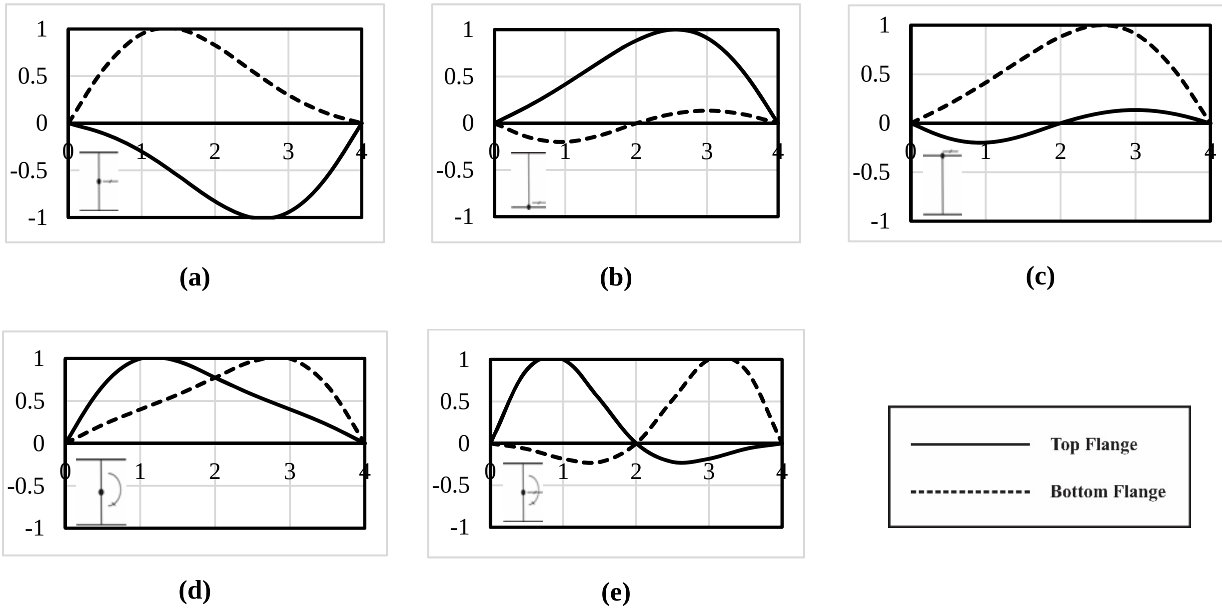

Figure 3-7 Normalized lateral displacement of the top flange and the bottom flange along the span (m) for various mid-span constraints: (a) Case 1, (b) Case 2, (c) Case 3, (d) Case 4 and (e) Case 5

3.9.4 Example 4: Effect of the lateral brace height on the critical moment

Among studies present in the literature review, the work of Powel and Klingner (1970), Kitipornchai and Richter (1978), Kitipornchai et al. (1984), Assadi and Roeder (1985) and Wang et al. (1995) investigated the effect of rigid lateral or torsional discrete intermediate restraints on LTB capacity of beams. Lateral restraints in these studies were assumed to act at the shear center. In practice, I-girders can be laterally restrained at various locations along the height. Thus, the present example aims at quantifying the effect of bracing height on the LTB resistance of beams. The simply supported beam investigated in the previous example is revisited here while considering mid-span lateral restraints located at various heights h relative to the shear center within the range $-d/2 \leq h \leq d/2$, in which d is the depth of cross-section (Figure 3-8). The resulting critical moments are normalized with respect to the solution based on $h = 0$ (i.e., the case of shear center lateral restraint). For the case of the reverse moments, the most effective bracing location is found to be at either flange while mid-height bracing is observed to be the least effective. The case of flange bracing corresponds to a 15% increase in the critical moments when compared to that of mid-height bracing.

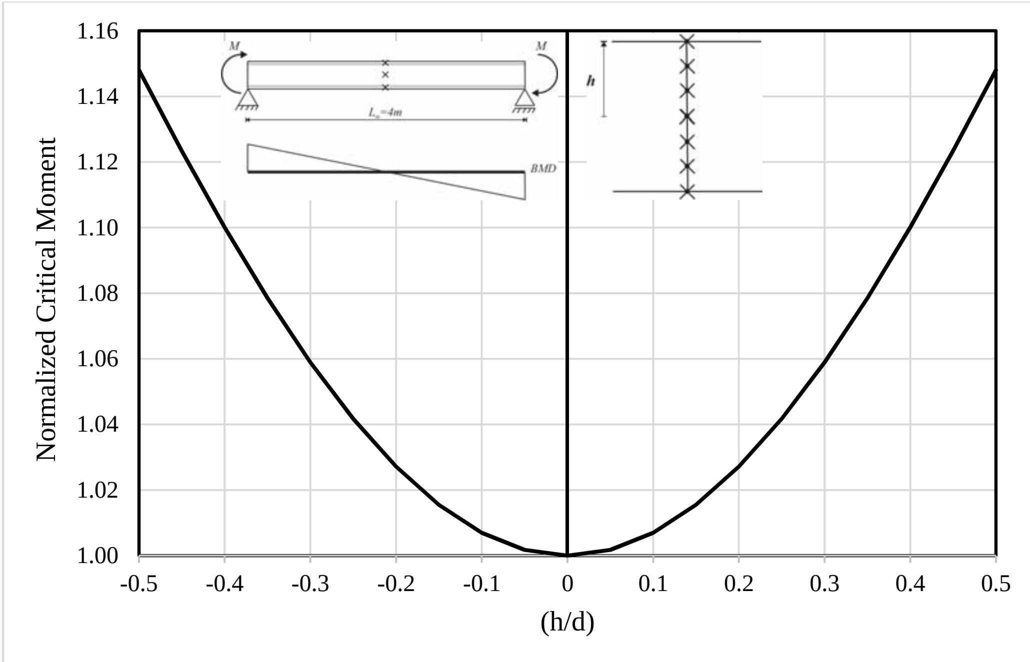

Figure 3-8 Effect of constraint's location on critical moment for a simply supported beam of 4m span

3.9.5 Example 5: Effect of mid-span restraints on buckling capacity of continuous beams

An evaluation of the effect of lateral and torsional restraints at the interior supports on the buckling capacity of a continuous beam is of practical importance. A two-span continuous beam with 8m spans [Figure 3-9(b)] is investigated in this example. As a reference case for comparison, another 8m span simply supported beam is also considered [Figure 3-9(a)]. Both beams are subjected to uniformly distributed loads. Four cases of lateral and/or torsional restraints are considered for the interior support [(Figure 3-9(c)]: (1) No lateral nor torsional restraints, (2) only a lateral restraint at the shear center, (3) only a torsional restraint, and (4) both lateral and torsional restraints.

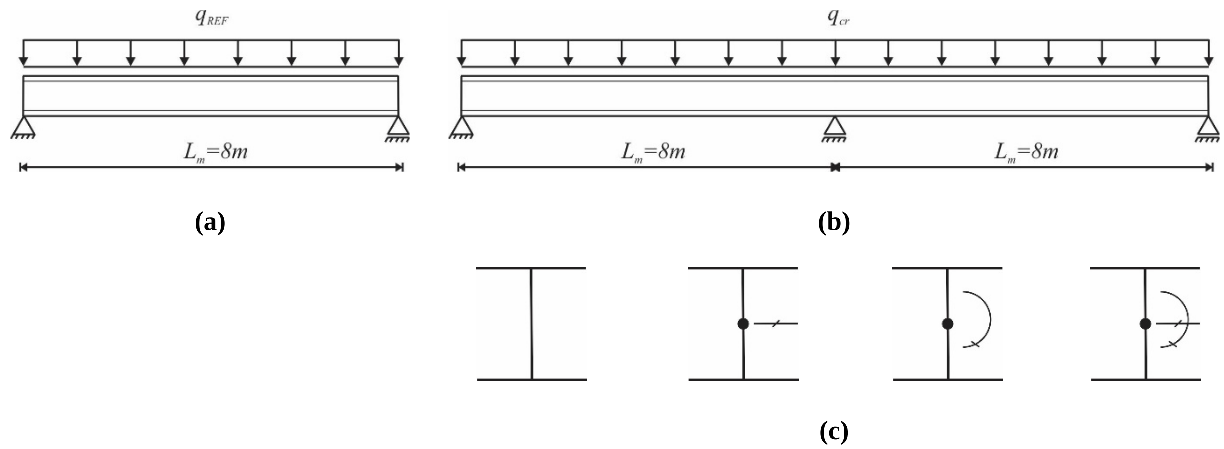

Figure 3-9 (a) Reference case, (b) Multi-span beam used for cases (1) to (4) and (c) Cross-sections at middle support for various cases (1) to (4)

Table 3.7 provides the critical loads based on 8 SM-M elements for each span. The critical load of the continuous two-span beam with no lateral nor twist restraint at the intermediate support (Case 1) is 8.9 kN, which is l2% less than that of the simply supported beam. The presence of a lateral support at the middle support (Case 2) is observed to marginally increase the buckling capacity (i.e., by 2%) of the continuous beam compared to the unrestrained case (Case 1). In contrast, the presence of a torsional brace (Case 3) is observed to significantly increase the lateral-torsional capacity compared to Case 1. The presence of both restraints (lateral and torsional) in Case 4 yields the same critical moment as that in Case 3. The comparison suggests that the presence of a torsional restraint at the intermediate support is most effective in increasing the LTB resistance of the continuous beam considered.

For the simply supported beam (i.e., the reference case), the critical load as predicted by 8 SM-M elements is 10.1 kN/m. Taking 8 SM-X elements provides a lower bound prediction of 9.39 kN/m for the critical load, while 8 SM-N elements provides an upper bound prediction of 10.9 kN/m. As observed in Example 3, increasing the number of elements leads to improved lower and upper predictions. For instance, by taking 24 elements, the critical load prediction is bounded between 9.69 kN/m and 10.2 kN/m.

Table 3.7 Summary of buckling loads for the reference case and cases (1) to (4) – Based on SM-M element

	# of Span(s)	Lateral restraint	Torsional restraint	$q_{cr}\,(kN/m)$	$q_{REF}\,(kN/m)$	q_{cr}/q_{REF}
Reference Case	1	N/A	N/A	-	10.1	1.0
Case (1)	2	✗	✗	8.90	-	0.88
Case (2)	2	✓	✗	9.10	-	0.90
Case (3)	2	✗	✓	20.2	-	2.0
Case (4)	2	✓	✓	20.2	-	2.0

3.9.6 Example 6: Effect of shear deformation

The cantilever beam problem in Example 1 is re-considered. The span is varied from 0.2m to 3.0m. The critical loads are obtained based on the SM-M, B31OS and BG elements. The results are illustrated in Table 3.8 and depicted in Figure 3-10.

Table 3.8 Critical loads $P_{cr}\,(kN)$ for various spans

L (m)	SM-M Element	B31OS Element	BG Element
0.2	135,400	150,000	292,800
0.4	28,820	29,580	37,250
0.6	10,010	10,140	11,340
0.8	4,598	4,640	4,955
1.0	2,510	2,528	2,640
1.2	1,536	1,546	1,594
1.4	1,019	1,025	1,049
1.6	716.3	720.8	733.7
1.8	526.8	530.11	537.7
2.0	401.2	403.7	408.5
2.2	314.2	316.2	319.3
2.4	251.8	253.4	255.4
2.6	205.6	206.9	208.3
2.8	170.6	171.7	172.7
3.0	143.5	144.4	145.2

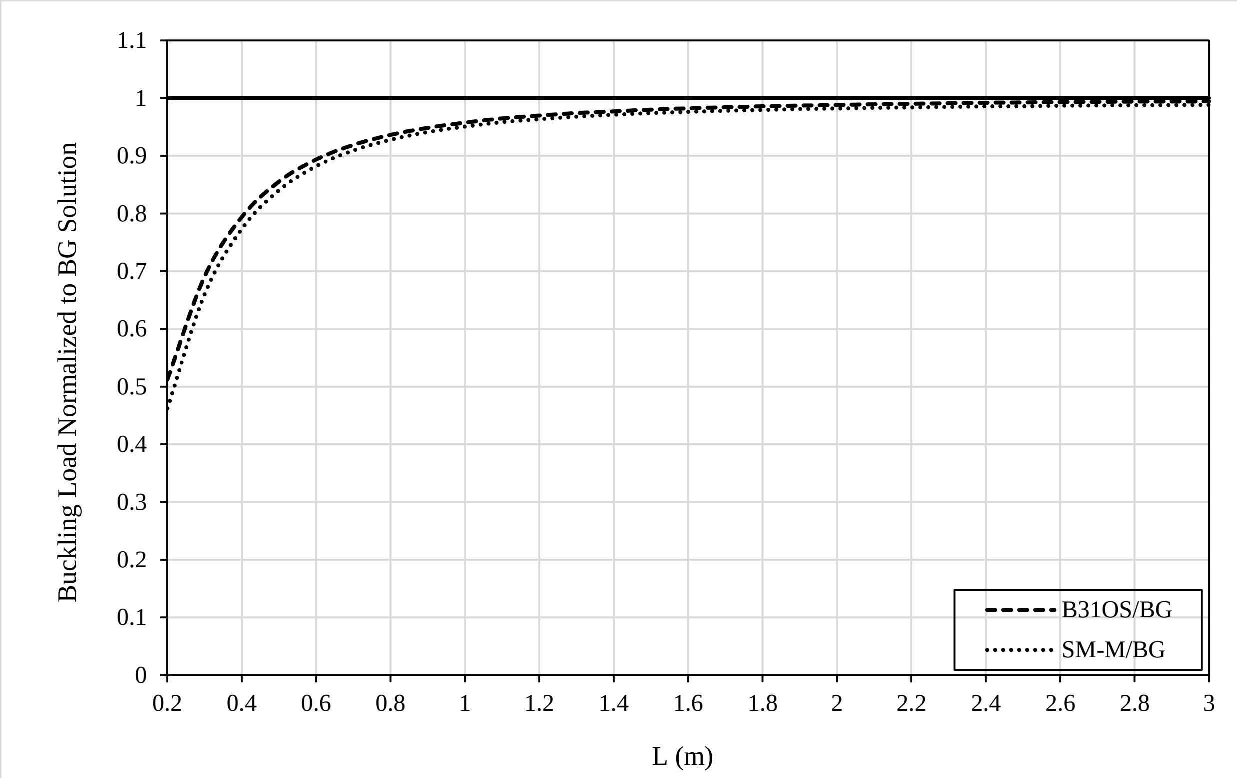

Figure 3-10 Normalized LTB loads for the cantilever example

As the span decreases, the difference between the non-shear deformable BG element predictions and the SM-M predictions is observed to increase since shear deformation effects become pronounced for shorter spans. The SM-M predictions are observed to be slightly below the shear deformable critical load predictions of the B31OS element. As discussed in Example 3, this is attributed to the fact that the B31OS element captures the effect of shear deformation due to bending, but omits shear deformation effects due to warping. In contrast, both features are incorporated in the SM-M formulation. For spans shorter than 0.6m, the ratio of the critical loads based on the SM-M element to those based on the BG element is less than 90%, highlighting the importance of shear deformation effects for short span members.

3.10 Summary and conclusions

1. A new family of three finite elements was developed for the lateral-torsional buckling analysis of beams with doubly-symmetric cross-sections. The elements capture warping torsion, shear deformation, and load position effects.

2. The results based on the three elements were in an excellent agreement with those based on shear deformable WM element (Wu and Mohareb (2011b)) and successfully avoid shear locking phenomena. Very good agreement is also observed with the B31OS ABAQUS element and the non-shear deformable Barsoum and Gallagher (1970) element for long span members.
3. A large number of numeric examples have shown that two of the elements are successful in bounding buckling load estimates. In all cases, mesh refinements are observed in narrowing the bounds for the predicted buckling load.
4. The SM-M element is observed to provide the fastest converging solution with a remarkably small number of degrees of freedom compared to the SM-N and SM-X and WM shear deformable element (Wu and Mohareb (2011b)) and is thus recommended if the analyst is seeking computational efficiency.
5. Within the limitations of the formulation, discretization errors in the SM-X element consistently provide lower bound estimates for the buckling loads. Element SM-X is recommended for design situations where the designer would rather err on the conservative side.
6. For the simply supported beam under full reverse moments considered, it was shown that torsional restraint at mid-span is most effective in increasing the LTB capacity compared to shear center or flange lateral restraints. Providing torsional and lateral restraints was observed to increase the buckling capacity by more than twofold compared to the case of no lateral and torsional restraints.
7. For the same problem, a brace at one of the flanges was shown to increase the LTB capacity of the beam by 15% compared to the case of web mid-height bracing.
8. At intermediate supports of two-span beams, the presence of torsional restraints was observed to significantly improve the lateral-torsional buckling capacity of continuous beams compared to lateral restraints and compared to the case of no lateral nor torsional restraints.

Acknowledgements

The authors gratefully acknowledge financial support from the Natural Sciences and Engineering Research Council (NSERC) of Canada.

3.11 Appendix A. Evaluating the simplifying assumption made to develop shape functions

This section provides a numeric example assessing the assumption made in formulating shape functions regarding the neglect of pre-buckling internal forces. Assuming constant pre-buckling internal as shown in Figure 3-2(b), Eq. (3.5) can be rewritten in a non-dimensional form as follows

$$\left[\begin{array}{c:c:c:c}
-\left(1+\dfrac{\lambda\bar{N}_p}{GD_{xx}}\right)\dfrac{d^2}{d\xi^2} & \dfrac{d}{d\xi} & \begin{array}{c}\left(\dfrac{\lambda\bar{M}_{xp}}{LGD_{xx}}\right)\dfrac{d^2\theta_{zb}}{d\xi^2}\\ +\left(\dfrac{\lambda\bar{V}_{yp}}{GD_{xx}}\right)\dfrac{d\theta_{zb}}{d\xi}\end{array} & 0 \\ \hdashline
\dfrac{d}{d\xi} & \dfrac{EI_{yy}}{GD_{xx}L^2}\dfrac{d^2}{d\xi^2}-1 & \dfrac{\lambda q_z y_{qz}}{GD_{xx}} & 0 \\ \hdashline
\begin{array}{c}\left(\dfrac{\lambda\bar{M}_{xp}}{LGD_{xx}}\right)\dfrac{d^2\theta_{zb}}{d\xi^2}\\ +\left(\dfrac{\lambda\bar{V}_{yp}}{GD_{xx}}\right)\dfrac{d\theta_{zb}}{d\xi}\end{array} & \dfrac{-\lambda q_z y_{qz}}{GD_{xx}} & \begin{array}{c}\dfrac{\lambda q_y y_{qy}}{GD_{xx}}+\left[-\dfrac{\left(J+D_{hh}\right)}{D_{xx}L^2}\right.\\ \left.-\lambda\bar{N}_p\dfrac{\left(I_{xx}+I_{yy}\right)}{GD_{xx}AL^2}\right]\end{array} & -\left(\dfrac{D_{hh}}{L^2D_{xx}}\right)\dfrac{d}{d\xi} \\ \hdashline
0 & 0 & -\left(\dfrac{D_{hh}}{L^2D_{xx}}\right)\dfrac{d}{d\xi} & \begin{array}{c}\dfrac{EI_{\omega\omega}}{D_{xx}L^4}\dfrac{d^2}{d\xi^2}\\ -\dfrac{D_{hh}}{L^2D_{xx}}\end{array}
\end{array}\right]\begin{Bmatrix}\dfrac{u_b}{L}\\ \theta_{yb}\\ \theta_{zb}\\ L\psi_b\end{Bmatrix}\approx\begin{Bmatrix}0\\0\\0\\0\end{Bmatrix} \tag{3.24}$$

in which $D = d/dz = d/Ld\xi$ is the first derivative of displacement fields with respect to the dimensionless coordinate $\xi = z/L$. It can be shown that for practical geometries, the term $\lambda\bar{N}_p/GD_{xx}$ in the first entry of the first equation in Eq. (3.24), is negligible compared to unity. Also, the terms $\lambda\bar{M}_{xp}/LGD_{xx}$ and $\lambda\bar{V}_{yp}/GD_{xx}$ in the third entry of the first equation are also negligible compared to the zero value. In a similar manner, the term located in the third row and third column including $\lambda\bar{N}_p\left(I_{xx}+I_{yy}\right)/GD_{xx}AL^2$ is found insignificant compared to $\left(J+D_{hh}\right)/D_{xx}L^2$. To numerically illustrate the above statements for practical problems, consider a simply supported member (cross-section is W250x45 and member span is taken as

$L_m = 120 r_y = 4189\ mm$), subject to a compressive axial force [Case (a) in Figure 3-11] and uniform bending moments [Case (b) in Figure 3-11]. To get an indication of the magnitude of the shear force involved, we also consider another loading case [Case (c) in Figure 3-11] which involves no axial force but equal reverse moments (thus inducing a linear moment gradient, or constant shear). Since no transverse forces offset from the shear center and no axial forces offset from the section centroid are applied, the terms $\left(\lambda q_y y_{qy}\right)$ and $\left(\lambda q_z y_{qz}\right)$ are omitted.

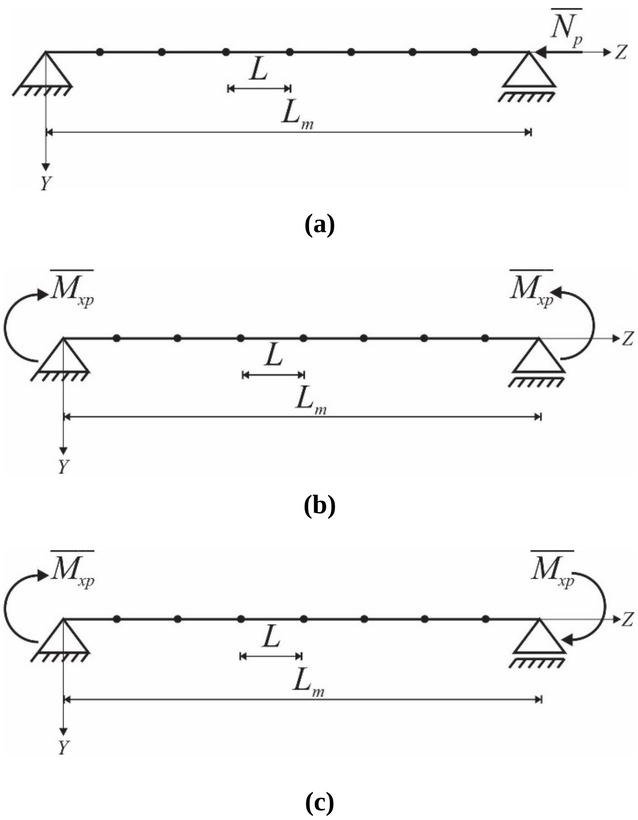

Figure 3-11 (a) Elevation of the beam under axial load, (b) Elevation of the beam under uniform bending moments, (c) Elevation of the beam under reverse bending moments

In Case (1), in the absence of bending moments, the buckling load predicted by the classical solution, would be $\overline{N}_p = \pi^2 EI_{yy} / L_m^2 = 791\ kN$. Also, in Case (2) in the absence of axial force and according to the classical solution, the critical buckling moment of the beam would be $\overline{M}_{xp} = \pi / L_m \sqrt{EI_{yy}\left(GJ + EI_{\omega\omega}\,\pi^2 / L_m^2\right)} = 160\ kNm$. For Case (3), the critical moment is given by $\lambda \overline{M}_{xp} = C_b \lambda \overline{M}_{xp}$, where C_b is a moment gradient factor ($C_b = 2.27$ for this case) given by AISC (2010), $C_b = \left(12.5 M_{\max}\right) / \left(2.5\left|M_{\max}\right| + 3\left|M_{L/4}\right| + 4\left|M_{L/2}\right| + 3\left|M_{3L/4}\right|\right)$, in which $M_{\max}$ is the maximum bending moment along the beam, $M_{L/4}$, $M_{L/2}$ and $M_{3L/4}$ are bending moments at the quarter, mid-point and three-quarter points of the beam span, respectively. The corresponding shear is given by $\lambda\bar{V}_{yp} = 2\lambda\bar{M}_{xp}/L_m = 2C_b\lambda\bar{M}_{xp}/L_m = 173\ kN$. Table 3.9 summarizes the numeric values and corresponding approximations considered for the relevant matrix entries.

Table 3.9 Justification of assumption made to obtain shape functions

Entry*	**Expression**	**Values and Comments**	**Approximation**
1,1	$-\left(1+\frac{\lambda\bar{N}_p}{GD_{xx}}\right)\frac{d^2}{d\xi^2}\left(\frac{u_b}{L}\right)$	$\lambda\bar{N}_p/GD_{xx} = 2.7\times10^{-3}$ (negligible compared to unity)	$-\frac{d^2}{d\xi^2}\left(\frac{u_b}{L}\right)$
1,3	$\left(\frac{\lambda\bar{M}_{xp}}{LGD_{xx}}\right)\frac{d^2\theta_{zb}}{d\xi^2}+\lambda\left(\frac{\bar{V}_{yp}}{GD_{xx}}\right)\frac{d\theta_{zb}}{d\xi}$	$\lambda\bar{M}_{xp}/LGD_{xx} = 5.4\times10^{-4}/L$ $\lambda\bar{V}_{yp}/GD_{xx} = 5.8\times10^{-4}$ (negligible terms)	0
3,3	$-\left[\frac{(J+D_{hh})}{D_{xx}L^2}+\lambda\bar{N}_p\frac{(I_{xx}+I_{yy})}{GD_{xx}AL^2}\right]$	$(J+D_{hh})/D_{xx}L^2$ $=1.6\times10^{-2}/L^2$ $\lambda\bar{N}_p(I_{xx}+I_{yy})/GD_{xx}AL^2$ $=3.7\times10^{-5}/L^2$ $<<(J+D_{hh})/D_{xx}L^2$	$\left[-\frac{(J+D_{hh})}{D_{xx}L^2}\right]\frac{d^2\theta_{zb}}{d\xi^2}$

* e.g., Entry (1,3) denotes the third term in the first row in Eq. (3.24)

The above approximations lead to the following simplified system of equilibrium equations

$$\left[\begin{array}{c:c:c:c} -\frac{d^2}{d\xi^2} & \frac{d}{d\xi} & 0 & 0 \\ \hdashline \frac{d}{d\xi} & \frac{EI_{yy}}{GD_{xx}L^2}\frac{d^2}{d\xi^2}-1 & 0 & 0 \\ \hdashline 0 & 0 & -\frac{(J+D_{hh})}{D_{xx}L^2}\frac{d^2}{d\xi^2} & -\left(\frac{D_{hh}}{L^2D_{xx}}\right)\frac{d}{d\xi} \\ \hdashline 0 & 0 & -\left(\frac{D_{hh}}{L^2D_{xx}}\right)\frac{d}{d\xi} & \frac{EI_{\omega\omega}}{D_{xx}L^4}\frac{d^2}{d\xi^2}-\frac{D_{hh}}{L^2D_{xx}} \end{array}\right]\begin{Bmatrix} \frac{u_b}{L} \\ \theta_{yb} \\ \theta_{zb} \\ L\psi_b \end{Bmatrix} \approx \begin{Bmatrix} 0 \\ 0 \\ 0 \\ 0 \end{Bmatrix} \tag{3.25}$$

which are the non-dimensional form of Eqs. (3.10)a-b used to obtain the shape functions.

3.12 Appendix B. Matrices needed to determine stiffness matrices

This appendix provides explicit expressions for matrices stiffness components. In Eq. (3.20), the elastic stiffness matrix components $\left[K_f\right],\left[K_{sv}\right],\left[K_s\right]$ and geometric stiffness components $\left[K_G\right]_N,\left[K_G\right]_M,\left[K_G\right]_V,\left[K_G\right]_{qy},\left[K_G\right]_{qz}$ were expressed as functions of matrices $\left[M_1\right],\left[M_2\right],...,\left[M_8\right]$. Matrices $\left[M_1\right],\left[M_2\right],...,\left[M_8\right]$ are provided as follows:

Elastic stiffness due to flexural stresses

Matrix $\left[M_1\right]$ related to $\left[K_f\right]$ is given by

$$\left[M_1\right]=EI_{yy}\left[\begin{array}{c|c}\left[S_1\right]_{4\times4} & \left[0\right]_{4\times4}\\ \hline \left[0\right]_{4\times4} & \left[S_2\right]_{4\times4}\end{array}\right],\ \left[S_1\right]=\begin{bmatrix}0&0&0&0\\ &0&0&0\\ &&4L&6L^2\\ Sym.&&&12L^3\end{bmatrix},\ \left[S_2\right]=\begin{bmatrix}0&0&0&0\\ &0&0&0\\ &&\bar{a}_{3,3}&\bar{a}_{3,4}\\ Sym.&&&\bar{a}_{4,4}\end{bmatrix}$$

(3.26)a-c

in which function $\bar{a}_{i,j}$ is defined as

$$\bar{a}_{i,j}=\frac{I_{\omega\omega}m_i^2m_j^2\left(e^{L\left(m_i+m_j\right)}-1\right)\left(D_{hh}+J\right)^2}{D_{hh}^2\left(m_i+m_j\right)I_{yy}} \tag{3.27}$$

Elastic stiffness due to Saint-Venant shear stresses

Matrix $\left[M_2\right]$ related to $\left[K_{sv}\right]$ is given by

$$\left[M_2\right]=GJ\left[\begin{array}{c|c}\left[0\right]_{4\times4} & \left[0\right]_{4\times4}\\ \hline \left[0\right]_{4\times4} & \left[S_3\right]_{4\times4}\end{array}\right],\quad \left[S_3\right]=\begin{bmatrix}0&0&0&0\\ &L&\bar{b}_3&\bar{b}_4\\ &&\bar{c}_{3,3}&\bar{c}_{3,4}\\ Sym.&&&\bar{c}_{4,4}\end{bmatrix} \tag{3.28)a-b$$

in which functions $\bar{b}_i$ and $\bar{c}_{i,j}$ are defined as

$$\bar{b}_i=e^{Lm_i}-1,\quad \bar{c}_{i,j}=\frac{m_im_j\left(e^{L\left(m_i+m_j\right)}-1\right)}{m_i+m_j} \tag{3.29)a-b$$

3.12.1 Elastic stiffness due to other shear stresses

Matrix $\left[M_3\right]$ related to $\left[K_s\right]$ is given by

$$\left[M_3\right]=\left[\begin{array}{c:c}\left[S_4\right]_{4\times4} & \left[0\right]_{4\times4}\\ \hdashline \left[0\right]_{4\times4} & \left[S_5\right]_{4\times4}\end{array}\right],\ \left[S_4\right]=\begin{bmatrix}0 & 0 & 0 & 0\\ & 0 & 0 & 0\\ & & 0 & 0\\ Sym. & & & \bar{\alpha}\end{bmatrix},\ \left[S_5\right]=\begin{bmatrix}0 & 0 & 0 & 0\\ & 0 & 0 & 0\\ & & \bar{d}_{3,3} & \bar{d}_{3,4}\\ Sym. & & & \bar{d}_{4,4}\end{bmatrix} \qquad \text{(3.30)a-c}$$

in which function $\bar{d}_{i,j}$ and constant $\bar{\alpha}$ are defined as

$$\bar{d}_{i,j}=\frac{GJ^2m_im_j\left(e^{L\left(m_i+m_j\right)}-1\right)}{D_{hh}\left(m_i+m_j\right)},\quad \bar{\alpha}=\frac{36E^2I_{yy}{}^2L}{GD_{xx}} \qquad \text{(3.31)a-b}$$

3.12.2 Geometric stiffness due to normal forces

Matrix $\left[M_4\right]$ related to $\left[K_G\right]_N$ is given by

$$\left[M_4\right]=N\left[\begin{array}{c:c}\left[S_6\right]_{4\times4} & \left[0\right]_{4\times4}\\ \hdashline \left[0\right]_{4\times4} & \left[S_7\right]_{4\times4}\end{array}\right],\left[S_6\right]=\begin{bmatrix}0 & 0 & 0 & 0\\ & L & L^2 & L^3\\ & & \frac{4L^3}{3} & \frac{3L^4}{2}\\ Sym. & & & \frac{9L^5}{5}\end{bmatrix},\left[S_7\right]=\begin{bmatrix}0 & 0 & 0 & 0\\ & \bar{\beta} & \bar{e}_3 & \bar{e}_3\\ & & \bar{f}_{3,3} & \bar{f}_{3,4}\\ Sym. & & & \bar{f}_{4,4}\end{bmatrix}$$

(3.32)a-c

in which functions $\bar{e}_i$, $\bar{f}_{i,j}$ and constant $\bar{\beta}$ are defined as

$$\bar{e}_i=\frac{\left(e^{Lm_i}-1\right)\left(I_{xx}+I_{yy}\right)}{A},\quad \bar{f}_{i,j}=\frac{m_im_j\left(e^{L\left(m_i+m_j\right)}-1\right)\left(I_{xx}+I_{yy}\right)}{A\left(m_i+m_j\right)},\quad \bar{\beta}=\frac{L\left(I_{xx}+I_{yy}\right)}{A} \qquad \text{(3.33)a-c}$$

3.12.3 Geometric stiffness due to bending moments

Matrix $\left[M_5\right]$ related to $\left[K_G\right]_M$ is given by

$$\left[M_5\right]=M\left[\begin{array}{c:c}\left[0\right]_{4\times4} & \left[S_8\right]_{4\times4}\\ \hdashline \left[S_8\right]_{4\times4}^T & \left[0\right]_{4\times4}\end{array}\right],\quad \left[S_8\right]=\begin{bmatrix}0 & 0 & 0 & 0\\ 0 & 0 & 0 & 0\\ 2L & L^2 & \bar{g}_3 & \bar{g}_4\\ 3L^2 & \left(2L^3+\dfrac{6EI_{yy}L}{GD_{xx}}\right) & \bar{h}_3 & \bar{h}_4\end{bmatrix} \tag{3.34)a-b}$$

in which functions $\bar{g}_i$ and $\bar{h}_i$ are defined as

$$\bar{g}_i=\frac{2\left(e^{Lm_i}-1\right)}{m_i},\quad \bar{h}_i=6\left(\frac{1}{m_i^{\,2}}+\frac{e^{Lm_i}\left(Lm_i-1\right)}{m_i^{\,2}}\right)+\frac{6EI_{yy}\left(e^{Lm_i}-1\right)}{GD_{xx}} \tag{3.35)a-b}$$

3.12.4 Geometric stiffness due to shear forces

Matrix $\left[M_6\right]$ related to $\left[K_G\right]_V$ is given by

$$\left[M_6\right]=V\left[\begin{array}{c:c}\left[0\right]_{4\times4} & \left[S_9\right]_{4\times4}\\ \hdashline \left[S_9\right]_{4\times4}^T & \left[0\right]_{4\times4}\end{array}\right],\quad \left[S_9\right]=\begin{bmatrix}0 & 0 & 0 & 0\\ 0 & 0 & 0 & 0\\ 0 & 0 & 0 & 0\\ \dfrac{6EI_{yy}L}{GD_{xx}} & \dfrac{3EI_{yy}L^2}{GD_{xx}} & \bar{k}_3 & \bar{k}_4\end{bmatrix} \tag{3.36)a-b}$$

in which function $\bar{k}_i$ is defined as

$$\bar{k}_i=-\frac{6EI_{yy}\left(e^{Lm_i}-1\right)}{GD_{xx}m_i} \tag{3.37}$$

3.12.5 Geometric stiffness due to distributed transverse load

Matrix $\left[M_7\right]$ related to $\left[K_G\right]_{qy}$ is given by

$$\left[M_7\right]=q_y y_{qy}\left[\begin{array}{c:c}\left[0\right]_{4\times4} & \left[0\right]_{4\times4}\\ \hdashline \left[0\right]_{4\times4} & \left[S_{10}\right]_{4\times4}\end{array}\right],\quad \left[S_{10}\right]=\begin{bmatrix}L & \dfrac{L^2}{2} & \bar{l}_3 & \bar{l}_4\\ & \dfrac{L^3}{3} & \bar{n}_3 & \bar{n}_4\\ & & \bar{o}_{3,3} & \bar{o}_{3,4}\\ Sym. & & & \bar{o}_{4,4}\end{bmatrix} \tag{3.38)a-b}$$

in which functions $\overline{l}_i$, $\overline{n}_i$ and $\overline{o}_{i,j}$ are defined as

$$\overline{l}_i = \frac{e^{Lm_i} - 1}{m_i}, \quad \overline{n}_i = \frac{1}{m_i^2} + \frac{e^{Lm_i}\left(Lm_i - 1\right)}{m_i^2}, \quad \overline{o}_{i,j} = \frac{e^{L\left(m_i + m_j\right)} - 1}{m_i + m_j} \tag{3.39)a-c}$$

3.12.6 Geometric stiffness due to distributed axial load

Matrix $\left[M_8\right]$ related to $\left[K_G\right]_{qz}$ is given by

$$\left[M_8\right] = q_z y_{qz} \left[\begin{array}{c|c} \left[0\right]_{4\times4} & \left[S_{11}\right]_{4\times4} \\ \hline \left[S_{11}\right]_{4\times4}^T & \left[0\right]_{4\times4} \end{array}\right], \quad \left[S_{11}\right] = \begin{bmatrix} 0 & 0 & 0 & 0 \\ -L & \dfrac{-L^2}{2} & \overline{p}_3 & \overline{p}_4 \\ -L^2 & \dfrac{-2L^2}{3} & \overline{q}_3 & \overline{q}_4 \\ \overline{\gamma} & \overline{\varepsilon} & \overline{r}_3 & \overline{r}_4 \end{bmatrix} \tag{3.40)a-b}$$

in which functions $\overline{p}_i$, $\overline{q}_i$, $\overline{r}_i$ and constants $\overline{\gamma}$ and $\overline{\varepsilon}$ are defined as

$$\begin{gathered} \overline{p}_i = \frac{\left(e^{Lm_i} - 1\right)}{m_i}, \quad \overline{q}_i = -2\left(\frac{1}{m_i^2} + \frac{e^{Lm_i}\left(Lm_i - 1\right)}{m_i^2}\right), \quad \overline{\gamma} = \frac{-L\left(GD_{xx}L^2 + 6EI_{yy}\right)}{GD_{xx}} \\ \overline{r}_i = 3\left(\frac{2}{m_i^3} - \frac{e^{Lm_i}\left(L^2 m_i^2 - 2Lm_i + 2\right)}{m_i^3}\right) - \frac{6EI_{yy}\left(e^{Lm_i} - 1\right)}{GD_{xx}m_i}, \quad \overline{\varepsilon} = \frac{-3L^2\left(GD_{xx}L^2 + 4EI_{yy}\right)}{4GD_{xx}} \end{gathered} \tag{3.41)a-e}$$

3.12.7 Load position matrix for concentrated transverse load

When a member is subject to a concentrated transverse load Q_y applied at $z = z_{Qy}$ and position y_{Qy} relative to the shear center, the load function in Eq. (3.2)g can be expressed as $q_y\left(z\right) = Q_y Dirac\left(z - z_{Qy}\right)$. Substituting this load function into Eq. (3.2)g, one obtains a new geometric stiffness matrix $\left[K_G\right]_{Qy}$ due to load position effect relative to the shear center *SC*. Matrix $\left[M_9\right]$ related to $\left[K_G\right]_{Qy}$ is given by

$$\left[M_9\right]=q_y y_{qy}\left[\begin{array}{c|c}\left[0\right]_{4\times4} & \left[0\right]_{4\times4} \\ \hline \left[0\right]_{4\times4} & \left[S_{12}\right]_{4\times4}\end{array}\right], \quad \left[S_{12}\right]=\begin{bmatrix}1 & z_{Qy} & \overline{s}_3 & \overline{s}_4 \\ & z_{Qy}^2 & \overline{t}_3 & \overline{t}_4 \\ & & \overline{u}_{3,3} & \overline{u}_{3,4} \\ Sym. & & & \overline{u}_{4,4}\end{bmatrix} \qquad \text{(3.42)a-b}$$

in which functions $\overline{s}_i$, $\overline{t}_i$ and $\overline{u}_{i,j}$ are defined as

$$\overline{s}_i=e^{m_i z_{Qy}}, \quad \overline{t}_i=z_{Qy}e^{m_i z_{Qy}}, \quad \overline{u}_{i,j}=e^{z_{Qy}\left(m_i+m_j\right)} \qquad \text{(3.43)a-c}$$

3.13 Notation

A	=	Cross-sectional area
$\left[B(z)\right]$	=	Matrix relating displacement fields to integration constants
$\left\{C_{st}\right\}$	=	Vector of integration constants
D_{hh}, D_{xx}	=	Properties of cross-section related to shear deformation
d	=	Depth of cross-section
$\left\langle d(z)\right\rangle^{T}$	=	Field displacements
E	=	Modulus of elasticity
$\left\{F\right\}$	=	Vector of Lagrange multipliers
G	=	Shear modulus
$\left[H\right]$	=	Matrix relating nodal displacements to integration constants
I_{xx}, I_{yy}	=	Moments of inertia of the cross-section about x-axis and y-axis respectively
$I_{\omega\omega}$	=	Warping Constant
J	=	St. Venant torsional constant
$\left[K_f\right]$	=	Stiffness matrix due to flexural stresses
$\left[K_G\right]_N$	=	Geometric matrix due to normal forces
$\left[K_G\right]_M$	=	Geometric matrix due to bending moments
$\left[K_G\right]_V$	=	Geometric matrix due to shear forces
$\left[K_G\right]_{qy}$	=	Geometric matrix due to load position effect of the distributed transverse load
$\left[K_G\right]_{qz}$	=	Geometric matrix due to load position effect of the distributed axial load
$\left[K_G\right]_{Qy}$	=	Geometric matrix due to load position effect of the concentrated transverse load

$\left[K_s\right]$	=	Stiffness matrix due to other shear stresses
$\left[K_{sv}\right]$	=	Stiffness matrix due to Saint Venant shear stresses
L	=	Length of a finite element
L_m	=	Span of the member
$\left[L(z)\right]$	=	Matrix of shape functions
m_i	=	Roots of quadratic eigenvalue problem
M_1, M_2	=	Internal bending moment at both end of an element
$M_{xp}(z)$	=	Strong axis bending moment as obtained from pre-buckling analysis
N_1, N_2	=	Internal normal forces at both ends of an element
$N_p(z)$	=	Resultant of the normal stresses obtained from pre-buckling Analysis
$\left[P\right]$	=	Matrix of user-input coefficients which linearly relate any set of nodal displacements
q_y, q_z	=	Distributed load applied to a member acting along the y- and z-direction respectively
$\left[S\right]$	=	Structure elastic stiffness matrix
$\left[S_G\right]$	=	Structure geometric stiffness matrix
$\left[S_i\right](i = 1 to 12)$	=	Sub-matrices needed to determine element stiffness matrices
u_b	=	Lateral buckling displacement
$\left\langle u_N \right\rangle^T$	=	Vector of nodal displacements
$\left\{u_s\right\}$	=	Vector of unknown displacements of the structure
U	=	Internal strain energy
V	=	Load potential energy
V_1, V_2	=	Internal shearing forces at both end of an element
$V_{yp}(z)$	=	Resultant of shear force component along y-direction obtained

		from pre-buckling analysis
x, y, z	=	Cartesian coordinates
β	=	End moment ratio
λ	=	Load multiplier
π	=	Total potential energy
θ_{yb}, θ_{zb}	=	Buckling rotation angles about y, z axes, respectively
$\omega(s)$	=	Warping function
ψ_b	=	Warping deformation (1/Length)

3.14 REFERENCES

Akay, H. U., C. P. Johnson and K. M. Will (1977). "Lateral and Local Buckling of Beams and Frames." Journal of the Structural Division, ASCE, ST9 103(9): 1821-1832.

Albert, C., H. S. Essa and D. J. L. Kennedy (1992). "Distortional buckling of steel beams in cantilever-suspended span construction." Canadian Journal of Civil Engineering 19(5): 767-780.

American Institute of Steel Construction, A. I. S. C. (2010). Specification for Structural Steel Buildings. ANSI/AISC 360-10. Chicago, IL.

Andrade, A., D. Camotim and P. Providência e Costa (2007). "On the evaluation of elastic critical moments in doubly and singly symmetric I-section cantilevers." Journal of Constructional Steel Research 63(7): 894-908.

Assadi, M. and C. Roeder (1985). "Stability of Continuously Restrained Cantilevers." Journal of Engineering Mechanics 111(12): 1440-1456.

Attard, M. M. (1990). "General non-dimensional equation for lateral buckling." Thin-Walled Structures 9(1–4): 417-435.

Attard, M. M. and M.-Y. Kim (2010). "Lateral buckling of beams with shear deformations – A hyperelastic formulation." International Journal of Solids and Structures 47(20): 2825-2840.

Austin, W. J., S. Yegian and T. P. Tung (1957). "Lateral Buckling of Elastically End-Restrained I-Beams." Transactions of the American Society of Civil Engineers 122(1): 374–388.

Barsoum, R. S. and R. H. Gallagher (1970). "Finite element analysis of torsional and torsional–flexural stability problems." International Journal for Numerical Methods in Engineering 2(3): 335-352.

Choo, K. M. (1987). Building Program BASP for Use on a Micro Computer MS, University of Texas at Austin.

Erkmen, R. E. (2014). "Shear deformable hybrid finite-element formulation for buckling analysis of thin-walled members." Finite Elements in Analysis and Design 82(0): 32-45.

Erkmen, R. E. and M. M. Attard (2011). "Lateral–torsional buckling analysis of thin-walled beams including shear and pre-buckling deformation effects." International Journal of Mechanical Sciences 53(10): 918-925.

Erkmen, R. E. and M. Mohareb (2008a). "Buckling analysis of thin-walled open members—A complementary energy variational principle." Thin-Walled Structures 46(6): 602-617.

Erkmen, R. E. and M. Mohareb (2008b). "Buckling analysis of thin-walled open members—A finite element formulation." Thin-Walled Structures 46(6): 618-636.

Erkmen, R. E., M. Mohareb and M. Bradford (2009). "Complementary Energy Based Formulation for Torsional Buckling of Columns." Journal of Engineering Mechanics 135(12): 1420-1426.

Essa, H. and D. Kennedy (1994). "Design of Cantilever Steel Beams: Refined Approach." Journal of Structural Engineering 120(9): 2623-2636.

Essa, H. and D. Kennedy (1995). "Design of Steel Beams in Cantilever-Suspended-Span Construction." Journal of Structural Engineering 121(11): 1667-1673.

Eurocode3 (1992). Comité Européen de Normalisation (CEN), Design of Steel Structures. Part 1-1: General rules and rules for buildings (ENV 1993-1-1). Brussels.

Gallagher, R. H. and J. Padlog (1963). "DISCRETE ELEMENT APPROACH TO STRUCTURAL INSTABILITY ANALYSIS." AIAA Journal 1(6): 1437-1439.

Geng-Shu, T. and C. Shao-Fan (1988). "Buckling of laterally and torsionally braced beams." Journal of Constructional Steel Research 11(1): 41-55.

Hartmann, A. J. (1967). "Elastic Lateral Buckling of Continuous Beams." Journal of the Structural Division 93(4): 11-26.

Hjaji, M. and M. Mohareb (2014). "Finite-Element Formulation for the Linear Steady-State Response of Asymmetric Thin-Walled Members under Harmonic Forces." Journal of Engineering Mechanics: 04014126.

Khelil, A. and B. Larue (2008). "Simple solutions for the flexural-torsional buckling of laterally restrained I-beams." Engineering Structures 30(10): 2923-2934.

Kim, N.-I. and D.-H. Choi (2013). "Super convergent shear deformable finite elements for stability analysis of composite beams." Composites Part B: Engineering 44(1): 100-111.

Kim, N.-I. and J. Lee (2013). "Lateral buckling of shear deformable laminated composite I-beams using the finite element method." International Journal of Mechanical Sciences 68(0): 246-257.

Kitipornchai, S., P. Dux and N. Richter (1984). "Buckling and Bracing of Cantilevers." Journal of Structural Engineering 110(9): 2250-2262.

Kitipornchai, S. and N. J. Richter (1978). "Elastic lateral buckling of I-beams with discrete intermediate restraints." Civil Engineering Transactions, Institution of Engineers, Australia CE20(No. 2): 105-111.

Krajcinovic, D. (1969). "A consistent discrete elements technique for thinwalled assemblages." International Journal of Solids and Structures 5(7): 639-662.

Larue, B., A. Khelil and M. Gueury (2007). "Elastic flexural–torsional buckling of steel beams with rigid and continuous lateral restraints." Journal of Constructional Steel Research 63(5): 692-708.

Lim, N.-H., N.-H. Park, Y.-J. Kang and I.-H. Sung (2003). "Elastic buckling of I-beams under linear moment gradient." International Journal of Solids and Structures 40(21): 5635-5647.

Nethercot, D. A. (1973a). "The Effective Length of Cantilevers as Governed by Lateral Buckling." The Structural Engineer 51(5): 161–168.

Nethercot, D. A. (1973b). "buckling of laterally or torsionally restrained beams." Journal of the Engineering Mechanics Division ASCE, 99(No. EM4): 773-791.

Nethercot, D. A. and K. C. Rockey (1971). "Finite element solutions for the buckling of columns and beams." International Journal of Mechanical Sciences 13(11): 945-949.

Nguyen, C. T., J. Moon, V. N. Le and H.-E. Lee (2010). "Lateral–torsional buckling of I-girders with discrete torsional bracings." Journal of Constructional Steel Research 66(2): 170-177.

Özdemir, K. M. and C. Topkaya (2006). "Lateral buckling of overhanging crane trolley monorails." Engineering Structures 28(8): 1162-1172.

Park, J. S., J. M. Stallings and Y. J. Kang (2004). "Lateral–torsional buckling of prismatic beams with continuous top-flange bracing." Journal of Constructional Steel Research 60(2): 147-160.

Poley, S. (1956). "Lateral Buckling of Cantilevered I-Beams Under Uniform Load." Transactions of the American Society of Civil Engineers 121(1): 786–790.

Powell, G. and R. Klingner (1970). "Elastic Lateral Buckling of Steel Beams." Journal of the Structural Division 96(9): 1919-1932.

Sahraei, A., L. Wu and M. Mohareb (2015). "Finite element formulation for lateral torsional buckling analysis of shear deformable mono-symmetric thin-walled members." Thin-Walled Structures 89(0): 212-226.

Salvadori, M. G. (1955). "Lateral Buckling of I-Beams." Transactions of the American Society of Civil Engineers 120(1): 1165-1177.

Santos, H. A. F. A. (2011). "Complementary-Energy Methods for Geometrically Non-linear Structural Models: An Overview and Recent Developments in the Analysis of Frames." Archives of Computational Methods in Engineering 18(4): 405-440.

Santos, H. A. F. A. (2012). "Variationally consistent force-based finite element method for the geometrically non-linear analysis of Euler–Bernoulli framed structures." Finite Elements in Analysis and Design 53(0): 24-36.

Serna, M. A., A. López, I. Puente and D. J. Yong (2006). "Equivalent uniform moment factors for lateral–torsional buckling of steel members." Journal of Constructional Steel Research 62(6): 566-580.

Trahair, N. S. (1993). Flexural-torsional buckling of structures, USA: CRC Press.

Trahair, N. S. (2008). "Lateral buckling of monorail beams." Engineering Structures 30(11): 3213-3218.

Wang, C. M., K. K. Ang and L. Wang (1995). "Optimization of bracing and internal support locations for beams against lateral buckling." Structural optimization 9(1): 12-17.

Wang, Y. C. and D. A. Nethercot (1990). "Bracing requirements for laterally unrestrained beams." Journal of Constructional Steel Research 17(4): 305-315.

Wu, L. (2010). Finite element formulations for lateral torsional buckling of shear deformable planar frames, PhD Dissertation. PhD Dissertation, University of Ottawa.

Wu, L. and M. Mohareb (2011a). "Buckling of shear deformable thin-walled members—I. Variational principle and analytical solutions." Thin-Walled Structures 49(1): 197-207.

Wu, L. and M. Mohareb (2011b). "Buckling formulation for shear deformable thin-walled members—II. Finite element formulation." Thin-Walled Structures 49(1): 208-222.

Yura, J. (2001). "Fundamentals of beam bracing." Engineering Journal, AISC (First Quarter): 11-26.

Chapter 4 Finite Element Formulation for Lateral Torsional Buckling Analysis of Shear Deformable Mono-symmetric Thin-walled Members

Abstract

A shear deformable theory and a computationally efficient finite element are developed to determine the lateral torsional buckling capacity of beams with mono-symmetric I-sections under general loading. A closed-form solution is also derived for the case of a mono-symmetric simply supported beam under uniform bending moments. The finite element is then used to provide solutions for simply supported beams, cantilevers, and developing moment gradient factors for the case of linear moments. The formulation is shown to successfully capture interaction effects between axial loads and bending moments as well as the load height position effect. The validity of the element is verified through comparisons with other established numerical solutions.

Keywords: Thin-walled members, Finite element, Mono-symmetric sections, Shear deformable members, Lateral torsional buckling

4.1 Motivation

Wide flange mono-symmetric sections are commonly used as girders in bridge structures. In buildings, they represent a viable design alternative as flexural members in cases such as roof members where positive bending moments induced by gravity load combinations involving gravity loads can be significantly larger than negative moments typically induced by wind uplift. When such members are used in large span laterally unsupported beams, their resistance is frequently governed by lateral torsional buckling resistance. Relatively recently, design standards (e.g., CAN/CSA S16 (2009), ANSI/AISC 360 (2005) and the subsequent edition ANSI/AISC 360 (2010)) have incorporated provisions for quantifying the lateral torsional buckling resistance for simply supported mono-symmetric members under general loading. More complex cases involving continuous beams, cantilever suspended constructions, cantilevers, are beyond the scope of North American design standards, although, as will be discussed in the literature review, past research has tackled some of these issues. The present study contributes to the existing body of knowledge by developing a theory and finite element for the buckling analysis of mono-symmetric sections. In a recent study, Wu and Mohareb (2011a, 2011b) developed a shear deformable theory and finite element formulation for lateral torsional buckling of thin-walled members. The theory was limited to members with doubly symmetric sections, and the resulting element exhibited slow convergence characteristics, thus requiring a several hundreds of degrees of freedom to model simple problems. Within this context, the present study is intended to advance the work in Wu and Mohareb (2011a, 2011b) in two respects; (a) it extends the developments to beams with mono-symmetric sections, and (b) it devises an effective interpolation scheme to accelerate the convergence characteristics of the resulting finite element.

4.2 Literature review

The present work is concerned with the lateral torsional buckling of beams of mono-symmetric sections based on a shear deformable thin-walled theory. Thus, within the vast body of research about lateral torsional buckling, the present review focuses on the work related to beams of mono-symmetric cross-sections (Section 4.2.1) and recent buckling solutions under shear deformable theories (Section 4.2.2).

4.2.1 Lateral torsional buckling for members of mono-symmetric cross-sections

Several studies have investigated the lateral torsional buckling resistance of mono-symmetric I-beams. Using the finite integral method, Anderson and Trahair (1972) developed tables for the critical loads of cantilevers and simply supported beams. Based on energy solutions, Robert and Burt (1985) developed a lateral torsional solution for beams with boundary conditions similar to those reported in Anderson and Trahair (1972). Both studies (Anderson and Trahair and Robert and Burt (1972, 1985)) focused on members under concentrated and uniformly distributed loads. Using the Raleigh Ritz method, Wang and Kitipornchai (1986) developed buckling solutions for cantilevers and simply supported beams (Wang and Kitipornchai (1986)) under concentrated and uniformly distributed loads. Also, Kitipornchai et al. (1986) investigated the effect of moment gradient on the buckling resistance of simply supported beams. Based on the stationarity condition of the total potential energy, Kitipornchai and Wang (1986) investigated the elastic lateral torsional buckling resistance of the simply supported tee beams under moment gradient. They showed that for inverted tee beams, uniform bending moment is not the most severe loading case and the cases involving high moment gradients ordinarily were more critical. Using shell finite element analysis, Helwig et al. (1997) modelled the lateral buckling capacity of girders subject to transverse point and uniformly distributed loads. Attard (1990) developed solutions for estimating elastic lateral torsional capacity of beams with mono-symmetric and doubly symmetric sections and general boundary conditions. Using Ritz and Galerkin's methods, Mohri et al. (2003) developed an analytical model for estimating the lateral torsional buckling resistance of simply supported beams under concentrated and uniformly distributed loads. Andrade et al. (2007) extended the application of three-factor lateral torsional buckling formula in the Eurocode (1992) to mono-symmetric cantilevers subject to uniformly distributed and concentrated transverse tip loads applied. Their solution incorporated the effect of load height. Based on the principle of stationarity of the second variation of the total potential energy, Zhang and Tong (2008) developed a new theory for estimating the lateral torsional buckling capacity of cantilevers subject to concentrated and uniformly distributed loads and uniform bending moments. Mohri et al. (2010) developed linear and nonlinear models to investigate into the lateral torsional buckling capacity of simply beams under moment gradient. Using a hyperelastic constitutive model, Attard and Kim (2010) formulated lateral torsional buckling solutions for shear deformable simply supported beams subject to uniform bending moment. Using the Generalized Beam Theory (GBT), Camotim et al. (2012) modeled beams with fork-type end supports under uniform moment, mid-span point load, two-point loads, distributed load and linear moments. They observed that among all loading conditions including end moments and transverse loads applied at shear center, the lowest critical buckling moments do not necessarily correspond to uniform bending moment. Mohri et al. (2013) developed a non-linear model to investigate the effect of axial forces on lateral torsional buckling resistance of simply supported I and H-sections. Their solutions involved concentrated and uniformly distributed loads.

In addition to the above solutions, several finite element formulations have been developed for the lateral torsional buckling of mono-symmetric sections. This includes the work of Krajcinovic (1969) and Barsoum and Gallagher (1970) who developed a finite element for buckling analysis based on the Vlasov thin-walled beam theory (1961). Based on the principle of stationarity of the second variation of the total potential energy, Attard (1986) developed two finite element formulations for estimating lateral torsional buckling loads of beams. Papangelis et al. (1998) developed a computer program to predict elastic lateral torsional buckling estimates of beams, beam-columns and plane frames. Distortional effects in doubly and mono-symmetric sections were also investigated in the work of Hancock et al. (1980), Bradford and Trahair (1981) and Bradford (1985). Using the Hellinger-Reissner principle, Erkmen (2014) developed a hybrid finite element formulation for shear deformable elements. Lateral torsional buckling solutions for web-tapered mono-symmetric beams were investigated in Bradford (1988), Bradford (1989), Andrade et al. (2007), Gelera and Park (2012), Yuan et al. (2013) and Trahair (2014). Also, solutions for laminated composite include the work of Lee (2006) and Kim and Lee (2013). Table 4.1 provides a comparative summary of the most relevant studies. As shown in the table, the present study aims at developing a general theory and finite element formulation for the lateral torsional buckling analysis of mono-symmetric members. The solution captures warping and shear deformation effects and excludes pre-buckling and distortional effects. It is applicable to general boundary and loading conditions and incorporates the destabilizing effects of axial loading, shearing force, and bending moments, albeit the P-delta effect in the pre-buckling analysis is omitted.

Table 4.1 Comparative studies on lateral-torsional buckling of mono-symmetric I-beams

Author(s)	Boundary Condition Types		Loading Types					Assumptions			Solutions Developed			Analysis Type
	Simply Supported	Cantilever	Concentrated Transverse Load(s)	Uniformly Distributed Load	Uniform Bending Moment	Linear Moment	Axial load	Distortional effects	Shear Deformations	Pre-buckling Deformations	Closed-form	FEA	Other Numerical Methods	
Anderson and Trahair (1972)	✓	✓	✓	✓									Finite Integral	
Bradford (1985)	✓	✓	✓	✓	✓	✓	✓	✓				✓		
Roberts and Burt (1985)	✓	✓	✓	✓						✓	✓		Stationarity of the Total Potential Energy	
Kitipornchai et al. (1986)	✓				✓	✓							Rayleigh-Ritz	
Wang and Kitipornchai (1986)	✓		✓	✓									Rayleigh-Ritz	
Wang and Kitipornchai (1986)		✓	✓	✓									Rayleigh-Ritz	
Attard (1990)	✓	✓	✓	✓	✓	✓				✓			Stationarity of the Total Potential Energy	
Helwig et al. (1997)	✓		✓	✓										Shell FEA
Mohri et al. (2003)	✓		✓	✓									Ritz and Galerkin	
Andrade et al. (2007)		✓	✓	✓									Rayleigh-Ritz	
Zhang and Tong (2008)		✓	✓	✓	✓								Stationarity of the Total Potential Energy	
Mohri et al. (2010)	✓	✓	✓	✓	✓	✓	✓			✓		✓		Beam 3D FEA
Attard and Kim (2010)	✓				✓				✓		✓			Hyperelastic
Camotim et al. (2012)	✓		✓	✓	✓	✓							Stationarity of the Total Potential Energy	LTBEAM Shell FEA GBT
Mohri et al. (2013)	✓		✓	✓			✓			✓	✓		Galerkin	Beam 3D FEA
Erkmen (2014)	✓	✓	✓	✓	✓	✓	✓		✓			✓	Hellinger-Reissner	
Present Study	✓	✓	✓	✓	✓	✓	✓		✓		✓	✓	**Stationarity of the Total Potential Energy**	

4.2.2 Buckling solutions under shear deformable theories

A common feature among the above studies is that they focused on mono-symmetric sections. Other shear deformable theories were also developed. This includes the work of Erkmen and Mohareb (2008a) who developed a complementary energy variational principle and formulated a finite element (Erkmen and Mohareb (2008b)) for doubly symmetric sections. In a subsequent study, focused on torsional buckling of columns, Erkmen et al. (2009) demonstrated that the elastic torsional buckling of columns is guaranteed to converge from below.

4.3 Assumptions

The following assumptions have been adopted:

1. The formulation is restricted to prismatic thin-walled members with mono-symmetric sections consisting of segments parallel to the principal axes,
2. Regarding shear/bending action, the cross-section remains rigid in its own plane during deformation but does not remain perpendicular to the neutral axis after deformation in line with the Timoshenko theory. The hypothesis is further generalized for torsion/warping action. Similar kinematics have been used in buckling problems in Saade (2004), Kollar (2001) Back and Will (2008), Attard and Kim (2010), Kim and Lee (2013) and Lee (2006), and Wu and Mohareb (2011a, 2011b).
3. The material is assumed to be linearly elastic and obeys Hooke's law,
4. Strains are assumed small but rotations are assumed to be moderate. Rotation effects are thus included in the formulation by retaining the non-linear strain components,
5. The member buckles in an inextensional mode (Trahair (1993)) which means that throughout buckling, the centroidal longitudinal strain and curvature in yz-plane remain zero. This signifies that the member is assumed to buckle under constant axial load and bending moments, and
6. The solution neglects pre-buckling deformation effects.

4.4 Variational formulation

This section outlines the details of the variational formulation. The treatment is similar to that presented in Wu and Mohareb (2011a) for doubly symmetric sections. As such, only important milestones are provided here and the reader is referred to Wu and Mohareb (2011a) for a more thorough discussion of the methodology. A right-handed Cartesian coordinate system is adopted in which the Z-axis is oriented along the axial direction of the member while X-axis and Y-axis are parallel to major and minor principal axes of the cross-section, respectively. The origin is taken to coincide with the cross-section centroid $C(x_c = 0, y_c = 0)$ while pole A_p is taken to coincide with the shear center $SC\ \left(x_A = 0, y_A\right)$.

4.4.1 Problem description and notation

The member is assumed to be subjected to a uniformly distributed transverse load q_y applied at a distance $y_{qy}(z)$ from the shear center and a uniformly distributed axial load q_z acting at distance $y_{qz}(z)$ from the origin. Under such external loads, the member deforms from configuration 1 to 2 as shown in Figure 4-1 and undergoes displacements $v_p(z)$, $w_p(z)$ and rotation $\theta_{xp}(z)$. As a convention, subscript *p* represents pre-buckling displacement, strain, and stress fields. The applied loads are assumed to increase by a factor λ and attain the values λq_y and λq_z at the onset of buckling (Configuration 3). Under the load increase, it is assumed that pre-buckling deformations linearly increase to $\lambda v_p(z)$, $\lambda w_p(z)$ and $\lambda \theta_p(z)$. The section then undergoes lateral torsional buckling (Configuration 4) manifested by lateral displacement u_b, weak-axis rotation θ_{yb}, angle of twist θ_{zb} and warping deformation ψ_b. Again, as a matter of convention, subscript *b* denotes field displacements, strains, or stresses, occurring during the buckling stage (i.e., in going from configuration 3 to 4) while superscripts * denotes the total fields (i.e., in going from configuration 1 to 4).

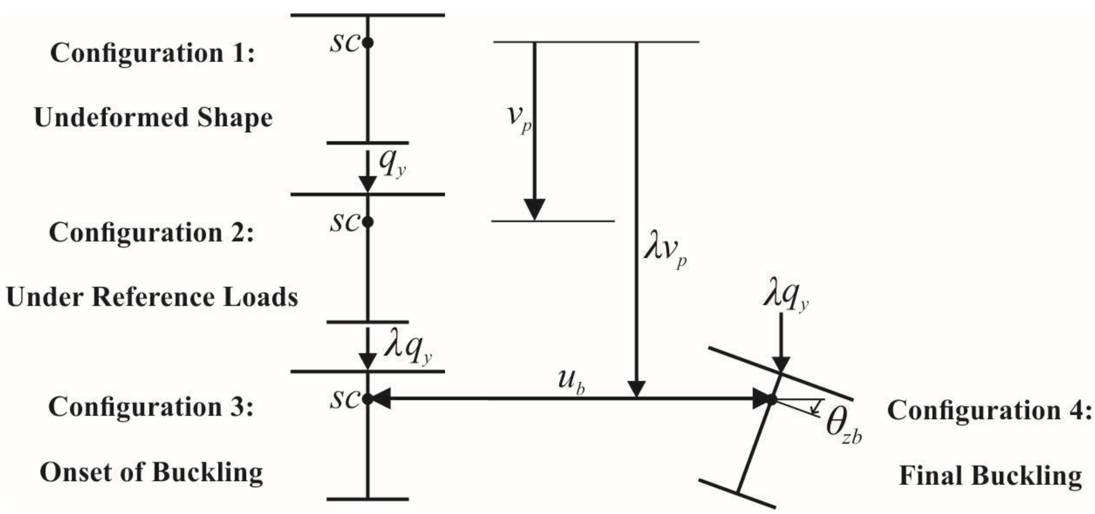

Figure 4-1 Different stages of deformation

4.4.2 Kinematic relations

Under the kinematic assumptions postulated above, a point S on the section mid-surface can be shown (Wu and Mohareb (2011a)) to undergo total displacements $u_s^*(s,z), v_s^*(s,z), w_s^*(s,z)$ given by

$$\begin{aligned}
u_s^*(s,z) &= u_b(z) - \left(y(s) - y_A\right)\theta_{zb}(z) \\
v_s^*(s,z) &= \lambda v_p(z) + x(s)\theta_{zb}(z) \\
w_s^*(s,z) &= \lambda w_p(z) + y(s)\lambda\theta_{xp}(z) - x(s)\theta_{yb}(z) + \omega(s)\psi_b(z) + x(s)\lambda\theta_{xp}(z)\theta_{zb}(z) \\
&\quad + y(s)\theta_{yb}(z)\theta_{zb}(z)
\end{aligned} \tag{4.1)a-c}$$

Figure 4-2 depicts the global coordinate system, displacements, and sign conventions adopted in this study.

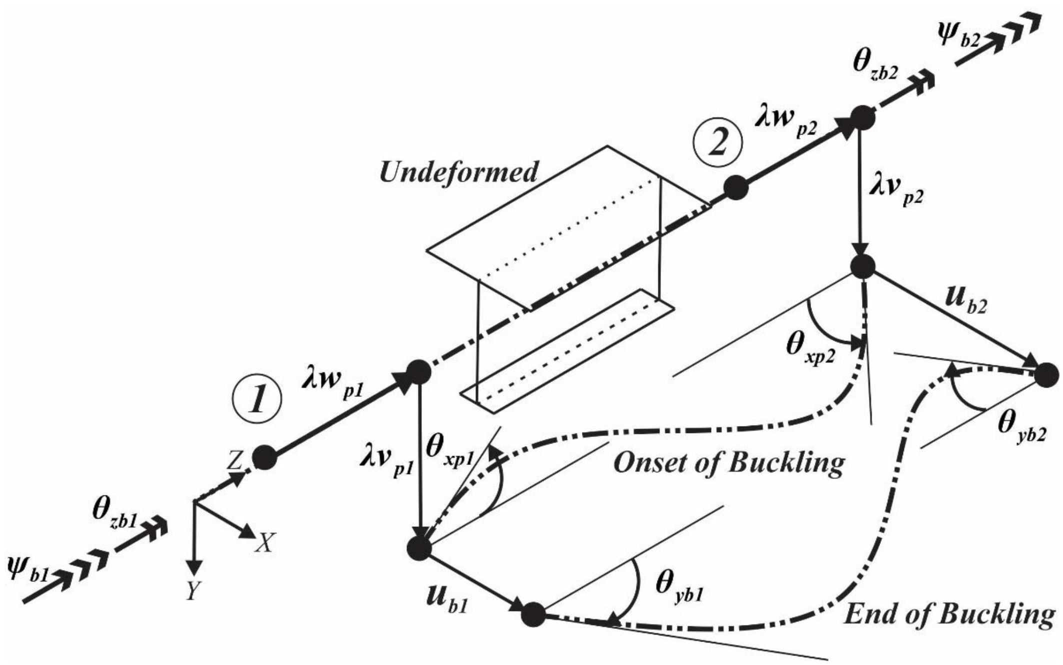

Figure 4-2 Global coordinate system and displacement components

4.4.3 Conditions of neutral stability

The condition of neutral stability is given by evoking the variation of the second variation of the total potential energy π, (Wu and Mohareb (2011a)), i.e.,

$$\delta\left(1/2\,\delta^2\pi\right)=\delta\left[1/2\left(\delta^2U+\delta^2V\right)\right]=0 \tag{4.2}$$

in which U is the internal strain energy and V is the load potential energy gained by externally applied loads. The variation of their second variation of U and V are given by

$$\delta\left[\frac{1}{2}\left(\delta^2U\right)\right]=\delta\left\{\frac{1}{2}\int_0^L\int_A\left\{\left[E\left(\delta\varepsilon_{zz_b}\right)^2+\lambda\sigma_{zz_p}\delta^2\varepsilon_{zz_b}\right]+\left[G\left(\delta\gamma_{zs_b}\right)^2+\lambda\gamma_{zs_p}\delta^2\tau_{zs_b}\right]\right\}dAdz+\frac{1}{2}\int_0^L GJ\left(\delta\theta'_{zb}\right)^2dz\right.$$

$$\left.\delta\left[\frac{1}{2}\left(\delta^2V\right)\right]=-\int_0^L\left[-\frac{1}{2}q_y\left(y_{qy}-y_A\right)\left(\delta\theta_{zb}\right)^2+q_z\left(y_{qz}\delta\theta_{yb}\delta\theta_{zb}\right)\right]dz\right\}$$

(4.3)a-b

Equations (4.1)a-c are differentiated with respect the appropriate coordinates to yield the strain expressions. The first variation and second variations of strains are

$$\delta\varepsilon_{zzb}=-x\delta\theta'_{yb}+\omega\delta\psi'_b$$

$$\delta\gamma_{zsb}=\frac{dx}{ds}\left(\delta u'_b-\delta\theta_{yb}\right)+h\left(\delta\theta'_{zb}+\delta\psi_b\right)$$

$$\delta^2\varepsilon_{zz_b}=\left(\delta u'_b\right)^2-2\left(y-y_A\right)\delta u'_b\delta\theta'_{zb}+\left[x^2+\left(y-y_A\right)^2\right]\left(\delta\theta'_{zb}\right)^2+2y\left(\delta\theta'_{yb}\delta\theta_{zb}+\delta\theta_{yb}\theta'_{zb}\right) \qquad \text{(4.4)a-d}$$

$$\delta^2\gamma_{zsb}=2\left[\frac{dy}{ds}\left(\delta\theta_{yb}\delta\theta_{zb}\right)+x\frac{dx}{ds}\left(\delta\theta_{yb}\delta\theta'_{yb}\right)-xh\left(\delta\psi_b\delta\theta'_{yb}\right)-\omega\frac{dx}{ds}\left(\delta\theta_{yb}\delta\psi'_b\right)\right.$$
$$\left.+\omega h\left(\delta\psi_b\delta\psi'_b\right)-\left(\frac{dy}{ds}\right)\left(\frac{dk}{ds}\right)\left(\delta u'_b\delta\theta_{zb}\right)+k\left(\frac{dk}{ds}\right)\left(\delta\theta'_{zb}\delta\theta_{zb}\right)\right]$$

where $h(s)=x(s)\sin\alpha(s)-\left[y(s)-y_A\right]\cos\alpha(s)$, $k(s)=x(s)\cos\alpha(s)+\left[y(s)-y_A\right]\sin\alpha(s)$. From Eqs. (4.4)a-d by substituting into the vibrational expression $\delta\left(1/2\,\delta^2\pi\right)=\delta\left[1/2\left(\delta^2U+\delta^2V\right)\right]=0$, and recalling the pre-buckling stress expressions $\sigma_{zzp}=N_p(z)/A+M_{xp}(z)\,y/I_{xx}$ and $\tau_{zz_p}=G\gamma_{zs_p}$, one obtains

$$\delta\left(\frac{1}{2}\delta^2\pi\right)=\delta\left[\frac{1}{2}\left(\delta^2U_b+\delta^2U_{sv}+\delta^2U_s+\delta^2V_N+\delta^2V_M+\delta^2V_V+\delta^2V_{qy}+\delta^2V_{qz}\right)\right]=0 \tag{4.5}$$

in which U_b is the internal strain energy due to normal stresses, U_{sv} is the internal strain energy due to Saint-Venant shear stress, U_s is the internal strain energy due to shear stresses, V_N is the destabilizing term of the total potential energy due to normal forces, V_M is the destabilizing term of the total potential energy due to bending moments, V_V is the destabilizing term of the total potential energy due to shear forces, V_{qy} is the destabilizing term of the total potential energy due to transverse load position effect, V_{qz} is the destabilizing term of the total potential energy due to longitudinal load position effect. Under this condition, the second variations are the above energy terms take the form

$$\delta^2 U_b = \int_0^L \left[EI_{yy} \left(\delta\theta'_{yb}\right)^2 + EI_{\omega\omega}\left(\delta\psi'_b\right)^2 \right] dz$$

$$\delta^2 U_{sv} = \int_0^L GJ\left(\delta\theta'_{zb}\right)^2 dz$$

$$\begin{aligned}\delta^2 U_s = G\int_0^L \Big[& \left(D_{xx}\delta u'_b - D_{xx}\delta\theta_{yb} + D_{xh}\delta\theta'_{zb} + D_{xh}\delta\psi_b\right)\delta u'_b \\ & + \left(-D_{xx}\delta u'_b + D_{xx}\delta\theta_{yb} - D_{xh}\delta\theta'_{zb} - D_{xh}\delta\psi_b\right)\delta\theta_{yb} \\ & + \left(D_{xh}\delta u'_b - D_{xh}\delta\theta_{yb} + D_{hh}\delta\theta'_{zb} + D_{hh}\delta\psi_b\right)\delta\theta'_{zb} \\ & + \left(D_{xh}\delta u'_b - D_{xh}\delta\theta_{yb} + D_{hh}\delta\theta'_{zb} + D_{hh}\delta\psi_b\right)\delta\psi_b \Big] dz\end{aligned}$$

$$\delta^2 V_N = -\lambda\int_0^L \left(\frac{N_p(z)}{A}\right)\left[-Au'^2_b - (2y_A A)u'_b\theta'_{zb} - \left(I_{xx} + I_{yy} + y_A{}^2 A\right)\theta'^2_{zb}\right] dz$$

$$\delta^2 V_M = -\lambda\int_0^L \left(\frac{M_{xp}(z)}{I_{xx}}\right)\left[-2I_{xx}(\theta'_{yb}\theta_{zb} + \theta_{yb}\theta'_{zb}) + 2I_{xx}u'_b\theta'_{zb} - \left(I_{px} - 2y_A I_{xx}\right)\theta'^{\,2}_{zb}\right] dz$$

$$\begin{aligned}\delta^2 V_V = -\lambda\int_0^L \left(\frac{2V_{yp}(z)}{D_{yy}}\right)\Big(& -D_{yy}\theta_{yb}\theta_{zb} + D_{yyk}u'_b\theta_{zb} - D_{yk}\theta'_{zb}\theta_{zb} - D_{xx'y'}\theta_{yb}\theta'_{yb} \\ & + D_{\omega x'y'}\theta_{yb}\psi'_b + D_{yh}\psi_b\theta'_{yb} - D_{y\omega h}\delta\psi_b\delta\psi'_b\Big) dz\end{aligned}$$

` (4.6)a-h

$$\delta^2 V_{qy} = -\lambda\int_0^L \left[-q_y\left(y_{qy} - y_A\right)\left(\delta\theta_{zb}\right)^2\right] dz$$

$$\delta^2 V_{qz} = -\lambda\int_0^L 2q_z y_{qz}\delta\theta_{yb}\delta\theta_{zb} dz$$

in which the following sectional properties have been defined

$$I_{yy} = \int_A x^2 dA \qquad I_{xy} = \int_A xy dA \qquad I_{\omega\omega} = \int_A \omega^2 dA \qquad I_{px} = \int_A y\left(x^2 + y^2\right) dA$$

$$S_x = \int_A y dA \qquad S_{x\omega} = \int_A x\omega dA \qquad D_{hh} = \int_A h^2 dA \qquad D_{xx} = \int_A \left(\frac{dx}{ds}\right)^2 dA$$

$$D_{xh} = \int_A h\left(\frac{dx}{ds}\right) dA \qquad D_{yy} = \int_A \left(\frac{dy}{ds}\right)^2 dA \qquad D_{yk} = \int_A k \frac{dy}{ds}\frac{dk}{ds} dA \qquad D_{yyk} = \int_A \left(\frac{dy}{ds}\right)^2 \frac{dk}{ds} dA$$

$$D_{yh} = \int_A xh\left(\frac{dy}{ds}\right) dA \qquad D_{y\omega h} = \int_A h\omega \frac{dy}{ds} dA \qquad D_{xx'y'} = \int_A x \frac{dx}{ds}\frac{dy}{ds} dA \qquad D_{\omega x'y'} = \int_A \omega \frac{dx}{ds}\frac{dy}{ds} dA$$

It is observed that for common cross-sections consisting exclusively of segments parallel to *x* and *y* axes (such as a mono-symmetric I section), all area integral terms containing the product $\left(dy/ds\right)\left(dx/ds\right)$ vanish, i.e., $D_{xx'y'} = D_{\omega x'y'} = 0$.

As a verification of the validity of Eqs. (4.6)a-h, when the cross-section is doubly symmetric constants $I_{xy}, I_{px}, S_x, S_{x\omega}, D_{xh}, D_{yk}, D_{yh}$ and $D_{y\omega h}$ vanish and the present variational statement reverts to that in Wu and Mohareb (2011a) when the coordinate system is taken to be orthogonal.

4.4.4 Finite Element Formulation I

The variational expressions in Eqs (4.6)a-h consist of the buckling displacement functions $u_b \quad \theta_{yb} \quad \theta_{zb} \quad \psi_b$ and their first derivatives with respect to coordinate *z*. Thus, each of the assumed four displacement functions needs to satisfy only C^0 continuity. By taking two nodes per element, and adopting a linear interpolation scheme between the two nodal values, the displacement fields $\left\langle u_b(z) \quad \theta_{yb}(z) \quad \theta_{zb}(z) \quad \psi_b(z)\right\rangle^T$ are related to the nodal displacements through

$$\left\langle u_b(z) \quad \theta_{yb}(z) \quad \theta_{zb}(z) \quad \psi_b(z)\right\rangle_{1\times 4} = \left\langle H_b(z)\right\rangle_{1\times 2} \left[\begin{Bmatrix} u_1 \\ u_2 \end{Bmatrix}_{2\times 1} \quad \begin{Bmatrix} \theta_{y1} \\ \theta_{y2} \end{Bmatrix}_{2\times 1} \quad \begin{Bmatrix} \theta_{z1} \\ \theta_{z2} \end{Bmatrix}_{2\times 1} \quad \begin{Bmatrix} \psi_1 \\ \psi_2 \end{Bmatrix}_{2\times 1} \right]$$

(4.7)a-d

in which $\left\langle H_b(z)\right\rangle_{1\times 2} = \left\langle (1 - z/L) \quad (z/L)\right\rangle$ is the vector of shape linear shape functions and $u_1, u_2, \theta_{y1}, ...\psi_2$ are the nodal displacement. In a similar manner, the pre-buckling stress resultants $N_p(z) \quad V_{yp}(z) \quad M_{xp}(z)$ are linearly interpolated between the internal forces

$N_1, N_2, V_1, V_2, M_1, M_2$ at the nodes as obtained from the pre-buckling analysis (Figure 4-3b, d, f), i.e.,

$$\langle N_p(z) \quad V_{yp}(z) \quad M_{xp}(z) \rangle = \langle H_b(z) \rangle_{1\times 2} \left[\begin{Bmatrix} N_1 \\ -N_2 \end{Bmatrix}_{2\times 1} \quad \begin{Bmatrix} V_1 \\ -V_2 \end{Bmatrix}_{2\times 1} \quad \begin{Bmatrix} M_1 \\ -M_2 \end{Bmatrix}_{2\times 1} \right] \tag{4.8)a-c}$$

The resulting element is similar to that reported in Wu and Mohareb (2011b) (and will be subsequently referred to as the WM element), with two differences. The present element is geared towards mono-symmetric sections, while the WM element is for doubly symmetric sections. Also, the present formulation is based on an orthogonal coordinate system, while the WM is based on general non-orthogonal coordinates.

4.4.5 Finite Element Formulation II

The element developed in Section 4.4.4 has a minimal number of degrees of freedom (8 DOFs for the buckling solution) but will be shown to exhibit slow convergence characteristics, thus needing hundreds of elements to solve simple problems. Within this context, the present section aims at developing an element which preserves the low number degrees of freedom per element while accelerating its convergence characteristics. This is achieved by adopting different interpolation schemes for pre-buckling internal forces and buckling displacement fields.

4.4.5.1 Approximation of pre-buckling internal forces

In general, the pre-buckling internal forces $N_p(z)$, $V_{yp}(z)$ and $M_{xp}(z)$ are non-constant functions. Under such conditions, the closed-form solution of the governing neutral stability conditions stemming from the above variational principle becomes unattainable. Thus, the non-constant internal forces obtained from pre-buckling analysis (Figure 4-3-a, c, e) are approximated as piecewise constant functions equal to the average values of the internal forces. Thus, one can set

$$N_p(z) \approx N_p = (N_1 - N_2)/2, \quad V_{yp}(z) \approx V_{yp} = (V_1 - V_2)/2, \quad M_{xp}(z) \approx M_{xp} = (M_1 - M_2)/2 \tag{4.9)a-c}$$

in the variational statement (Eqs. (4.6)a-h) within the subdomain L_e (Figure 4-3-b, d, f) of the element. When the number of elements is sufficiently large, the piecewise representation of pre-buckling internal forces would approach that of actual internal force distributions and the resulting approximate total potential energy expression of the system will approach that based on Eqs. (4.6) a-h. This treatment will be shown rather advantageous from a computational viewpoint and will lead to desirable convergence characteristics.

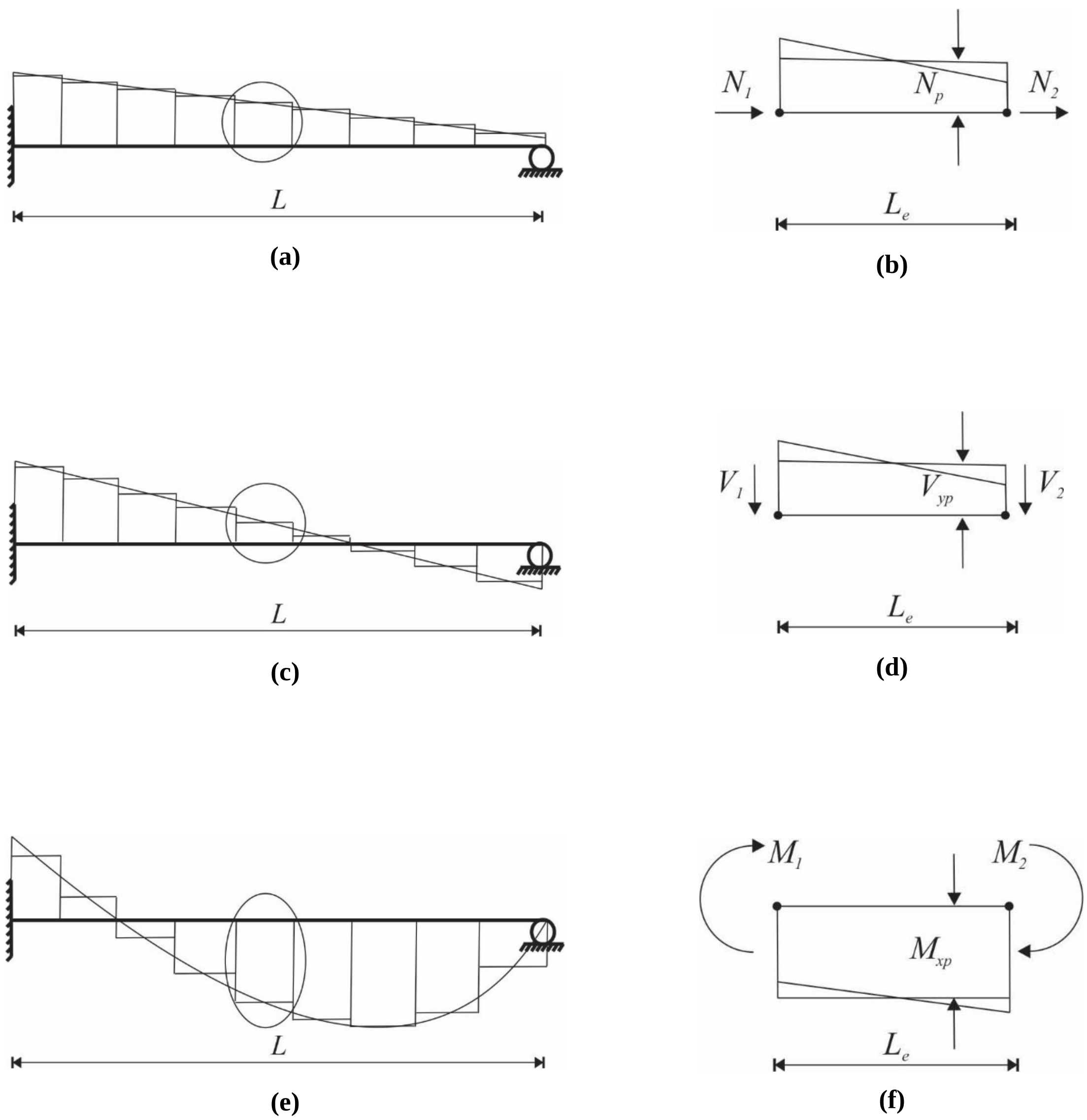

Figure 4-3 Internal forces for a beam-column: (a) Normal forces within member, (b) Idealized constant normal force within the element, (c) Shearing forces within member, (d) Idealized constant shearing force within the element, (e) Bending moments within member, and (f) Idealized bending moment within the element

4.4.5.2 Approximate equations of neutral stability

Under the approximations introduced in Section 4.4.5.1, Eqs. (4.6)a-h are integrated by parts and like terms are grouped together. Noting that the functions δu_b, $\delta\theta_{yb}$, $\delta\theta_{zb}$ and $\delta\psi_b$ are arbitrary, one recovers the conditions of neutral stability

$$
\left[\begin{array}{c|c|c|c}
-\left(1+\frac{\lambda N_p}{GD_{xx}}\right)\frac{d^2}{d\xi^2} & \frac{d}{d\xi} & \begin{array}{c}\left[\left(-\frac{D_{xh}}{L_eD_{xx}}+\frac{-y_A\lambda N_p}{L_eGD_{xx}}+\frac{\lambda M_{xp}}{L_eGD_{xx}}\right)\right]\frac{d^2\theta_{zb}}{d\xi^2}\\ +\lambda\left(\frac{V_{yp}}{GD_{xx}}\right)\frac{d\theta_{zb}}{d\xi}\end{array} & -\left(\frac{D_{xh}}{L_eD_{xx}}\right)\frac{d}{d\xi} \\ \hline
\frac{d}{d\xi} & \frac{EI_{yy}}{GD_{xx}L_e^2}\frac{d^2}{d\xi^2}-1 & \left(\frac{D_{xh}}{L_eD_{xx}}\right)\frac{d}{d\xi} & \frac{D_{xh}}{L_eD_{xx}} \\ \hline
\begin{array}{c}\left[-\frac{D_{xh}}{L_eD_{xx}}+\frac{-y_A\lambda N_p}{L_eGD_{xx}}\right.\\ \left.+\frac{\lambda M_{xp}}{L_eGD_{xx}}\right]\frac{d^2}{d\xi^2}\\ +\lambda\left(\frac{V_{yp}}{GD_{xx}}\right)\frac{d}{d\xi}\end{array} & \left(\frac{D_{xh}}{L_eD_{xx}}\right)\frac{d}{d\xi} & \begin{array}{l}\lambda q_y\frac{\left(y_{qy}-y_A\right)}{GD_{xx}}+\left[-\frac{\left(J+D_{hh}\right)}{D_{xx}L_e^2}\right.\\ -\lambda N_p\frac{\left(I_{xx}+I_{yy}+y_A{}^2A\right)}{GD_{xx}AL_e^2}\\ \left.-\lambda M_{xp}\frac{\left(I_{px}-2y_AI_{xx}\right)}{GD_{xx}I_{xx}L_e^2}\right]\frac{d^2}{d\xi^2}\\ -\lambda V_{yp}\left[\frac{D_{yk}}{GD_{xx}D_{yy}L_e}\right.\\ \left.+\frac{\left(I_{px}-2y_AI_{xx}\right)}{GD_{xx}I_{xx}L_e}\right]\frac{d}{d\xi}\end{array} & -\left(\frac{D_{hh}}{L_e^2D_{xx}}\right)\frac{d}{d\xi} \\ \hline
-\left(\frac{D_{xh}}{L_eD_{xx}}\right)\frac{d}{d\xi} & \frac{D_{xh}}{L_eD_{xx}} & -\left(\frac{D_{hh}}{L_e^2D_{xx}}\right)\frac{d}{d\xi} & \begin{array}{c}\frac{EI_{\omega\omega}}{GD_{xx}L_e^4}\frac{d^2}{d\xi^2}\\ -\frac{D_{hh}}{L_e^2D_{xx}}\end{array}
\end{array}\right]
\times\begin{Bmatrix}\frac{u_b}{L_e}\\ \theta_{yb}\\ \theta_{zb}\\ L_e\psi_b\end{Bmatrix}=\begin{Bmatrix}0\\0\\0\\0\end{Bmatrix}
\tag{4.10}
$$

in which $D = d/dz = d/L_e d\xi$ is the first derivative of displacement fields with respect to the dimensionless coordinate $\xi = z/L_e$.

4.4.5.3 Formulating shape functions

It is proposed to generate shape functions which satisfy Eq. (4.10). The presence of the unknowns $\lambda N_p, \lambda V_{yp}, \lambda M_{xp}$ makes such a solution unattainable given that λ is unknown a-priori. As such, the terms involving $\lambda N_p, \lambda V_{yp}, \lambda M_{xp}$ are assumed negligible. This assumption turns out to be accurate for beams of practical dimensions.

Another issue arising when solving Eq. (4.10) is the need to estimate. $\lambda q_y \left(y_{qy} - y_A\right)/GD_{xx}$ When the load λq_y is a applied at the shear center, i.e., $y_{qy} = y_A$, it is clear that $\lambda q_y \left(y_{qy} - y_A\right)/GD_{xx}$ would vanish. Otherwise, the order of magnitude for maximum for the distributed load λq_y can be estimated by equating the lateral torsional buckling resistance of the beam $C_b \left(\pi^2 EI_{yy}/2L^2\right)\left[\beta_x + \sqrt{\beta_x^2 + 4\left(GJL^2/\pi^2 EI_{yy} + I_{\omega\omega}/I_{yy}\right)}\right]$, in which $C_b = 1.14$, to the external moments $\lambda q_y L^2/8$ for a simply supported beam, and solving for λq_y. It is clear that the proposed scheme will yield approximate value for λq_y since it does not necessarily capture the end conditions of the element, yielding approximate shape functions. Nevertheless, the approximate functions thus obtained will be shown to have superior convergence characteristics compared to that in Formulation I.

4.4.5.4 Closed-form Solution for the field equations

The coupled system of equations (Eq. (4.10)) has constant coefficients. Its solution is assumed to take the form $\left\langle u_b/L_e, \theta_{yb}, \theta_{zb}, L_e\psi_b\right\rangle^T = \left\langle A_i, B_i, C_i, D_i\right\rangle^T e^{m_i z}$. By substituting into Eq. (4.10), one obtains the quadratic eigenvalue problem

$$\left(m_i^2\left[\bar{A}\right] + m_i\left[\bar{B}\right] + \left[\bar{C}\right]\right)_{4\times4}\left\{\varphi_i\right\}_{4\times1} = \left\{0\right\}_{4\times1} \tag{4.11}$$

in which matrices $\left[\bar{A}\right]$, $\left[\bar{B}\right]$ and $\left[\bar{C}\right]$ are defined this time in dimensional form as

$$\left[\bar{A}\right]=\left[\begin{array}{c|c|c|c} -GD_{xx} & 0 & -GD_{xh} & 0 \\ \hline 0 & EI_{yy} & 0 & 0 \\ \hline -GD_{xh} & 0 & -G\left(J+D_{hh}\right) & 0 \\ \hline 0 & 0 & 0 & EI_{\omega\omega} \end{array}\right] \tag{4.12}$$

$$\left[\bar{B}\right]=\left[\begin{array}{c|c|c|c} 0 & GD_{xx} & 0 & -GD_{xh} \\ \hline GD_{xx} & 0 & GD_{xh} & 0 \\ \hline 0 & GD_{xh} & 0 & -GD_{hh} \\ \hline -GD_{xh} & 0 & -GD_{hh} & 0 \end{array}\right] \tag{4.13}$$

$$\left[\bar{C}\right]=\left[\begin{array}{c|c|c|c} 0 & 0 & 0 & 0 \\ \hline 0 & -GD_{xx} & 0 & GD_{xh} \\ \hline 0 & 0 & \lambda q_y\left(y_{qy}-y_A\right) & 0 \\ \hline 0 & GD_{xh} & 0 & -GD_{hh} \end{array}\right] \tag{4.14}$$

in which φ_i is the eigenvector corresponding the eigenvalue m_i. Equation (4.11) can be expressed into the following equivalent linear eigenvalue problem

$$\left(\left[\begin{array}{c|c} \left[\bar{B}\right] & \left[\bar{C}\right] \\ \hline \left[-I\right] & \left[0\right] \end{array}\right]_{8\times 8}+m_i\left[\begin{array}{c|c} \left[\bar{A}\right] & \left[0\right] \\ \hline \left[0\right] & \left[I\right] \end{array}\right]_{8\times 8}\right)\left\{\begin{array}{c} m_i\{\varphi_i\} \\ \hline \{\varphi_i\} \end{array}\right\}_{8\times 1}=\left\{\begin{array}{c} 0 \\ \hline 0 \end{array}\right\}_{8\times 1} \tag{4.15}$$

in which $\left[I\right]=Diag\left\langle 1 \quad 1 \quad 1 \quad 1\right\rangle^T$ is the identity matrix. The above eigenvalue problem is observed to have four zero roots, i.e., $m_1=m_2=m_3=m_4=0$. Thus, the closed-form solution takes the form

$$\begin{aligned} u_b &= A_1+A_2z+A_3z^2+A_4z^3+A_5e^{m_5z}+A_6e^{m_6z}+A_7e^{m_7z}+A_8e^{m_8z} \\ \theta_{yb} &= B_1+B_2z+B_3z^2+B_4z^3+B_5e^{m_5z}+B_6e^{m_6z}+B_7e^{m_7z}+B_8e^{m_8z} \\ \theta_{zb} &= C_1+C_2z+C_3z^2+C_4z^3+C_5e^{m_5z}+C_6e^{m_6z}+C_7e^{m_7z}+C_8e^{m_8z} \\ \psi_b &= D_1+D_2z+D_3z^2+D_4z^3+D_5e^{m_5z}+D_6e^{m_6z}+D_7e^{m_7z}+D_8e^{m_8z} \end{aligned} \tag{4.16)a-d$$

The remaining four roots m_i (i=5 to 8) can either be obtained by solving the right eigenvalue problem in Eq. (4.15) or from the equivalent bi-quadratic characteristic equation

$$G\left\{\left(-D_{xh}^2 E^2 G I_{\omega\omega} I_{yy} + D_{hh} D_{xx} E^2 G I_{\omega\omega} I_{yy} + D_{xx} E^2 G I_{\omega\omega} I_{yy} J\right) m^4 + \left[E D_{xh}^2 G^2 I_{yy} J - E D_{hh} D_{xx} G^2 I_{yy} J \right.\right.$$
$$\left.\left. + D_{xx} E^2 I_{\omega\omega} I_{yy} q_y y_A\right] m^2 + E G I_{yy} q_y y_A \left(D_{xh}^2 - D_{hh} D_{xx}\right)\right\} = 0 \tag{4.17}$$

It is observed that for the special case of doubly symmetric sections, one has $D_{xh} = y_A = 0$ and the last coefficient of Eq. (4.17) vanishes. In such a case, one obtains six repeated zero roots, and Eqs. (4.16)a-d becomes an invalid solution. Thus, as stated in Assumption 1, the present solution is restricted to mono-symmetric sections.

By substituting Eqs. (4.16)a-d and their derivatives into the field equations (Eq. (4.10)), and performing algebraic simplifications, the 32 integration constants $A_i - D_i \ (i = 1...8)$ can be reduced to eight independent constants $A_i \ (i = 1...8)$. The field displacements $\langle d(z)\rangle^T = \langle u_b(z) \quad \theta_{yb}(z) \quad \theta_{zb}(z) \quad \psi_b(z)\rangle^T$ are thus related to integration constants $\langle A\rangle^T = \langle A_1 \quad A_2 \quad A_3 \quad A_4 \quad A_5 \quad A_6 \quad A_7 \quad A_8\rangle^T$ through

$$\{d(z)\} = [B(z)]_{4\times8} \{A\}_{8\times1} \tag{4.18}$$

where

$$[B(z)]_{4\times8} = \left[[F(z)]_{4\times4} \;\middle|\; [\Phi]_{4\times4}[E(z)]_{4\times4}\right], \quad [F(z)]_{4\times4} = \left[\begin{array}{c|c|c|c} 1 & z & z^2 & z^3 \\ \hline 0 & 1 & 2z & 3z^2 - \dfrac{6EI_{yy}D_{hh}}{G\left(D_{xh}{}^2 - D_{hh}D_{xx}\right)} \\ \hline 0 & 0 & 0 & 0 \\ \hline 0 & 0 & 0 & \dfrac{-6EI_{yy}D_{xh}}{G\left(D_{xh}{}^2 - D_{hh}D_{xx}\right)} \end{array}\right] \tag{4.19a-b}$$

and $[\Phi]_{4\times4} = \left[\{\phi\}_1 \quad \{\phi\}_2 \quad \{\phi\}_3 \quad \{\phi\}_4\right]$ is the matrix of eigenvectors of the quadratic eigenvalue problem defined in Eq. (4.15) and $[E(z)]_{4\times4} = Diag\left[e^{m_5 z}, e^{m_6 z}, e^{m_7 z}, e^{m_8 z}\right]$ is the diagonal matrix of exponential functions. The Integration constants A_i can be related to the nodal displacements

$\langle u_N \rangle^T = \langle u_{b1} \quad \theta_{yb1} \quad \theta_{zb1} \quad \psi_{b1} \quad u_{b2} \quad \theta_{yb2} \quad \theta_{zb2} \quad \psi_{b2} \rangle^T$ by setting $z=0$ and $z=L$ in Eq. (4.18) leading to

$$\{u_N\}_{8\times1} = [H]_{8\times8}\{A\}_{8\times1} \tag{4.20}$$

in which

$$[H]_{8\times8} = \left[\begin{array}{c:c} [F(0)]_{4\times4} & [\Phi]_{4\times4}[E(0)]_{4\times4} \\ \hdashline [F(l)]_{4\times4} & [\Phi]_{4\times4}[E(l)]_{4\times4} \end{array}\right] \tag{4.21}$$

From Eq. (4.20) by solving for the integration constants and substituting into Eq. (4.18), one obtains

$$\{d(z)\} = [L(z)]_{4\times8}\{u_N\}_{8\times1} \tag{4.22}$$

in which $[L(z)]_{4\times8} = [B(z)]_{4\times8}[H]^{-1}_{8\times8}$ is a matrix of shape function, and

$$\begin{aligned} u_b(z) &= \langle L_1(z)\rangle_{1\times8}^{\ T}\{u_N\}_{8\times1} = \langle p_1\rangle_{1\times4}^T [L(z)]_{4\times8}\{u_N\}_{8\times1} \\ \theta_{yb}(z) &= \langle L_2(z)\rangle_{1\times8}^{\ T}\{u_N\}_{8\times1} = \langle p_2\rangle_{1\times4}^T [L(z)]_{4\times8}\{u_N\}_{8\times1} \\ \theta_{zb}(z) &= \langle L_3(z)\rangle_{1\times8}^{\ T}\{u_N\}_{8\times1} = \langle p_3\rangle_{1\times4}^T [L(z)]_{4\times8}\{u_N\}_{8\times1} \\ \psi_b(z) &= \langle L_4(z)\rangle_{1\times8}^{\ T}\{u_N\}_{8\times1} = \langle p_4\rangle_{1\times4}^T [L(z)]_{4\times8}\{u_N\}_{8\times1} \end{aligned} \tag{4.23)a-d}$$

and, $\langle p_1\rangle^T_{1\times4} = \langle 1 \quad 0 \quad 0 \quad 0\rangle_{1\times4}$, $\langle p_2\rangle^T_{1\times4} = \langle 0 \quad 1 \quad 0 \quad 0\rangle_{1\times4}$, $\langle p_3\rangle^T_{1\times4} = \langle 0 \quad 0 \quad 1 \quad 0\rangle_{1\times4}$, and $\langle p_4\rangle^T_{1\times4} = \langle 0 \quad 0 \quad 0 \quad 1\rangle_{1\times4}$ have been defined. It is noted that when a section is doubly symmetric, matrix $[H]_{8\times8}$ becomes singular and the shape functions introduced in Eq. (4.22) become unattainable. From Eqs. (4.23)a-d, by substituting into Eqs. (4.6)a-h and then Eq. (4.5), one obtains

$$\langle \delta u_n\rangle^T \left\{[K]_f + [K]_{sv} + [K]_s + \lambda\left([K_G]_N + [K_G]_M + [K_G]_V + [K_G]_{qy} + [K_G]_{qz}\right)\right\}\{\delta u_n\} = 0 \tag{4.24}$$

in which $[K]_f$ is the elastic stiffness matrix due to flexural stresses, $[K]_{sv}$ is the elastic stiffness matrix due to Saint Venant shear stresses, $[K]_s$ is the elastic matrix due to the remaining shear stresses, $[K_G]_N$ is the geometric matrix due to normal forces, $[K_G]_M$ is the geometric matrix due to bending moments, $\left[K_G\right]_V$ is the geometric matrix due to shear forces, $\left[K_G\right]_{qy}$ is the geometric matrix due to the distributed transverse load and $\left[K_G\right]_{qz}$ is the geometric matrix due to the distributed axial load. These stiffness matrices are obtained from

$$\begin{aligned}&\left\{\left[K_f\right],\left[K_{sv}\right],\left[K_s\right],\left[K_G\right]_N,\left[K_G\right]_M,\left[K_G\right]_V,\left[K_G\right]_{qy},\left[K_G\right]_{qz}\right\} = \\ &\left[H^{-1}\right]_{8\times 8}^T\left\{\left[M_1\right],\left[M_2\right],\left[M_3\right],\left[M_4\right],\left[M_5\right],\left[M_6\right],\left[M_7\right],\left[M_8\right]\right\}\left[H\right]_{8\times 8}^{-1}\end{aligned} \tag{4.25}$$

in which $\left[M_1\right]$ to $\left[M_8\right]$ are provided in Appendix A.

4.5 Examples

This section provides various buckling examples aimed at assessing the quality of the results, and illustrate its various features. All examples assume steel material with $E = 200,000$ MPa and $G = 77,000$ MPa and all the examples (excluding Example 7), are related to the section illustrated in Figure 4-4. Cross-sectional properties are $I_{xx} = 5.6987\times 10^7\,\text{mm}^4$, $I_{yy} = 1.42155\times 10^7\,\text{mm}^4$, $A = 8\times 10^3\,\text{mm}^2$, $I_{\omega\omega} = 3.2080\times 10^{10}\,\text{mm}^6$, $I_{px} = 2.1056\times 10^9\,\text{mm}^5$, $y_A = -58\text{mm}$, $J = 8.61867\times 10^5\,\text{mm}^4$, $D_{xx} = 5.600\times 10^3\,\text{mm}^2$, $D_{hh} = 5.71264\times 10^7\,\text{mm}^4$, $D_{yy} = 2.400\times 10^3\,\text{mm}^2$, $D_{xh} = -2.52800\times 10^5\,\text{mm}^3$, and $D_{yk} = -72000\text{mm}^3$.

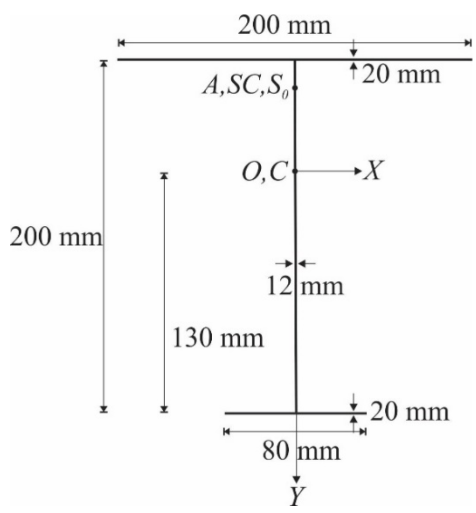

Figure 4-4 Dimensions of the mono-symmetric cross-section

4.5.1 Example 1: Closed-form solution for a simply supported beam under uniform bending moment

A simply supported beam of length L with a mono-symmetric cross-section is subject to uniform bending moment M_x. All other internal forces are assumed to vanish. By setting $\left(M_{xp}\left(z\right)=M_{xp}\neq 0, N_z=V_y=q_y=q_z=0\right)$ in the governing differential equations (Eq. (4.10)) and solving the resulting coupled system of differential equations, one obtains

$$\left\{d\left(z\right)\right\}=\left[B(z)\right]_{4\times 8}\left\{A\right\}_{8\times 1} \tag{4.26}$$

The relevant boundary conditions are

$$\begin{aligned}
&u_b\left(0\right)=0,\quad EI_{yy}\theta'_{yb}\left(0\right)+M_{xp}\theta_{zb}\left(0\right)=0,\quad \theta_{zb}\left(0\right)=0,\quad \psi'_b\left(0\right)=0\\
&u_b\left(L\right)=0,\quad EI_{yy}\theta'_{yb}\left(L\right)+M_{xp}\theta_{zb}\left(L\right)=0,\quad \theta_{zb}\left(L\right)=0,\quad \psi'_b\left(L\right)=0
\end{aligned} \qquad \text{(4.27)a-h}$$

From Eq. (4.26) by substituting into the displacement field equations in Eqs. (4.27)a-h, one obtains

$$\begin{aligned}
M_{cr}&=\lambda M_{xp_{1,2}}=\frac{-b\pm\sqrt{d}}{2a}\\
a&=\left[-E^2I_{yy}I_{\omega\omega}\left(\frac{\pi}{L}\right)^4-GE\left(D_{hh}I_{yy}+D_{xx}I_{\omega\omega}\right)\left(\frac{\pi}{L}\right)^2+G^2\left(D_{xh}^2-D_{hh}D_{xx}\right)\right]\\
b&=EGI_{yy}\left(\frac{\pi}{L}\right)^2\left[EI_{\omega\omega}\left(2D_{xh}+\beta_xD_{xx}\right)\left(\frac{\pi}{L}\right)^2-G\beta_x\left(D_{xh}^2-D_{hh}D_{xx}\right)\right]\\
c&=EG^2I_{yy}\left(\frac{\pi}{L}\right)^2\left[EI_{\omega\omega}\left(-D_{xh}^2+D_{hh}D_{xx}+D_{xx}J\right)\left(\frac{\pi}{L}\right)^2-GJ\left(D_{xh}^2-D_{hh}D_{xx}\right)\right]\\
d&=b^2-4ac
\end{aligned} \qquad \text{(4.28)a-e}$$

In Eqs. (4.28)a-e, it can be verified that by setting $D_{xh}=\beta_x=0$, one recovers the critical moment expression M_{crd} based on the shear deformable theory as provided in Wu and Mohareb (2011a), i.e.,

$$M_{crd}=\pm G\pi\sqrt{\frac{D_{hh}D_{xx}E^2I_{\omega\omega}I_{yy}\pi^2+D_{xx}E^2I_{\omega\omega}I_{yy}J\pi^2+ED_{hh}D_{xx}GI_{yy}JL^2}{D_{hh}D_{xx}G^2L^4+E^2I_{\omega\omega}I_{yy}\pi^4+ED_{hh}GI_{yy}\pi^2L^2+ED_{xx}GI_{\omega\omega}\pi^2L^2}} \tag{4.29}$$

Also, for a large spans L, one has $-b\left\{\left[\left(\pi/L\right)^2 EI_{yy}\right]/2\beta_x^2\right\}\Big/2a\left\{\left[\left(\pi/L\right)^2 EI_{yy}/2\beta_x^2\right]^2-e\right\}\to 0$,

$b\sqrt{e}\Big/2a\left\{\left[\left(\pi/L\right)^2 EI_{yy}/2\beta_x^2\right]^2-e\right\}\to 0$,

$\left\{\left[\sqrt{d/2a}\left(\pi/L\right)^2 EI_{yy}\right]/2\beta_x^2\right\}\Big/\left\{\left[\left(\pi/L\right)^2 EI_{yy}/2\beta_x^2\right]^2-e\right\}\to 0$,

$-\sqrt{ed/2a}\Big/\left\{\left[\left(\pi/L\right)^2 EI_{yy}/2\beta_x^2\right]^2-e\right\}\to 1$,

in which $e=\left\{\left[\left(\pi/L\right)^2 EI_{yy}\right]/2\right\}^2\left\{\beta_x^2+4\left[\left(GJL^2/\pi^2 EI_{yy}\right)+\left(I_{\omega\omega}/I_{yy}\right)\right]\right\}$ and one can show that the critical moment expression in Eq. (4.28)a approaches that of the classical solution (Trahair (1993)), i.e.,

$$M_{cl}=\frac{\pi^2 EI_{yy}}{2L^2}\left[\beta_x\pm\sqrt{\beta_x^2+4\left(\frac{GJL^2}{\pi^2 EI_{yy}}+\frac{I_{\omega\omega}}{I_{yy}}\right)}\right] \qquad (4.30)\text{a-b}$$

In Eqs. (4.28)a and (4.30), the positive sign is taken when the large flange is in compression.

4.5.2 Example 2: Mesh density analysis

Consider a 2m span cantilever section subject to a vertical concentrated load located at the tip and acting at the shear center. The critical load as determined by the present formulation is provided for various discretizations. Results based on the present formulation (i.e., based on formulation II are compared to those predicted by a) the WM element, b) the classical non-shear deformable element by Barsoum and Gallagher (1970) (referred to as BG) and c) the WM element (Table 4.2). Also, for comparison, a solution was performed under the ABAQUS S4R shell element. ABAQUS S4R solution yields the lowest buckling load estimate of 282.3 kN. This is due to the fact that the shell element captures both the distortional and shear deformation effects and thus provides the most flexible representation of all solutions. The present element and the WM element predict nearly equal buckling loads of 287.2 kN and 288.0 kN, respectively. These values are slightly higher than that based on the shell solution. While shear deformation is captured in both formulations, they do not account for distortional effect and thus they provide a slightly stiffer representation for the member. The largest buckling load is that based on the BG which predicts a buckling load of 329.5 kN. This is expected since the BG element neglects shear distortional and shear deformation effects and thus provides the stiffest representation of the member among all solutions. Under the present formulation, it is observed that no more than eight elements are needed to attain convergence, in a manner similar to the BG element, but in contrast with the significantly larger number of WM elements needed.

The present solution converges from below for the problem, i.e., a coarser mesh tends to under-predict the buckling loads. This contrasts to the WM and BG elements, which consistently converge from above. However, convergence from below cannot be guaranteed. This is illustrated by considering a 5m span simply supported beam under end reverse moments (Table 4.3). For the case of a single element, the approximation $M_{xp}(z) \approx M_{xp} = (M_1 - M_2)/2$ introduced in Eq. (4.9) c yields, $M_{xp} = 0$, thus vanishing the destabilizing term due to bending moment, and the only destabilizing term remaining is due to shear (which is minor in the present 5m span beam), yielding a high buckling moment prediction of 286,800 kNm. A significant predictive improvement is obtained by taking eight elements.

Table 4.2 Mesh density study for cantilever under a concentrated load at the tip

(Span=2m, ABAQUS critical load=282.3 kN)

Present Study			**WM Element**			**BG Element**		
Number of Elements	**Buckling Load (kN)**	**Present Study/ ABAQUS**	**Number of Elements**	**Buckling Load (kN)**	**WM/ ABAQUS**	**Number of Elements**	**Buckling Load (kN)**	**BG/ ABAQUS**
2	275.9	97.73%	32	302.7	107.2%	2	332.2	117.7%
3	283.6	100.4%	64	291.4	103.2%	3	330.0	116.9%
4	285.7	101.2%	128	288.4	102.2%	4	329.7	116.8%
5	286.5	101.5%	256	288.0	102.0%	5	329.6	116.8%
6	286.9	101.6%	-	-	-	6	329.6	116.8%
8	287.2	101.7%	-	-	-	8	329.5	116.7%
10	287.2	101.7%	-	-	-	-	-	-

Table 4.3 Convergence study for a simply supported beam (span=5m) under reverse end moments

Number of Elements	**Buckling Moment (kNm)**
1	286.8×10^{3}
2	602.4
4	529.9
8	499.9
10	498.1

4.5.3 Example 3: Influence of span on shear deformation effects

A cantilever is subject to a transverse concentrated load applied at the shear center of the free end. Two spans are examined in this example: 1000 and 4000 mm. The lateral torsional buckling load is estimated based on four solutions: (1) The classical BG solution which neglects shear deformations and distortional effects, (2) the WM solution (Wu and Mohareb (2011b)) which captures shear deformations but neglects distortional effects, (3) the present formulation which also captures shear deformations and neglects distortional effects and (4) the ABAQUS shell analysis which considers both effects. As suggested in Example 2, eight elements were used for the BG solution, 64 elements per meter were used for the WM element, and eight elements were used for the present solution. In the ABAQUS model, 10 elements per top flange, four elements per bottom flange, 10 elements along the web height and 50 elements in the longitudinal direction were taken to model the beam. The results are presented in Table 4.4. As observed in Example 2, the ABAQUS shell element solution provides the lowest buckling prediction. This is attributed to the fact that the shell formulation is the only solution that captures distortional effects, which tend to be more significant in a short span cantilever. This is illustrated in Figure 4-5a where the web of the 1m span cantilever is observed to undergo minor distortion near the top flange (relative to the shown straight reference line). In contrast, the web for the 4m span (Figure 4-5b) cantilever is observed to essentially undergo no distortion compared to the straight reference line. Since both the WM element and the present element capture shear deformation effects, their buckling load predictions are smaller than those based on the BG element. As illustrated by results, the shear deformation effect is more pronounced in the short span cantilever. This is evident by the 24%

difference observed between the buckling load prediction based on the present element and the BG element. The difference is only 6% for the longer span cantilever.

Table 4.4 Buckling loads (kN) for a mono-symmetric cantilever beam under a tip vertical concentrated load

Span (mm)	ABAQUS	Present Element	WM Element	BG Element	Present /ABAQUS	WM/ ABAQUS	BG/ ABAQUS
1000	866.5	**925.5**	930.8	1223	1.07	1.07	1.41
4000	81.86	**84.50**	84.90	89.70	1.03	1.04	1.10

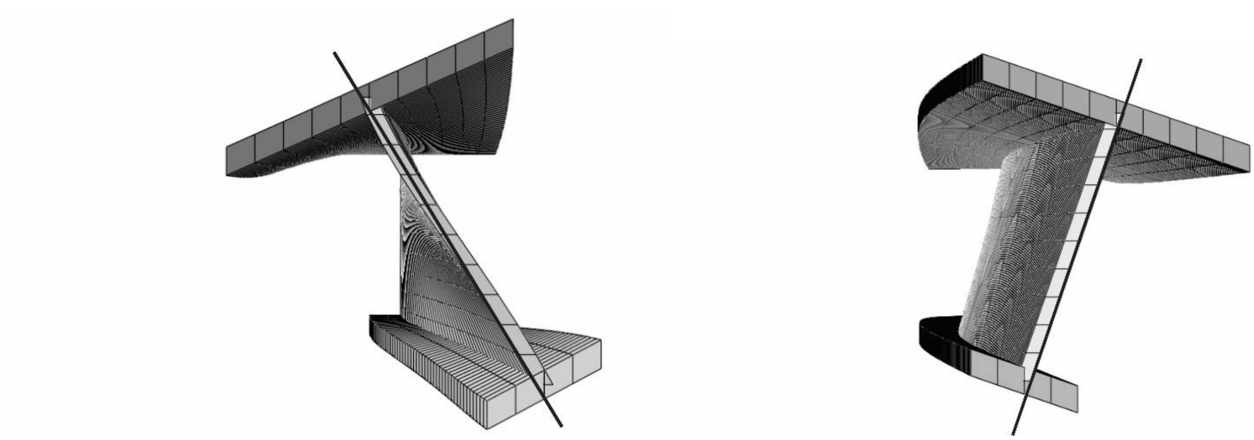

(a) **(b)**

Figure 4-5 Distorted cross-section at free end: (a) span=1000 mm, (b) span=4000 mm

4.5.4 Example 4: Beam under linear bending moment

A simply supported mono-symmetric beam is subject to a linear bending moment distribution as shown in Figure 4-6a. A strong axis moment M_x is a applied at the left end and a moment vary βM_x at the other end where $-1 \le \beta \le 1$. Two cases are considered: In Case 1, the larger flange is located in the top of the section so that the larger flange is under compression (Figure 4-6b) and in Case 2, the smaller flange is in the top so that the smaller flange is under compression (Figure 4-6c). Spans were taken to vary from 1m to 5m. For Case 1 under uniform moments, i.e., $\beta = -1$, the lateral torsional buckling capacity is predicted based on three different FEA solutions including the present element (with eight elements along the span), and the WM and BG elements, the closed-form as provided in Eq. (4.28)a-e as well as the classical solution as given by Eq. (4.30) a-b while retaining the positive sign. Table 4.5 shows that the critical moment as predicted by the present FEA and closed form solution agree well with the classical solution for large spans (2m and larger). For the 1m span, where shear deformation effects are significant, the critical moment as predicted by the present shear deformable solution is less than that predicted by the classical solution which neglects shear deformation effects. It is noted that the results based on the present element nearly coincide the WM element with a significantly lower number of DOFs.

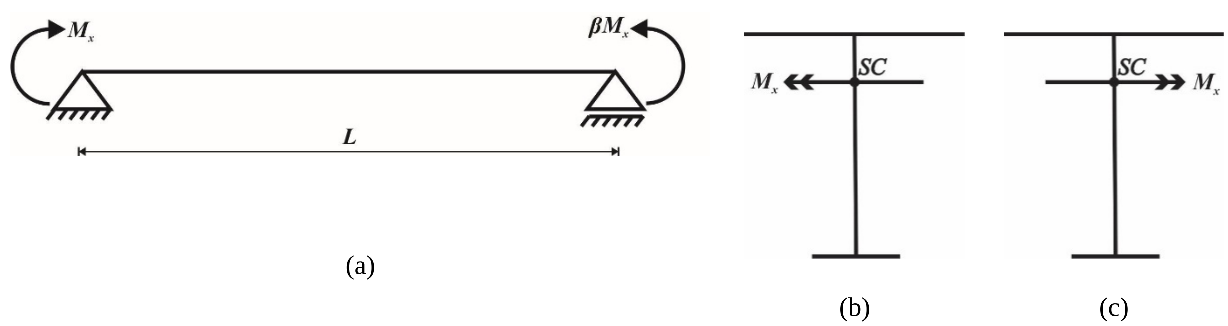

Figure 4-6 Simply supported beam under moment gradient (a) Elevation, (b) Cross-section for Case (1) - Moments M_x induces compression in larger flange, and (c) Cross-Section for Case (2) – Moments M_x induces compression in smaller flange

Table 4.5 Lateral torsional buckling loads (kNm) for a simply supported beam under uniform bending moment (Case 1-larger flange in compression)

Span (m)	**1**	**2**	**3**	**4**	**5**
Present Finite Element (8 elements)	**4652**	**1441**	**767.8**	**508.4**	**376.4**
WM Element (64 elements/m)	4658	1444	768.9	509.0	376.6
BG Element (8 elements)	5017	1466	773.0	510.0	376.9
Closed-form Solution Present Study - (Eq. 28a)	**4647**	**1440**	**764.5**	**508.2**	**376.0**
Classical Closed-form Solution M_{cl} - (Eq. 30a)	5017	1466	772.9	510.0	376.9
Present/Classical	0.93	0.98	0.99	1.00	1.00

For non-uniform moments, the moment gradient factor is defined as the ratio of the critical moment as predicted by the present study to that of classical solution as given by Eq. (4.30)a. This ratio accounts for the end moment ratios β and the span. The results are depicted in Figure 4-7 for Case 1 where moments induce compression in the larger flange and Figure 4-8 for Case 2 where the smaller flange is under compression. For the longer spans, the moment gradient factor is observed to be almost identical for 3m, 4m and 5m spans (and larger spans –not shown on the figure) in the moment gradient range $-1 \leq \beta \leq 0$ i.e., when the larger flange is under entirely under compression. For shorter spans, smaller moment gradient factors are obtained given that shear deformation effects gain significance in such short spans. When moments induce compression in the smaller flange, the moment gradient factor monotonically increases with the end moment ratio β (Figure 4-8). In contrast, for the case where the larger flange is under compression, the moment gradient factors peak around $\beta = 0.5$ for 3, 4, 5m spans and close to $\beta = 0.0$ for the short span beams.

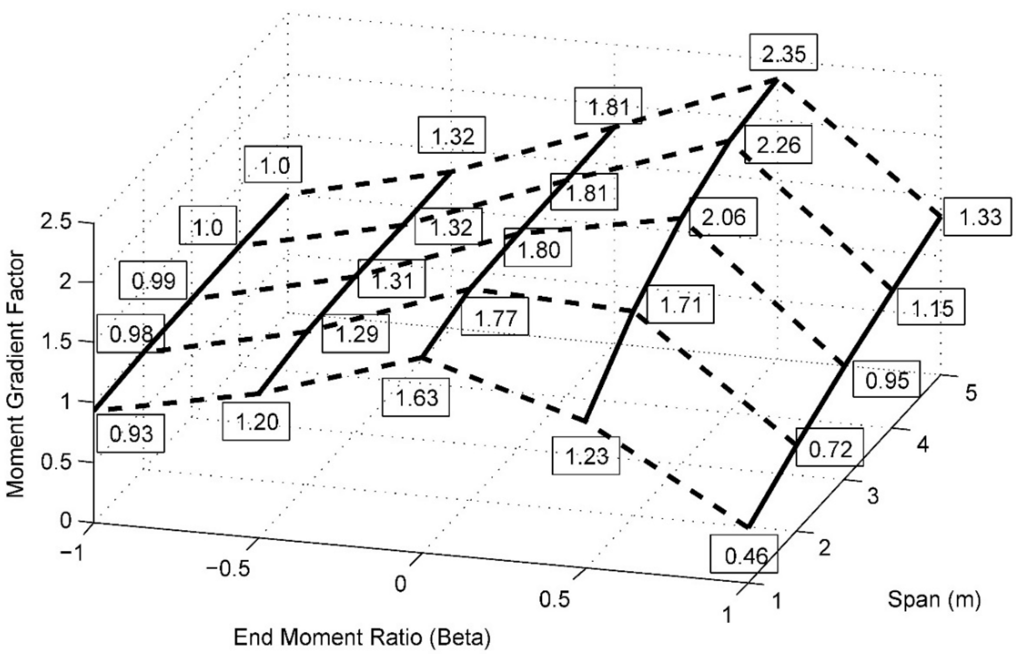

Figure 4-7 Moment gradient factor versus various end moment ratios β and spans (m) – for Case (1): Larger flange under compression

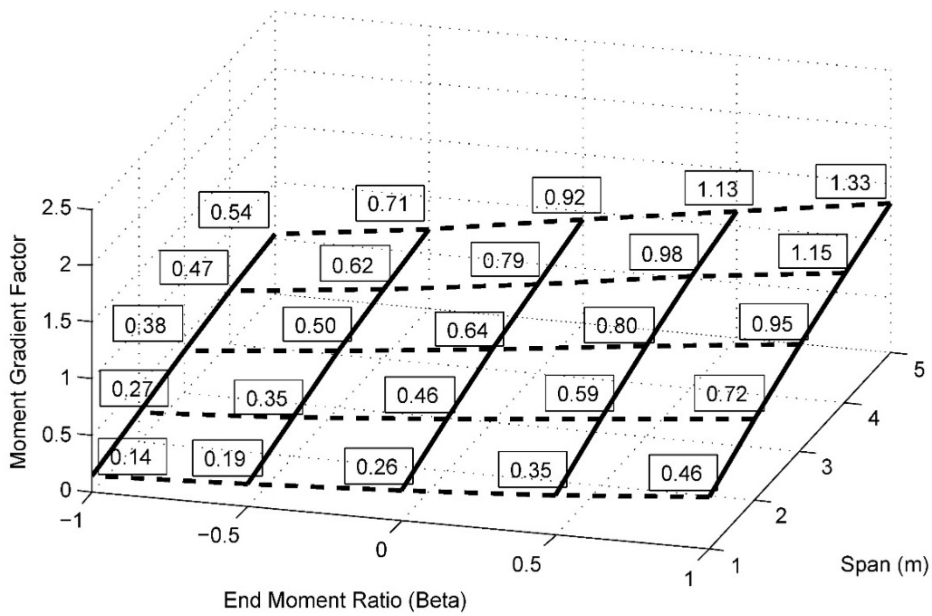

Figure 4-8 Moment gradient factor versus various end moment ratios β and spans (m) – for Case (2): Smaller flange under compression

4.5.5 Example 5: Axial force-bending interaction

A simply supported member has a 4m span and is subject to an axial compressive force Q_z and two equal end moments. In the absence of uniform bending moment, the flexural-torsional buckling load Q_{z0} obtained is 1580.6 kN, while from Example 4, the buckling moment M_{x0} in the absence of the axial load is 508.4 kNm. In order to develop the $Q_z - M_x$ buckling interaction diagram, several load combinations $\left(Q_{zi}, M_{xi}\right)$ $i = 1,...,n$ are applied to the member and the buckling eigenvalues are obtained for each case. This gives $i = 1,...,n$ critical load combinations $\lambda_i\left(Q_{zi}/Q_{z0}, \lambda_i M_{xi}/M_{x0}\right)$ in which each load combination has been normalized with respect to Q_{z0} and M_{x0}. The resulting normalized interaction curve is depicted in Figure 4-9.

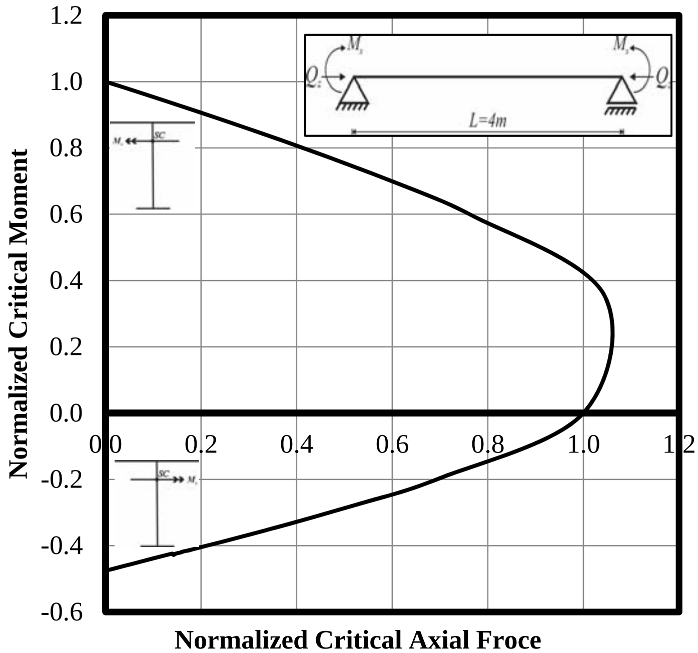

Figure 4-9 Normalized Interaction Diagram

As can be seen, unlike doubly symmetric sections, the diagram is non-symmetric about the horizontal axis. This observation is in line with what is observed in Mohri et al. (2013). The higher critical moment ratio $\lambda M_x / M_{x0} = 1$ is obtained when the section is under pure bending and when the top flange is under compression.

4.5.6 Example 6: Effect of load height position for a member under concentrated transverse load

A cantilever spanning 5m is subject to a concentrated transverse load applied at the tip. Three different load positions are considered: (a) top flange, (b) shear center and (c) bottom flange. The results are shown to agree well with those based on the shell finite element analysis (Table 4.6). Due to the destabilizing effect of the top flange loading, buckling loads are lower than that based on shear center loading. Bottom flange loading is associated with a stabilizing effect which increases the buckling load.

Table 4.6 Load position effect on lateral torsional buckling estimates (kN) of a cantilever beam under a tip vertical load

Load Position	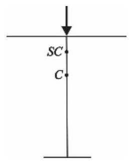	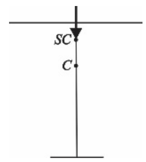	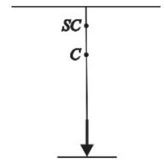
(1) Present Study	**55.3**	**56.4**	**68.0**
(2) ABAQUS	53.5	54.4	63.2
Percentage difference ((1)-(2))/(2)	3.3%	3.7%	7.6%

4.5.7 Example 7: Mono-symmetric I-girder

The present example illustrates the applicability of the formulation for other types of mono-symmetric sections. A simply supported girder (Cross-section given in Figure 4-10) is subject to a mid-span point load applied at the shear center. Four spans are examined in this example; 2000, 4000, 6000 and 8000 mm. The lateral torsional buckling load estimated based on the present study is compared to those obtained from the classical BG element. Sectional properties are $I_{xx} = 1.2 \times 10^9 \,\mathrm{mm}^4$, $I_{yy} = 3.73 \times 10^8 \,\mathrm{mm}^4$, $A = 3 \times 10^4 \,\mathrm{mm}^2$, $I_{\omega\omega} = 2.39 \times 10^{13} \,\mathrm{mm}^6$, $I_{px} = 1.70 \times 10^{10} \,\mathrm{mm}^5$, $y_A = -105 \mathrm{mm}$, $J = 4.0 \times 10^6 \,\mathrm{mm}^4$, $D_{xx} = 16000 \mathrm{mm}^2$, $D_{hh} = 1.44 \times 10^9 \,\mathrm{mm}^4$, $D_{yy} = 14000 \mathrm{mm}^2$, $D_{xh} = -2.107 \times 10^6 \,\mathrm{mm}^3$, and $D_{yk} = 4.27 \times 10^5 \,\mathrm{mm}^3$.

As dicussed in previous examples, as the beam span increases, shear deformation effects become less significant. Consequently in Table 4.7, the buckling load ratio varies from 0.82 at a span of 2m to 0.97 at a span of 12m.

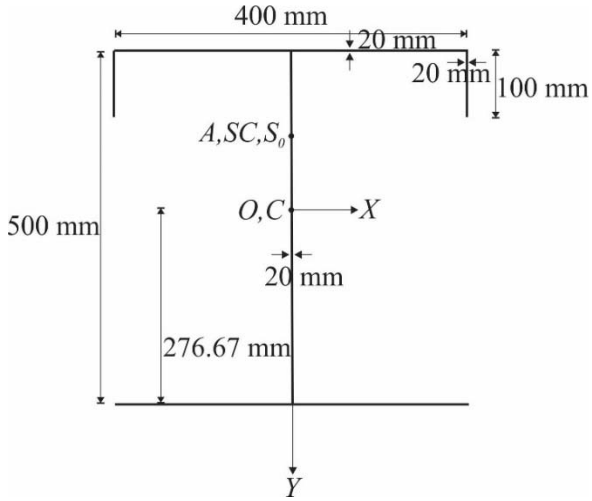

Figure 4-10 Dimensions of the I-girder cross-section

Table 4.7 Lateral torsional buckling loads (kN) for a simply supported beam under mid-span point load

Span (m)	**2**	**4**	**6**	**8**	**12**
Present Solution	$\mathbf{8.984\times10^{4}}$	$\mathbf{1.286\times10^{4}}$	**4154**	**1921**	**705.1**
BG Element	1.098×10^{5}	1.432×10^{4}	4521	2062	727.6
Present Solution/BG element	0.82	0.90	0.92	0.93	0.97

4.6 Summary and Conclusions

1. A general shear deformable element was developed for buckling analysis of members with mono-symmetric sections.
2. Compared to the shear deformable WM element (Wu and Mohareb (2011b)), the number of degrees of freedom needed for convergence was observed to reduce significantly.
3. A closed-form solution was derived for the buckling moments of shear deformable mono-symmetric simply supported beams under uniform bending moments.
4. Results obtained based on the present element and the WM element were found to provide results in close agreement.
5. For long spans, excellent agreement was obtained with ABAQUS FEA shell results. For shorter spans, the present solution provides higher buckling predictions compared to

ABAQUS results, but lower than those based on the classical BG element. This is a natural outcome of the fact that ABAQUS shell model captures shear deformation and distortional effects, thus providing the most flexible representation, while the present solution captures shear deformation effects but not the distortional effect and the classical solution captures neither effects.

6. Based on the present formulation, moment gradient factors were developed for the mono-symmetric section investigated in the study and were shown to depend upon the end moment ratio as well as the span. Beyond a certain span (3m in the present problem) when $-1 \leq \beta \leq 0$ and the lager flange is under compression, the moment gradient factors were observed to become independent of the span.
7. Interaction effects between moments and axial force as well as the load height position effects were successfully captured through the present element.

4.7 Appendix A. Matrices needed to determine stiffness matrices

This appendix provides explicit expressions for matrices forming stiffness matrices. In Eq. (4.25) , the elastic stiffness matrix components $\left[K_f\right],\left[K_{sv}\right],\left[K_s\right]$ and geometric stiffness components $\left[K_G\right]_N,\left[K_G\right]_M,\left[K_G\right]_V,\left[K_G\right]_{qy},\left[K_G\right]_{qz}$ were expressed as a function of matrices $\left[M_1\right],\left[M_2\right],...,\left[M_8\right]$. In order to obtain elastic and geometric stiffness matrices, firstly, $\left[M_1\right],\left[M_2\right],...,\left[M_8\right]$ matrices should be calculated numerically as follows

4.7.1 Elastic stiffness due to flexural stresses

Matrix $\left[M_1\right]$ related to $\left[K_f\right]$ is given by

$$[M_1] = EI_{yy}\begin{bmatrix} 0 & 0 & 0 & 0 & 0 & 0 & 0 & 0 \\ & 0 & 0 & 0 & 0 & 0 & 0 & 0 \\ & & 4L & 6L^2 & \bar{a}_1 & \bar{a}_2 & \bar{a}_3 & \bar{a}_4 \\ & & & 12L^3 & \bar{b}_1 & \bar{b}_2 & \bar{b}_3 & \bar{b}_4 \\ & & & & \bar{c}_{1,1} & \bar{c}_{1,2} & \bar{c}_{1,3} & \bar{c}_{1,4} \\ & & & & & \bar{c}_{2,2} & \bar{c}_{2,3} & \bar{c}_{2,4} \\ & & Sym. & & & & \bar{c}_{3,3} & \bar{c}_{3,4} \\ & & & & & & & \bar{c}_{4,4} \end{bmatrix} \tag{4.31}$$

in which functions $\bar{a}_i$, $\bar{b}_i$ and $\bar{c}_{i,j}$ are defined as

$$\bar{a}_i = 2\varphi_{2i}\left(e^{Lm_i} - 1\right)$$
$$\bar{b}_i = 6\varphi_{2i}m_i\left(\frac{1}{m_i^2} + \frac{e^{Lm_i}\left(Lm_i - 1\right)}{m_i^2}\right) \tag{4.32)a-c}$$
$$\bar{c}_{i,j} = \frac{m_i m_j\left(I_{yy}\varphi_{2i}\varphi_{2j} + I_{\omega\omega}\varphi_{4i}\varphi_{4j}\right)\left(e^{Lm_i + Lm_j} - 1\right)}{I_{yy}\left(m_i + m_j\right)}$$

and φ_{ij} denotes the jth element of eigenvector $\{\varphi_i\}$.

4.7.2 Elastic stiffness due to Saint Venant shear stress

Matrix $[M_2]$ related to $[K_{sv}]$ is given by

$$[M_2] = GJ\begin{bmatrix} 0 & 0 & 0 & 0 & 0 & 0 & 0 & 0 \\ & 0 & 0 & 0 & 0 & 0 & 0 & 0 \\ & & 0 & 0 & 0 & 0 & 0 & 0 \\ & & & 0 & 0 & 0 & 0 & 0 \\ & & & & \bar{d}_{1,1} & \bar{d}_{1,2} & \bar{d}_{1,3} & \bar{d}_{1,4} \\ & & & & & \bar{d}_{2,2} & \bar{d}_{2,3} & \bar{d}_{2,4} \\ & & Sym. & & & & \bar{d}_{3,3} & \bar{d}_{3,4} \\ & & & & & & & \bar{d}_{4,4} \end{bmatrix} \tag{4.33}$$

in which function $\bar{d}_{i,j}$ are defined as

$$\bar{d}_{i,j}=\frac{\left(\varphi_{3i}\varphi_{3j}\right)\left(m_i m_j\right)\left(e^{Lm_i+Lm_j}-1\right)}{m_i+m_j} \tag{4.34}$$

4.7.3 Elastic stiffness due to shear stresses

Matrix $\left[M_3\right]$ related to $\left[K_s\right]$ is given by

$$\left[M_3\right]=\begin{bmatrix} 0 & 0 & 0 & 0 & 0 & 0 & 0 & 0 \\ & 0 & 0 & 0 & 0 & 0 & 0 & 0 \\ & & 0 & 0 & 0 & 0 & 0 & 0 \\ & & & \bar{\alpha} & \bar{e}_1 & \bar{e}_2 & \bar{e}_3 & \bar{e}_4 \\ & & & & \bar{g}_1 & \bar{f}_{1,2} & \bar{f}_{1,3} & \bar{f}_{1,4} \\ & & & & & \bar{g}_2 & \bar{f}_{2,3} & \bar{f}_{2,4} \\ & Sym. & & & & & \bar{g}_3 & \bar{f}_{3,4} \\ & & & & & & & \bar{g}_4 \end{bmatrix} \tag{4.35}$$

in which functions $\bar{e}_i$, $\bar{f}_{i,j}$, and $\bar{g}_i$ are defined as

$$\bar{e}_i=\frac{6EI_{yy}\left(e^{Lm_i}-1\right)\left(\varphi_{2i}-\varphi_{1i}m_i\right)}{m_i}$$

$$\begin{aligned}\bar{f}_{i,j}=&\frac{G\left(e^{Lm_i+m_j}-1\right)}{m_i+m_j}\Big(D_{hh}\left(\varphi_{4i}\varphi_{4j}+\varphi_{3i}\varphi_{4j}m_i+\varphi_{3j}\varphi_{4i}m_j+\varphi_{3i}\varphi_{3j}m_im_j\right)\\&+D_{xx}\left(\varphi_{2i}\varphi_{2j}-\varphi_{1i}\varphi_{2j}m_i-\varphi_{1j}\varphi_{2i}m_j+\varphi_{1i}\varphi_{1j}m_im_j\right)\\&+D_{xh}\left(-\varphi_{2i}\varphi_{4j}-\varphi_{2j}\varphi_{4i}+\varphi_{1i}\varphi_{4j}m_i-\varphi_{2j}\varphi_{3i}m_i+\varphi_{1j}\varphi_{4i}m_j-\varphi_{2i}\varphi_{3j}m_j+\varphi_{1i}\varphi_{3j}m_im_j+\varphi_{1j}\varphi_{3i}m_im_j\right)\Big)\end{aligned}$$

$$\begin{aligned}\bar{g}_i=&\frac{G\left(e^{2Lm_i}-1\right)\left(2D_{hh}\varphi_{3i}\varphi_{4i}-2D_{xx}\varphi_{1i}\varphi_{2i}+2D_{xh}\varphi_{1i}\varphi_{4i}-2D_{xh}\varphi_{2i}\varphi_{3i}\right)}{2}\\&+\frac{Gm_i\left(e^{2Lm_i}-1\right)\left(D_{xx}\varphi_{1i}{}^2+2D_{xh}\varphi_{1i}\varphi_{3i}+D_{hh}\varphi_{3i}{}^2\right)}{2}+\frac{G\left(e^{2Lm_i}-1\right)\left(D_{xx}\varphi_{2i}{}^2-2D_{xh}\varphi_{2i}\varphi_{4i}+D_{hh}\varphi_{4i}{}^2\right)}{2m_i}\end{aligned}$$

(4.36)a-c

and parameter $\bar{\alpha}$ is

$$\bar{\alpha}=\frac{-36D_{hh}E^2I_{yy}{}^2L}{G\left(D_{xh}{}^2-D_{hh}D_{xx}\right)} \tag{4.37}$$

4.7.4 Geometric stiffness due to normal forces

Matrix $\left[M_4\right]$ related to $\left[K_G\right]_N$ is given by

$$\left[M_4\right] = N\begin{bmatrix} 0 & 0 & 0 & 0 & 0 & 0 & 0 & 0 \\ & L & L^2 & L^3 & \bar{h}_1 & \bar{h}_2 & \bar{h}_3 & \bar{h}_4 \\ & & \dfrac{4L^3}{3} & \dfrac{3L^4}{2} & \bar{k}_1 & \bar{k}_2 & \bar{k}_3 & \bar{k}_4 \\ & & & \dfrac{9L^5}{5} & \bar{n}_1 & \bar{n}_2 & \bar{n}_3 & \bar{n}_4 \\ & & & & \bar{p}_1 & \bar{o}_{1,2} & \bar{o}_{1,3} & \bar{o}_{1,4} \\ & & & & & \bar{p}_2 & \bar{o}_{2,3} & \bar{o}_{2,4} \\ & Sym. & & & & & \bar{p}_3 & \bar{o}_{3,4} \\ & & & & & & & \bar{p}_4 \end{bmatrix} \tag{4.38}$$

in which functions $\bar{h}_i$, $\bar{k}_i$, $\bar{n}_i$, $\bar{o}_{i,j}$ and $\bar{p}_i$ are defined as

$$\begin{aligned} \bar{h}_i &= \left(\varphi_{1i} + \varphi_{3i} y_A\right)\left(e^{Lm_i} - 1\right) \\ \bar{k}_i &= \frac{2\left(\varphi_{1i} + \varphi_{3i} y_A\right)\left(Lm_i e^{Lm_i} - e^{Lm_i} + 1\right)}{m_i} \\ \bar{n}_i &= \frac{3\left(\varphi_{1i} + \varphi_{3i} y_A\right)\left(2e^{Lm_i} + L^2 m_i^{\,2} e^{Lm_i} - 2Lm_i e^{Lm_i} - 2\right)}{m_i^{\,2}} \\ \bar{o}_{i,j} &= \frac{m_i m_j \left(e^{L\left(m_i + m_j\right)} - 1\right)\left(A\varphi_{1i}\varphi_{1j} + \left(Ay_A^2 + I_{xx} + I_{yy}\right)\varphi_{3i}\varphi_{3j} + Ay_A\left(\varphi_{1i}\varphi_{3j} + \varphi_{1j}\varphi_{3i}\right)\right)}{A\left(m_i + m_j\right)} \\ \bar{p}_i &= \frac{m_i\left(e^{2Lm_i} - 1\right)\left(\varphi_{1i}^2 + 2\varphi_{1i}\varphi_{3i} y_A + \varphi_{3i}^2 y_A^2\right)}{2} + \frac{m_i\left(e^{2Lm_i} - 1\right)\left(\left(I_{xx} + I_{yy}\right)\varphi_{3i}^2\right)}{2A} \end{aligned} \tag{4.39a-e}$$

4.7.5 Geometric stiffness due to bending moments

Matrix $\left[M_5\right]$ related to $\left[K_G\right]_M$ is given by

$$\left[M_5\right]=M\begin{bmatrix} 0 & 0 & 0 & 0 & 0 & 0 & 0 & 0 \\ & 0 & 0 & 0 & 0 & 0 & 0 & 0 \\ & & 0 & 0 & \overline{q}_1 & \overline{q}_2 & \overline{q}_3 & \overline{q}_4 \\ & & & 0 & \overline{r}_1 & \overline{r}_2 & \overline{r}_3 & \overline{r}_4 \\ & & & & \overline{t}_1 & \overline{s}_{1,2} & \overline{s}_{1,3} & \overline{s}_{1,4} \\ & & & & & \overline{t}_2 & \overline{s}_{2,3} & \overline{s}_{2,4} \\ & Sym. & & & & & \overline{t}_3 & \overline{s}_{3,4} \\ & & & & & & & \overline{t}_4 \end{bmatrix} \tag{4.40}$$

in which functions $\overline{q}_i$, $\overline{r}_i$, $\overline{s}_{i,j}$ and $\overline{t}_i$ are defined as

$$\begin{aligned}
\overline{q}_i &= \frac{2\varphi_{3i}\left(e^{Lm_i}-1\right)}{m_i} \\
\overline{r}_i &= 6\varphi_{3i}\left(\frac{1}{m_i^{\,2}}+\frac{e^{Lm_i}\left(Lm_i-1\right)}{m_i^{\,2}}\right)-\frac{6ED_{hh}I_{yy}\varphi_{3i}\left(e^{Lm_i}-1\right)}{G\left(D_{xh}^{\;2}-D_{hh}D_{xx}\right)} \\
\overline{s}_{i,j} &= \frac{\left(e^{L\left(m_i+m_j\right)}-1\right)\begin{pmatrix}\left(\varphi_{2i}\varphi_{3j}+\varphi_{2j}\varphi_{3i}\right)m_i+\left(\varphi_{2i}\varphi_{3j}+\varphi_{2j}\varphi_{3i}\right)m_j+\dfrac{I_{px}}{I_{xx}}\varphi_{3i}\varphi_{3j}m_i m_j \\ -\left(\varphi_{1i}\varphi_{3j}+\varphi_{1j}\varphi_{3i}\right)m_i m_j-2\varphi_{3i}\varphi_{3j}y_A m_i m_j\end{pmatrix}}{\left(m_i+m_j\right)} \\
\overline{t}_i &= \frac{I_{px}\varphi_{3i}^2 m_i\left(e^{2Lm_i}-1\right)}{2I_{xx}}-\frac{\varphi_{3i}\left(e^{2Lm_i}-1\right)\left(2\varphi_{1i}m_i-4\varphi_{2i}+2\varphi_{3i}m_i y_A\right)}{2}
\end{aligned} \tag{4.41)a-d}$$

4.7.6 Geometric stiffness due to shear forces

Matrix $\left[M_6\right]$ related to $\left[K_G\right]_V$ is given by

$$\left[M_6\right]=V\begin{bmatrix} 0 & 0 & 0 & 0 & 0 & 0 & 0 & 0 \\ & 0 & 0 & 0 & 0 & 0 & 0 & 0 \\ & & 0 & 0 & 0 & 0 & 0 & 0 \\ & & & 0 & \overline{u}_1 & \overline{u}_2 & \overline{u}_3 & \overline{u}_4 \\ & & & & \overline{w}_1 & \overline{v}_{1,2} & \overline{v}_{1,3} & \overline{v}_{1,4} \\ & & & & & \overline{w}_2 & \overline{v}_{2,3} & \overline{v}_{2,4} \\ & Sym. & & & & & \overline{w}_3 & \overline{v}_{3,4} \\ & & & & & & & \overline{w}_4 \end{bmatrix} \tag{4.42}$$

in which functions $\bar{u}_i$, $\bar{v}_{i,j}$ and $\bar{w}_i$ are defined as

$$\begin{aligned}
\bar{u}_i &= -\frac{6ED_{hh}I_{yy}\varphi_{3i}\left(e^{Lm_i}-1\right)}{Gm_i\left(D_{xh}{}^2-D_{hh}D_{xx}\right)} \\
\bar{v}_{i,j} &= \frac{\left(e^{L\left(m_i+m_j\right)}-1\right)\left(\varphi_{2i}\varphi_{3j}+\varphi_{2j}\varphi_{3i}-\varphi_{1i}\varphi_{3j}m_i-\varphi_{1j}\varphi_{3i}m_j+\dfrac{D_{yk}}{D_{yy}}\varphi_{3i}\varphi_{3j}\left(m_i+m_j\right)\right)}{\left(m_i+m_j\right)} \qquad \text{(4.43)a-c} \\
\bar{w}_i &= \frac{\varphi_{3i}\left(e^{2Lm_i}-1\right)\left(D_{yy}\varphi_{2i}-D_{yy}\varphi_{1i}m_i+D_{yk}\varphi_{3i}m_i\right)}{D_{yy}m_i}
\end{aligned}$$

4.7.7 Geometric stiffness due to distributed transverse load

Matrix $\left[M_7\right]$ related to $\left[K_G\right]_{qy}$ is given by

$$\left[M_7\right]=q_y\begin{bmatrix}
0 & 0 & 0 & 0 & 0 & 0 & 0 & 0 \\
 & 0 & 0 & 0 & 0 & 0 & 0 & 0 \\
 & & 0 & 0 & 0 & 0 & 0 & 0 \\
 & & & 0 & 0 & 0 & 0 & 0 \\
 & & & & \bar{y}_1 & \bar{x}_{1,2} & \bar{x}_{1,3} & \bar{x}_{1,4} \\
 & & & & & \bar{y}_2 & \bar{x}_{2,3} & \bar{x}_{2,4} \\
 & Sym. & & & & & \bar{y}_3 & \bar{x}_{3,4} \\
 & & & & & & & \bar{y}_4
\end{bmatrix} \qquad (4.44)$$

in which functions $\bar{x}_{i,j}$ and $\bar{y}_i$ are defined as

$$\begin{aligned}
\bar{x}_{i,j} &= \frac{-\varphi_{3i}\varphi_{3j}\left(e^{L\left(m_i+m_j\right)}-1\right)\left(y_A-y_{qy}\right)}{m_i+m_j} \qquad \text{(4.45)a-b} \\
\bar{y}_i &= \frac{-\varphi_{3i}{}^2\left(y_A-y_{qy}\right)\left(e^{2Lm_i}-1\right)}{2m_i}
\end{aligned}$$

4.7.8 Geometric stiffness due to distributed axial load

Matrix $\left[M_8\right]$ related to $\left[K_G\right]_{qz}$ is given by

$$[M_8] = q_z \begin{bmatrix} 0 & 0 & 0 & 0 & 0 & 0 & 0 & 0 \\ & 0 & 0 & 0 & \overline{z}_1 & \overline{z}_2 & \overline{z}_3 & \overline{z}_4 \\ & & 0 & 0 & \hat{a}_1 & \hat{a}_2 & \hat{a}_3 & \hat{a}_4 \\ & & & 0 & \hat{b}_1 & \hat{b}_2 & \hat{b}_3 & \hat{b}_4 \\ & & & & \hat{d}_1 & \hat{c}_{1,2} & \hat{c}_{1,3} & \hat{c}_{1,4} \\ & & & & & \hat{d}_2 & \hat{c}_{2,3} & \hat{c}_{2,4} \\ & Sym. & & & & & \hat{d}_3 & \hat{c}_{3,4} \\ & & & & & & & \hat{d}_4 \end{bmatrix} \tag{4.46}$$

in which functions $\overline{z}_i$, $\hat{a}_i$, $\hat{b}_i$, $\hat{c}_i$ and $\hat{d}_i$ are defined as

$$\begin{aligned}
\overline{z}_i &= \frac{-\varphi_{3i} y_{qz} \left(e^{Lm_i} - 1\right)}{m_i} \\
\hat{a}_i &= -2\varphi_{3i} y_{qz} \left(\frac{1}{m_i^{\,2}} + \frac{e^{Lm_i}\left(Lm_i - 1\right)}{m_i^{\,2}} \right) \\
\hat{b}_i &= 3\varphi_{3i} y_{qz} \left(\frac{2}{m_i^{\,3}} - \frac{e^{Lm_i}\left(L^2 m_i^{\,2} - 2Lm_i + 2\right)}{m_i^{\,3}} \right) + \frac{6ED_{hh} I_{yy} \varphi_{3i} y_{qz} \left(e^{Lm_i} - 1\right)}{Gm_i \left(D_{xh}^{\,2} - D_{hh} D_{xx}\right)} \\
\hat{c}_{i,j} &= \frac{-y_{qz}\left(e^{L\left(m_i + m_j\right)} - 1\right)\left(\varphi_{2i}\varphi_{3j} + \varphi_{2j}\varphi_{3i}\right)}{m_i + m_j} \\
\hat{d}_i &= \frac{-\varphi_{2i}\varphi_{3i} y_{qz}\left(e^{2Lm_i} - 1\right)}{m_i}
\end{aligned} \tag{4.47)a-e$$

4.7.9 Load position matrix for concentrated transverse load

When a member is subject to a concentrated transverse load Q_y applied at $z = z_{Qy}$ and position y_{Qy} relative to the shear center, the load function in Eq. (4.6)g can be demonstrated as $q_y(z) = Q_y Dirac\left(z - z_{Qy}\right)$. Substituting this load function into Eq. (4.6)g, one can obtain a new geometric stiffness matrix $[K_G]_{Qy}$ due to load position effect relative to the shear center *SC*. Matrix $[M_9]$ related to $[K_G]_{Qy}$ is given by

$$[M_9] = -Q_y\left(y_{Qy} - y_A\right)\begin{bmatrix} 0 & 0 & 0 & 0 & 0 & 0 & 0 & 0 \\ & 0 & 0 & 0 & 0 & 0 & 0 & 0 \\ & & 0 & 0 & 0 & 0 & 0 & 0 \\ & & & 0 & 0 & 0 & 0 & 0 \\ & & & & \hat{f}_1 & \hat{e}_{1,2} & \hat{e}_{1,3} & \hat{e}_{1,4} \\ & & & & & \hat{f}_2 & \hat{e}_{2,3} & \hat{e}_{2,4} \\ & \mathit{Sym.} & & & & & \hat{f}_3 & \hat{e}_{3,4} \\ & & & & & & & \hat{f}_4 \end{bmatrix} \tag{4.48}$$

in which functions $\hat{e}_{i,j}$ and $\hat{f}_i$ are defined as

$$\begin{aligned} \hat{e}_{i,j} &= \varphi_{3i}\varphi_{3j}e^{z_{Qy}\left(m_i+m_j\right)} \\ \hat{f}_i &= \varphi_{3i}{}^2 e^{2z_{Qy}m_i} \end{aligned} \tag{4.49a-b}$$

4.8 List of Symbols

$\bar{a}_i$ *to* $\bar{z}_i$	Elements of stiffness matrices
$\hat{a}_i$ *to* $\hat{f}_i$	Elements of stiffness matrices
$\left[\bar{A}\right],\left[\bar{B}\right],\left[\bar{C}\right]$	Matrices which are coefficients of quadratic eigenvalue problem
A	Cross-sectional area
A_p	A pole
$A_i\left(i=1to8\right)$	Integration constants
$\left[B(z)\right]$	Matrix relating displacement fields to integration constants
C	Section centroid
$D_{hh}, D_{xh}, D_{xx}, D_{yk}$, $D_{yyk}, D_{yh}, D_{y\omega h}$, $D_{xx'y'}, D_{\omega x'y'}$	Properties of cross-section related to shear deformation
$\left\langle d(z)\right\rangle^T$	Field displacements
E	Modulus of elasticity
$\left[E\left(z\right)\right]$	Diagonal matrix of exponential functions
G	Shear modulus
$\left[H\right]$	Matrix relating nodal displacements to integration constants
$\left[I\right]$	Identity matrix
I_{xx}, I_{yy}	Moments of inertia of the cross-section about x-axis and y-axis respectively
I_{px}	Polar moment of inertia about x-axis
$I_{\omega\omega}$	Warping Constant
J	St. Venant torsional constant
$\left[K_f\right]$	Stiffness matrix due to flexural stresses
$\left[K_G\right]_N$	Geometric matrix due to normal forces
$\left[K_G\right]_M$	Geometric matrix due to bending moments

$\left[K_G\right]_V$	Geometric matrix due to shear forces
$\left[K_G\right]_{qy}$	Geometric matrix due to load position effect of the distributed transverse load
$\left[K_G\right]_{qz}$	Geometric matrix due to load position effect of the distributed axial load
$\left[K_G\right]_{Qy}$	Geometric matrix due to load position effect of the concentrated transverse load
$\left[K_s\right]$	Stiffness matrix due to shear stresses
$\left[K_{sv}\right]$	Stiffness matrix due to Saint Venant shear stress
l	Length of a finite element
L	Span of the member
$\left[L(z)\right]$	Matrix of shape functions
m_i	Roots of quadratic eigenvalue problem
M_1, M_2	Internal bending moment at both end of an element
$M_{xp}(z)$	Resultant of the moments of the normal stresses obtained from pre-buckling analysis
N_1, N_2	Internal normal forces at both end of an element
$N_p(z)$	Resultant of the normal stresses obtained from pre-buckling analysis
O	Origin of the Cartesian coordinates *x*, *y* and *z*
q_y, q_z	Distributed load applied to a member acting along the y- and z- direction respectively
S_0	Sectorial origin
SC	Shear center of the cross-section
u_b	Lateral buckling displacement
$\langle u_N \rangle^T$	Vector of nodal displacements
U	Internal strain energy
V	Potential energy

V_1, V_2	Internal shearing forces at both end of an element
$V_{yp}(z)$	Resultant of shear force component along y-direction obtained from pre-buckling analysis
x, y, z	Cartesian coordinates
y_A	Coordinate of the shear center along y-direction
$\bar{\alpha}$	Constant
β	End moment ratio
λ	Load multiplier
π	Total potential energy
$\delta\pi$	Variation of total potential energy
θ_{yb}, θ_{zb}	Buckling rotation angles about y, z axes, respectively
$[\Phi]$	Matrix of eigenvectors
σ_{zz}	Normal stress along z direction
τ_{zs}	Shear stress on the cross-section mid-surface
$\omega(s)$	Warping function or sectorial area of a cross-section
ψ_b	Warping deformation (1/Length)

4.9 REFERENCES

Eurocode3 Design of Steel Structures, (1992). Part 1.1: General Rules for Buildings. European Committee for Standartisation. Brussels, Draft Document ENV 1993-1-1.

American Institute of Steel Construction, (AISC), (2005). Specification for Structural Steel Buildings, ANSI/AISC 360-05, AISC. Chicago, IL.

Canadian Standards Association, (CSA), (2009). Limit States Design of Steel Structures, CAN/CSA S16-09. Toronto, Ontario, Canada.

American Institute of Steel Construction, (AISC), (2010). Specification for Structural Steel Buildings, ANSI/AISC 360-10, AISC. Chicago, IL.

Anderson, J. M. and N. S. Trahair (1972). "Stability of monosymmetric beams and cantilevers." Journal of Structural Division, ASCE 98(ST1): 269–286.

Andrade, A., D. Camotim and P. B. Dinis (2007). "Lateral-torsional buckling of singly symmetric web-tapered thin-walled I-beams: 1D model vs. shell FEA." Computers & Structures 85(17–18): 1343-1359.

Andrade, A., D. Camotim and P. Providência e Costa (2007). "On the evaluation of elastic critical moments in doubly and singly symmetric I-section cantilevers." Journal of Constructional Steel Research 63(7): 894-908.

Attard, M. M. (1986). "Lateral buckling analysis of beams by the fem." Computers & Structures 23(2): 217-231.

Attard, M. M. (1990). "General non-dimensional equation for lateral buckling." Thin-Walled Structures 9(1–4): 417-435.

Attard, M. M. and M.-Y. Kim (2010). "Lateral buckling of beams with shear deformations – A hyperelastic formulation." International Journal of Solids and Structures 47(20): 2825-2840.

Back, S. Y. and K. M. Will (2008). "Shear-flexible thin-walled element for composite I-beams." Engineering Structures 30(5): 1447-1458.

Barsoum, R. S. and R. H. Gallagher (1970). "Finite element analysis of torsional and torsional–flexural stability problems." International Journal for Numerical Methods in Engineering 2(3): 335-352.

Bradford, M. A. (1985). "Distortional buckling of monosymmetric I-beams." Journal of Constructional Steel Research 5(2): 123-136.

Bradford, M. A. (1988). "Stability of tapered I-beams." Journal of Constructional Steel Research 9(3): 195-216.

Bradford, M. A. (1989). "Inelastic buckling of tapered monosymmetric I-beams." Engineering Structures 11(2): 119-126.

Bradford, M. A. and N. S. Trahair (1981). "Distortional buckling of I-beams." Journal of Structural Division, ASCE 107(2): 355-370.

Camotim, D., A. Andrade and C. Basaglia (2012). "Some thoughts on a surprising result concerning the lateral-torsional buckling of monosymmetric I-section beams." Thin-Walled Structures 60(0): 216-221.

Erkmen, R. E. (2014). "Shear deformable hybrid finite-element formulation for buckling analysis of thin-walled members." Finite Elements in Analysis and Design 82(0): 32-45.

Erkmen, R. E. and M. Mohareb (2008a). "Buckling analysis of thin-walled open members—A complementary energy variational principle." Thin-Walled Structures 46(6): 602-617.

Erkmen, R. E. and M. Mohareb (2008b). "Buckling analysis of thin-walled open members—A finite element formulation." Thin-Walled Structures 46(6): 618-636.

Erkmen, R. E., M. Mohareb and M. Bradford (2009). "Complementary Energy Based Formulation for Torsional Buckling of Columns." Journal of Engineering Mechanics 135(12): 1420-1426.

Gelera, K. and J. Park (2012). "Elastic lateral torsional buckling strength of monosymmetric stepped I-beams." KSCE Journal of Civil Engineering 16(5): 785-793.

Hancock, G. J., M. A. Bradford and N. S. Trahair (1980). "Web distortion and flexural-torsional buckling." Journal of Structural Division, ASCE 106(7): 1557-1571.

Helwig, T., K. Frank and J. Yura (1997). "Lateral-Torsional Buckling of Singly Symmetric I-Beams." Journal of Structural Engineering 123(9): 1172-1179.

Kim, N.-I. and J. Lee (2013). "Lateral buckling of shear deformable laminated composite I-beams using the finite element method." International Journal of Mechanical Sciences 68(0): 246-257.

Kitipornchai, S., C. Wang and N. Trahair (1986). "Buckling of Monosymmetric I-Beams under Moment Gradient." Journal of Structural Engineering 112(4): 781-799.

Kitipornchai, S. and C. M. Wang (1986). "Lateral buckling of tee beams under moment gradient." Computers & Structures 23(1): 69-76.

Kollár, L. P. (2001). "Flexural–torsional buckling of open section composite columns with shear deformation." International Journal of Solids and Structures 38(42–43): 7525-7541.

Krajcinovic, D. (1969). "A consistent discrete elements technique for thinwalled assemblages." International Journal of Solids and Structures 5(7): 639-662.

Lee, J. (2006). "Lateral buckling analysis of thin-walled laminated composite beams with monosymmetric sections." Engineering Structures 28(14): 1997-2009.

Mohri, F., A. Brouki and J. C. Roth (2003). "Theoretical and numerical stability analyses of unrestrained, mono-symmetric thin-walled beams." Journal of Constructional Steel Research 59(1): 63-90.

Mohri, F., N. Damil and M. Potier-Ferry (2010). "Linear and non-linear stability analyses of thin-walled beams with monosymmetric I sections." Thin-Walled Structures 48(4–5): 299-315.

Mohri, F., N. Damil and M. Potier-Ferry (2013). "Buckling and lateral buckling interaction in thin-walled beam-column elements with mono-symmetric cross sections." Applied Mathematical Modelling 37(5): 3526-3540.

Papangelis, J. P., N. S. Trahair and G. J. Hancock (1998). "Elastic flexural–torsional buckling of structures by computer." Computers & Structures 68(1–3): 125-137.

Roberts, T. M. and C. A. Burt (1985). "Instability of monosymmetric I-beams and cantilevers." International Journal of Mechanical Sciences 27(5): 313-324.

Saadé, K., B. Espion and G. Warzée (2004). "Non-uniform torsional behavior and stability of thin-walled elastic beams with arbitrary cross sections." Thin-Walled Structures 42(6): 857-881.

Trahair, N. S. (1993). Flexural-torsional buckling of structures, USA: CRC Press.

Trahair, N. S. (2014). "Bending and buckling of tapered steel beam structures." Engineering Structures 59(0): 229-237.

Vlasov, V. Z. (1961). Thin-Walled Elastic Beams. Jerusalem, Israel, Program for Scientific Translation.

Wang, C. and S. Kitipornchai (1986). "Buckling Capacities of Monosymmetric I-Beams." Journal of Structural Engineering 112(11): 2373-2391.

Wang, C. M. and S. Kitipornchai (1986). "On stability of monosymmetric cantilevers." Engineering Structures 8(3): 169-180.

Wu, L. and M. Mohareb (2011a). "Buckling of shear deformable thin-walled members—I. Variational principle and analytical solutions." Thin-Walled Structures 49(1): 197-207.

Wu, L. and M. Mohareb (2011b). "Buckling formulation for shear deformable thin-walled members—II. Finite element formulation." Thin-Walled Structures 49(1): 208-222.

Yuan, W.-b., B. Kim and C.-y. Chen (2013). "Lateral–torsional buckling of steel web tapered tee-section cantilevers." Journal of Constructional Steel Research 87(0): 31-37.

Zhang, L. and G. S. Tong (2008). "Elastic flexural-torsional buckling of thin-walled cantilevers." Thin-Walled Structures 46(1): 27-37.

Chapter 5 Generalized Lateral Torsional Buckling Analysis of Plane Frames

Abstract

A finite element formulation is developed to predict the lateral torsional buckling resistance of plane frames with moment connections. The solution focuses on the simple characterization the elastic warping behavior of moment connections in a manner that allows them to interface seamlessly with existing beam buckling finite elements, thus providing means for the realistic lateral torsional buckling modelling of general plane frames. Special attention is devoted to the finite rotation effects of the joints. The technique successfully captures the interaction between beams and columns of frames, an effect that is neglected in present design methodologies based on individual member checks. The solution is shown to predict lateral torsional buckling resistance predictions in very good agreement with shell based finite element solutions at a fraction of the modelling and computational effort. For typical frames that are laterally supported at the joints, the study suggests that present design methodologies that isolate the member from the rest of the structure provide conservative buckling resistance predictions. Conversely, for frames with no lateral restraints at some of the joints, the present solution predicts lateral torsional buckling resistances that are significantly different from those based on design standard equations, suggesting the need to account for interaction effects in such situations.

Keywords: Lateral torsional buckling, plane frames, finite element, joint element, interaction buckling

5.1 Motivation

Present structural steel design standards (CAN-CSA S16 2014, ANSI AISC 360-16) stipulate isolating the member from the surrounding structure when investigating its capacity through interaction checks. The idea of separating a member from the surrounding structure when determining its lateral torsional buckling (LTB) resistance may be traced to the work of Salvadori (1953) who advocated that such an approach yields conservative estimates for the critical moment capacity of the member. The approach of separating individual members from other members of the frame neglects interactions between various elements of the structure. Existing beam buckling finite elements provide effective means of capturing interaction effects between adjacent elements when characterising the LTB capacity of the structure, but are primarily intended to collinear structures (e.g., continuous beams). For non-collinear structures such as typical frames, the modelling of interaction effects between various elements of a structure when characterizing their LTB strength is possible through shell analysis for the whole structure, an impractical option when the frame consists of multiple storey and/or multiple bays. Relatively recent work has extended the use existing beam buckling solutions to the LTB analysis of frames, but is limited to rather simple frame configurations. Within this context, the present study aims at developing more general means of incorporating interaction effects between various adjoining non-collinear elements (beams, columns) when characterizing their LTB resistance for multi-story frames.

5.2 Literature review

An extensive body of research has been developed for the LTB analysis of collinear beams with doubly symmetric cross-sections. Classical solutions based on the Vlasov beam theory include the work of Krajcinovic (1969), Barsoum and Gallagher (1970) and Powel and Klingner (1970). The classical Vlasov treatment neglects shear deformation and distortional effects. More recent solutions account for shear deformation effects and include the work of Erkmen and Mohareb (2008a, 2008b), Wu and Mohareb (2011a, 2011b), Attard and Kim (2010), Erkmen and Attard (2011) Erkmen (2014) and Sahraei and Mohareb (2016). The LTB analysis of mono-symmetric sections include the work of Kitipornchai et al. (1986), Wang and Kitipornchai (1986, 1986), Mohri et al. (2003, 2010, 2013), Andrade et al. (2007), Zhang and Tong (2008), and Sahraei et al. (2015). Distortional LTB investigations include the work of Johnson and Will (1974), Hancock et al. (1980), Bradford and Trahair (1981, 1982), Bradford (1985, 1986, 1992a, 1992b), and Bradford and Ronagh (1997) who developed finite element solutions for a variety of boundary conditions and loading cases.

While the above studies and others have focused on the LTB analysis of collinear members, relatively fewer studies investigated the LTB capacity of non-collinear members involving beams, columns, and connecting joints. Hartmann and Munse (1966) numerically investigated the LTB of portal frames with rigid joints. Vacharajittiphan and Trahair (1974) developed a finite element model to examine the effect of member length, joint angle and stiffener arrangement on the warping restraint provided by joints. Morrel (1979) experimentally examined the effects of the common joint details including one, two or three pairs of stiffeners on the torsional behavior of Γ-shaped frames containing channel cross-sections. Ettouney and Kirby (1981) and Yang and McGuire (1984) expressed the warping degree of freedom in terms of other degrees of freedom at a joint and adopted a warping spring to characterize the warping boundary conditions. Sharman (1985) incorporated the effect of warping into the standard stiffness matrix of open section thin-walled beams by assuming the twist rate of a member to be equal to that of the adjacent member at the intersection joint in the Γ-shaped frames. Krenk and Damkidle (1991) characterize the warping and distortion of connections of beams with I-shaped cross-sections. Four connections types were investigated: (1) unstiffened, (2) partially stiffened with a single diagonal stiffener, (3) a pair of perpendicular stiffeners, and (4) fully stiffened with three pairs of stiffeners. Pi and Trahair (2000) investigated the effect of end-supports on the lateral distortional buckling and warping resistance of I-beams. Masarria (2002) investigated the effect of joint details with various stiffener arrangements on the lateral torsional buckling of plane frames. Mohareb and Dabbas (2003) and Zinoviev and Mohareb (2004) showed design procedures in standards which neglect member interaction, are unable to predict the buckling strength of plane frames with no lateral restraints at the joints and advocated the use of shell finite element analysis for such problems. Tong et al. (2005) developed a warping transmission model for beam-to-column rigid joints with diagonal stiffeners. The model captures the bending and twist effect of the diagonal stiffener and the twist restrain of the diagonal stiffener. Using the generalized beam theory, Basaglia et al. (2012) simulated the transmission of warping deformation at frame joints consisting of non-collinear U- and I-section members. Shayan and Rasmussen (2014) developed a joint model and incorporated it into buckling finite element analysis. This joint element considers the effect of partial warping transmission between members of a plane frame. Wu and Mohareb (2012) developed a joint element for LTB analysis of portal and Γ-shaped frames. The joint element can be used to characterize the stiffness of moment connections at the intersection of two members at 90 degrees. The above studies provided various treatments of the partial fixity conditions at beam to column junctions for specific frame configurations on the LTB capacity of the frames as a whole. In this context, one of the aims of the present study is to provide a generalized treatment for beam to column joints in more general plane frame configurations while considering the effect of finite rotations on the LTB analysis.

5.3 Assumptions

The following assumptions have been adopted:

1. The solution is applicable to plane frames consisting of doubly symmetric I-shaped cross-sections;
2. All members are assumed to be connected at right angles through welded moment connections consisting of two pairs of horizontal and vertical stiffeners;
3. The material is assumed linearly elastic, isotropic, and obeying Hooke's law;
4. Second-order effects throughout pre-buckling deformations are considered negligible;
5. Throughout buckling, the joint is assumed to: (a) displace and rotate as a rigid body and (b) warp elastically along the sides of adjoining members such that they match the warping deformations of the adjoining members; and
6. All rotations under Item 5a are assumed moderate.

5.4 Outline of the solution

A general plane frame structure is subjected to general planar loads (Figure 5-1a). The frame can be idealized as an assembly of elements (either collinear or intersecting at 90 degrees) and joint elements connecting the elements (Figure 5-1b). A typical member ab (Figure 5-1c) has two nodes with four buckling degrees of freedom per node (Figure 5-1c): lateral displacement u, weak axis rotation θ_y, angle of twist θ_z and warping deformation ψ. Throughout buckling, a generic joint such as $4-kj$ undergoes rigid body lateral displacement u_0 and rotations θ_{y0},θ_{z0} as shown in Figure 5-1d. The warping stiffness of the joint is to be characterized by an independent elastic analysis based on a shell model (Figure 5-1e). The degrees of freedom of the shell model of the joint are then to be condensed into four warping degrees of freedom (Figure 5-1f) associated with each of the four faces of the joint. A block diagram of the steps for the proposed solution is provided in Figure 5-1g. Module I loops on the straight elements to calculate their elastic and geometric stiffness matrices and send the contributions to the structure stiffness matrix. Several beam buckling elements can be adopted such as (Krajcinovic (1969), Barsoum and Gallagher (1970), Powel and Klingner (1970), Erkmen and Mohareb (2008b), Wu and Mohareb (2011b), Sahraei and Mohareb (2016), etc.). Unlike co-linear structures, where finite rotation effects are negligible Krajcinovic (1969), Barsoum and Gallagher (1970), Powel and Klingner (1970), Erkmen and Mohareb (2008b) and Wu and Mohareb (2011b), the present study incorporates finite rotation effects which is shown to be in accurately characterizing the LTB buckling of laterally unsupported frames with free ends (Examples 1-3). Such finite rotation effects will be presented in Section 5.5.5. Module II adds the joint contributions. The kinematic constraints related to rigid body motion are to be incorporated in Module II.1 in Figure 5-1g and the underlying formulation is provided under Section 5.5.2. For each joint, an independent shell analysis is conducted to characterize the relation between four warping degrees of freedom (Figure 5-1e) and corresponding warping-bimoment relations are to be determined from the edge reaction and incorporated in Module II.3 in Figure 5-1g. The underlying formulations are provided under Section 5.5.3.

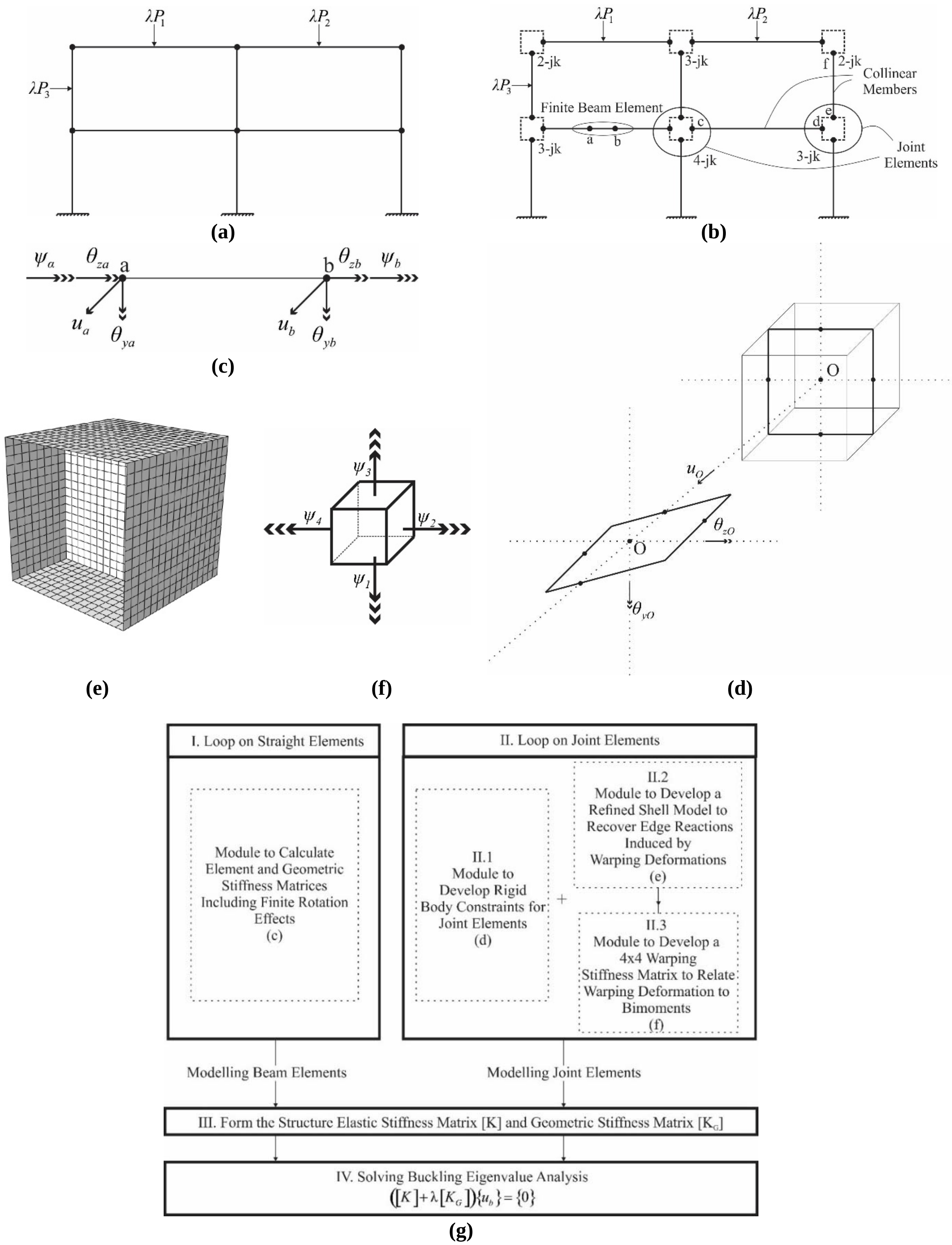

Figure 5-1 (a) Conventional representation of a frame, (b) Model proposed in present research, (c) DOFs of a beam finite element, (d) Rigid body displacements and rotations for joint, (e) Shell joint model, (f) warping deformations for joint element and (g) Block diagrams showing various components of the analysis to conduct LTB analysis for frame

5.5 Variational formulation

When a frame attains a neutral stability state, the variation of the second variation of the total potential energy π has to vanish (Bazant and Cedolin (1991)) i.e.,

$$\delta\left(\frac{1}{2}\delta^2\pi\right)=\delta\left[\frac{1}{2}\delta^2\left(\pi_m+\pi_c+\pi_j\right)\right]=0 \tag{5.1}$$

where $\pi_m =$ total potential energy for all collinear member elements undergoing elastic bucking deformations, π_c is the term resulting from the Lagrange multipliers to enforce the kinematic constraints describing the rigid body motion (postulated under Assumption 5a), which relate the displacements of Nodes 1 to those of nodes 2-4 within each joint element, and $\pi_j =$ total potential energy of the joint elements undergoing elastic buckling warping deformation (as per Assumption 5b and Figure 5-2). Symbol δ denotes the variation of the argument functionals with respect to the buckling displacements. The following three sections formulate the expressions for π_m, π_c and π_j respectively.

5.5.1 Stiffness matrices for members

The second variation of the total potential energy of the members, $\delta^2\pi_m$ takes the form

$$\begin{aligned}\frac{1}{2}\delta^2\pi_m &= \sum_{i=1}^{n}\frac{1}{2}\left\langle\delta\left({}^{ei}U_{nl}\right)\right\rangle^T\left\{\left[{}^{ei}K\right]-\lambda\left[{}^{ei}K_G\right]\right\}\left\{\delta\left({}^{ei}U_{nl}\right)\right\}\\ &= \sum_{i=1}^{n}\frac{1}{2}\left\langle\delta\left({}^{ei}U_{nl}\right)\right\rangle^T\left[\mathbf{T}(\varphi_{ei})\right]^T\left\{\left[{}^{ei}K\right]-\lambda\left[{}^{ei}K_G\right]\right\}\left[T\left(\varphi_{ei}\right)\right]\left\{\delta\left({}^{ei}U_{nl}\right)\right\}\end{aligned} \tag{5.2}$$

in which $\left\langle\delta\left({}^{ei}U_{nl}\right)\right\rangle^T=\left\langle {}^{ei}_{1}u_{bl}\quad {}^{ei}_{1}\theta_{ybl}\quad {}^{ei}_{1}\theta_{zbl}\quad {}^{ei}_{1}\psi_{bl}\ \middle|\ {}^{ei}_{2}u_{bl}\quad {}^{ei}_{2}\theta_{ybl}\quad {}^{ei}_{2}\theta_{zbl}\quad {}^{ei}_{2}\psi_{bl}\right\rangle$ denotes the buckling nodal displacement of the member and are expressed in terms of the local coordinates. As a notation convention, symbols e in the left superscripts denote that the generalized displacements pertain to an element (as opposed to a joint), and $i=1,...,n$ denotes the element number. In the notation of the nodal displacements, the left subscript takes the values 1 or 2 to denote the first or second nodes of the element, respectively. Identifier l in the right subscript indicates that nodal displacements $\{U_{nl}\}$ are defined in local coordinates, while identifier g denotes that nodal displacements $\{U_{ng}\}$ are defined in global coordinates. The entries of the stiffness matrices $\left[{}^{ei}K\right]$ and $\left[{}^{ei}K_G\right]_C$ can be adopted from any of past solutions (e.g., Barsoum and Gallagher (1970), Erkmen and Mohareb (2008b), Wu and Mohareb (2011b) and Sahraei and Mohareb (2016)). In the present study, the classical solution in Barsoum and Gallagher (1970) and the shear deformable SM-M element in Sahraei and Mohareb (2016) are adopted. In Eq. (5.2), the nodal displacements $\left\{{}^{ei}U_{nl}\right\}$ in local coordinates are related to the nodal displacements $\left\{{}^{ei}U_{ng}\right\}$ in global coordinates through the transformation

$$\left\{{}^{ei}U_{nl}\right\}_{8\times1}=\left[T\left(\varphi_{ei}\right)\right]_{8\times8}\left\{{}^{ei}U_{ng}\right\}_{8\times1} \tag{5.3}$$

where

$$\left[T\left(\varphi_{ei}\right)\right]_{8\times8}=\begin{bmatrix}1 & 0 & 0 & 0 & 0 & 0 & 0 & 0\\ 0 & \cos\varphi_{ei} & \sin\varphi_{ei} & 0 & 0 & 0 & 0 & 0\\ 0 & -\sin\varphi_{ei} & \cos\varphi_{ei} & 0 & 0 & 0 & 0 & 0\\ 0 & 0 & 0 & 1 & 0 & 0 & 0 & 0\\ 0 & 0 & 0 & 0 & 1 & 0 & 0 & 0\\ 0 & 0 & 0 & 0 & 0 & \cos\varphi_{ei} & \sin\varphi_{ei} & 0\\ 0 & 0 & 0 & 0 & 0 & -\sin\varphi_{ei} & \cos\varphi_{ei} & 0\\ 0 & 0 & 0 & 0 & 0 & 0 & 0 & 1\end{bmatrix}_{8\times8} \tag{5.4}$$

and angle $\varphi_{ei}=$ counter clockwise rotation angle from the global z_g direction to the local z_{ei} direction for member i. For frames consisting exclusively of horizontal and vertical members, φ_{ei} takes one of the values $0,\ \pi/2,\ \pi,\ 3\pi/2$. As a notation convention, total field variables (i.e., those describing the motion from Configuration 1 to 4 will be denoted by superscript $*$, variables with subscripts b denote buckling variables (i.e., those describing the motion from Configuration 3 to 4) while those with a superscript p denote pre-buckling displacements (i.e., those describing the motion from Configuration 1 to 2). Variables without subscripts or a superscript $*$ are generic and applicable to pre-buckling, buckling, or total field variables.

5.5.2 Kinematic constraints at the joints

When a laterally unsupported plane frame undergoes LTB, a generic joint k is assumed to undergo rigid body displacements within the plane of the frame from the initial state (Configuration 1 in Figure 5-2) to an equilibrium state (Configuration 2). This pre-buckling movement is characterized by two orthogonal displacements ${}^{jk}_{2}v_{pl}$ and ${}^{jk}_{2}w_{pl}$ at an arbitrary point (e.g., Node 2) and a rotation angle ${}^{jk}_{2}\theta_{xpl}$. Subscript l denotes displacements that are defined in the local coordinates of the joint. In the left superscript, j denotes that the generalized displacement is related to a joint (as opposed to a member), and k denotes the joint number. The left subscript takes the values $1,\ldots,4$ to denote the first through fourth nodes of the joint element, respectively. When the loads are magnified by factor λ, the structure is assumed to reach the state of onset of buckling (Configuration 3), and the associated displacements are assumed to become $\lambda\left({}^{jk}_{2}v_{pl}\right)$, $\lambda\left({}^{jk}_{2}w_{pl}\right)$ and $\lambda\left({}^{jk}_{2}\theta_{xpl}\right)$. This assumption neglects pre-buckling second order effects (in line with Assumption 4).

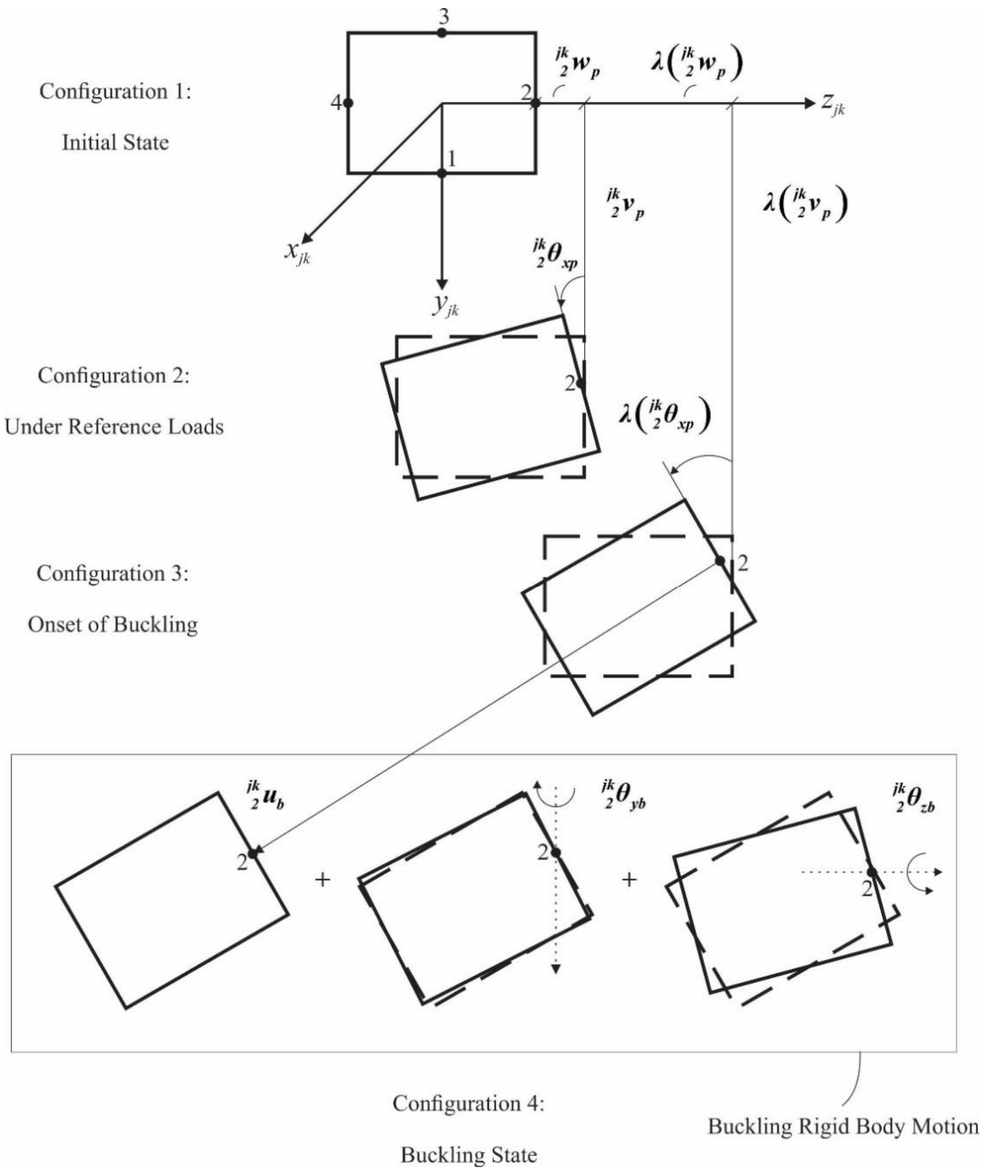

Figure 5-2 Rigid body motion of a joint from initial state to buckled configuration

When the frame buckles laterally, the joint undergoes additional rigid body motion consisting of out of plane displacement ${}_{2}^{jk}u_{bl}$ and two rotations ${}_{2}^{jk}\theta_{ybl}$ and ${}_{2}^{jk}\theta_{zbl}$ (Figure 5-3). In addition, the joint undergoes elastic warping deformations ${}_{1}^{jk}\psi_{bl}$ through ${}_{4}^{jk}\psi_{bl}$ at Faces 1 through 4 which are connected to Elements 1 through 4, respectively. Warping deformation ${}_{1}^{jk}\psi_{bl}$ induces angles of rotation ${}_{1}^{jk}\theta_{\psi bl}$ at edge $5'-5''$ and $-{}_{1}^{jk}\theta_{\psi bl}$ at edge $8'-8''$. Also, warping deformation ${}_{2}^{jk}\psi_{bl}$ induces angles of rotation ${}_{2}^{jk}\theta_{\psi bl}$ and $-{}_{2}^{jk}\theta_{\psi bl}$ at edges $5'-5''$ and $6'-6''$. Similarly, warping deformation ${}_{3}^{jk}\psi_{bl}$ angles rotation ${}_{3}^{jk}\theta_{\psi bl}$ and $-{}_{3}^{jk}\theta_{\psi bl}$ at edges $6'-6''$ and $7'-7''$, and warping deformation ${}_{4}^{jk}\psi_{bl}$ induces an angles of rotation ${}_{4}^{jk}\theta_{\psi bl}$ and $-{}_{4}^{jk}\theta_{\psi bl}$ at $8'-8''$ and $7'-7''$. The joint element consists of four nodes, each having three pre-buckling and four buckling generalized displacements. In local coordinates, the pre-buckling nodal displacement vector is

$$\left\{{}^{jk}U_{pl}\right\} = \left\langle {}_{1}^{jk}v_{pl} \quad {}_{1}^{jk}w_{pl} \quad {}_{1}^{jk}\theta_{xpl} \;\middle|\; {}_{2}^{jk}v_{pl} \quad {}_{2}^{jk}w_{pl} \quad {}_{2}^{jk}\theta_{xpl} \;\middle|\; {}_{3}^{jk}v_{pl} \quad {}_{3}^{jk}w_{pl} \quad {}_{3}^{jk}\theta_{xpl} \;\middle|\; {}_{4}^{jk}v_{pl} \quad {}_{4}^{jk}w_{pl} \quad {}_{4}^{jk}\theta_{xpl} \right\rangle^{T}$$

and the buckling displacement vector is

$$\left\{{}^{jk}U_{bl}\right\} = \left\langle {}_{1}^{jk}u_{bl} \quad {}_{1}^{jk}\theta_{ybl} \quad {}_{1}^{jk}\theta_{zbl} \quad {}_{1}^{jk}\psi_{bl} \;\middle|\; {}_{2}^{jk}u_{bl} \quad {}_{2}^{jk}\theta_{ybl} \quad {}_{2}^{jk}\theta_{zbl} \quad {}_{2}^{jk}\psi_{bl} \;\middle|\; {}_{3}^{jk}u_{bl} \quad {}_{3}^{jk}\theta_{ybl} \quad {}_{3}^{jk}\theta_{zbl} \quad {}_{3}^{jk}\psi_{bl} \;\middle|\; {}_{4}^{jk}u_{bl} \quad {}_{4}^{jk}\theta_{ybl} \quad {}_{4}^{jk}\theta_{zbl} \quad {}_{4}^{jk}\psi_{bl} \right\rangle^{T}.$$

Each node of the joint element is intended to interface with that of an adjoining beam element. For example, the first node (Figure 5-4) connects to the end of element e_1 through global node N_1 which has global nodal displacements ${}^{N_1}u_{bg}$, ${}^{N_1}\theta_{ybg}$, ${}^{N_1}\theta_{zbg}$ and ${}^{N_1}\psi_{bg}$. Likewise, the second node connects to the end of element e_2 through global node N_2 with nodal displacements ${}^{N_2}u_{bg}$, ${}^{N_2}\theta_{ybg}$, ${}^{N_2}\theta_{zbg}$ and ${}^{N_2}\psi_{bg}$.

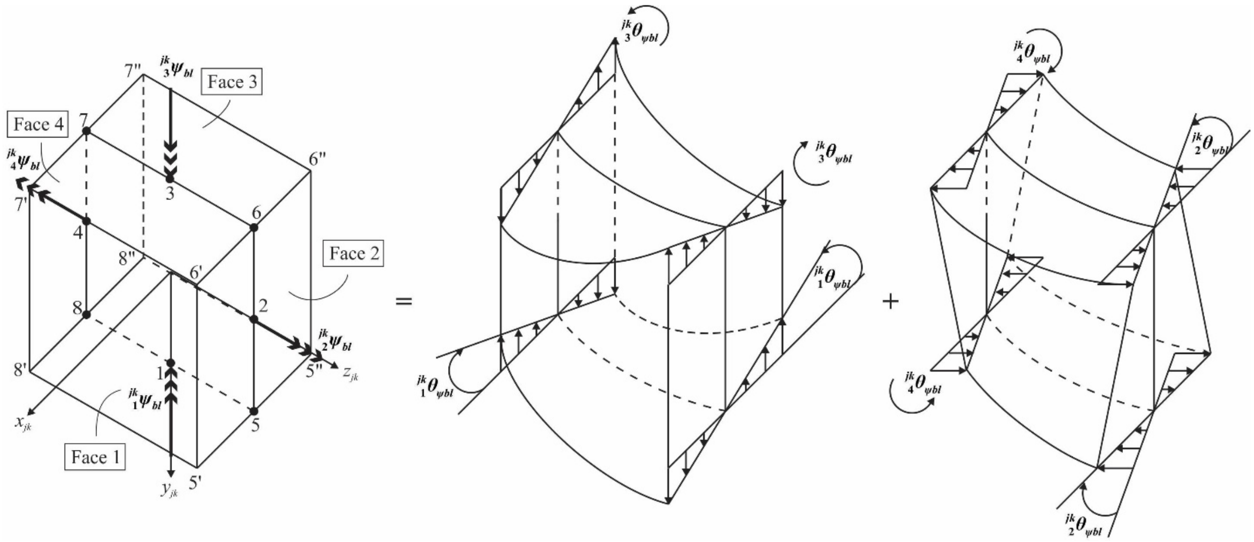

Figure 5-3 Warping deformations of joint *k* and sign conventions

The plane frame is assumed to consist of $i = 1, 2...n$ members, $k = 1, 2..m$ joints, and o nodes. As shown in Figure 5-4, each member element has its own element local coordinate system $\left(x_{ei},\, y_{ei},\, z_{ei}\right)$Also, each joint member k has its own local coordinate system $\left(x_{jk},\, y_{jk},\, z_{jk}\right)$. Coordinate system $\left(x_{ei},\, y_{ei},\, z_{ei}\right)$ defines the positive directions of the nodal displacements within member element i, while coordinate system $\left(x_{jk},\, y_{jk},\, z_{jk}\right)$ defines the positive directions of the nodal displacements within joint element k. Finally, the nodal degrees of freedom at nodes $1, 2, ..., o$ are oriented along global coordinate system $\left(x_g,\, y_g,\, z_g\right)$.

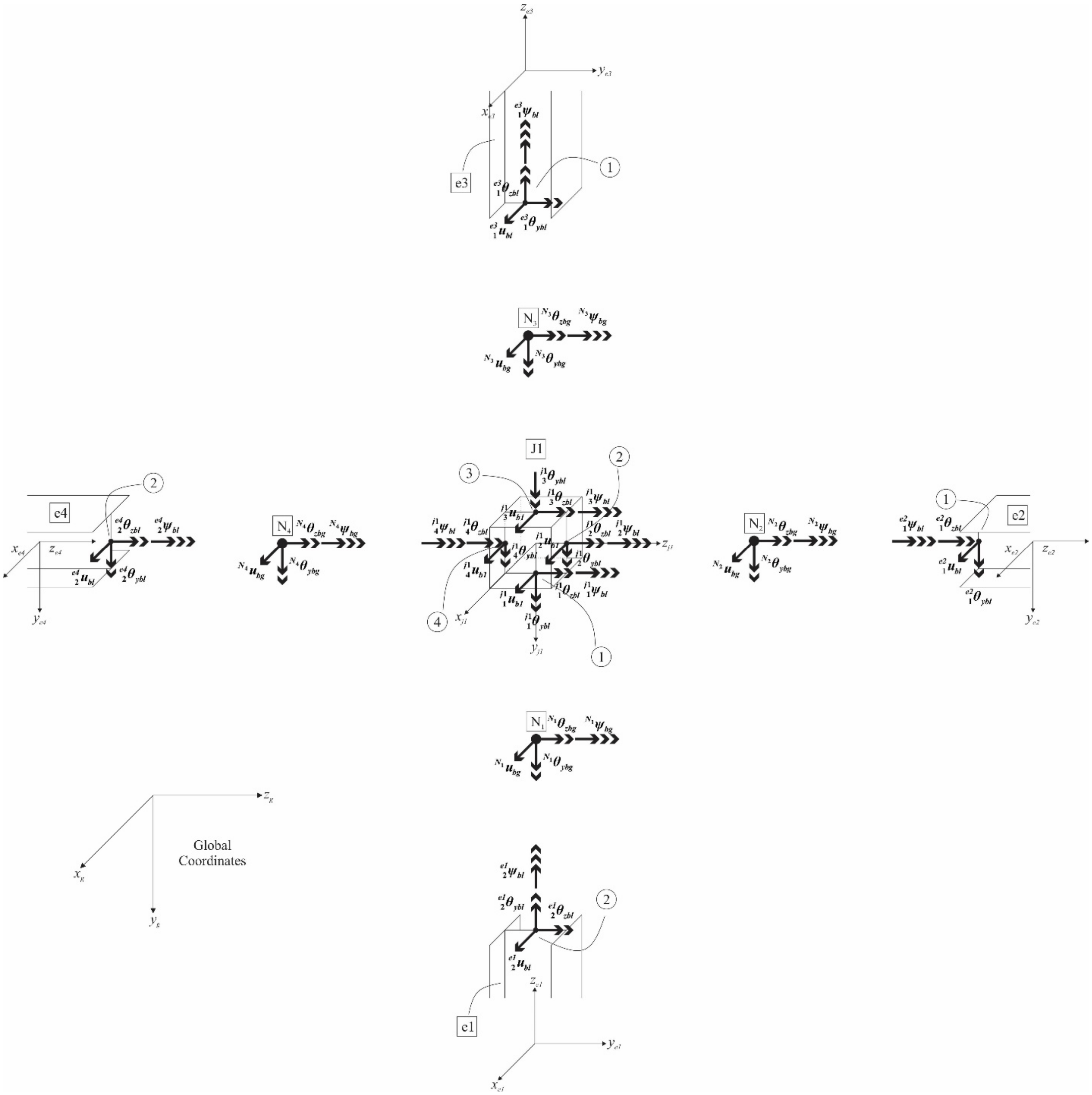

Figure 5-4 Connectivity of joint and members (displacements of Global nodes N1-N4 are shown in global directions, displacements of joint J1 and elements e1-e4 are shown in local directions)

The three pre-buckling degrees of freedom (DOFs) for each of the nodes $i = 2,3,4$ (Figure 5-2) can be related those of node 1, considered as the master node. Nine pre-buckling rigid body constraints can be expressed in the form

$$\begin{aligned} v_{pi} &= v_{p1} + \left(z_i - z_1\right)\theta_{xpi1} \\ w_{pi} &= w_{p1} - \left(y_i - y_1\right)\theta_{xpi1} \qquad i = 2,3,4 \\ \theta_{xpi} &= \theta_{xp1} \end{aligned} \tag{5.5}$$

Based on Figure 5-5, for a given joint $k = 1,...,m$ with local coordinate system $\left(x_{jk}, y_{jk}, z_{jk}\right)$, position vectors $\{x_1\}$ to $\{x_8\}$ in the un-deformed configuration for points 1 to 8 are given by

$$\{x_1\} = \begin{Bmatrix} 0 \\ h_2/2 \\ 0 \end{Bmatrix}, \quad \{x_2\} = \begin{Bmatrix} 0 \\ 0 \\ h_1/2 \end{Bmatrix}, \quad \{x_3\} = \begin{Bmatrix} 0 \\ -h_2/2 \\ 0 \end{Bmatrix}, \quad \{x_4\} = \begin{Bmatrix} 0 \\ 0 \\ -h_1/2 \end{Bmatrix}$$

$$\{x_5\} = \begin{Bmatrix} 0 \\ h_2/2 \\ h_1/2 \end{Bmatrix}, \quad \{x_6\} = \begin{Bmatrix} 0 \\ -h_2/2 \\ h_1/2 \end{Bmatrix}, \quad \{x_7\} = \begin{Bmatrix} 0 \\ -h_2/2 \\ -h_1/2 \end{Bmatrix}, \quad \{x_8\} = \begin{Bmatrix} 0 \\ h_2/2 \\ -h_1/2 \end{Bmatrix} \tag{5.6)a-h$$

from which position vector $\langle x_{21}\rangle^T$ for point 2 relative to point 1 is given by

$$\langle x_{21}\rangle^T = \langle x_2\rangle^T - \langle x_1\rangle^T = \langle 0 \quad -h_2/2 \quad h_1/2\rangle \tag{5.7}$$

Also, position vectors $\langle x_{31}\rangle^T$ and $\langle x_{41}\rangle^T$ for points 3 and 4 relative to point 1 are

$$\begin{aligned} \langle x_{31}\rangle^T &= \langle x_3\rangle^T - \langle x_1\rangle^T = \langle 0 \quad -h_2 \quad 0\rangle \\ \langle x_{41}\rangle^T &= \langle x_4\rangle^T - \langle x_1\rangle^T = \langle 0 \quad -h_2/2 \quad -h_1/2\rangle \end{aligned} \tag{5.8)a-b$$

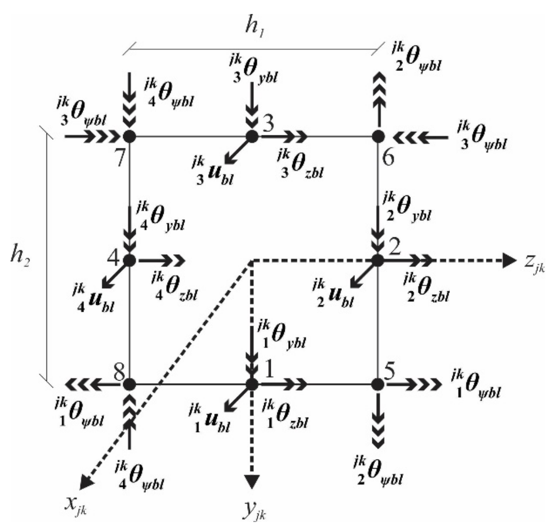

Figure 5-5 Buckling degrees of freedom for a joint element in local coordinates (displacements are shown as single-headed arrows, rotations as double-headed arrows, and rotations induced by warping triple-headed arrows)

Rigid body constraints are such that buckling rotations at nodes 1 and $i = 2,3,4$ must be identical in line with assumption (5a), i.e.,

$$\left(-{}_{i}^{jk}\theta_{yb} + {}_{1}^{jk}\theta_{yb}\right) = 0 \qquad i = 2,3,4 \tag{5.9}$$

$$\left(-{}_{i}^{jk}\theta_{zb} + {}_{1}^{jk}\theta_{zb}\right) = 0 \qquad i = 2,3,4 \tag{5.10}$$

The lateral displacement ${}_{i}^{jk}u_b$ of nodes $i = 2,3,4$ is expressed in the terms of other nodal displacements at node 1 $\left({}_{1}^{jk}u_b, {}_{1}^{jk}\theta_{yb}, {}_{1}^{jk}\theta_{zb}\right)$ and warping displacements ${}_{1}^{jk}\psi_b$ and ${}_{i}^{jk}\psi_b$. First, displacement vector $\langle u_i\rangle^T = \left\langle {}_{i}^{jk}u_b^* \quad {}_{i}^{jk}v_p^* \quad {}_{i}^{jk}w_p^* \right\rangle^T$ at node i due to rigid body displacements $\langle u_1\rangle^T = \left\langle {}_{1}^{jk}u_b^* \quad {}_{1}^{jk}v_p^* \quad {}_{1}^{jk}w_p^* \right\rangle^T$ and rotations at node 1 is obtained through

$$\{u_i\}_{3\times1} = \{u_1\}_{3\times1} + [R]_{3\times3}\{x_{i1}\}_{3\times1} \tag{5.11)a-c}$$

where $[R]$ is the moderate rotation matrix (Wu and Mohareb (2012)) given as

$$[R]_{3\times3} = \begin{bmatrix} -\frac{1}{2}\left[\left({}_{1}^{jk}\theta_{yb}\right)^2 + \left({}_{1}^{jk}\theta_{zb}\right)^2\right] & -{}_{1}^{jk}\theta_{zb} + \frac{1}{2}\lambda\left({}_{1}^{jk}\theta_{xp}\right){}_{1}^{jk}\theta_{yb} & {}_{1}^{jk}\theta_{yb} + \frac{1}{2}\lambda\left({}_{1}^{jk}\theta_{xp}\right){}_{1}^{jk}\theta_{zb} \\ {}_{1}^{jk}\theta_{zb} + \frac{1}{2}\lambda\left({}_{1}^{jk}\theta_{xp}\right){}_{1}^{jk}\theta_{yb} & -\frac{1}{2}\left[\lambda^2\left({}_{1}^{jk}\theta_{xp}\right)^2 + \left({}_{1}^{jk}\theta_{zb}\right)^2\right] & -\lambda\left({}_{1}^{jk}\theta_{xp}\right) + \frac{1}{2}\,{}_{1}^{jk}\theta_{yb}\,{}_{1}^{jk}\theta_{zb} \\ -{}_{1}^{jk}\theta_{yb} + \frac{1}{2}\lambda\left({}_{1}^{jk}\theta_{xp}\right){}_{1}^{jk}\theta_{zb} & \lambda\left({}_{1}^{jk}\theta_{xp}\right) + \frac{1}{2}\,{}_{1}^{jk}\theta_{yb}\,{}_{1}^{jk}\theta_{zb} & -\frac{1}{2}\left[\lambda^2\left({}_{1}^{jk}\theta_{xp}\right)^2 + \left({}_{1}^{jk}\theta_{yb}\right)^2\right] \end{bmatrix}$$

(5.12)

Lateral displacements of nodes 2-4 $\left({}_{i}^{jk}u_b^*, \;\; i = 2,3,4\right)$ are related to the lateral displacement of node 1 ${}_{1}^{jk}u_b^*$ by expanding the first row resulting from Eqs. (5.11)a-c, yielding

$$\begin{aligned} {}_{2}^{jk}u_b^* &= {}_{1}^{jk}u_b^* + \frac{h_2}{2}\left({}_{1}^{jk}\theta_{zb}\right) + \frac{h_1}{2}\left({}_{1}^{jk}\theta_{yb}\right) \\ {}_{3}^{jk}u_b^* &= {}_{1}^{jk}u_b^* + h_2\left({}_{1}^{jk}\theta_{zb}\right) \\ {}_{4}^{jk}u_b^* &= {}_{1}^{jk}u_b^* + \frac{h_2}{2}\left({}_{1}^{jk}\theta_{zb}\right) - \frac{h_1}{2}\left({}_{1}^{jk}\theta_{yb}\right) \end{aligned} \tag{5.13)a-c}$$

in which one recalls that superscripts * denotes the total field variables of a node (i.e., going from configuration 1 to 4 as shown in Figure 5-2. It is noted that the pre-buckling rotation term is neglected in the context of linearized buckling solutions (Barsoum and Gallagher (1970) and Wu and Mohareb (2011a). Thus, terms containing θ_{xp} have been neglected in Eq. (5.11)a-c. Besides the displacements derived in Section 5.5.2, warping deformation $\left({}_{i}^{jk}\psi_b \quad i=1,2,3,4 \right)$ induce the following additional lateral displacements at faces 2, 3, and 4 (Appendix A).

$$-{}_{2}^{jk}u_b + {}_{1}^{jk}u_b - \frac{h_1 h_2}{4}\left({}_{2}^{jk}\psi_b \right) + \frac{h_1}{2}\left({}_{1}^{jk}\theta_{yb} \right) + \frac{h_2}{2}\left({}_{1}^{jk}\theta_{zb} \right) + \frac{h_1 h_2}{4}\left({}_{1}^{jk}\psi_b \right) \approx 0$$

$$-{}_{3}^{jk}u_b + {}_{1}^{jk}u_b + h_2\left({}_{1}^{jk}\theta_{zb} \right) + \frac{h_1 h_2}{4}\left({}_{1}^{jk}\psi_b \right) + \frac{h_1 h_2}{4}\left({}_{3}^{jk}\psi_b \right) \approx 0 \tag{5.14)a-c}$$

$$-{}_{4}^{jk}u_b + {}_{1}^{jk}u_b + \frac{h_1 h_2}{4}\left({}_{4}^{jk}\psi_b \right) - \frac{h_1}{2}\left({}_{1}^{jk}\theta_{yb} \right) + \frac{h_2}{2}\left({}_{1}^{jk}\theta_{zb} \right) + \frac{h_1 h_2}{4}\left({}_{1}^{jk}\psi_b \right) \approx 0$$

By grouping Eqs. (5.9), (5.10), (5.13)a-c and (5.14)a-c, one obtains 12 constraint equations for the four-faced joint. Constraints for all joints k are then assembled in the matrix form

$$\left[B \right]_{jk} \left\{ {}^{k}U_{bg} \right\} = \left\{ 0 \right\} \tag{5.15}$$

where the entries of $\left[B \right]_{jk}$ depend on the width h_1 and height h_2 of joint element k and $\left\{ {}^{k}U_{bg} \right\}$ is the nodal buckling displacement vector of the joint k in the global coordinates. The constraints in Eq. (5.15) are enforced through a Lagrange multiplier vector $\left\{ L_j \right\}$. By summation over the joints in the frame, one obtains the resulting energy term

$$\pi_c = \sum_{j=1}^{m} \left\langle L_j \right\rangle^T \left[B_{jk} \right] \left\{ {}^{k}U_{bg} \right\} \tag{5.16}$$

which is the one sought in Eq. (5.1) to augment the total potential energy functional. It ensures that the functional is minimized subject to the constraints provided in Eq. (5.15).

5.5.3 Warping stiffness matrices for joints connecting four elements

As a member of a frame undergoes LTB, it tends to warp at its ends. This action is in part elastically restrained by the adjacent joint. This section aims at characterizing such warping restraint and devising a simplified generalized warping stiffness matrix for the joint element. One recalls that, in addition to the rigid body motion previously characterizing the joint behaviour, the joint has four warping degrees of freedom (Figure 5-3) ${}_{1}^{jk}\psi_{bl}$ - ${}_{4}^{jk}\psi_{bl}$ at Faces 1-4, respectively. Such warping degrees of freedom need to be related to the corresponding bimoments ${}_{1}^{jk}B_{bl}$ through ${}_{4}^{jk}B_{bl}$ acting at Faces 1-4 through a 4×4 warping stiffness matrix. The warping-bimoment relationships of the joint are obtained from a separate shell analysis for the five-plate assembly of the joint.

(Figure 5-1e). To obtain the warping stiffness matrix of joint k (Figure 5-6), the joint is first subjected to a unit warping deformation ${}_1^{jk}\psi_{bl} = 1$ at Face 1. The warping ${}_1^{jk}\psi_{bl} = 1$ is applied by applying a rotation angle ${}_1^{jk}\theta_{\psi bl} = h_1/2 \times {}_1^{jk}\psi_{bl} = h_1/2$ about axis z_{jk} at edge $5'-5''$ and an equal but opposite angle $-{}_1^{jk}\theta_{\psi bl} = -h_1/2$ at edge $8'-8''$ (Figure 5-6a), while setting the warping deformations ${}_2^{jk}\psi_{bl}$ - ${}_4^{jk}\psi_{bl}$ to zero at Faces 2- 4 (by restraining the rotations of edges $6'-6''$ and $7'-7''$ in Figure 5-6b along the z_{jk} direction and edges $5'-5''$, $6'-6''$, $7'-7''$ and $8'-8''$ along the y_{jk} direction). The corresponding bimoment ${}_{11}^{jk}B_{bl}$ induced at Face 1 is determined from the reactions ${}_1^{jk}R_{yr5'-5''}$, ${}_1^{jk}R_{yr8'-8''}$ $(r = 1,...,\alpha)$ (Figure 5-6b) obtained from the shell finite-element model, that is

$$ {}_{11}^{jk}B_{bl} = \int_{A_1} \sigma_1 \omega_1(s) dA \approx \sum_{r=1}^{nr} \left({}^{jk}R_{yr5'-5''} \right) \left(\frac{h_1}{2} x_{r5'-5''} \right) + \sum_{r=1}^{nr} \left({}^{jk}R_{yr8'-8''} \right) \left(\frac{-h_1}{2} x_{r8'-8''} \right) \tag{5.17} $$

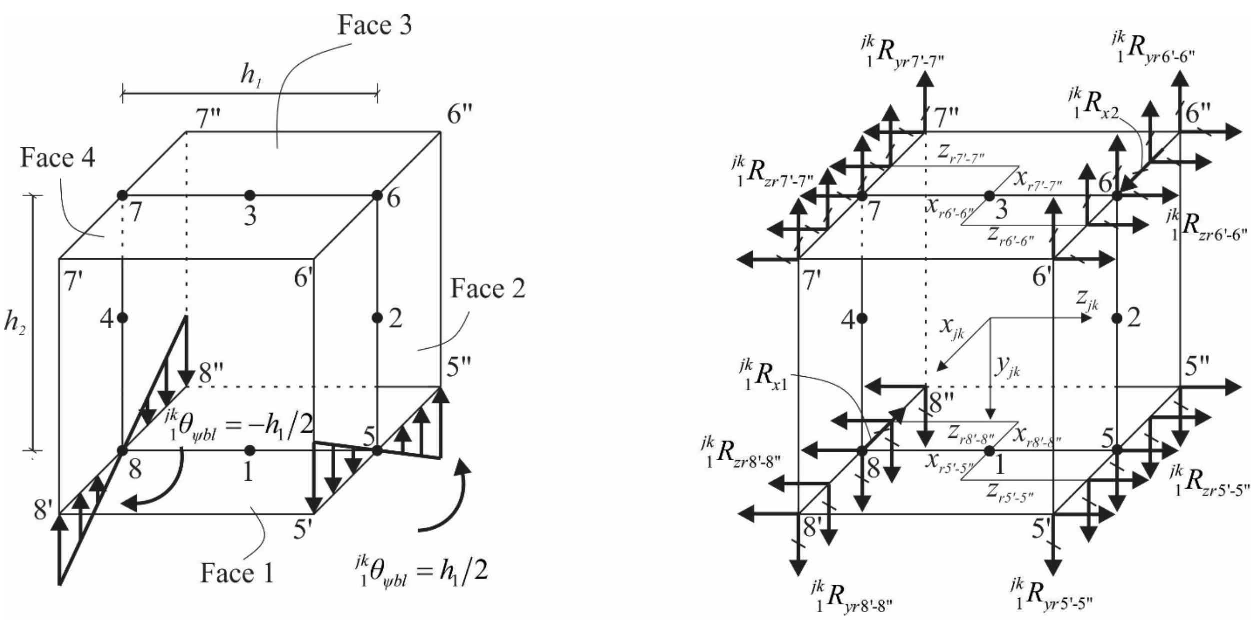

(a) **(b)**

Figure 5-6 (a) Unit warping deformation applied at Face 1; (b) boundary conditions and reactions

In Eq. (5.17), the warping function $\omega_1(s)$ illustrated in Figure 5-4 is obtained by $\omega_1(s) = \pm(h_1/2)\, x_r(s)$ along edges $5'-5''$ and $8'-8''$. Similarly, bimoments ${}_{21}^{jk}B_{bl}$, ${}_{31}^{jk}B_{bl}$ and ${}_{41}^{jk}B_{bl}$ induced at Faces 2- 4, respectively, are determined from reactions through

$$
\begin{aligned}
{}^{jk}_{21}B_{bl} &= \int_{A_1} \sigma_2 \omega_2(s) dA \approx \sum_{r=1}^{nr} \left({}^{jk}R_{zr5'-5''} \right) \left(\frac{h_2}{2} x_{r5'-5''} \right) + \sum_{r=1}^{nr} \left({}^{jk}R_{zr6'-6''} \right) \left(\frac{-h_2}{2} x_{r6'-6''} \right) \\
{}^{jk}_{31}B_{bl} &= \int_{A_1} \sigma_3 \omega_3(s) dA \approx \sum_{r=1}^{nr} \left(R_{yr6'-6''} \right) \left(\frac{-h_1}{2} x_{r6'-6''} \right) + \sum_{r=1}^{nr} \left({}^{jk}R_{yr7'-7''} \right) \left(\frac{h_1}{2} x_{r7'-7''} \right) \\
{}^{jk}_{41}B_{bl} &= \int_{A_1} \sigma_4 \omega_4(s) dA \approx \sum_{r=1}^{nr} \left({}^{jk}R_{zr8'-8''} \right) \left(\frac{-h_2}{2} x_{r8'-8''} \right) + \sum_{r=1}^{nr} \left({}^{jk}R_{zr7'-7''} \right) \left(\frac{h_2}{2} x_{r7'-7''} \right)
\end{aligned} \qquad (5.18)\text{a-c}
$$

The following step is to subject the joint to a unit warping deformation ${}^{jk}_{2}\psi_{bl} = 1$ at Face 2 while setting to zero the warping deformations ${}^{jk}_{1}\psi_{bl}$, ${}^{jk}_{3}\psi_{bl}$ and ${}^{jk}_{4}\psi_{bl}$ at Faces 1,3 and 4. The resulting reactions are extracted from the finite element model and the corresponding bimoments induced at Faces 1-4 are calculated by the expressions given in Appendix B. The procedure is repeated by successively imposing unit warping deformation ${}^{jk}_{3}\psi_{bl} = 1$, ${}^{jk}_{4}\psi_{bl} = 1$ one at a time at Faces 3 and 4, while setting remaining warping deformations to zero, the corresponding induced bimoment at Faces 1 to 4 (Appendix B).

The total bimoments ${}^{jk}_{1}B_{bl}$ - ${}^{jk}_{4}B_{bl}$ acting on Faces 1-4 induced warping deformations ${}^{jk}_{1}\psi_{bl}$ - ${}^{jk}_{4}\psi_{bl}$ are obtained by superposition of Eqs. (5.17), (5.18)a-c, (5.57)a-d, (5.58)a-d and (5.59)a-d yielding

$$
\left\{ {}^{jk}B_{bl} \right\} = \left[{}^{jk}K_{\psi bl} \right] \left\{ {}^{jk}U_{\psi bl} \right\}, \qquad \left[{}^{jk}K_{\psi bl} \right] = \begin{bmatrix} {}^{jk}_{11}B_{bl} & {}^{jk}_{21}B_{bl} & {}^{jk}_{31}B_{bl} & {}^{jk}_{41}B_{bl} \\ {}^{jk}_{12}B_{bl} & {}^{jk}_{22}B_{bl} & {}^{jk}_{32}B_{bl} & {}^{jk}_{42}B_{bl} \\ {}^{jk}_{13}B_{bl} & {}^{jk}_{23}B_{bl} & {}^{jk}_{33}B_{bl} & {}^{jk}_{43}B_{bl} \\ {}^{jk}_{14}B_{bl} & {}^{jk}_{24}B_{bl} & {}^{jk}_{34}B_{bl} & {}^{jk}_{44}B_{bl} \end{bmatrix} \qquad (5.19)\text{a-b}
$$

Eq. (5.19)a-b defines the warping matrix $\left[{}^{jk}K_{\psi bl} \right]$ which relates the nodal bimoments $\left\langle {}^{jk}B_{bl} \right\rangle^T = \left\langle {}^{jk}_{1}B_{bl} \quad {}^{jk}_{2}B_{bl} \quad {}^{jk}_{3}B_{bl} \quad {}^{jk}_{4}B_{bl} \right\rangle$ to the nodal warping deformations $\left\langle {}^{jk}U_{\psi bl} \right\rangle^T = \left\langle {}^{jk}_{1}\psi_{bl} \quad {}^{jk}_{2}\psi_{bl} \quad {}^{jk}_{3}\psi_{bl} \quad {}^{jk}_{4}\psi_{bl} \right\rangle$. The energy contribution of the warping matrices for the joints of the structure

$$
\frac{1}{2}\delta^2 \pi_j = \sum_{k=1}^{m} \frac{1}{2} \delta^2 \left({}^{jk}\pi_k \right) = \sum_{k=1}^{m} \frac{1}{2} \left\langle \delta \left({}^{jk}U_{\psi bl} \right) \right\rangle_{1\times 4}^T \left[{}^{jk}K_{\psi bl} \right]_{4\times 4} \left\{ \delta \left({}^{jk}U_{\psi bl} \right) \right\}_{4\times 1} \qquad (5.20)
$$

where the summation is over the number of joints m in the structure.

5.5.4 Special considerations for joints connecting fewer than four elements

Eq. (5.19)a-b provides the general form of warping stiffness matrix $\left[{}^{jk}K_{\psi bl}\right]$ for the case of a joint interfacing between four members. When a joint connects only two or three members, the bimoments acting on the unconnected faces of the joint vanish and static condensation is needed to formulate the warping stiffness matrices for such cases. It is expedient to re-order the warping degrees of freedom in Eq. (5.19)a-b so that the non-vanishing bimoments $\{B_1\}$ and corresponding warping deformations $\{\psi_1\}$ are grouped in a first partition and the vanishing bimoments $\{B_2\}$ and corresponding warping deformations $\{\psi_2\}$ are grouped in the second partition. The procedure is systematically achieved by introducing permutation matrices $[P]_c$ for various cases $c = 1, 2, 3, 4$ as defined in Table 5.1. Also, given in the table are the sizes of vectors $\{B_1\}$, $\{\psi_1\}$, $\{B_2\}$, and $\{\psi_2\}$ for the joint configurations depicted in Figure 5-1b and can be generalized to other cases. In all cases, the permutation matrices meet the condition $[P]_c [P]_c = [I]$ while re-arranging the degrees of freedom so that the vanishing bimoments are moved to bottom partition, i.e.,

$$[P]_c \left\{{}^{jk}B_{bl}\right\} = \left\{\begin{array}{c}\{B_1\}\\ \hline \{B_2\}\end{array}\right\}, [P]_c \left\{{}^{jk}U_{\psi bl}\right\} = \left\{\begin{array}{c}\{\psi_1\}\\ \hline \{\psi_2\}\end{array}\right\} \tag{5.21)a-b (}$$

By pre-multiplying Eq. (5.19)a by $[P]_c$ and inserting $[P]_c [P]_c = [I]$ in the right hand side term, one obtains

$$[P]_c \left\{{}^{jk}B_{bl}\right\} = [P]_c \left[{}^{jk}K_{\psi bl}\right][P]_c [P]_c \left\{{}^{jk}U_{\psi bl}\right\}, \text{ or}$$

$$\left\{\begin{array}{c}\{B_1\}\\ \hline \{B_2\}\end{array}\right\} = \left[\begin{array}{c:c}[K_{11}] & [K_{12}]\\ \hdashline [K_{12}]^T & [K_{22}]\end{array}\right]\left\{\begin{array}{c}\{\psi_1\}\\ \hline \{\psi_2\}\end{array}\right\}, \qquad \left[\begin{array}{c:c}[K_{11}] & [K_{12}]\\ \hdashline [K_{12}]^T & [K_{22}]\end{array}\right] = [P]_c \left[{}^{jk}K_{\psi bl}\right][P]_c \tag{5.22)a-b (}$$

By setting $\{B_2\} = \{0\}$, expanding Eq. (5.22)a-b along the second partition, and solving for $\{\psi_2\}$, one obtains

$$\{\psi_2\} = -[K_{22}]^{-1}[K_{12}]^T\{\psi_1\} \tag{5.23}$$

By expanding the first partition of Eq. (5.22)a-b and substituting from Eq. (5.23), one obtains

$$\left([K_{11}] - [K_{12}][K_{22}]^{-1}[K_{12}]^T\right)\{\psi_1\} = \{B_1\} \tag{5.24}$$

where the bracketed term represents the modified stiffness matrix sought which accounts for the condition $\{B_2\}=\{0\}$. The numeric values of the warping matrix for different types of joint configurations of the Examples, reviewed in the present study, will be provided in Appendix C.

Table 5.1 Permutation matrices and sizes of nodal bimoment and warping vectors for various joint configurations

Case	**(1)**	**(2)**	**(3)**	**(4)**
Joint configuration	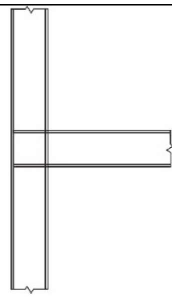	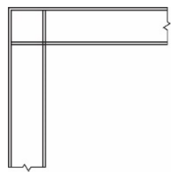	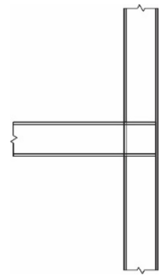	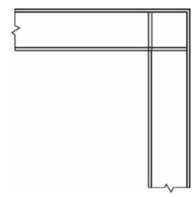
Numbering of faces where bimoments vanish	4	3,4	2	2,3
Permutation matrix $[P]_c$	$[I]$	$[I]$	$\begin{bmatrix} 1 & & & \\ & & & 1 \\ & & 1 & \\ & 1 & & \end{bmatrix}$	$\begin{bmatrix} 1 & & & \\ & & & 1 \\ & & 1 & \\ & 1 & & \end{bmatrix}$
Size of $\{B_1\},\{\psi_1\}$	3x1	2x1	3x1	2x1
Size of $\{B_2\},\{\psi_2\}$	1x1	2x1	1x1	2x1

5.5.5 Destabilizing contribution of joints due to finite rotation effects

Consider the four-nodded joint element k as a part of 2D frame shown in Figure 5-7a. Under reference loads (Configuration 2 in Figure 5-2) the joint is in equilibrium and the sum of moments M at faces $i=1,\ldots,4$ must vanish, i.e.,

$$\sum_{i=1}^{4} {}^{jk}_{i}M = 0 \Rightarrow {}^{jk}_{1}M = -{}^{jk}_{2}M - {}^{jk}_{3}M - {}^{jk}_{4}M \tag{5.25}$$

At the onset of buckling (Configuration 3 in Figure 5-2), this equilibrium equation takes the form

$$\sum_{i=1}^{4} \lambda\left({}^{jk}_{i}M\right) = 0 \tag{5.26}$$

Moments ${}^{jk}_{i}M\ (i=1,...,4)$ are depicted as a couple of tensile and compressive forces ${}^{jk}_{i}F_3$ (Figure 5-7b) applied at Faces 1 to 4 where the right subscript takes the value 3 to denote Configuration 3 (Figure 5-2) at the onset of buckling. When the structure buckles, the joint undergoes rotations θ_{yb} and θ_{zb}. If the moments rotate with the joint (non-conservative moments), the points of application of forces ${}^{jk}_{i}F_3$ (Figure 5-7b) move by a distance $(d/2)\ {}^{jk}\theta_{yb}$ and thus forces ${}^{jk}_{i}F_3$ induce a second order weak axis moment $\lambda\ {}^{jk}_{i}F_3 d\ {}^{jk}\theta_{yb}$ as shown in Figure 5-7c. When the joint undergoes rotation ${}^{jk}\theta_{zb}$, the weak axis moment $\lambda\ {}^{jk}_{i}F_3 d\ {}^{jk}\theta_{yb}$ induces a load potential gain $\lambda\left({}^{jk}_{i}M\right)\left({}^{jk}\theta_{yb}\right)\left({}^{jk}\theta_{zb}\right)$ (Figure 5-7d). The second order moments induced about y-axis and z-axis on all faces are respectively shown in Figure 5-7e and Figure 5-7f. Subscripts 4 for forces $\lambda\ {}^{jk}_{i}F_4$ denote the equivalent forces at Configuration 4 in Figure 5-2 (i.e., at the buckled configuration). The load potential gained by the second order moments at all four faces due to the joint undergoing θ_{yb} and θ_{zb} is

$$V_{FR} = \lambda\left(-\,{}^{jk}_{1}M + {}^{jk}_{2}M - {}^{jk}_{3}M + {}^{jk}_{4}M\right)\ {}^{jk}\theta_{yb}\ {}^{jk}\theta_{zb} \tag{5.27}$$

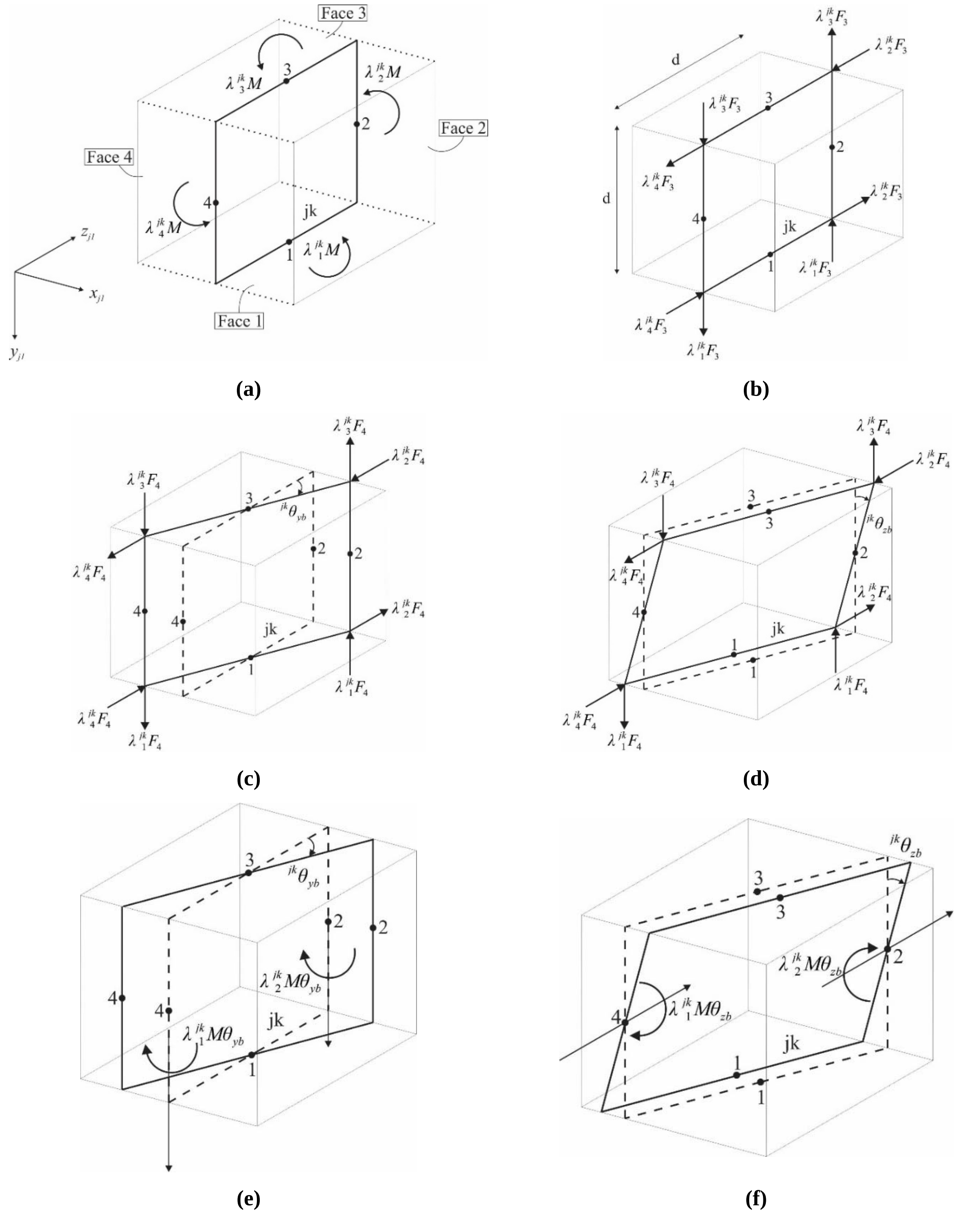

Figure 5-7 (a) Joint element under moments at the onset of buckling, (b) Joint element with equivalent force couples, (c) Joint after rotation about weak-axis, (d) Final position of the joint after rotation about z-axis, (e) Induced weak-axis moments, and (f) Second order moments due to rotation

Considering the special cased where only two collinear members are connected to faces 1 and 3, Eqs. (5.25) and (5.27) lead to the simplification

$$V_{FR} = \lambda \left(-{}_{1}^{jk}M - {}_{3}^{jk}M \right) {}^{jk}\theta_{yb} \, {}^{jk}\theta_{zb} = \lambda \left({}_{3}^{jk}M - {}_{3}^{jk}M \right) {}^{jk}\theta_{yb} \, {}^{jk}\theta_{zb} = 0 \tag{5.28}$$

Thus, for collinear members, the contribution of the finite rotation effect vanishes. Unlike the general case of a joint connected to four elements where the omission of finite rotation effects destroys joint equilibrium, for collinear members, the omission of finite rotation effects does not disturb the joint equilibrium and the omission of finite rotation effects still leads to correct buckling solutions. This approach was successfully used in various collinear solutions (e.g., Barsoum and Gallagher (1970), Erkmen and Mohareb (2008b), Wu and Mohareb (2011b) and Sahraei and Mohareb (2016)).

Consider the case of a joint k connecting two perpendicular members at Faces 1 and 2. Unlike the case of collinear members, the potential energy gain induced by second order moments due to moments ${}_{1}^{jk}M$ and ${}_{2}^{jk}M$ will not cancel one another and the load potential energy gain due to finite rotation effects is

$$V_{FR} = \lambda \left(-{}_{1}^{jk}M + {}_{2}^{jk}M \right) {}^{jk}\theta_{yb} \, {}^{jk}\theta_{zb} \neq 0 \tag{5.29}$$

In such a case, the incorporation of the finite rotation effect becomes essential for the proper prediction of the critical load of the frame.

5.5.6 Condition of neutral stability for the structure

The structure stiffness matrix $\left[K\right]_s$, reflecting the stiffness contributions of the members, the warping stiffness contributions of joints, and the structure geometric stiffness $\left[K_G\right]_s$ are formed using conventional assembly technique. From the kinematic conditions in Eq. (5.16), by substituting into Eq. (5.1), one obtains the variational statement for the structure

$$\delta\left(\frac{1}{2}\delta^2\pi\right) = \delta\left\{\frac{1}{2}\left\langle \delta u_s \right\rangle^T \left(\left[K\right]_s + \lambda\left[K_G\right]_s\right)\left\{\delta u_s\right\} + \left\langle \delta u_s \right\rangle^T \left[B\right]\left\{\delta L\right\}\right\} = 0 \tag{5.30}$$

in which $\{u_s\}$ is the vector nodal displacements for the structure. By evoking the stationarity conditions $\partial\left(1/2\,\delta^2\pi\right)/\partial\{\delta u_s\} = \{0\}$, $\partial\left(1/2\,\delta^2\pi\right)/\partial\{\delta L\} = \{0\}$ one recovers the following eigenvalue problem in the unknown load multiplier λ

$$\left(\begin{bmatrix} \left[K\right]_s & \left[B\right]^T \\ \left[B\right] & \left[0\right] \end{bmatrix} + \lambda \begin{bmatrix} \left[K_g\right]_s & \left[0\right] \\ \left[0\right] & \left[0\right] \end{bmatrix}\right) \begin{Bmatrix} \{u_s\} \\ \{L\} \end{Bmatrix} = \{0\} \tag{5.31}$$

5.6 Examples

5.6.1 Example 1: Γ-shaped frame

A laterally unsupported Γ-shaped frame (Figure 5-8a) consisting of a column of height $L_c = 4000m$ and a horizontal cantilever of span $L_b = 0.8m$ connected through a moment connection consisting of two pairs of stiffeners. The frame is subjected to a gravity load P acting at the shear center at the tip of the cantilever. The frame is assumed to remain within its elastic range of deformation. The cross-section profile is W200x59. The sectional properties for the idealized cross section (i.e., while neglecting the fillets) rather than the real sections were adopted to be consistent with the shell finite-element analysis model, which does not model the fillets. The idealized cross-sectional properties are provided in Figure 5-8b. It is required to determine the elastic lateral buckling load of the frame based on various solutions, including the one developed in the current study by considering the effect of finite rotations.

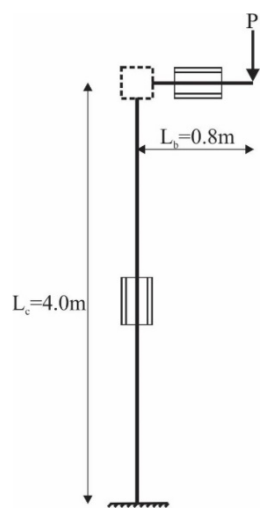

(a)

Width $b\ (mm)$	204.0
Height $h\ (mm)$	195.8
Flange thickness $t\ (mm)$	14.20
Web thickness $w\ (mm)$	9.100
Principal moment of inertia $I_x\ (mm^4)$	61.32×10^6
Principal moment of inertia $I_y\ (mm^4)$	20.10×10^6
Torsional constant $J\ (mm^4)$	4.390×10^5
Warping constant $I_\omega\ (mm^6)$	1.930×10^{11}
Area $A\ (mm^2)$	7575

(b)

Figure 5-8 Γ-shaped frame for Example 1 (a) Geometry and (b) Sectional properties for W200x59 section

Seven solutions were conducted and summarized in Table 5.2. The number of elements used in each model is provided to provide an indication of the computational effort for each analysis. Solution 1 is based on a shell element analysis using the S4R element in ABAQUS. Solution 2 is based on the joint formulation developed in conjunction with the shear deformable elements of Sahraei and Mohareb (2016) to represent the beam and columns. Solution 3 is based on the ABAQUS shear deformable B31OS element which captures shear deformation due to bending but omits shear deformation due to warping (Sahraei and Mohareb (2016)). Solution 4 is based on the present joint element in conjunction with the classical element by Barsoum and Gallagher (1970). Solution 5 is based on shear deformable elements while assuming the warping deformation is continuous (in line with the solutions developed in Mohareb and Dabbas (2003), Zinoviev and Mohareb (2004), Rizzi and Varano (2011), and Basaglia et al. (2012)). Solution 6 is based on a rigid representation of the joint (by assuming zero warping deformation at the column top and beam left end) in conjunction with shear deformable elements, while Solution 7 is based on a rigid representation of the joint in conjunction with classical finite elements. The rigid joint representation adopted in Solutions 6 and 7 would be approached only if the joint had three pairs of stiffeners including a diagonal pair of stiffeners (Trahair (1993)) and its use in the present problem with two pairs of stiffeners providing only partial warping restraints is expected to overestimate buckling loads.

Table 5.2 provides buckling load predictions of the frame based on several idealizations. Given the large number of degrees of freedom involved in the shell model in Solution 1, the corresponding buckling load prediction $P_{cr1} = 170.9kN$ provides the most accurate prediction. The critical load P_{cr1} is used as a reference value against which other buckling predictions are compared. Solution 2, based on the joint element developed in the present study, and including finite rotation effects, provides a very close prediction of the buckling load, only 1.2% higher than that based on the shell solution at a fraction of the computational cost. The difference is attributed to distortional effects, captured in the shell solution but not in the SM-M element. If the finite rotation effect is excluded from Solution 2, the predicted critical load is found to be 231.1 kN, grossly overestimating the buckling load by 35% compared to Solution 1. The comparison illustrates the importance of incorporating the finite rotation effect in the formulation.

Table 5.2 Critical loads (kN) for Gamma-shaped frame based on different solutions

Solution type			**Critical load (kN)**	**Critical load relative to P_{cr1}**
P_{cr}	**Member representation**	**Joint representation**		
P_{cr1}	Shell (S4R)-finite element analysis solution (column: 2400 elements; beam: 480 elements)	320 shell-finite element analysis solution (S4R)	170.9	----
P_{cr2}	SM-M element (Sahraei and Mohareb (2016)) fully deformable in shear (column: 20 elements; beam 4 elements)	Present joint formulation Including finite rotation effects	173.0	1.012
P_{cr3}	ABAQUS B31OS beam element (shear deformable in bending but not in warping; column: 20 elements; beam 10 elements)	Treated as a two-noded joint connected with rigid multi-point constraints and different warping deformations	173.1	1.013
P_{cr4}	Classical non-shear deformable element (Barsoum and Gallagher (1970)) (column: 20 elements; beam 4 elements)	Present joint formulation Including finite rotation effects	176.8	1.035
P_{cr5}	SM-M (Sahraei and Mohareb (2016)) element fully deformable in shear (column: 20 elements; beam 4 elements)	Continuous warping deformation	178.1	1.042
P_{cr6}	SM-M (Sahraei and Mohareb (2016)) element fully deformable in shear (column: 20 elements; beam 4 elements)	Rigid joint representation with full warping restraint	209.8	1.228
P_{cr7}	Classical non-shear deformable element (Barsoum and Gallagher (1970)) (column: 20 elements; beam 4 elements)	Rigid joint representation with full warping restraint	210.4	1.231

Solution 3 provides a critical load estimate based on the ABAQUS thin-walled shear deformable B31OS element while modeling the joint using two nodes rigidly connected using Multi Point Constraints. The comparison shows almost identical results with Solution 2. Similar to the SM-M element, B31OS element does not capture distortional effects and thus predicts higher critical moment predictions compared to that of S4R shell solution.

Solution 4 based on the classical non-shear deformable element overestimates buckling loads by 3.5% compared to Solution 1. The difference is caused by the fact that the classical solution captures neither distortional nor shear deformation effects.

The influence of the method of representation of the joint is assessed by comparing Solutions 2 and 6, in which a rigid jointed representation with full warping restraints (Solution 6) is found to over-predict the buckling load by about 21.6% compared to Solution 2 based on the more realistic representation of the joint introduced in the present study. When warping deformation is assumed continuous by equating the warping deformation at the column top to that at the cantilever left end (Solution 5), the solution was found to over-predict the buckling load by 4.2% -1.2%=3.0% compared to Solution 2. The comparison suggests that the joint formulation developed in the current study provides the most flexible representation of the joint flexibility and thus yields the closest results compared to the shell element solution (Solution 1). The continuous warping deformation assumption is found to lead to a stiffer higher critical and thus provides the second best representation of the joint, while the rigid joint representation grossly overestimates the stiffness provided by the joint. A similar conclusion is reached when comparing Solutions 4 and 7, both based on the classical element, in which the Solution 7 based on a rigid joint representation is found to overestimate the buckling load by $23.1-3.5=19.6\%$ compared with Solution 4 (based on a partially restrained joint representation).

The scenario where the beam is separated from the frame and the flexibility of the column at the cantilever root is omitted is investigated conducting a buckling analysis of the beam with 8 fully shear deformable elements [12]. The critical load is found to be 9,980 kN, grossly overestimating the buckling load compared to other solutions which account for beam-column interaction. Contrary to the widely accepted proposition by Salvadori (1953), separating the member from the whole frame and assuming idealized end boundary conditions, leads to un-conservative critical moment predictions in the present frame. The case where the frame is laterally braced at the cantilever root and tip is further discussed in Appendix D.

5.6.2 Example 2: Single story portal frame

The portal frame studied in Zinoviev and Mohareb (2004) is re-investigated. Column heights are $L_c = 4m$ and beam span is $L_b = 6m$. Cross-sections are W200x59. Columns are fully fixed at the bases (Figure 5-9a) while the rest of frame is laterally unsupported out of the plane of the frame as no lateral restraints are provided at the beam to column junctions. Two point loads P are acting at third-span points. The relevant idealized cross-section properties have been provided in Figure 5-8b. The elastic lateral buckling load for the frame is sought. It is considered that the (a) yield strength of the frame is high enough so that the capacity of the frame is not governed by yielding considerations.

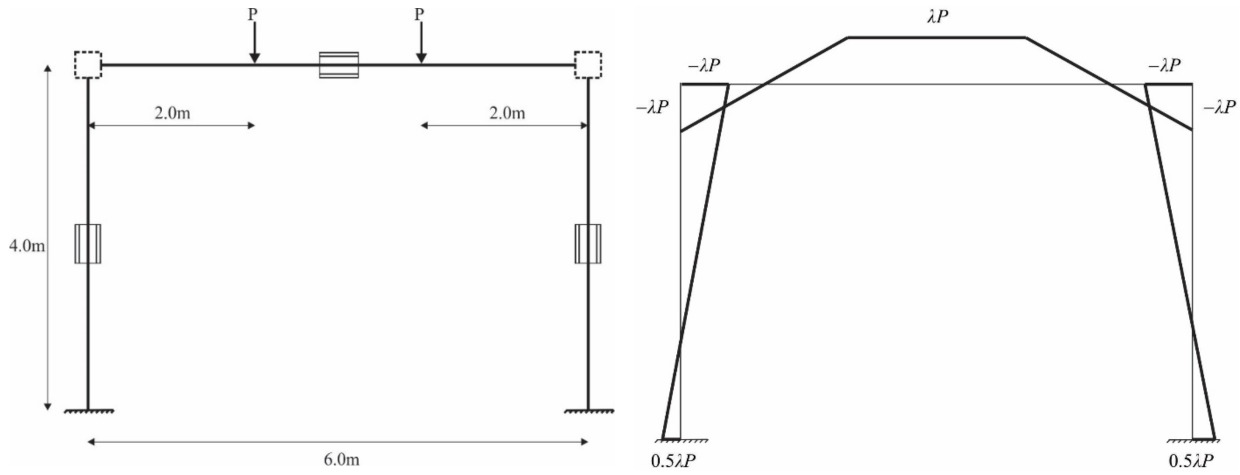

(a) **(b)**

Figure 5-9 Portal frame (a) geometry and reference loading, and (b) Bending moment diagram at onset of bucking

The bending moment diagram under the applied reference loads is shown in Figure 5-9b. In a manner similar to example 1, seven solution are conducted to predict the critical moment of the portal frame. The number of elements adopted in each solution are provided in Table 5.3.

Solution 1 based on the shell analysis provides the lowest critical load prediction P_{cr1} and is taken as a reference against which the remaining solutions are compared.

The buckling load prediction of Solution 2 (based on the present joint formulation including finite rotation effects and shear deformable elements) is found to be 5.8% higher than that based on the shell FEA and is the closest to the shell solution. The difference between both solutions is higher than in Example 1, suggesting that distortional effects for the portal frame are more significant than the Gamma-shaped frame. When the finite rotation effect is omitted, the critical load is found to increase to 244.7 kN (not shown in Table 5.3), thus over-predicting the buckling load by 11.4% compared to Solution 1. The effect of finite rotation results in an 11.4%-5.8%=6.4% over-prediction of the critical load, which is significantly lower than the 35% difference observed for the Gamma-shaped frame in Example 1. The large difference from the finite rotation effect observed in Example 1 is attributed to the fact that the column in example 1 undergoes significant twist throughout LTB compared to that in Example 2, thus increasing the contribution of the destabilizing term $\lambda\left(-{}_{1}^{jk}M + {}_{2}^{jk}M\right){}^{jk}\theta_{yb}\,{}^{jk}\theta_{zb}$ arising in Eq. (5.29).

Solution 3 overestimates the critical load by $P_{cr3}/P_{cr1} - P_{cr2}/P_{cr1} = 1.117 - 1.058 = 5.9\%$ compared to Solution 2. As discussed in Example 1, the difference is due to shear deformation effects induced by warping. Solution 4 fully omits shear deformation in members and is observed to predict a higher buckling load compared to Solution 2 which captures shear deformation. The difference between both solutions is $P_{cr4}/P_{cr1} - P_{cr2}/P_{cr1} = 1.131 - 1.058 = 7.3\%$, which is larger than the 2.3% difference observed in Example 1, suggesting that shear deformation has a more pronounced effect for the portal frame. The finding is consistent with the fact that a portal frame, with two fixed supports, is more constrained than the Γ-shaped frame with a single support at the base, thus increasing the effect of shear deformation.

Solutions 5 based on continuous warping restraint is observed to over-predict the buckling load by $P_{cr5}/P_{cr1} - P_{cr2}/P_{cr1} = 1.151 - 1.058 = 9.3\%$ compared to Solution 2 which adopts the present joint formulation. The 9.3% difference is larger than 3.0% difference in Example 1 since the warping stiffness and kinematic relations for the two joints involved in Example 2 are more pronounced compared to Example 1 where only one joint was modeled through kinematic relations.

A rigid joint representation with shear deformable elements (Solution 6) and with non-shear deformable elements (solution 7) are observed to over-predict the buckling load by $P_{cr6}/P_{cr1} - P_{cr2}/P_{cr1} = 1.202 - 1.058 = 14.4\%$ and $P_{cr7}/P_{cr1} - P_{cr2}/P_{cr1} = 1.316 - 1.058 = 25.8\%$, respectively, compared to Solution 2. Both results illustrate (a) the importance of accounting for joint flexibility and (b) that shear deformation effects are more pronounced in the present example compared to the corresponding percent differences of 21.6% and 21.9% obtained in for Solutions 6 and 7 of Example 1.

Present standards (CAN/CSA S16 (2014), ANSI/AISC 360 (2016)) isolate members from the rest of structure and quantify their critical moments separately in line with the Salvadori hypothesis (1953). The methodology is applied to the horizontal member by separating it from the rest of the portal frame. The member is subjected to the two point loads and the end moments as obtained from the pre-bucking analysis shown in Figure 5-9b. Idealized pinned boundary conditions are assumed for the vertical displacement, lateral displacement, and angle of twist. Based on ANSI/AISC 360-16, the moment gradient factor is $C_{AISC} = 12.5M_{\max}/\left(2.5M_{\max} + 3M_A + 4M_B + 3M_C\right)$ where M_A, M_B and M_C are the quarter point moments, and $M_{\max}$ is the peak moment, yielding $C_{AISC} = 1.316$, and the corresponding critical moment is $M_{cr-AISC} = C_{AISC}\left(\pi/L_u\right)\sqrt{EI_yGJ + \left(\pi E/L_u\right)^2 I_yC_w} = 291\ kNm$. Under the Canadian standards CSA-S16-14, the moment gradient factor is given by $C_{CAN} = 4M_{\max} \Big/ \sqrt{M_{\max}^2 + 4M_A^2 + 7M_B^2 + 4M_C^2} = 1.265$, yielding a critical moment prediction $M_{cr-CAN} = C_{CAN}\left(\pi/L_u\right)\sqrt{EI_y GJ + \left(\pi E/L_u\right)^2 I_y C_w} = 280\ kNm$. The corresponding axial force in the member at the onset of buckling under the reference load $C_f = 0.374\lambda = 0.374 \times 232 = 89.6\ kN$ is relatively small compared to the buckling strength $C_{ry} = 1102 kN$ of the column (i.e., $C_f / C_{ry} = 0.08$) suggesting that the buckling strength of the member is predominantly induced by strong axis bending. Both standard-based elastic critical moment predictions are observed to over-predict the critical moment based on the shell analysis $\left(219.7\ kNm\right)$ and the present solution. This is the case since the quarter point moment gradient equations are only approximate and are intended for beam segments that are restrained laterally and torsionally but free to warp and undergo lateral rotation at both ends. Such idealized conditions are not representative of the end conditions of the horizontal member where both ends are partially restrained relative to the lateral displacement, twist, warping, and weak axis rotation through the adjoining columns. The example suggests the importance of accounting for interaction effects between the beam and columns as is the case in the ABAQUS shell solution and the present solution.

Table 5.3 Critical Loads (kN) for single story portal frame

Solution type			Critical load (kN)	Critical load relative to P_{cr1}
P_{cr}	**Member representation**	**Joint representation**		
P_{cr1}	Shell (S4R)-finite element analysis solution (column: 2400 elements; beam: 3600 elements)	320 shell-finite element analysis solution (S4R)	219.7	----
P_{cr2}	SM-M element (Sahraei and Mohareb (2016)) fully deformable in shear (column: 20 elements; beam 30 elements)	Present joint formulation Including finite rotation effects	232.4	1.058
P_{cr3}	ABAQUS B31OS beam element (shear deformable in bending but not in warping; column: 20 elements; beam 30 elements)	Treated as a two-noded joint connected with rigid multi-point constraints and different warping deformations	245.4	1.117
P_{cr4}	Classical (Barsoum and Gallagher (1970)) non-shear deformable element (column: 20 elements; beam 30 elements)	Present joint formulation Including finite rotation effects	248.4	1.131
P_{cr5}	SM-M (Sahraei and Mohareb (2016)) element fully deformable in shear (column: 20 elements; beam 30 elements)	Continuous warping deformation	252.8	1.151
P_{cr6}	SM-M (Sahraei and Mohareb (2016)) element fully deformable in shear (column: 20 elements; beam 30 elements)	Rigid joint representation with full warping restraint	264.1	1.202
P_{cr7}	Classical (Barsoum and Gallagher (1970)) non-shear deformable element (column: 20 elements; beam 30 elements)	Rigid joint representation with full warping restraint	289.2	1.316

5.6.3 Example 3: Three-story single-bay frame

The three-storey single-bay frame shown in Figure 5-10a is fixed at bases A and B and subjected to the shown uniformly distributed gravity load applied to the third-story beam. All members are assumed to have W200x46 cross-section and connected through moment resisting connections. Cross-sectional properties of W200x46 are: $b = 203.0\,mm$, $h = 192.0\ mm$, $t = 11\,mm$, $w = 7.2\,mm$, $I_x = 4.545\times10^7\ mm^4$, $I_y = 1.534\times10^7\,mm^4$, $J = 2.040\times10^5\ mm^4$, $I_\omega = 1.413\times10^{11}\,mm^6$ and $A = 5848\ mm^2$. It is required to determine the elastic LTB resistance of the frame based on two scenarios: (a) All beam-column junctions are restrained against lateral displacement (as is commonly the case in conventional buildings), and (b) No lateral restraints are provided at the beam-column junction except junctions E and F (as may be the case in some pipe rack configurations in industrial plants). The yield strength of steel is assumed to be high enough so that the resistance of the frame is governed by its elastic lateral torsional buckling resistance.

The bending moment and normal force diagrams under the reference load based on a pre-buckling analysis are provided in (Figure 5-10b-c). The critical load combination of the whole three-story frame was determined for the laterally restrained and unrestrained scenarios using three solutions: (1) A shell finite-element analysis based on the S4R element in ABAQUS; (2) A solution based on the joint element developed under the present solution in conjunction with shear deformable beam elements (based on Sahraei and Mohareb (2016)) to model the straight segments; and (3) A solution based on the B31OS element in ABAQUS with an assumed continuous warping restraint at the joints. The critical load multipliers λ based on the three solutions are summarized in Table 5.4.

As expected, Solution 1 predicts the smallest critical load since it provides the most flexible representation of the structure. The corresponding buckling load multiplier is considered as a benchmark against which the validity of other two solutions are assessed. Using the joint element developed in the current study with the shear deformable beam elements leads to a closer buckling prediction to the shell solution when compared to that based on the B31OS element with continuous warping at the joints, which tend to overestimate the buckling resistance of the frame. The present solution overestimates the buckling strength of the frame by 2% for the laterally restrained frame and by 7% for the case of no lateral restraint. The number of degrees of freedom involved in the present study is two orders of magnitudes less than that of the shell analysis. As expected, the present solution provides a more realistic representation of the joint behaviour and the beam to column junctions. Figure 5-11 depicts the buckling configurations for both scenarios based on the ABAQUS simulation. The top beam deforms the most and thus the frame global buckling is attributed predominantly to the top beam.

By restraining the frame at all the junctions (Scenario (a)), Solutions 1-3 yield considerably higher buckling loads compared to Scenario (b) where lateral restraints are provided only at junctions E and F. For instance, the present solution predicts a peak critical moment of 315.3 kNm for Scenario (a) and only 125.2 kNm under Scenario (b). As observed in Figure 5-10b, the peak bending moment occurs at mid-span of beam GH. In line with the standards procedure, member GH beam is isolated from the structure and its critical moment is determined from ANSI/AISC 360-16. The corresponding moment gradient factor is $C_{AISC} = 1.285$, and the corresponding critical moment is

$M_{cr-AISC} = 231.8\ kNm$. According to CAN/CSA S16-14, the moment gradient factor of $C_{CAN} = 1.246$ and the corresponding critical moment is $M_{cr-CAN} = 224.8\ kNm$. Both values are lower than the critical moment of the braced frame (a), suggesting that the common standard practice of isolating the member from the structure based on the Salvadori hypothesis (1953) leads to conservative predictions of the critical moments. In contrast, for the laterally unbraced frame (b), the procedure overestimates the lateral torsional buckling resistance of the member. The example suggests restricting the adoption of the Salvadori hypothesis to structures where members are laterally braced at both ends. Further discussions are provided in Appendix E.

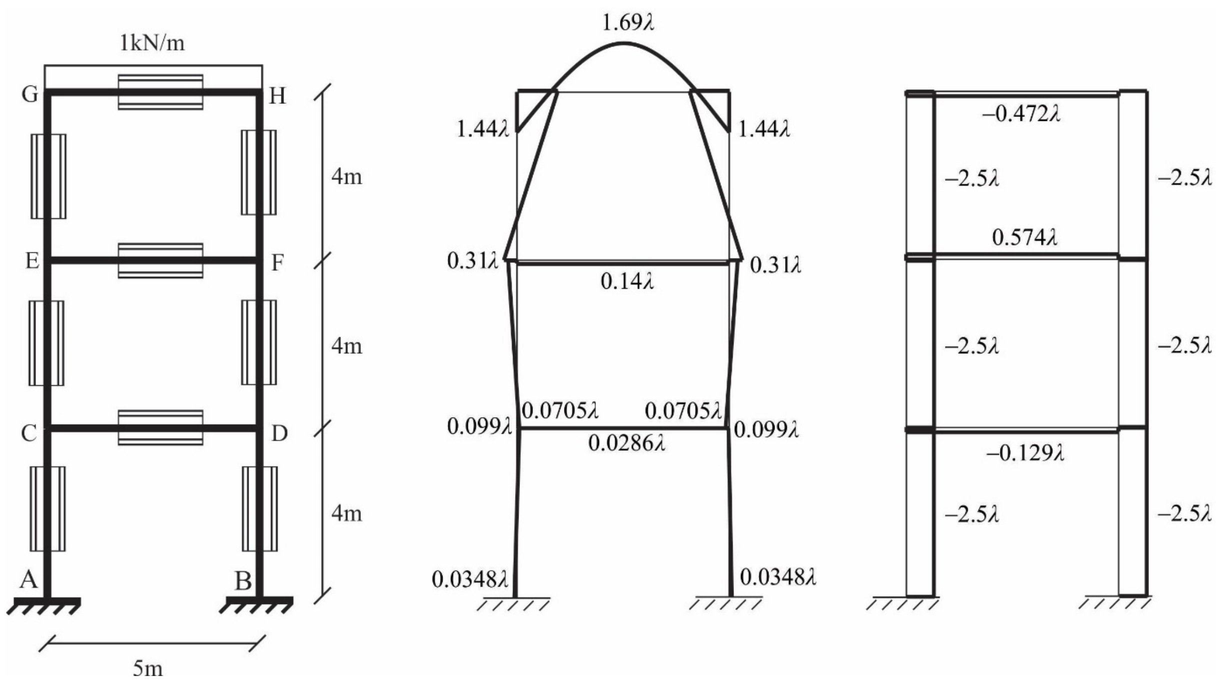

(a) **(b)** **(c)**

Figure 5-10 Three -story frame under gravity load (a) Geometry, (b) Bending Moment diagram, and (c) Normal force diagram

(a)

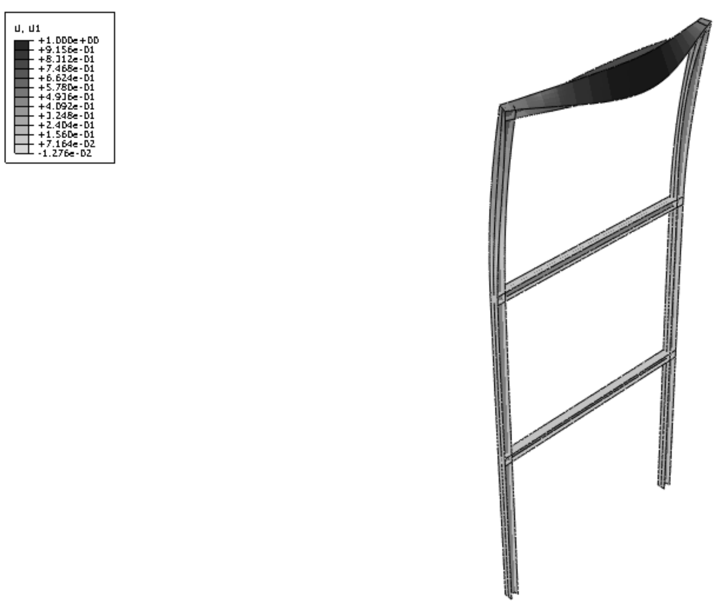

(b)

Figure 5-11 buckling configurations for (a) Scenario (a) Frame laterally restrained at joints and (b) Scenario (b) Frame is laterally unrestrained at some of the joints

Table 5.4 Buckling load multipliers for 3-story frame with and without lateral restraints at junctions

Type of solution	Number of degrees of freedom	**Scenario (1) with lateral restraints at joints**			**Scenario (2) no lateral restraints except at junctions E, F**		
		Load multiplier λ	Critical moment kNm in Member BG	Load multiplier relative to λ_1	Load multiplier λ	Critical moment kNm in Member BG	Load multiplier relative to λ_1
λ_1 : ABAQUS shell model of the whole structure (S4R element)	63,498	183.5	310.1	----	69.50	117.5	----
λ_2 : present Joint element and shear deformable elements for the whole structure	567	186.7	315.3	1.02	74.11	125.2	1.07
λ_3 : Continuous warping restraint and ABAQUS B31OS elements of the whole structure	497	207.0	349.6	1.13	77.66	131.2	1.12

5.7 Summary and conclusions

1. The present study developed a generalized joint finite element that accurately quantifies the partial warping restraint provided by common moment connections to adjoining members framing at right angles.
2. The generalized four-node joint element developed is based on an initial shell analysis for the joint and is condensed into a reduced 4 DOF element. The joint element interfaces seamlessly with the classical 14 degrees of freedom beam finite element in Barsoum and Gallagher (1970) or that based on the shear deformable theory developed in Sahraei and Mohareb (2016).
3. The new developed element provides a more accurate representation of the joint stiffness than the continuous warping deformation assumption and provides LTB moment estimates closer to those based on a shell-finite element analysis.
4. The developed joint element successfully extends functionality of existing beam elements to analyze non-collinear structures and enables a more accurate and less un-conservative prediction of the elastic buckling resistance of plane frames when compared with a rigid joint representation. The gain in accuracy is achieved while keeping the degrees of freedom involved to a minimum.

5. The joint finite rotation effect was systematically incorporated into the formulation. Its importance for the accurate prediction of frame buckling loads was illustrated through numerical examples.
6. Compared to the number of degrees of freedom involved in shell-finite element solutions, the newly developed element is found to involve considerably fewer degrees of freedom. The underlying analysis can be conducted in a fraction of time and expense compared to shell-based solutions.
7. The limitations of the Salvadori hypothesis adopted in present design standards whereby the buckling loads for members are quantified by separating the members from the entire structure are illustrated through examples. The hypothesis is shown to lead to conservative results when frames are laterally restrained at the joints but can lead to un-conservative predictions when some of the frame joints are not laterally restrained. In contrast, the present solution accounts for interaction, and enables the whole frame to attain a buckling strength intermediate between the buckling strength of the column alone the buckling strength of the beam alone (Chapter 5).
8. The joint element can be used to model the entire structure including straight and joint elements. Thus, to attain buckling load predictions as close as possible to shell elements, it is recommended to use the generalized joint elements developed in the current study in conjunction with the shear deformable element in Sahraei and Mohareb (2016).

5.8 Appendix A. Lateral displacements due to warping

This appendix provides the formulation on obtaining the lateral displacements induced by warping deformation. Four lateral displacement contributions result from each of warping deformations at each of the four faces of the joints. These contributions are provided in each of the following subsections.

5.8.1 A.1. Contributions of warping at faces 1 and 2

The displacements at Point 2 on face 2 are related to those of Point 1 at face 1 through point 5 located at their intersection (Figure 5-5). The position vectors of points 1 and 2 relative to point 5 are:

$$\begin{aligned} \langle x_{15} \rangle^T &= \langle x_1 \rangle^T - \langle x_5 \rangle^T = \langle 0 \quad 0 \quad -h_1/2 \rangle \\ \langle x_{25} \rangle^T &= \langle x_2 \rangle^T - \langle x_5 \rangle^T = \langle 0 \quad -h_2/2 \quad 0 \rangle \end{aligned} \tag{5.32}$$

A positive warping deformation ${}^{jk}_{2}\psi_b$ at face 2 induces a positive angle of rotation ${}^{jk}_{2}\theta_{\psi b} = +(h_2/2)\, {}^{jk}_{2}\psi_b$ about the y_{jk} axis at Point 5 and an equal and opposite angle of rotation at point 6. Angle ${}^{jk}_{2}\theta_{\psi b}$ at point 5 induces an additional lateral displacement at Point 1, $\langle {}^{jk}_{1}U^*_{\psi 2} \rangle^T = \langle {}^{jk}_{1}u^*_b \quad {}^{jk}_{1}v^*_p \quad {}^{jk}_{1}w^*_p \rangle^T$ given by

$$\{ {}^{jk}_{1}U^*_{\psi 2} \} = [R_{\psi 2}]\{x_{15}\} \tag{5.33}$$

where the rotation matrix $[R_{\psi 2}]$ is defined as

$$[R_{\psi 2}]_{3\times 3} = \begin{bmatrix} -\frac{1}{2}\left(\frac{h_2}{2}\right)^2 \left({}^{jk}_{2}\psi_b\right)^2 & \frac{-h_2}{4}\lambda\left({}^{jk}_{2}\theta_{xp}\right)\left({}^{jk}_{2}\psi_b\right) & \frac{h_2}{2}\left({}^{jk}_{2}\psi_b\right) \\ \frac{h_2}{4}\lambda\left({}^{jk}_{2}\theta_{xp}\right)\left({}^{jk}_{2}\psi_b\right) & -\frac{1}{2}\lambda^2\left({}^{jk}_{2}\theta_{xp}\right)^2 & -\lambda\left({}^{jk}_{2}\theta_{xp}\right) \\ -\frac{h_2}{2}\left({}^{jk}_{2}\psi_b\right) & \lambda\left({}^{jk}_{2}\theta_{xp}\right) & -\frac{1}{2}\left[\lambda^2\left({}^{jk}_{2}\theta_{xp}\right)^2 + \left(\frac{h_2}{2}\right)^2\left({}^{jk}_{2}\psi_b\right)^2\right] \end{bmatrix} \tag{5.34}$$

The additional lateral displacement induced at Face 1 due to warping at face 2 is obtained by expanding the first row of right hand side of Eq. (5.33) yielding

$${}^{jk}_{1}u^*_b = -(h_1 h_2/4)\, {}^{jk}_{2}\psi_b \tag{5.35}$$

Similarly, the additional displacement at Point 2, $\left\langle {}_{2}^{jk}U_{\psi 1}^{*}\right\rangle^{T}=\left\langle {}_{2}^{jk}u_{b}^{*} \quad {}_{2}^{jk}v_{p}^{*} \quad {}_{2}^{jk}w_{p}^{*}\right\rangle^{T}$ is given by

$$\left\{{}_{2}^{jk}U_{\psi 1}^{*}\right\}=\left[R_{\psi 1}\right]\left\{x_{25}\right\} \tag{5.36}$$

where

$$\left[R_{\psi 1}\right]_{3\times 3}=\begin{bmatrix} -\frac{1}{2}\left(\frac{h_1}{2}\right)^2\left({}_{1}^{jk}\psi_b\right)^2 & -\frac{h_1}{2}\left({}_{1}^{jk}\psi_b\right) & \frac{h_1}{4}\lambda\left({}_{1}^{jk}\theta_{xp}\right)\left({}_{1}^{jk}\psi_b\right) \\ \frac{h_1}{2}\left({}_{1}^{jk}\psi_b\right) & -\frac{1}{2}\left(\frac{h_1}{2}\right)^2\left({}_{1}^{jk}\psi_b\right)^2 & -\lambda\left({}_{1}^{jk}\theta_{xp}\right) \\ \frac{h_1}{4}\lambda\left({}_{1}^{jk}\theta_{xp}\right)\left({}_{1}^{jk}\psi_b\right) & \lambda\left({}_{1}^{jk}\theta_{xp}\right) & -\frac{1}{2}\lambda^2\left({}_{1}^{jk}\theta_{xp}\right)^2 \end{bmatrix} \tag{5.37}$$

The additional lateral displacement induced at Face 2 due to warping deformation at Face 1 is obtained by expanding the first row of the right hand side of Eq. (5.36) yielding

$${}_{2}^{jk}u_{b}^{*}=\left(h_1 h_2/4\right){}_{1}^{jk}\psi_b \tag{5.38}$$

The total out of plane displacement at point 2 obtained by summation of Eqs. (5.14)a, (5.35) and (5.38) yielding

$$-{}_{2}^{jk}u_b+{}_{1}^{jk}u_b-\frac{h_1 h_2}{4}\left({}_{2}^{jk}\psi_b\right)+\frac{h_1}{2}\left({}_{1}^{jk}\theta_{yb}\right)+\frac{h_2}{2}\left({}_{1}^{jk}\theta_{zb}\right)+\frac{h_1 h_2}{4}\left({}_{1}^{jk}\psi_b\right)\approx 0 \tag{5.39}$$

5.8.2 A.2. Contributions of warping at faces 1 and 3

Using the same methodology described in Section 5.8.1 [Eqs. (5.33) and (5.36)], the DOFs of node 2 are related to those of node 3. Then, using Eq. (5.39) to relate the DOFs of node 2 to those of node 1, one can obtain the relationship between the DOFs of nodes 3 and 1 by eliminating DOFs of node 2. Displacements of node 2 are related to those of node 3 to form the rigid body motion as follows

$$\left\{u_2\right\}_{3\times 1}=\left\{u_3\right\}_{3\times 1}+\left[R\right]_{3\times 3}\left\{x_{23}\right\}_{3\times 1} \tag{5.40}$$

Expanding the right hand side of Eq. (5.40) about the first row leads to

$${}_{2}^{jk}u_{b}^{*}={}_{3}^{jk}u_{b}^{*}-\frac{h_2}{2}\left({}_{3}^{jk}\theta_{zb}\right)+\frac{h_1}{2}\left({}_{3}^{jk}\theta_{yb}\right) \tag{5.41}$$

5.8.3 A.3. Contributions of warping at faces 2 and 3

Displacements at point 2 of face 2 are related to those of at point 3 of face 3 through point 6 located at their junctions as follows

$$\begin{aligned}\langle x_{36}\rangle^T &= \langle x_3\rangle^T - \langle x_6\rangle^T = \langle 0 \quad 0 \quad -h_1/2\rangle \\ \langle x_{26}\rangle^T &= \langle x_2\rangle^T - \langle x_6\rangle^T = \langle 0 \quad h_2/2 \quad 0\rangle\end{aligned} \tag{5.42}$$

The angle ${}^{jk}_{2}\theta_{\psi b}$ acting at point 6 induces an additional lateral displacement at point 3, $\left\langle {}^{jk}_{3}U^*_{\psi 2}\right\rangle^T = \left\langle {}^{jk}_{3}u^*_b \quad {}^{jk}_{3}v^*_p \quad {}^{jk}_{3}w^*_p\right\rangle^T$ given by

$$\left\{ {}^{jk}_{3}U^*_{\psi 2}\right\} = \left[R_{\psi 2}\right]\left\{x_{36}\right\} \tag{5.43}$$

The additional lateral displacement induced at the face 3 due to warping deformation at face 2 is obtained by expanding the right hand side of Eq. (5.43) about the first row as follows

$${}^{jk}_{3}u^*_b = -\left(h_1 h_2/4\right) {}^{jk}_{2}\psi_b \tag{5.44}$$

Similarly, the additional lateral displacement induced at the face 2 due to warping deformation at face 3 is obtained through

$$\left\{ {}^{jk}_{2}U^*_{\psi 3}\right\} = \left[R_{\psi 3}\right]\left\{x_{26}\right\} \tag{5.45}$$

Expanding the right hand side of Eq. (5.45) about the first row leads to

$${}^{jk}_{2}u^*_b = -\left(h_1 h_2/4\right) {}^{jk}_{3}\psi_b \tag{5.46}$$

where

$$\left[R_{\psi 3}\right]_{3\times 3} = \begin{bmatrix} -\frac{1}{2}\left(\frac{h_1}{2}\right)^2\left({}^{jk}_{3}\psi_b\right)^2 & -\frac{h_1}{2}\left({}^{jk}_{3}\psi_b\right) & \frac{h_1}{4}\lambda\left({}^{jk}_{3}\theta_{xp}\right)\left({}^{jk}_{3}\psi_b\right) \\ \frac{h_1}{2}\left({}^{jk}_{3}\psi_b\right) & -\frac{1}{2}\left(\frac{h_1}{2}\right)^2\left({}^{jk}_{3}\psi_b\right)^2 & -\lambda\left({}^{jk}_{3}\theta_{xp}\right) \\ -\frac{h_1}{4}\lambda\left({}^{jk}_{3}\theta_{xp}\right)\left({}^{jk}_{3}\psi_b\right) & \lambda\left({}^{jk}_{3}\theta_{xp}\right) & -\frac{1}{2}\lambda^2\left({}^{jk}_{3}\theta_{xp}\right)^2 \end{bmatrix} \tag{5.47}$$

Finally, the total out of plane displacement at point 2 obtained by summation of Eqs. (5.40), (5.44) and (5.46) resulting in

$$-{}^{jk}_{2}u_b + {}^{jk}_{3}u_b - \frac{h_2}{2}\left({}^{jk}_{3}\theta_{zb}\right) + \frac{h_1}{2}\left({}^{jk}_{3}\theta_{yb}\right) - \left(\frac{h_1 h_2}{4}\right){}^{jk}_{2}\psi_b - \left(\frac{h_1 h_2}{4}\right){}^{jk}_{3}\psi_b \approx 0 \tag{5.48}$$

In Eq. (5.39), DOFs of node 2 are related to those of node 1 through

$$-{}_{2}^{jk}u_b - \frac{h_1 h_2}{4}\left({}_{2}^{jk}\psi_b\right) + {}_{1}^{jk}u_b + \frac{h_1}{2}\left({}_{1}^{jk}\theta_{yb}\right) + \frac{h_2}{2}\left({}_{1}^{jk}\theta_{zb}\right) + \frac{h_1 h_2}{4}\left({}_{1}^{jk}\psi_b\right) \approx 0 \tag{5.39}$$

Substituting Eq. (5.48) into Eq. (5.39) and using Eqs. (5.39) and (5.10), $\left({}_{3}^{jk}\theta_{yb} = {}_{1}^{jk}\theta_{yb},\ {}_{3}^{jk}\theta_{zb} = {}_{1}^{jk}\theta_{zb}\right)$, DOFs of node 3 will be related to those of node 1 through

$$-{}_{3}^{jk}u_b + {}_{1}^{jk}u_b + h_2\left({}_{1}^{jk}\theta_{zb}\right) + \frac{h_1 h_2}{4}\left({}_{1}^{jk}\psi_b\right) + \frac{h_1 h_2}{4}\left({}_{3}^{jk}\psi_b\right) \approx 0 \tag{5.49}$$

5.8.4 A.4. Contributions of warping at faces 1 and 4

Displacements at point 4 of face 4 are related to those of at point 1 of face 1 through point 8 located at their junctions as follows

$$\begin{aligned} \langle x_{18}\rangle^T &= \langle x_1\rangle^T - \langle x_8\rangle^T = \langle 0 \quad 0 \quad h_1/2\rangle \\ \langle x_{48}\rangle^T &= \langle x_4\rangle^T - \langle x_8\rangle^T = \langle 0 \quad -h_2/2 \quad 0\rangle \end{aligned} \tag{5.50}$$

The angle ${}_{4}^{jk}\theta_{\psi 4}$ acting at point 8 induces an additional lateral displacement at point 1, $\left\langle {}_{1}^{jk}U_{\psi 1}^{*}\right\rangle^T = \left\langle {}_{1}^{jk}u_b^{*} \quad {}_{1}^{jk}v_p^{*} \quad {}_{1}^{jk}w_p^{*}\right\rangle^T$ given by

$$\left\{{}_{1}^{jk}U_{\psi 4}^{*}\right\} = \left[R_{\psi 4}\right]\left\{x_{18}\right\} \tag{5.51}$$

The additional lateral displacement induced at the face 1 due to warping deformation at face 4 is obtained by expanding the right hand side of Eq. (5.51) about the first row as follows

$${}_{1}^{jk}u_b^{*} = \left(h_1 h_2/4\right)\,{}_{4}^{jk}\psi_b \tag{5.52}$$

where

$$\left[R_{\psi 4}\right]_{3\times 3} = \begin{bmatrix} -\frac{1}{2}\left(\frac{h_2}{2}\right)^2\left({}_{4}^{jk}\psi_b\right)^2 & -\frac{h_2}{4}\lambda\left({}_{4}^{jk}\theta_{xp}\right)\left({}_{4}^{jk}\psi_b\right) & \frac{h_2}{2}\left({}_{4}^{jk}\psi_b\right) \\ \frac{h_2}{4}\lambda\left({}_{4}^{jk}\theta_{xp}\right)\left({}_{4}^{jk}\psi_b\right) & -\frac{1}{2}\lambda^2\left({}_{4}^{jk}\theta_{xp}\right)^2 & -\lambda\left({}_{4}^{jk}\theta_{xp}\right) \\ -\frac{h_2}{2}\left({}_{4}^{jk}\psi_b\right) & \lambda\left({}_{4}^{jk}\theta_{xp}\right) & -\frac{1}{2}\left[\lambda^2\left({}_{4}^{jk}\theta_{xp}\right)^2 + \left(\frac{h_2}{2}\right)^2\left({}_{4}^{jk}\psi_b\right)^2\right] \end{bmatrix} \tag{5.53}$$

Similarly, on has

$$\left\{{}_{4}^{jk}U_{\psi 1}^{*}\right\} = \left[R_{\psi 1}\right]\left\{x_{48}\right\} \tag{5.54}$$

Similarly, the additional lateral displacement induced at the face 4 due to warping deformation at face 1 is obtained by expanding the right hand side of Eq. (5.54) about the first row as follows

$${}_{4}^{jk}u_b^* = \left(h_1 h_2/4\right) {}_{1}^{jk}\psi_b \tag{5.55}$$

Finally, the total out of plane displacement at point 4 obtained by summation of Eqs. (5.14)c, (5.52) and (5.55)

$$-{}_{4}^{jk}u_b + {}_{1}^{jk}u_b + \frac{h_1 h_2}{4}\left({}_{4}^{jk}\psi_b\right) - \frac{h_1}{2}\left({}_{1}^{jk}\theta_{yb}\right) + \frac{h_2}{2}\left({}_{1}^{jk}\theta_{zb}\right) + \frac{h_1 h_2}{4}\left({}_{1}^{jk}\psi_b\right) \approx 0 \tag{5.56}$$

5.9 Appendix B. Bimoments due to warping deformation

This appendix presents the formulation on obtaining the bimoments induced by warping deformation on Faces 2 to 4. Using the same methodology depicted in Section 5.5.3, bimoments induced on Face 2 can be determined through the following Eq. (5.57)a-d as shown in Figure 5-12.

$$
\begin{aligned}
{}_{12}^{jk}B_{bl} &= \int_{A_1} \sigma_1 \omega_1(s) dA \approx \sum_{r=1}^{nr} \left({}^{jk}R_{yr5'-5''} \right) \left(\frac{-h_1}{2} x_{r5'-5''} \right) + \sum_{r=1}^{nr} \left({}^{jk}R_{yr8'-8''} \right) \left(\frac{h_1}{2} x_{r8'-8''} \right) \\
{}_{22}^{jk}B_{bl} &= \int_{A_1} \sigma_2 \omega_2(s) dA \approx \sum_{r=1}^{nr} \left({}^{jk}R_{zr5'-5''} \right) \left(\frac{-h_2}{2} x_{r5'-5''} \right) + \sum_{r=1}^{nr} \left({}^{jk}R_{zr6'-6''} \right) \left(\frac{h_2}{2} x_{r6'-6''} \right) \\
{}_{32}^{jk}B_{bl} &= \int_{A_1} \sigma_3 \omega_3(s) dA \approx \sum_{r=1}^{nr} \left(R_{yr6'-6''} \right) \left(\frac{h_1}{2} x_{r6'-6''} \right) + \sum_{r=1}^{nr} \left({}^{jk}R_{yr7'-7''} \right) \left(\frac{-h_1}{2} x_{r7'-7''} \right) \\
{}_{42}^{jk}B_{bl} &= \int_{A_1} \sigma_4 \omega_4(s) dA \approx \sum_{r=1}^{nr} \left({}^{jk}R_{zr8'-8''} \right) \left(\frac{h_2}{2} x_{r8'-8''} \right) + \sum_{r=1}^{nr} \left({}^{jk}R_{zr7'-7''} \right) \left(\frac{-h_2}{2} x_{r7'-7''} \right)
\end{aligned}
\qquad (5.57)\text{a-d}
$$

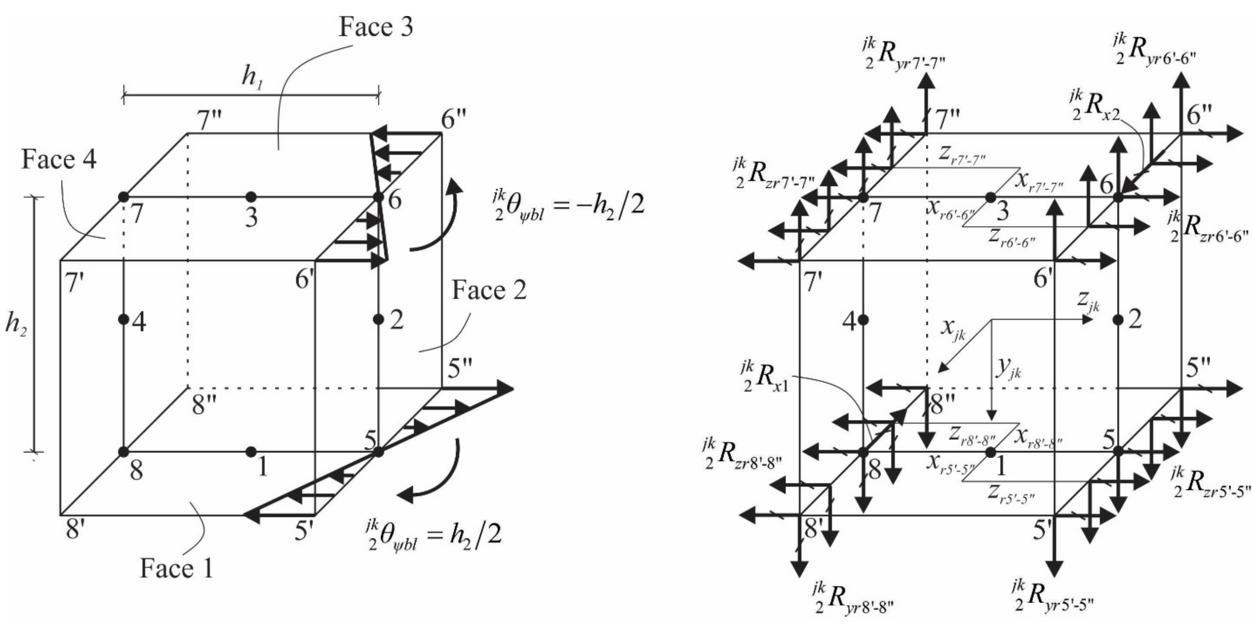

(a) **(b)**

Figure 5-12 (a) Unit warping deformation applied at Face 2; (b) boundary conditions and reactions

As shown in Figure 5-13 and Figure 5-14, are determined from

$$
\begin{aligned}
{}^{jk}_{13}B_{bl} &= \int_{A_1} \sigma_1 \omega_1(s)dA \approx \sum_{r=1}^{nr}\left({}^{jk}R_{yr5'-5''}\right)\left(\frac{-h_1}{2}x_{r5'-5''}\right) + \sum_{r=1}^{nr}\left({}^{jk}R_{yr8'-8''}\right)\left(\frac{h_1}{2}x_{r8'-8''}\right) \\
{}^{jk}_{23}B_{bl} &= \int_{A_1} \sigma_2 \omega_2(s)dA \approx \sum_{r=1}^{nr}\left({}^{jk}R_{zr5'-5''}\right)\left(\frac{-h_2}{2}x_{r5'-5''}\right) + \sum_{r=1}^{nr}\left({}^{jk}R_{zr6'-6''}\right)\left(\frac{h_2}{2}x_{r6'-6''}\right) \\
{}^{jk}_{33}B_{bl} &= \int_{A_1} \sigma_3 \omega_3(s)dA \approx \sum_{r=1}^{nr}\left(R_{yr6'-6''}\right)\left(\frac{h_1}{2}x_{r6'-6''}\right) + \sum_{r=1}^{nr}\left({}^{jk}R_{yr7'-7''}\right)\left(\frac{-h_1}{2}x_{r7'-7''}\right) \\
{}^{jk}_{43}B_{bl} &= \int_{A_1} \sigma_4 \omega_4(s)dA \approx \sum_{r=1}^{nr}\left({}^{jk}R_{zr8'-8''}\right)\left(\frac{h_2}{2}x_{r8'-8''}\right) + \sum_{r=1}^{nr}\left({}^{jk}R_{zr7'-7''}\right)\left(\frac{-h_2}{2}x_{r7'-7''}\right)
\end{aligned}
\qquad (5.58)\text{a-d}
$$

$$
\begin{aligned}
{}^{jk}_{14}B_{bl} &= \int_{A_1} \sigma_1 \omega_1(s)dA \approx \sum_{r=1}^{nr}\left({}^{jk}R_{yr5'-5''}\right)\left(\frac{-h_1}{2}x_{r5'-5''}\right) + \sum_{r=1}^{nr}\left({}^{jk}R_{yr8'-8''}\right)\left(\frac{h_1}{2}x_{r8'-8''}\right) \\
{}^{jk}_{24}B_{bl} &= \int_{A_1} \sigma_2 \omega_2(s)dA \approx \sum_{r=1}^{nr}\left({}^{jk}R_{zr5'-5''}\right)\left(\frac{-h_2}{2}x_{r5'-5''}\right) + \sum_{r=1}^{nr}\left({}^{jk}R_{zr6'-6''}\right)\left(\frac{h_2}{2}x_{r6'-6''}\right) \\
{}^{jk}_{34}B_{bl} &= \int_{A_1} \sigma_3 \omega_3(s)dA \approx \sum_{r=1}^{nr}\left(R_{yr6'-6''}\right)\left(\frac{h_1}{2}x_{r6'-6''}\right) + \sum_{r=1}^{nr}\left({}^{jk}R_{yr7'-7''}\right)\left(\frac{-h_1}{2}x_{r7'-7''}\right) \\
{}^{jk}_{44}B_{bl} &= \int_{A_1} \sigma_4 \omega_4(s)dA \approx \sum_{r=1}^{nr}\left({}^{jk}R_{zr8'-8''}\right)\left(\frac{h_2}{2}x_{r8'-8''}\right) + \sum_{r=1}^{nr}\left({}^{jk}R_{zr7'-7''}\right)\left(\frac{-h_2}{2}x_{r7'-7''}\right)
\end{aligned}
\qquad (5.59)\text{a-d}
$$

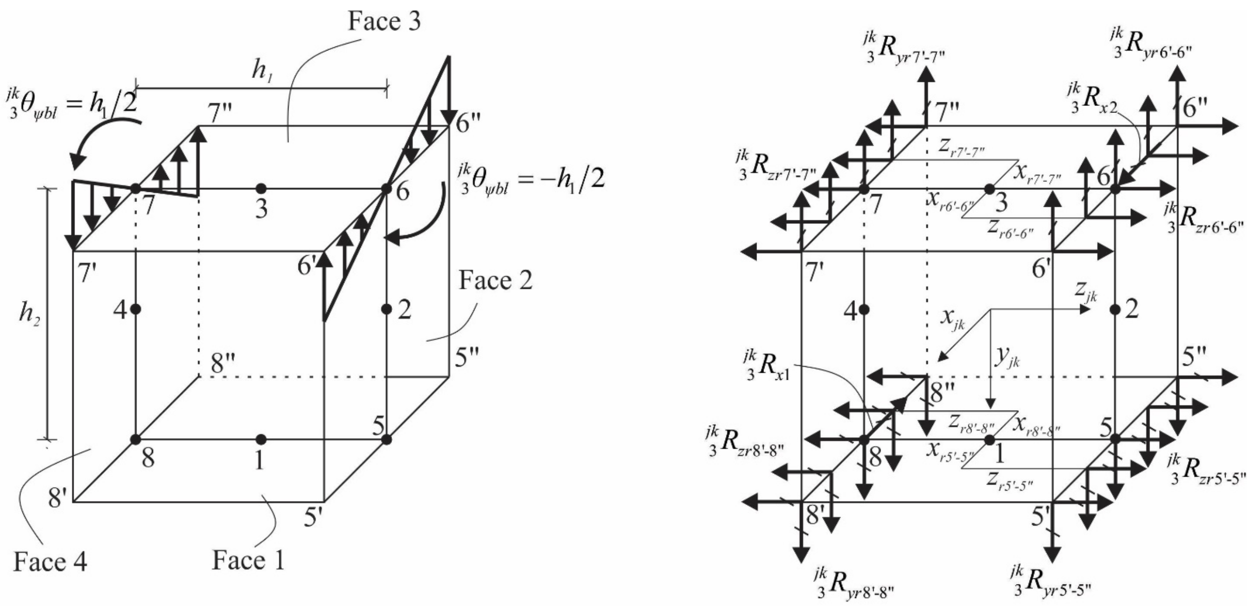

(a) **(b)**

Figure 5-13 (a) Unit warping deformation applied at Face 3; (b) boundary conditions and reactions

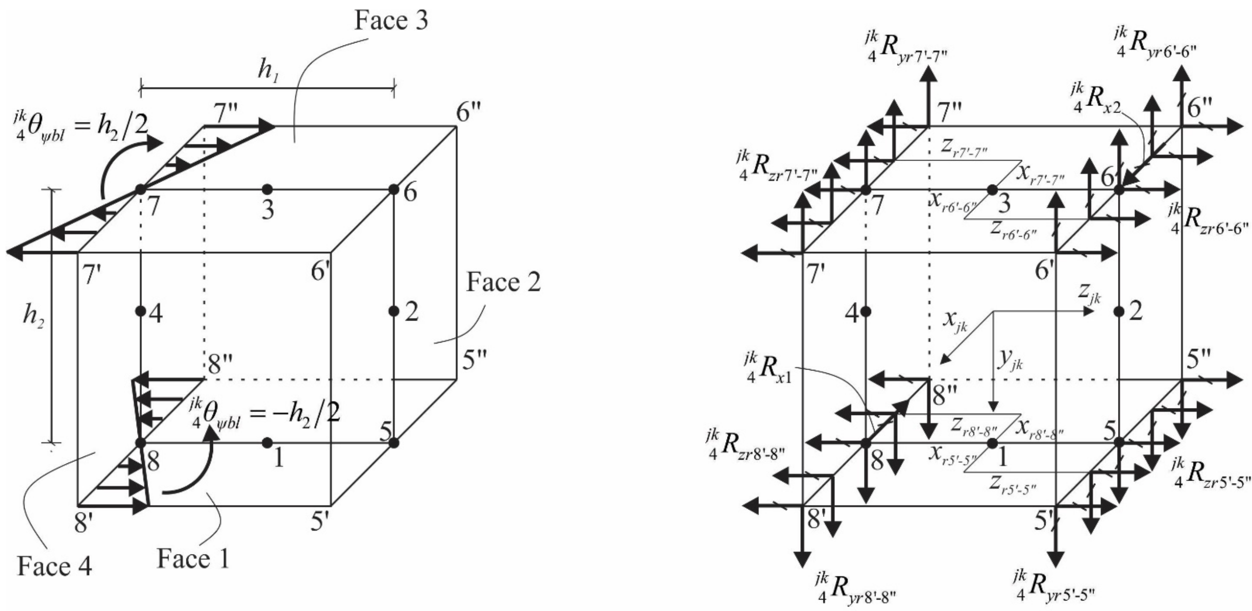

(a) **(b)**

Figure 5-14 (a) Unit warping deformation applied at Face 4; (b) boundary conditions and reactions

5.10 Appendix C. Entries of the warping spring stiffness matrices

This section provides the entries of coupled spring warping stiffness matrices obtained from shell analysis to determine the critical moment for the Examples 1-3. All units are Nmm^2/rad in all Cases. For the Examples 1 and 2, the section used is W200x59 and the coupled warping stiffness matrix takes the form

$$\left[{}^{jk}K_{\psi bl} \right]_{4\times4} = 10^8 \times \begin{bmatrix} 27.2 & -6.99 & 12.7 & -6.98 \\ -6.99 & 27.2 & 6.98 & -12.7 \\ 12.7 & 6.98 & 27.2 & 6.99 \\ -6.98 & -12.7 & 6.99 & 27.2 \end{bmatrix} \tag{5.60}$$

Also, the 3x3 and 2x2 versions at the left and right of the frame are given by

$$\left[{}^{jk}K_{\psi bl} \right]_{3\times3} = 10^9 \times \begin{bmatrix} 2.54 & -1.02 & 1.45 \\ -1.02 & 2.13 & 1.02 \\ 1.45 & 1.02 & 2.54 \end{bmatrix}, \quad \left[{}^{jk}K_{\psi bl} \right]_{2\times2} = 10^9 \times \begin{bmatrix} 1.72 & -1.61 \\ -1.61 & 1.72 \end{bmatrix} \tag{5.61)a-b (}$$

For the Example 3, the cross-section is W200x46 and the corresponding warping stiffness matrix takes the form

$$\left[{}^{jk}K_{\psi bl} \right]_{4\times4} = 10^8 \times \begin{bmatrix} 20.6 & -5.26 & 9.83 & -5.26 \\ -5.26 & 20.6 & 5.26 & -9.83 \\ 9.83 & 5.26 & 20.6 & 5.26 \\ -5.26 & -9.83 & 5.26 & 20.6 \end{bmatrix} \tag{5.62}$$

Again, the 3x3 and 2x2 versions at the left and right of the frame are given by

$$\left[{}^{jk}K_{\psi bl} \right]_{3\times3} = 10^8 \times \begin{bmatrix} 19.3 & -7.77 & 11.2 \\ -7.77 & 15.9 & 7.77 \\ 11.2 & 7.77 & 19.3 \end{bmatrix}, \quad \left[{}^{jk}K_{\psi bl} \right]_{2\times2} = 10^9 \times \begin{bmatrix} 1.28 & -1.23 \\ -1.23 & 1.28 \end{bmatrix} \tag{5.63)a-b (}$$

5.11 Appendix D. Design of braced Gamma-shaped frame

5.11.1 Statement of the problem

It is required to first investigate the buckling capacity of the Gamma-shaped frame of Example 1 when lateral braces (depicted as red crosses in Figure 5-15) are provided at the top of the column and the cantilever root and tip. It is then required to use the solution based on the present study to assess the safety of both members based on the out-of-plane stability interaction equations provided in the CAN/CSA S16-14 standards. Two cases will be considered: (1) an applied load of 150 kN at the tip with a steel yield strength of $F_y = 350\ MPa$, and (2) the applied load is increased to 280 kN with a steel yield strength increased to $F_y = 480\ MPa$.

5.11.2 Design calculations for Case 1

The axial force and bending moment diagrams under the applied load $P = 150\ kN$ $\left(F_y = 350\ MPa\right)$ are shown in Figure 5-15. In the following, the conventional design approach is first presented.

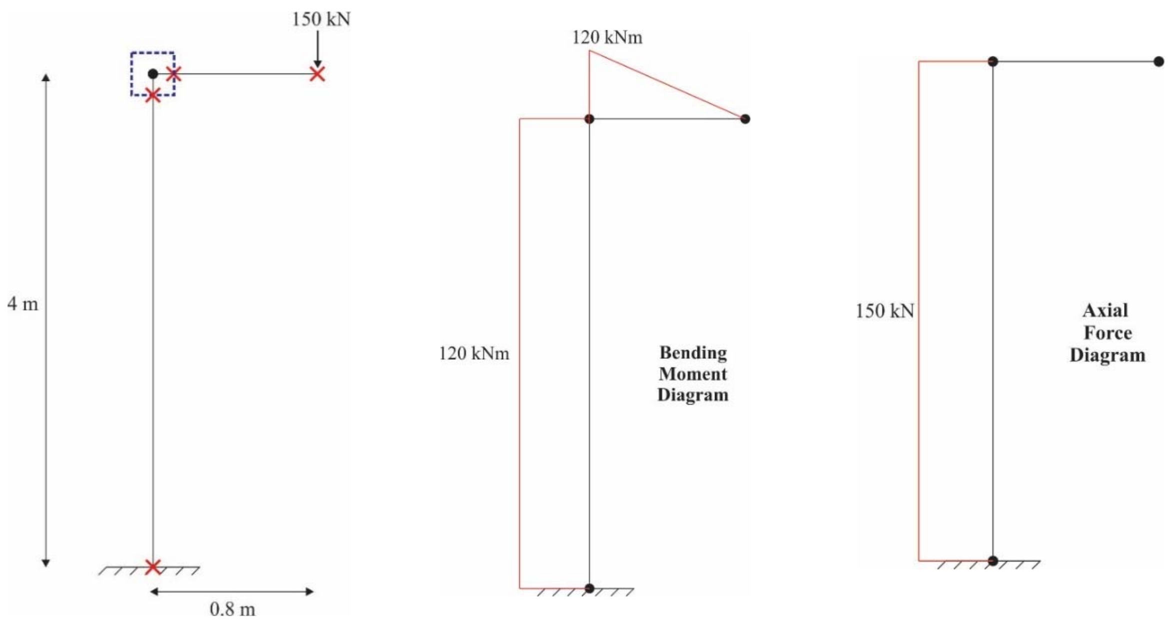

(a) **(b)** **(c)**

Figure 5-15 Internal forces for frame under P=150 kN (a) bracing configuration and loading (b) Bending moment diagram, and (c) Axial force diagram

5.11.2.1 Solution based on CAN/CSA S16-14

For the case $F_y = 350\ MPa$, the section is found to be class 1 since $b/2t = 7.75 \le 145/\sqrt{F_y}$ and $h/w = 20 \le 1100/\sqrt{F_y}\left(1.0 - 0.391 C_f / \phi C_y\right)$. Hence, the design will be based on the plastic moment resistance $M_p = Z_x F_y = 228\ kNm$. Given the moment gradient factor $\omega_2 = 1.75$ for the horizontal member, one obtains

$$M_u = \frac{\omega_2 \pi}{L}\sqrt{EI_y GJ + \left(\frac{\pi E}{L}\right)^2 I_y C_w} = 1.75 \times 6245 = 10{,}929\ kNm$$

Since $M_u \ge 0.67 M_p$, the beam capacity is calculated based on

$$M_{rx} = 1.15 \phi M_p \left[1 - 0.28 \frac{M_p}{M_u}\right] = 234\ kNm > \phi M_p = 205\ kNm$$

i.e., $M_{rx} = 205\ kNm$ and the flexural resistance of the short cantilever is dictated by material failure. There is no axial force contribution for the horizontal member and the interaction equation takes the form

$$\frac{M_{fx}}{M_{rx}} = \frac{120}{205} = 0.59 \le 1.00$$

The result suggests that the section is 59% utilized. For the vertical member, given the moment gradient factor $\omega_2 = 1.00$, one obtains

$$M_u = \frac{\omega_2 \pi}{L}\sqrt{EI_y GJ + \left(\frac{\pi E}{L}\right)^2 I_y C_w} = 1.00 \times 378 = 378\ kNm$$

Since $M_u \ge 0.67 M_p$, the flexural capacity of the vertical member is calculated based on

$$M_{rx} = 1.15 \phi M_p \left[1 - 0.28 \frac{M_p}{M_u}\right] = 196\ kNm \le \phi M_p = 205\ kNm$$

Thus, the Canadian standards predict a flexural resisting moment of $M_{rx} = 196\ kNm$. Also, the compressive resistance of the member can be obtained by computing the slenderness parameter

$$\lambda_y = \frac{1.0L}{r_y}\sqrt{\frac{F_y}{\pi^2 E}} = 1.0 \times 76.8 \sqrt{\frac{350}{\pi^2 \times 2 \times 10^5}} = 1.023$$

and then applying the column resistance equation

$$C_r = \phi A F_y \left[1+\lambda^{2n}\right]^{-\frac{1}{n}} = 1382\ kN$$

To assess the safety of the member, one needs to check the following two interaction equations:

$$\frac{C_f}{C_r} + 0.85\frac{U_{1x} M_{fx}}{M_{rx}} = \frac{150}{1382} + 0.85\frac{1\times 120}{196} = 0.63 \le 1.00$$

$$\frac{M_{fx}}{M_{rx}} = \frac{120}{196} = 0.61 \le 1.00$$

i.e., the out-of-plane stability check of the Canadian standards provisions indicates that the section is 63% utilized.

5.11.2.2 Solution based on the present study

An eigenvalue buckling analysis is conducted for the frame based on the present model. As expected, providing lateral braces is found to increase the buckling capacity of the frame from $P_{cr} = 173\ kN$ (based on the unbraced scenario) to $P_{cr} = 971\ kN$. The corresponding critical moments at the intersection of the centerlines of both members are found to be $M_u\left(FEA\right) = 777\ kNm$.

It is of interest to note that the elastic critical moment for the system (vertical + horizontal members), $M_u\left(FEA\right) = 777\ kNm$, as predicted by the present model lies in between that calculated for the horizontal member alone $\left(M_u = 10{,}929\ kNm\right)$ and for the vertical member alone $\left(M_u = 378\ kNm\right)$ as calculated by lateral torsional buckling provisions in CAN/CSA S16-14.

Since the critical load is based on an elastic analysis and as such does not account for inelastic effects nor residual stresses, these effects will then be accounted for by using the inelastic design provisions in the standards. For the horizontal member, since $M_u\left(FEA\right) \ge 0.67 M_p$, the member capacity is calculated by

$$M_{rx}\left(FEA\right) = 1.15\phi M_p \left[1 - 0.28\frac{M_p}{M_u\left(FEA\right)}\right] = 216\ kNm > \phi M_p = 205\ kNm$$

Since $M_{rx}\left(FEA\right) > \phi M_p$, the flexural resistance is governed by yielding and $M_{rx}\left(FEA\right) = 205\ kNm$. Unlike the CAN/CSA S16-14 solution, which predicts a flexural resistance of $205\ kNm$ for the horizontal member (governed by yielding) and $196\ kNm$ for the vertical member (as dictated by inelastic lateral torsional buckling), the present solution predicts a flexural resistance of $205\ kNm$ as predicted by yielding in both cases.

There is no axial force for the horizontal member and thus the interaction equation takes the form

$$\frac{M_{fx}}{M_{rx}\left(FEA\right)} = \frac{120}{205} = 0.59 \leq 1.00$$

According to the FEA analysis, the section is 59% utilized. The result is identical to that based on the conventional CAN/CSA S16-14 procedure since under both methods the design is found to be governed by yielding as opposed to lateral torsional buckling.

Unlike the conventional treatment in the standards, the flexural resistance for the vertical and horizontal members are equal. The corresponding elastic factored compressive buckling resistance of the member as determined from the eigenvalue analysis is $C_f\left(FEA\right) = P_{cr} = 971\ kN$. Again, such a buckling load does not capture inelastic effects, residual stresses, nor initial out-of-straightness. Such effects will then be incorporated using the provisions in the standards for inelastic column design. Firstly, the buckling stress F_{eyz} is obtained by dividing the computed buckling load by the cross-section area A, i.e., $F_{eyz} = C_f\left(FEA\right)/A = 129\ MPa$. Secondly, the corresponding compressive resistance of the member is determined from the slenderness parameter $\lambda_{yz} = \sqrt{F_y/F_{eyz}} = 1.60$ and then applying the column buckling relation, yielding

$$C_r\left(FEA\right) = \phi A F_y \left[1 + \lambda^{2n}\right]^{-\frac{1}{n}} = 733\ kN$$

It is of interest to note the drastic drop in the computed value $C_r\left(FEA\right) = 733\ kN$ from that based on the conventional calculation of the axial resistance of the column $C_r = 1382\ kN$. To assess the safety of the member, the out-of-plane stability interaction checks are applied:

$$\frac{C_f}{C_r} + 0.85\frac{U_{1x}M_{fx}}{M_{rx}} = \frac{150}{733} + 0.85\frac{1\times120}{205} = 0.70 \leq 1.00$$

$$\frac{M_{fx}}{M_{rx}} = \frac{120}{205} = 0.59 \leq 1.00$$

The analysis signifies that, under the present lateral buckling solution, the section is 70% utilized according to the interaction equations provided by CAN/CSA S16-14. This value compares with a 63% utilization factor as predicted by the conventional design methodology in CAN/CSA S16-

14, suggesting that the standards procedure is slightly un-conservative. The outcome is not necessarily alarming since the bi-linear interaction equations in the Canadian standards

$$\frac{C_f}{C_r} + 0.85\frac{U_{1x}M_{fx}}{M_{rx}} < 1.0, \qquad \frac{M_{fx}}{M_{rx}} < 1.0$$

are, generally, conservative approximations of the convex moment-axial force interaction relations (as was shown in Figure 4.9). A comparison of the results are summarized in Table 5.5.

Table 5.5 Summary of interaction relation results for Case 1 - $F_y = 350\ MPa$

Member	**Conventional Solution**		**Present Solution**	
	$\frac{C_f}{C_r} + 0.85\frac{U_{1x}M_{fx}}{M_{rx}}$	$\frac{M_{fx}}{M_{rx}}$	$\frac{C_f}{C_r} + 0.85\frac{U_{1x}M_{fx}}{M_{rx}}$	$\frac{M_{fx}}{M_{rx}}$
Horizontal	---	0.59	---	0.59
Vertical	0.63	0.61	0.70	0.59

5.11.3 Design calculations for Case 2

The axial force and bending moment diagrams under the applied load $P = 280\ kN$ $\left(F_y = 480\ MPa\right)$ are depicted in Figure 5-16.

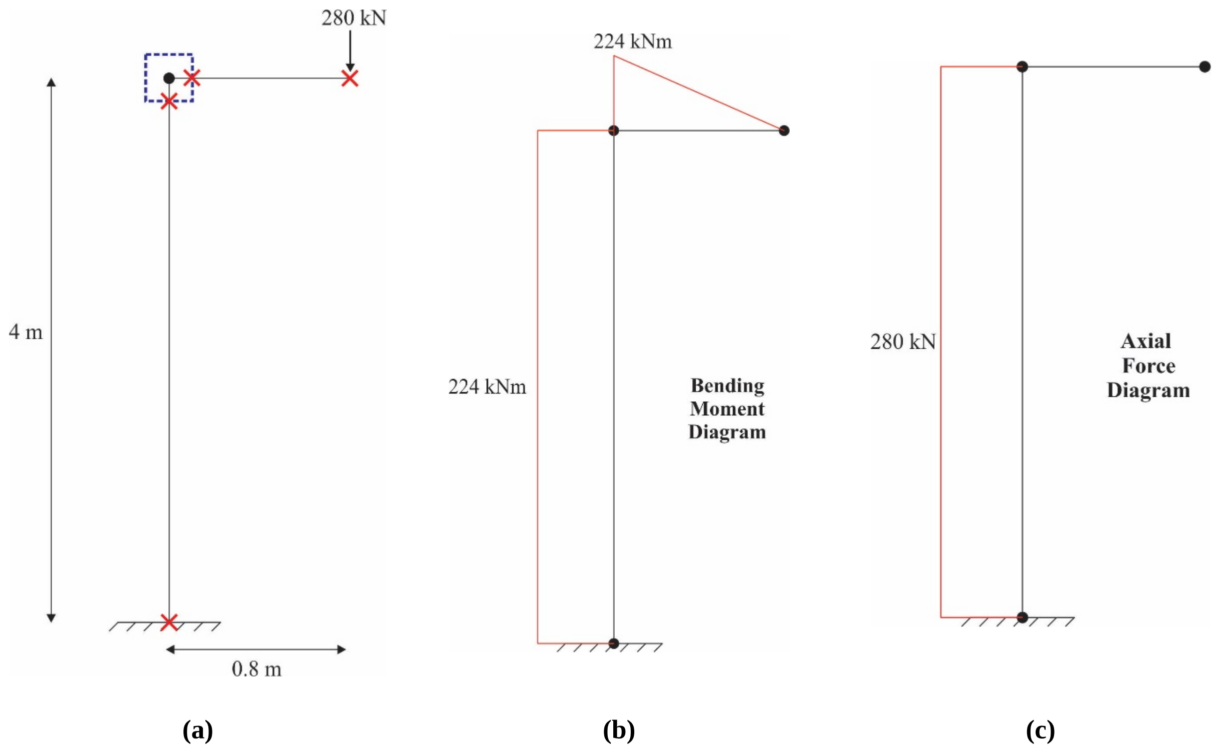

Figure 5-16 Internal forces for frame under P=280 kN (a) bracing configuration and loading (b) Bending moment diagram, and (c) Axial force diagram

5.11.3.1 Solution based on CAN/CSA S16-14

For the case $F_y = 480\ MPa$, the section is also found to be Class 1 and the plastic moment resistance is $M_p = Z_x F_y = 312\ kNm$. The elastic buckling moment remains $M_u = 10{,}929\ kNm$. Since $M_u \geq 0.67 M_p$, the beam capacity is calculated by

$$M_{rx} = 1.15\phi M_p \left[1 - 0.28\frac{M_p}{M_u}\right] = 320\ kNm > \phi M_p = 281\ kNm$$

or $M_{rx} = 281\ kNm$ and the design is governed by yielding. There is no axial force contribution for the horizontal member and the interaction equation takes the form

$$\frac{M_{fx}}{M_{rx}} = \frac{224}{281} = 0.80 \le 1.00$$

i.e., the section is 80% utilized. For the vertical member, the elastic lateral torsional buckling moment remains $M_u = 378\ kNm$. Since $M_u \ge 0.67 M_p$, the beam capacity is calculated from

$$M_{rx} = 1.15\phi M_p \left[1 - 0.28\frac{M_p}{M_u}\right] = 248\ kNm \le \phi M_p = 281\ kNm$$

Thus, the Canadian standards predict a flexural resistance of $M_{rx} = 248\ kNm$ and the design is governed by inelastic lateral torsional buckling. Also, the compressive resistance of the member is found to be $C_r = 1585\ kN$. The out-of-plane stability interaction checks take the form

$$\frac{C_f}{C_r} + 0.85\frac{U_{1x} M_{fx}}{M_{rx}} = \frac{280}{1585} + 0.85\frac{1 \times 224}{248} = 0.94 \le 1.00$$

$$\frac{M_{fx}}{M_{rx}} = \frac{224}{248} = 0.90 \le 1.00$$

i.e., the Canadian standards predict a 94% utilization factor.

5.11.3.2 Solution based on the present study

Under the elastic buckling formulation developed in the present study, no changes are observed in the predicted values of the critical moments from those found for Case 1, i.e., $M_u = 777\ kNm$. Since $M_u \ge 0.67 M_p$, the beam capacity is obtained by

$$M_{rx}(FEA) = 1.15\phi M_p \left[1 - 0.28\left(M_p / M_u(FEA)\right)\right] = 287\ kNm > \phi M_p = 281\ kNm$$

Since $M_{rx} > \phi M_p$, the flexural resistance for both members is governed once again by yielding and $M_{rx}(FEA) = 281\ kNm$. Again, there is no axial force contribution for the horizontal member and the interaction equation takes the form

$$\frac{M_{fx}}{M_{rx}(FEA)} = \frac{224}{281} = 0.80 \le 1.00$$

i.e., the section is 80% utilized. For the vertical member, one has the same buckling stress $F_{eyz} = 129\ MPa$ as in Case 1. However, due to the different yield strength F_y, one obtains a higher compressive resistance of $C_r\left(FEA\right)=776\ kN$. To assess the safety of the member, one needs to check the following two interaction equations:

$$\frac{C_f}{C_r}+0.85\frac{U_{1x}M_{fx}}{M_{rx}}=\frac{280}{776}+0.85\frac{1\times 224}{281}=1.04>1.00$$

$$\frac{M_{fx}}{M_{rx}}=\frac{224}{281}=0.80\leq 1.00$$

i.e., the section is 104% utilized. The use of the procedure in the standards in the present example leads to a safe design prediction while employing the present solution leads to a slightly unsafe design prediction. The results have been summarized in Table 5.6.

Table 5.6 Summary of interaction relation results for Case 2 - $F_y=480\ MPa$

Member	**Conventional Solution**		**Present Program**	
	$\frac{C_f}{C_r}+0.85\frac{U_{1x}M_{fx}}{M_{rx}}$	$\frac{M_{fx}}{M_{rx}}$	$\frac{C_f}{C_r}+0.85\frac{U_{1x}M_{fx}}{M_{rx}}$	$\frac{M_{fx}}{M_{rx}}$
Horizontal	---	0.80	---	0.80
Vertical	0.94	0.90	1.04	0.80

5.12 Appendix E. Buckling capacity of member EG in Example 3

The global lateral torsional buckling analysis in Example 3 predicts a load multiplier of $\lambda = 186.1$ for the braced frame (Scenario a) and $\lambda = 74.11$ for the unbraced frame (Scenario b). Since the peak reference moments $M_{cr} = 1.69\lambda\ kNm$ were found to occur at mid-span, the corresponding peak critical moments based on a global lateral torsional buckling capacity were found to be $M_{cr} = 315.3\ kNm$ and $M_{cr} = 125.2\ kNm$, respectively. For the braced frame (Scenario a) the global lateral torsional buckling capacity was found not to govern the capacity of the frame since the member lateral torsional buckling capacity turned out to be lower than the global buckling capacity. The reverse was observed for the unbraced frame (Scenario b).

This appendix further investigates whether the low global buckling capacity of the unbraced frame can be attributed to column buckling of member ACEG as opposed to lateral torsional buckling. Segment EG is partially fixed in the lateral direction at E and laterally free at G. The effective length factor for such a condition is expected to exceed 2.0 and the capacity of the column is determined based a separate eigenvalue column buckling analysis under S-Frame (2016) for the whole column ACEG. The analysis accounts for the lateral fixity conditions at A, C, E, and G. The elastic buckling capacity of column EG is found to be $C_r = 155.7\ kN$ which corresponds to an effective length factor for Segment EG of 3.49. This value is inferior to the axial load $C_f = 2.5\lambda = 2.5 \times 74.11 = 185.3\ kN$ at the onset of buckling based on a global lateral torsional buckling analysis. The corresponding axial force ratio is $C_f / C_r = 185.3/155.7 = 1.19 > 1.0$. In column segment EG, the peak moment at the onset of buckling is given by $M_f = 1.44\lambda = 1.44 \times 74.11 = 106.7\ kNm$ based on the present formulation. The bending resistance of the member as determined from the Canadian code provisions is obtained by computing the moment gradient factor $C_{CAN} = 4M_{\max} \Big/ \sqrt{M_{\max}^2 + 4M_A^2 + 7M_B^2 + 4M_C^2} = 2.010$. The corresponding critical moment is $M_r = C_{CAN}\left(\pi/L_u\right)\sqrt{EI_y GJ + \left(\pi E/L_u\right)^2 I_y C_w} = 2.010 \times 250.5 = 526\ kNm$ and the moment ratio is $M_f / M_r = 106.7/526 = 0.203$. The sum of the interaction ratios is $C_f / C_r + M_f / M_r = 1.19 + 0.203 = 1.393 > 1.0$, suggesting that at the onset of buckling, the column has tendency to buckle. In contrast, beam GH has

$C_f / C_r + M_f / M_r \approx 34.98/1211 + 125/224.8 = 0.585 < 1.0$ tendency to restrain the column from buckling. The Salvadori solution based on the separation of members neglects the interaction between both members and would lead to the conclusion that the column is unsafe while the beam is safe. In contrast the present solution accounts for interaction, and enables the whole frame to attain a buckling strength intermediate between the buckling strength of the column alone and the buckling strength of the beam alone.

5.13 List of Symbols

$[B]$	A user-input coefficient matrix
${}^{jk}_{mn}B_{bl}$	Bimoment at face m induced by warping at face n in local coordinates of joint k
C	Moment gradient factor
C_w	Warping Constant
h_1	Width of Face 1
h_2	Height of Face 2
$\left[{}^{ei}K\right]$	Elastic stiffness matrix of member element i
$\left[{}^{ei}K_G\right]$	Geometric stiffness matrix of member element i
$\left[{}^{jk}K_{\psi bl}\right]$	Buckling warping matrix relates the bimoments to warping deformations
$\left[R_{\psi n}\right]$	Rotation matrix induced by warping on face n, that is, $\left({}^{jk}_{n}\psi_{bl}\right)$
$\left[T\left(\varphi_{ei}\right)\right]$	Transformation matrix of member element i from global coordinates to local coordinates
$\left\{{}^{ei}U_{ng}\right\}$	Vector of buckling nodal displacements of member element i in global coordinates
$\left\{{}^{ei}U_{nl}\right\}$	Vector of buckling nodal displacements of member element i in local coordinates
E	Modulus of elasticity
$\left\{{}^{jk}_{m}U^{*}_{\psi n}\right\}$	Additional displacement vector at point m because of warping at face n of joint k
G	Shear modulus
I_y	Moment of inertia of the cross-section about y-axis
J	St. Venant torsional constant

${}^{jk}_{2}u_{bl}$, ${}^{jk}_{2}\theta_{ybl}$, ${}^{jk}_{2}\theta_{zbl}$	Buckling displacement and rotations of the second node in the local coordinates of joint element k
${}^{Ni}u_{bg}$, ${}^{Ni}\theta_{ybg}$, ${}^{Ni}\theta_{zbg}$, ${}^{Ni}\psi_{bg}$	Buckling displacement and rotations of virtual node i in global coordinates, and the node connects a member element and a joint: $i = 1, 2, 3, 4$
${}^{jk}_{2}v_{pl}$, ${}^{jk}_{2}w_{pl}$, ${}^{jk}_{2}\theta_{xpl}$	Pre-buckling displacement and rotations of the second node in the local coordinates of joint element k
x_{ei}, y_{ei}, z_{ei}	Local coordinates for member element i
x_g, y_g, z_g	Global coordinates for the frame
x_{jk}, y_{jk}, z_{jk}	Local coordinates for joint element k
δ	First variation of the argument functional
δ^2	Second variation of the argument functional
${}^{jk}_{i}\theta_{\psi bl}$	Rotation angle of the edges at Face i as a result of warping
λ	Load factor (eigenvalue)
π	Total potential energy of a frame
π_c	Additional energy term enforcing rigid body constraints between the degrees of freedom of Nodes 1, 2, 3 and 4 of joint elements through Lagrange's multipliers
π_j	Total potential energy of all the joint elements because of buckling warping deformation
π_m	Total potential energy for all collinear member elements
φ_{ei}	Orientation of member element i, which is positively defined when global axis z_g rotates counter clockwise to local axis z_{ei}
${}^{jk}_{i}\psi_{bl}$	Warping of the joint element k at Face i
$\psi(z)$	Rate of change of the longitudinal displacement as a result of warping along the z-axis (1/length dimension); and
$\omega(s)$	Warping function (sectorial area) of a point s

M_1, M_2	Internal bending moment at both end of an element
$[P]$	Permutation matrix
σ_{zz}	Normal stress along z direction
τ_{zs}	Shear stress on the cross-section mid-surface

5.14 REFERENCES

Canadian Standards Association, (CSA), (2014). Limit States Design of Steel Structures, CAN/CSA S16-14. Toronto, Ontario, Canada.

American Institute of Steel Construction, (AISC), (2016). Specification for Structural Steel Buildings, ANSI/AISC 360-16, AISC. Chicago, IL.

S-FRAME Software Inc. (2016). Vancouver, Canada.

Andrade, A., D. Camotim and P. Providência e Costa (2007). "On the evaluation of elastic critical moments in doubly and singly symmetric I-section cantilevers." Journal of Constructional Steel Research 63(7): 894-908.

Attard, M. M. and M.-Y. Kim (2010). "Lateral buckling of beams with shear deformations – A hyperelastic formulation." International Journal of Solids and Structures 47(20): 2825-2840.

Barsoum, R. S. and R. H. Gallagher (1970). "Finite element analysis of torsional and torsional–flexural stability problems." International Journal for Numerical Methods in Engineering 2(3): 335-352.

Basaglia, C., D. Camotim and N. Silvestre (2012). "Torsion warping transmission at thin-walled frame joints: Kinematics, modelling and structural response." Journal of Constructional Steel Research 69(1): 39-53.

Bazant, Z. P. and L. Cedolin (1991). Stability of structures. Oxford, U.K., Oxford University Press.

Bradford, M. and H. Ronagh (1997). "Generalized Elastic Buckling of Restrained I-Beams by FEM." Journal of Structural Engineering 123(12): 1631-1637.

Bradford, M. A. (1985). "Distortional buckling of monosymmetric I-beams." Journal of Constructional Steel Research 5(2): 123-136.

Bradford, M. A. (1986). "Inelastic distortional buckling of I-beams." Computers & Structures 24(6): 923-933.

Bradford, M. A. (1992a). "Buckling of doubly-symmetric cantilevers with slender webs." Engineering Structures 14(5): 327-334.

Bradford, M. A. (1992b). "Lateral-Distortional buckling of steel I—Section members." Journal of Constructional Steel Research 23(1–3): 97-116.

Bradford, M. A. and N. S. Trahair (1981). "Distortional buckling of I-beams." Journal of the Structural Division 107(2): 355–370.

Bradford, M. A. and N. S. Trahair (1982). "Distortional buckling of thin-web beam-columns." Engineering Structures 4(1): 2-10.

Erkmen, R. E. (2014). "Shear deformable hybrid finite-element formulation for buckling analysis of thin-walled members." Finite Elements in Analysis and Design 82(0): 32-45.

Erkmen, R. E. and M. M. Attard (2011). "Lateral–torsional buckling analysis of thin-walled beams including shear and pre-buckling deformation effects." International Journal of Mechanical Sciences 53(10): 918-925.

Erkmen, R. E. and M. Mohareb (2008a). "Buckling analysis of thin-walled open members—A complementary energy variational principle." Thin-Walled Structures 46(6): 602-617.

Erkmen, R. E. and M. Mohareb (2008b). "Buckling analysis of thin-walled open members—A finite element formulation." Thin-Walled Structures 46(6): 618-636.

Ettouney, M. M. and J. B. Kirby (1981). "Warping restraint in threedimensional frames." journal of the Structural Division 107(8): 1643–1656.

Hancock, G. J., M. A. Bradford and N. S. Trahair (1980). "Web distortion and flexural-torsional buckling." Journal of the Structural Division 106(7): 1557–1571.

Hartmann, A. J. and W. H. Munse (1966). "Flexural torsional buckling of planar frames." Journal of Engineering Mechanics Division 92(2): 37-60.

Johnson, C. P. and K. M. Will (1974). "Beam buckling by finite element procedure." Journal of the Structural Division 100(3): 669–685.

Kitipornchai, S., C. Wang and N. Trahair (1986). "Buckling of Monosymmetric I-Beams under Moment Gradient." Journal of Structural Engineering 112(4): 781-799.

Krajcinovic, D. (1969). "A consistent discrete elements technique for thinwalled assemblages." International Journal of Solids and Structures 5(7): 639-662.

Krenk, S. and L. Damkilde (1991). "Warping of Joints in I-Beam Assemblages." Journal of Engineering Mechanics 117(11): 2457-2474.

Masarira, A. (2002). "The effect of joints on the stability behaviour of steel frame beams." Journal of Constructional Steel Research 58(10): 1375-1390.

Mohareb, M. and A. Dabbas (2003). Lateral stability of partially restrained cantilever supports. Proc. of the Annual Technical Session and Meeting, Structural Stability Research Council, Rolla, MO.

Mohri, F., A. Brouki and J. C. Roth (2003). "Theoretical and numerical stability analyses of unrestrained, mono-symmetric thin-walled beams." Journal of Constructional Steel Research 59(1): 63-90.

Mohri, F., N. Damil and M. Potier-Ferry (2010). "Linear and non-linear stability analyses of thin-walled beams with monosymmetric I sections." Thin-Walled Structures 48(4–5): 299-315.

Mohri, F., N. Damil and M. Potier-Ferry (2013). "Buckling and lateral buckling interaction in thin-walled beam-column elements with mono-symmetric cross sections." Applied Mathematical Modelling 37(5): 3526-3540.

Morrel, P. J. B. (1979). The influence of joint detail on the torsional behaviour of thin-walled structures having an axial discontinuity. Proceeding International Conference Thin-Walled Structures. University of Strathclyde, Glasgow, Scotland: 539–556.

Pi, Y. and N. Trahair (2000). "Distortion and Warping at Beam Supports." Journal of Structural Engineering 126(11): 1279-1287.

Powell, G. and R. Klingner (1970). "Elastic Lateral Buckling of Steel Beams." Journal of the Structural Division 96(9): 1919-1932.

Rizzi, N. L. and V. Varano (2011). "The effects of warping on the postbuckling behaviour of thin-walled structures." Thin-Walled Structures 49(9): 1091-1097.

Sahraei, A. and M. Mohareb (2016). "Upper and lower bound solutions for lateral-torsional buckling of doubly symmetric members." Thin-Walled Structures 102: 180-196.

Sahraei, A., L. Wu and M. Mohareb (2015). "Finite element formulation for lateral torsional buckling analysis of shear deformable mono-symmetric thin-walled members." Thin-Walled Structures 89(0): 212-226.

Salvadori, M. G. (1953). "Stability of I-Beams under thrust and unequal end moments." Proceeding ASCE 79(291): 1–25.

Sharman, P. W. (1985). "Analysis of structures with thin-walled open sections." International Journal of Mechanical Sciences 27(10): 665-677.

Shayan, S. and K. J. R. Rasmussen (2014). "A model for warping transmission through joints of steel frames." Thin-Walled Structures 82: 1-12.

Tong, G. S., X. X. Yan and L. Zhang (2005). "Warping and bimoment transmission through diagonally stiffened beam-to-column joints." Journal of Constructional Steel Research 61(6): 749-763.

Trahair, N. S. (1993). Flexural-Torsional Buckling of Structures, CRC Press. USA.

Vacharajittiphan, P. and N. S. Trahair (1974). "Warping and distortion at I-section Joints." Journal of the Structural Division 100(3): 547-564.

Wang, C. and S. Kitipornchai (1986). "Buckling Capacities of Monosymmetric I-Beams." Journal of Structural Engineering 112(11): 2373-2391.

Wu, L. and M. Mohareb (2011a). "Buckling of shear deformable thin-walled members—I. Variational principle and analytical solutions." Thin-Walled Structures 49(1): 197-207.

Wu, L. and M. Mohareb (2011b). "Buckling formulation for shear deformable thin-walled members—II. Finite element formulation." Thin-Walled Structures 49(1): 208-222.

Wu, L. and M. Mohareb (2012). "Finite-Element Formulation for the Lateral Torsional Buckling of Plane Frames." Journal of Engineering Mechanics 139(4): 512-524.

Yang, Y.-B. and W. McGuire (1984). "A procedure for analysing space frames with partial warping restraint." International Journal for Numerical Methods in Engineering 20(8): 1377-1398.

Zhang, L. and G. S. Tong (2008). "Elastic flexural-torsional buckling of thin-walled cantilevers." Thin-Walled Structures 46(1): 27-37.

Zinoviev, I. and M. Mohareb (2004). "Analysis and design of laterally unsupported portal frames for out-of-plane stability." Canadian Journal of Civil Engineering 31(3): 440–452

Chapter 6 Summary, Conclusions and Recommendations

6.1 Summary

The present study contributed to the advancement of methods of lateral torsional buckling analysis of thin-walled beams in several respects as summarized in the following:

1. Developing a family of three beam finite elements for the lateral torsional buckling analysis of members with doubly symmetric cross-sections (Chapter 3) and a technique to incorporate general linear multi-node constraints. The formulation offers several desirable features compared to other solutions. These are:

a) The elements capture beam buckling effects including bending and shear and columns effects including axial forces, as well as beam-column interactions.

b) The elements capture warping, shear deformation, and load position effects.

c) The solution adopts a special interpolation scheme and thus avoid shear locking. These are shown to be an excellent agreement with those based on shear deformable WM element. Very good agreement is also observed with the B31OS ABAQUS element and the non-shear deformable Barsoum and Gallagher element for long span members.

d) A comprehensive number of numeric examples have shown that elements SM-N and SM-X are successful in bounding the buckling loads from above and below. In all cases, mesh refinements are shown to narrow the bounds for the predicted buckling load.

e) The SM-M element provides a fast converging solution with a remarkably small number of degrees of freedom compared to the SM-N, the SM-X and the WM shear deformable elements and is thus recommended when the analyst is seeking computational efficiency.

f) Within the limitations of the formulation, discretization errors in the SM-X element consistently provides lower bound estimates for the buckling loads. Element SM-X is recommended for design situations where the designer would rather err on the conservative side. This guaranteed lower bound property is a feature unique to the element as the author is unaware of other beam elements guaranteed to provide a lower bound buckling solution.

g) The multi-point constraint feature provides a means to model lateral bracing effects that are offset from the shear center.

2. Formulating a closed-form expression for the buckling moments of shear deformable mono-symmetric simply supported beams under uniform bending moments (Chapter 4). The expression is shown to converge to the conventional non-shear deformable solution when the beam span is long.

3. Developing a shear deformable beam element for the lateral torsional buckling analysis of beams mono-symmetric open cross-sections including wide flange sections with unequal flanges and crane-like beams (Chapter 4). The formulation has desirable features similar to those to those of the doubly symmetric element, namely:

a) It captures beam buckling effects including bending and shear and columns effects including axial forces, as well as beam-column interactions.
b) The elements capture warping, shear deformation, and load position effects.
c) The formulation is based on a special interpolation scheme that avoids shear locking phenomena that takes place in the WM element. As a result, the number of degrees of freedom needed for convergence was observed to reduce significantly compared to the WM element.
d) Results obtained based on the element were found to be in close agreement with those based on the WM element.
e) For long spans, excellent agreement was obtained with ABAQUS FEA shell results. For shorter spans, the present element was shown to provide higher buckling predictions compared to ABAQUS shell results, but lower predictions than those based on the classical BG element.

4. Devising a technique to extend existing lateral torsional buckling solutions for beams to non-co-linear plane frames (Chapter 5). Such extensions included the following features:

a) Developing a generalized four-node joint finite element that accurately quantifies the partial warping restraint provided by common moment connections to adjoining members framing at right angles. The joint element interfaces seamlessly with the classical and shear deformable 14 DOF beam finite elements. A systematic static condensation scheme was devised to adapt the joint element for cases where a joint interfaces with only two or three elements.

b) Careful consideration was taken to incorporate the finite rotation effect of the joint element into the formulation, an effect that has been omitted in most lateral torsional buckling solutions, but turns out to be important in the lateral torsional buckling analysis of frames.
c) The formulation adopts the multi-point constraints to characterize the pre-buckling in-plane behavior and out of plane buckling behavior of the joints.

The methodology is found to involve considerably fewer degrees of freedom while leading to accurate critical load predictions in a fraction of the computational and modelling time when compared to shell-based solutions.

5. The various formulations developed in the present thesis were coded under the MATLAB platform. This includes the following analyses:

1. Pre-buckling analysis of shear deformable thin-walled members
2. Lateral torsional buckling analysis of shear deformable doubly symmetric cross-sections based on the formulation developed in Chapter 3,
3. Lateral torsional buckling analysis mono-symmetric shear deformable cross-sections to implement lateral torsional buckling analysis based on the formulation developed in Chapter 4, and
4. Lateral torsional buckling analysis of planar frames involving the joint element which captures partial joint warping restraints and the finite rotation effect, both based on the formulation in Chapter 5.
5. Multiple point constraint features in the pre-buckling and buckling stages are included in steps (1) through (4).

6.2 Observations and conclusions

1. For a simply supported beam with doubly symmetric sections (Chapter 3) under full reverse moments, a torsional restraint at mid-span was found to be most effective in increasing the LTB capacity compared to a lateral restraint at the shear center or at one of the flanges. Providing combined torsional and lateral restraints was observed to increase the buckling capacity by more than twofold compared to the case of no lateral and torsional restraints.
2. For the same problem, a brace at one of the flanges was shown to increase the LTB capacity of the beam by 15% compared to the case of web mid-height bracing.

3. At the intermediate support of a two-span continuous beams, the presence of torsional restraints was observed to significantly improve the lateral torsional buckling capacity of continuous beams compared to the case of lateral restraints and to that of no lateral nor torsional restraints.
4. The solutions developed for doubly symmetric sections (in Chapter 3) and mono-symmetric sections (in chapter 4) show that the omission of shear deformation effects in classical solutions and design standards tends to over-predict the lateral torsional buckling resistance of beams with short spans. For common steel grades (with a yield strength of 350 MPa), the buckling resistance over-prediction for such short members is inconsequential in most cases, given that, short member strength tends to be dictated predominantly by yield criteria rather than elastic lateral torsional buckling. For higher strength steel members, the capacity of relatively short members will tend to be more influenced by lateral torsional buckling strength. In such cases, the analyst may need to resort to the present shear deformable solution for a more accurate critical moment prediction.
5. Moment gradient factors were developed for beams with mono-symmetric sections subjected to linear moments (Chapter 4). The moment gradients were shown to depend upon (a) the end moment ratio and (b), unlike doubly symmetric sections, on the beam span. When the lager flange is under compression, for beams over a certain span, the moment gradient factors become dependent solely on the end moment ratio.
6. When determining the elastic lateral torsional buckling strength of plane frames in Chapter 5, the importance of the finite rotation effect was assessed for a variety of structures. It was concluded that, unlike co-linear structures, the finite rotation effect is key for the correct prediction of the critical loads in most plane frame configurations.
7. The limitations of the Salvadori hypothesis commonly adopted in present design standards whereby the buckling loads for a member are quantified by separating the member from the rest of the structure were investigated through examples. The hypothesis was shown to lead to conservative predictions of the LTB strength when frames are laterally restrained at the joints but was found to lead to un-conservative predictions when some of the joints are laterally unrestrained. For frames with laterally unrestrained joints, a global lateral torsional buckling analysis is recommended. In this respect, the formulation developed in Chapter 5 provides an effective means to conduct such an analysis.

8. While the present research has exclusively focused on determining the elastic lateral torsional buckling resistance of members, the findings have direct impact on the quantification of inelastic lateral torsional buckling resistance for members with moderate spans. This is the case since design standards determine the inelastic lateral torsional buckling resistance based on empirical equations that depend upon the elastic lateral torsional buckling strength and the yield or plastic moments.

6.3 Recommendations for further research

1. In steel construction, lateral braces are frequently offset from the section shear center. The effect of bracing height on the critical moment has seen little attention in the literature. In this respect, the present study has illustrated the ability of the present multi-point constraint feature developed in Chapter 3 in capturing the bracing height effect for the case of reverse moments. It is recommended to adopt the multi-point constraint feature to investigate the effect of bracing height for other loading patterns and potentially develop simplified magnification/reduction expressions that account for bracing height.
2. It is recommended to adopt the solution developed in Chapter 4 for members with mono-symmetric cross-sections to investigate the load height and bracing height effects. While Section 4.5.4 has illustrated the applicability of the present formulation to develop moment gradient factors for the special case of linear moment gradients, moment gradient expressions can be developed for other loading cases and cross-sections. Also, Section 4.5.5 illustrated the ability of the present solution to generate buckling interaction diagrams for the specific case of beam-columns under a mid-span point load. The findings can be extended to other transverse load patterns (e.g., uniformly distributed loads, multiple point loads, etc.) in addition to axial forces.
3. The pre-buckling multi-point constraint feature developed in the present study can be used in conjunction with various buckling formulations to determine critical differential settlements values at which continuous members or frames tend to undergo lateral torsional buckling.
4. The frame lateral torsional buckling formulation developed in Chapter 5 was applied to a limited number of frame configurations. It would be of practical interest to adopt the present formulation to investigate other frame configurations involving multiple spans and multi-stories, where the use of shell buckling analysis would be prohibitively computationally

intensive. Such global lateral buckling analyses based on the present formulation would provide a basis to further assess the validity of conventional design methodologies based on the separation of the member from the surrounding structure.

5. The formulation presented in Chapter 5 has focused on frames where members intersect at 90 degrees. While such frames are representative of a large number of practical cases, further extensions of the work are needed for other frame configurations where members frame at different angles (e.g., gable frames, etc.).
6. The solutions developed in the present study have neglected the effect of the second order analysis effects in the pre-buckling analysis, where pre-buckling deformations were assumed to be proportional to the pre-buckling effects. In flexible structures and/or those subjected to high axial loads, geometric non-linear effects can play a role in the pre-buckling stage. It is of interest to incorporate such geometric non-linear effects in the pre-buckling deformation stage.